ISBN 978-82-326-2770-7 (printed version)
ISBN 978-82-326-2771-4 (electronic version)
ISSN 1503-8181

Doctoral Thesis
Astrid H. Brodtkorb

Doctoral theses at NTNU, 2017:351

Astrid H. Brodtkorb

Hybrid Control of Marine Vessels

Dynamic Positioning in Varying Conditions

NTNU
Norwegian University of
Science and Technology
Faculty of Engineering
Department of MarineTechnology

NTNU
Norwegian University of
Science and Technology

Doctoral theses at NTNU, 2017:351
NTNU

NTNU
Norwegian University of
Science and Technology

Astrid H. Brodtkorb

Hybrid Control of Marine Vessels

Dynamic Positioning in Varying Conditions

Thesis for the degree of Philosophiae Doctor

Trondheim, December 2017

Norwegian University of Science and Technology
Faculty of Engineering
Department of MarineTechnology

NTNU
Norwegian University of
Science and Technology

NTNU
Norwegian University of Science and Technology

Thesis for the degree of Philosophiae Doctor

Faculty of Engineering
Department of MarineTechnology

ISBN 978-82-326-2770-7 (printed version)
ISBN 978-82-326-2771-4 (electronic version)
ISSN 1503-8181

Doctoral theses at NTNU, 2017:351

Printed by Skipnes Kommunikasjon as

Blue,
green,
grey,
white,
or black;
smooth, ruffled, or mountainous;
that ocean is not silent.

- H. P. Lovecraft

Abstract

The next generation marine control systems will, as a step towards increased autonomy, have more automatic functionality in order to cope with a set of complex operations in unknown and varying environments, while maintaining safety and keeping costs low. In this thesis, a hybrid control concept for marine vessels is proposed, in order to increase the operational window of marine vessels in varying environmental conditions, with automatic switching of observers and controllers based on performance monitoring of the system states and signals, and characterizations of the sea state. The concept provides functional redundancy in the design methodology, giving better robustness to failures. The estimation and control algorithms presented in this work, are primarily designed for dynamic positioning (DP) control systems. A vessel in DP uses the thrusters to automatically maintain a fixed position, or move along a track at low speed. Vessels with DP capabilities are useful for marine operations in many marine applications, for instance; offshore oil and gas, offshore wind, aquaculture, fisheries, rescue, ocean science, and tourism.

As a result of more automatic functionality and system integration in marine control systems, control engineers must handle increasingly larger and more intricate systems. Typically, transit and maneuvering speed operation functionality can be merged with the DP functionality, giving one unified system for all speed ranges, modes of operation and environmental conditions. This is a hybrid control system, with continuous-time vessel dynamics and discrete-time (automatic) switching between candidate algorithms. Performance monitoring functions decide which candidate algorithms to use in closed-loop control, detect faults, issue alarms to the operator, and provide decision support. By applying a hybrid mathematical framework for marine control system modeling, rigorous analysis of the system, including switching dynamics, can be done, and stability constraints and robustness properties may be found. In order for a hybrid control system to be reliable, good switching criteria that are robust to measurement noise and system errors need to be established for the vessel speed, use modes, and environmental conditions. Some highlights from the thesis include:

- A residual calculation-based computationally efficient and reliable sea state estimation algorithm is proposed. The algorithm uses the heave, roll and pitch response spectra and simplified semi-analytical expressions for the motion transfer functions to compute an estimate of the wave spectrum. From this, characteristic periods, wave height, and the wave direction are derived. The algorithm may be used in performance monitoring functions of a hybrid

controller.

- Two ways of improving the transient response of a vessel in DP are investigated. Combining signal-based and model-based observers into one hybrid observer, and a time-varying model-based observer are both promising approaches. The strategies include a performance monitoring function that detects when a transient occurs.
- A novel signal-based observer concept is proposed for position and velocity estimation in DP. Noisy measurements with different, not necessarily periodic, sampling rates are combined into a hybrid system. The observer reacts fast to transients, and produces estimates of lower signal variance than the measurements.

The proposed sea state estimation, observer and controller algorithms are tested through simulations and model-scale experiments in the Marine Cybernetics Laboratory (MCLab) at NTNU. Some of the algorithms are also tested in full-scale sea trials on the NTNU owned Research Vessel Gunnerus.

The thesis is edited as a collection of papers.

Preface

This thesis is submitted in partial fulfillment of the requirements for the degree of philosophiae doctor (PhD) at the Norwegian University of Science and Technology (NTNU). The work is part of the Norwegian Center of Excellence (SFF) Centre for Autonomous Marine Operations and Systems (NTNU AMOS), Project 7 called *Autonomous marine operations in extreme seas, violent water-structure interactions, deep waters and Arctic*. It is a part of the Research Council of Norway (RCN) funding scheme, project number 223254.

I have done this work at the Department of Marine Technology (IMT) at NTNU. My main supervisor has been Professor Asgeir J. Sørensen at IMT NTNU, and my co-supervisors have been Professor Andrew R. Teel at Institute of Electrical and Electronics Engineers, University of California at Santa Barbara (UCSB) and Associate Professor Ulrik D. Nielsen at Department of Mechanical Engineering, Technical University of Denmark (DTU). During the spring of 2016 I had the pleasure of visiting Professor Andrew R. Teel at University of California, Santa Barbara (UCSB). I am very grateful for the hospitality.

The prelude to this thesis started in the fall of 2013 when I was starting the final year of my master studies. Professor Teel was visiting NTNU to hold lectures for a PhD course on hybrid systems. It seemed like an interesting topic, especially applied to marine control systems, and shortly after I was enrolled as an *Integrated PhD candidate*. After a couple of tough semesters I had completed my Master's thesis, presented a paper at my first conference (Paper D included in this thesis), and completed two PhD courses. In August 2014 when the *integrated* part of the PhD was up, and the 3-year PhD program started, I was already well into the research field.

Acknowledgments

I would like to thank Professor Asgeir J. Sørensen for being a continuous source of inspiration over many years, for sharing his knowledge of marine control systems, and for encouraging me to make my own judgements. Asgeir always finds the time to give good advice related to work, and on life in general. A great thanks to Professor Andrew R. Teel for good collaboration on applied hybrid systems, answering lengthy emails encouragingly, and for motivating me to pursue hybrid systems in the first place. I would like to thank Associate Professor Ulrik D. Nielsen for good and fruitful discussions related to vessel response, and sea state estimation, and for showing such enthusiasm for my work. I am very grateful for having such

a good team of supervisors, and without contributions from all three, the contents of this thesis would look very different.

Thanks to Torgeir Wahl (NTNU) for giving valuable help in the Marine Cybernetics Laboratory (MCLab) during six experiment periods, each with a duration of a couple of days up to two weeks. Thanks to Trond Innset (NTNU) and Lars Øien (Sintef Ocean) for building the cradle and completing oscillation tests for the model ship Cybership 3, so that the correct weight distribution could be calculated.

I have had the pleasure of joining the pioneering project AMOS DP Research Cruise 2016 (ADPRC'16), which was a collaboration between Kongsberg Maritime and NTNU PhD candidates and researchers. I would also like to thank the participants on the ADPRC'16 project for a great cruise with valuable learning outcomes. Especially thanks to Professor Roger Skjetne for initiating the project, Vincenzo Calabrò and the team at Kongsberg Maritime for making the DP test interface, the coding team Øivind Kjerstad, Mikkel E. N. Sørensen, and Svenn Are T. Værnø, and to Hans-Martin Heyn for helping me install the IMU (Inertial measurement unit) system on the R/V Gunnerus on very short notice.

Thanks to my fellow PhD candidates and postdocs for being great colleagues and friends. We have had many interesting discussions during lunch and coffee breaks over the years. Svenn Are deserves a special thanks for being a great office mate and co-author, for lengthy discussions of theory and ideas, and for close collaboration on simulation models, model-scale experiments and full-scale experiments.

Thanks to my family for always for being there for me, and showing interest in what I do, my parents for encouraging me to set my goals high, and for being proud of me, and finally a special thanks to my finacé Tor. You mean the world to me.

Trondheim, September 14$^{\text{th}}$ 2017 *Astrid H. Brodtkorb*

Contents

List of Acronyms

ADPRC	AMOS DP Research Cruise
AMOS	Centre for Autonomous Marine Operations and Systems
CG	Center of gravity
COLREG	Regulations for the prevention of collision of ships at sea
CPM	Control plant model
C/S	Cybership
DOF	Degree of freedom
DP	Dynamic positioning
ECEF	Earth-centered Earth-fixed reference frame
FFT	Fast Fourier transform
FMEA	Failure mode and effect analysis
GNSS	Global navigation satellite system
GPS	Global positioning system
HHT	Hilbert Huang Transform
HiL	Hardware-in-the-loop
IMO	International Maritime Organization
IMU	Inertial measurement unit
INS	Inertial navigation system
ISSC	International Ship and Offshore Structure Congress
JONSWAP	Join North Sea Wave Project
MCLab	Marine Cybernetics Laboratory
MCSim	Marine Cybernetics Simulator
MSS	Marine systems simulator
NED	North East Down reference frame
NORSOK	Norwegian continental shelf standard improving competitive position
NPO	Nonlinear passive observer
NTNU	Norwegian University of Science and Technology
OSC	Outer semi-continuous
PID	Proportional integral derivative
PPM	Process plant model
PSV	Platform supply vessel
ROV	Remotely operated vehicle
R/V	Research vessel
SiL	Software-in-the-loop

List of Figures

List of Tables

Part I

Thesis Overview and Background
- Stringing It All Together -

Chapter 1

Introduction

In this chapter the motivation and background for the thesis, research questions and methodology, list of papers and scientific contributions are introduced. The thesis organization and relationship between the papers, appearing in Part II, are discussed at the end of the chapter.

1.1 Motivation and Background

The demand for resources like food, energy, minerals, and trade is increasing worldwide. Roughly 70% of the world is covered by oceans that contain vast amounts of resources on the surface, within the water column, on and below the sea floor. At the same time the oceans remain some of the least explored places on Earth, and therefore it is important to develop sustainable technologies for responsible extraction and use of ocean resources. This includes developing marine vessels that are safe, environmentally friendly, and at the same time can operate for prolonged periods of time in varying environmental conditions. An overview of the topics considered in this thesis is found in Figure 1.1. It shows a marine vessel with its operational conditions and a block diagram of a general hybrid marine control system. Generally, several dimensions of vessel operation conditions may be defined. For illustration purposes (Figure 1.1) a 3-dimensional illustration is shown. The vessel operational conditions with *use mode, speed*, *environment* and (although not shown explicitly in the figure) *loading condition* indicates how the vessel performs different tasks with varying speed in an unknown and changing environment. The use mode includes algorithms that satisfy different control objectives such as stationkeeping, maneuvering, and target tracking, which is closely linked with the vessel speed. Environment refers to the state of the environment consisting of wind, waves and current, and loading condition is the mass distribution and draught of the vessel. Naturally, certain operations can only be performed in calm conditions. Because different physical effects matter for the various vessel operational conditions, there are distinct models and control strategies which are designed specifically for the various operational conditions.

Automatic ship motion control started more than 100 years ago with the invention of the gyroscope-aided autopilot in 1911 (Grumman, 2017) and rigorous

analysis of the proportional integral derivative (PID) controller (Minorsky, 1922). In the 1960s faster and smaller computers (Teknikum29, 2017), improved state estimation (Kalman, 1960), and the installation of the first dynamic positioning (DP) system, for automatic stationkeeping on a drillship using only thrusters, contributed to increased complexity in marine motion control systems. Today, marine (motion) control systems have strict requirements for redundancy and reliability, and the ability for re-configuration in the case of failure. Testing and verification is important to ensure safe systems with high integrity, see for instance Sørensen (2005), Sørensen (2011), and Fossen (2011). The complexity of marine control systems may differ from application to application, though the DP system remains one the more sophisticated control systems. A DP system is defined as *the complete installation necessary for dynamically positioning a vessel comprised of the power system, thruster system, and DP control system* (DNV-GL, 2017). The DP control system consists of computers including hardware and software, sensor system, displays and operator panels, positioning reference system, and the associated cabling. Some of the software modules for marine control systems are shown in the block diagram in Figure 1.1. Sensors measure the operational status and vessel motions, and signal processing software filters, weights and votes between redundant measurements, rejecting bad signals. The vessel observer estimates unmeasured states, filters out the wave-frequency vessel motion so that these do not enter in the control loop, and provides prediction of vessel states in the case of measurement loss. The guidance system provides waypoints for the vessel to follow, and the controller uses the estimated vessel motion to compute the desired generalized forces in order to satisfy the specified control objective. The control objective can for instance be setpoint regulation, path following and target tracking. The control allocation calculates setpoints for the actuators, in communication with the power system, so that sufficient power is available, and the local actuator control algorithms steer the individual actuators, like rotatable thrusters, propellers, rudders, and fins, to the setpoints.

The demand for increased levels of autonomy and system integration for marine vessels have forced control engineers to deal with increasingly larger and more complex systems. Higher levels of autonomy may lead to performance improvement in terms of increased precision, larger operational windows, lower fuel consumption and increased safety for passengers, crew and equipment. Typically the transit and maneuvering speed operation functionality merges with the DP functionality, giving one unified system for all speed ranges, use modes, loading and environmental conditions. Traditionally, control engineers have used continuous-time models to describe the interaction between the process plant and the controller, since for continuous-time models there are powerful control techniques like linear, nonlinear, robust or adaptive control, that provide formal proofs of performance. A marine vessel operating in waves can be modeled using continuous-time models, and observers and controllers for each operational condition can be designed using continuous-time control techniques. However, when the controllers for different vessel operational conditions are combined into one system using performance monitoring and switching logic, dynamics arise that differential equations on their own cannot describe. Systems that include both continuous- and discrete-time dynamics are called hybrid dynamical systems, or just hybrid systems, and the interaction

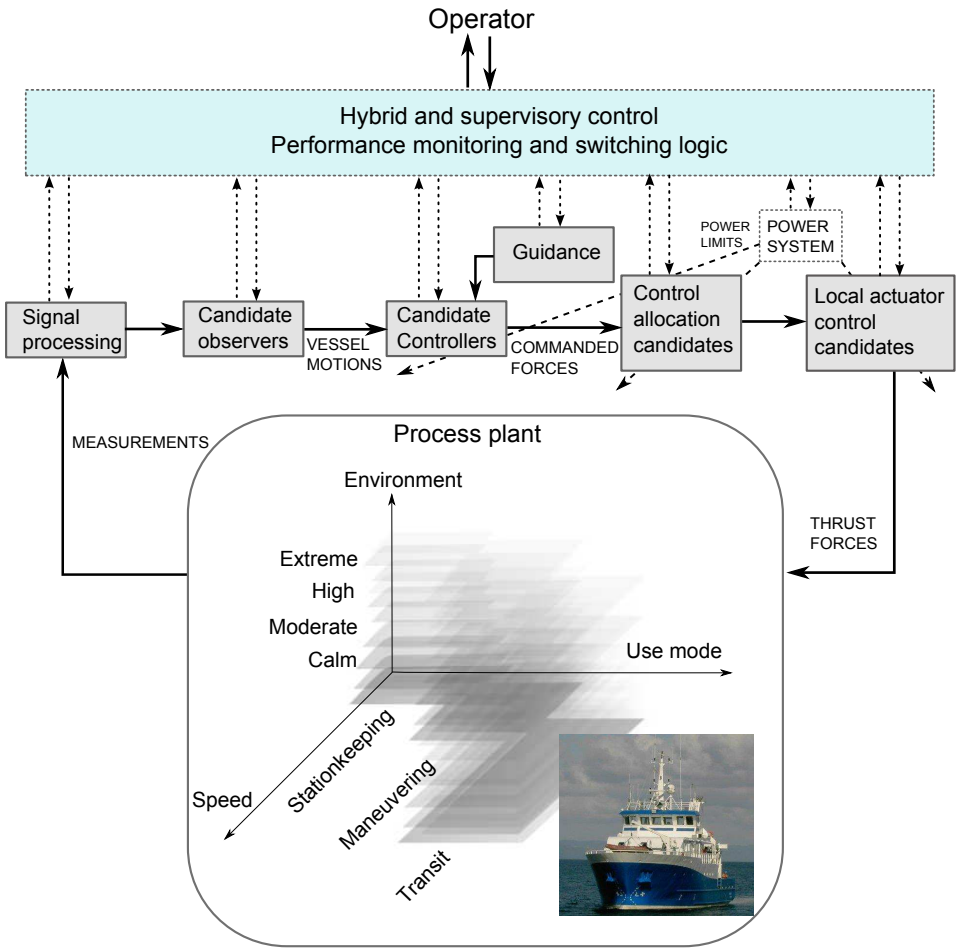

Figure 1.1: Hybrid control system for a marine vessel in a changing environment in different speed ranges and for various operational use modes. The ship is R/V Gunnerus.

between the different types of dynamics leads to challenging modeling and control problems.

Developing theory for hybrid systems is not a new area. As early as in the 1960's (Witsenhausen, 1966) systems with continuous and discrete dynamics were modeled and analyzed, and during the last 20 years, formal mathematical tools for modeling, stability and robustness analysis of hybrid systems have been developed. Examples of systems that can be modeled using hybrid frameworks include impulsive differential equations, systems with distinct logical states (also called hybrid automata), switching control systems, resetting control algorithms, synchronized behaviour that occurs in biological systems, and systems in networks. Since there are so many types of hybrid systems, naturally there are also a number of mathe-

matical frameworks for modeling and stability analysis, see for instance; Branicky (1995), Lygeros (1996), Henzinger (2000), Hespanha and Morse (2002), Goebel et al. (2012), and Arcak et al. (2016), to name a few. Hybrid systems frameworks are especially suited for describing marine vessel dynamics because the large diversity in dynamical behaviour for various vessel operational conditions can be captured using different sub-models merged into one hybrid system. Control system design based on hybrid vessel models that involve logic may be analyzed using diverse tools, and stability criteria may be obtained, ensuring safer, smarter and greener marine operations. A large inspiration for the work presented in this thesis are the works by Nguyen (2006), which applies switching control theory (Hespanha and Morse, 2002) to design hybrid controllers for changing sea states (Nguyen et al., 2007), and different speed ranges (Nguyen et al., 2008).

1.2 Research Questions and Methodology

In this thesis, a hybrid control concept is proposed, using the hybrid framework presented in Goebel et al. (2012). Several ways of improving the marine control system performance is investigated, focusing on the DP system, by looking into characterization and monitoring of the environment, improving the transient vessel response, and fusing measurements with different fidelities. The research questions of the thesis may be formulated as:

1. How can the sea state be characterized and monitored in order to improve operational availability and safety?
2. How can the operational window of a marine control system, subject to a varying sea state, be increased by automatic switching from a bank of observers and controllers based on performance monitoring of the system states and algorithms?
3. How can a theoretical control concept using a hybrid systems framework be developed in order to support 1 and 2?

The research methodology followed in the present work includes theoretical analysis, simulations, model-scale experiments and full-scale experiments. The research questions touch many different areas in the crossroads between the disciplines marine control systems, hybrid systems theory and wave-induced vessel response. Theory within these areas is used to inspire ideas for new concepts, and evaluate their theoretical validity and applicability. Simulations are used as a design tool in the first phase of a new concept, and later as a validation tool by identifying strengths and weaknesses through tuning and testing in different conditions. The simulator used for most of the numerical studies is based on the Matlab/Simulink MCSim (Sørensen et al., 2003), built over the last years by Master students and PhD candidates. Extensive simulations are done of the model ships in the Marine Cybernetics Laboratory (MCLab) and of the Research Vessel (R/V) Gunnerus before experiments are conducted. Model-scale experiments are performed in the MCLab on two different model ships; a platform supply vessel (PSV) model called Cybership 3, and an Arctic drillship model called C/S Inocean Cat 1 Drillship. Model-scale testing is an efficient way of testing the algorithms in a controlled environment. It is not as expensive as full-scale experiments, and the environment

can be turned on and off at leasure. Full-scale experiments are done onboard the NTNU-owned and operated R/V Gunnerus during the AMOS DP Research Cruise in October and November 2016 (ADPRC'16).

1.3 List of Publications and Scientific Contributions

This thesis summarizes a number of publications. Included in this thesis are seven authored and four co-authored papers. The papers are listed in the same order as they appear in Part II, which is according to topics and in chronological publication order within these. The scientific contribution of each paper is stated below the reference to the paper. Papers A-C are on sea state estimation, Papers D-I consider non-hybrid and hybrid observers and controllers for DP, and Papers J-K are on sensor fusion using hybrid systems theory.

A: Conference paper
Astrid H. Brodtkorb, Ulrik D. Nielsen, and Asgeir J. Sørensen (2015). **Sea State Estimation Using Model-scale DP Measurements.** *OCEANS 2015 - MTS/IEEE Washington, Washington, DC, 2015, pp. 1-7. doi: 10.23919/OCEANS.2015.7404402*

Contribution: The Fourier transforms of the vessel response in heave, roll and pitch are used directly to obtain an estimate of the peak wave frequency. The algorithm is computationally efficient, and validated on model-scale measurements.

B: Peer-reviewed journal paper
Astrid H. Brodtkorb, Ulrik D. Nielsen, and Asgeir J. Sørensen (2017). **Sea State Estimation Using Vessel Response in Dynamic Positioning.** *Accepted for publication in Applied Ocean Research 2017.*

Contribution: A novel method for estimating the sea state parameters based on the heave, roll and pitch response of a vessel in DP is developed. The algorithm finds the wave spectrum estimate from the response measurements by solving a set of linear equations through iteration, and as a result it is computationally efficient.

C: Peer-reviewed journal paper
Ulrik D. Nielsen, Astrid H. Brodtkorb, and Asgeir J. Sørensen (2017). **A Brute-force Spectral Approach for Wave Estimation Using Measured Vessel Responses.** *Submitted to Marine Structures.*

Contribution: The sea state estimation procedure from Paper B is generalized for vessels with forward speed and short-crested sea states. The procedure's performance is evaluated by use of numerical simulation of motion measurements, and it is shown that accurate wave spectrum estimates can be obtained for all wave directions in short-crested waves, composed of both wind-generated sea and swell.

D: Peer-reviewed conference paper
Astrid H. Brodtkorb, Asgeir J. Sørensen, and Andrew R. Teel (2014). **Increasing the Operation Window of Dynamic Positioned Vessels Using the Concept of Hybrid Control.** *Proc. 33rd International Conference on Ocean, Offshore and Arctic Engineering (OMAE) 2014, Volume 1A, V01AT01A046. doi: 10.1115/OMAE2014-23601.*

Contribution: A hybrid controller for a DP vessel in a varying sea state is proposed. An earlier version of the algorithm presented in Paper A, using the surge, sway and yaw motion is used to track the peak frequency of the sea state, and the controller performance is demonstrated through simulations. The controller yields the origin globally asymptotically stable.

E: Peer-reviewed conference paper
Astrid H. Brodtkorb, Svenn Are T. Værnø, Andrew R. Teel, Asgeir J. Sørensen, and Roger Skjetne (2016). **Hybrid Observer for Improved Transient Performance of a Marine Vessel in Dynamic Positioning.** *10th IFAC Symposium on Nonlinear Control Systems (NOLCOS 2016). IFAC-PapersOnLine. vol. 49 (18), pp 245-250, doi: 10.1016/j.ifacol.2016.10.189.*

Contribution: A hybrid observer including a signal-based part and a model-based part is designed. The model-based observer is used in steady-state conditions since it is especially good at filtering out first-order wave-induced motions, and predicting states in the case of signal loss, and the signal-based observer typically has superior performance during transients. The observer performance is monitored, and the part that provides the best estimate of the vessel position and heading is used in closed-loop control. Stability is analyzed, and the concept is validated through simulations.

F: Peer-reviewed journal paper
Astrid H. Brodtkorb, Svenn Are T. Værnø, Andrew R. Teel, Asgeir J. Sørensen, and Roger Skjetne (2017). **Hybrid Controller Concept for Marine Vessels with Experimental Results.** *Submitted to Automatica 2017*

Contribution: As a continuation of Paper E, a hybrid concept is proposed, allowing a structured way to develop a control system with a bank of controllers and observers improving DP performance in stationary dynamics, improving transient performance, and giving robustness to measurement errors and software bugs. The performance of the hybrid control system, including two observer candidates and one controller candidate, is demonstrated in model-scale experiments and on full-scale field data. The hybrid system has global stability properties.

G: Peer-reviewed conference paper
Svenn Are T. Værnø, Astrid H. Brodtkorb, Roger Skjetne, and Asgeir J. Sørensen (2016). **An Output Feedback Controller with Improved Transient Response of Marine Vessels in Dynamic Positioning.** *The 10th IFAC Conference on Control Applications in Marine Systems (CAMS 2016).*

IFAC-PapersOnLine. vol. 49 (23), pp. 133-138, doi: 10.1016/j.ifacol.2016.10.33.

Contribution: An output feedback controller is proposed for DP of marine surface vessels, that has good performance in steady-state conditions and during transients. This is achieved by having time-varying gains in the observer, and using the bias estimate from the observer as integral action. Validation of the concept is done in simulations.

H: Peer-reviewed journal paper
Svenn Are T. Værnø, Astrid H. Brodtkorb, Roger Skjetne, and Vincenzo Calabrò (2017). **Time-varying Model-based Observer for Marine Surface Vessels in Dynamic Positioning.** *IEEE Access, vol. 5, pp. 14787-14796, doi: 10.1109/ACCESS.2017.2731998*

Contribution: As a continuation of Paper G, the time-varying model-based observer design is enhanced to provide even better estimates during transients, and validation of the concept is done in simulations and in full-scale closed-loop experiments onboard R/V Gunnerus.

I: Peer-reviewed conference paper
Roger Skjetne, Mikkel E. N. Sørensen, Morten Breivik, Svenn Are T. Værnø, Astrid H. Brodtkorb, Asgeir J. Sørensen, Øivind K. Kjerstad, Vincenzo Calabrò, and Bjørn Ole Vinje (2017). **AMOS DP Research Cruise 2016: Academic Full-scale Testing of Experimental Dynamic Positioning Control Algorithms Onboard R/V Gunnerus.** *36th International Conference on Ocean, Offshore and Arctic Engineering (OMAE) 2017, Trondheim, Norway Paper no: OMAE2017-62045.*

Contribution: In order to validate relevant DP control algorithms in a realistic environment, a full-scale DP test campain, the AMOS DP Research Cruise 2016 (ADPRC'16), was organized in a collaboration between the NTNU Centre for Autonomous Marine Operations and Systems (NTNU AMOS) and the company Kongsberg Maritime. To the author's knowledge, closed loop DP feedback control algorithms have never been tested full-scale on a ship in an academic research experiment before. This paper reports the experimental setup, test program, and an overview of results from the ADPRC'16 campain.

J: Peer-reviewed conference paper
Astrid H. Brodtkorb, Andrew R. Teel and Asgeir J. Sørensen (2015). **Sensor-based Hybrid Observer for Dynamic Positioning.** *54th IEEE Conference on Decision and Control (CDC 2015), Osaka, pp. 948-953. doi: 10.1109/CDC.2015.7401995*

Contribution: A sensor-based (later referred to as *signal-based*) hybrid observer combining noisy acceleration, velocity and position measurements of a vessel in DP is presented. The concept assumes that noisy position and velocity measurements are available only occasionally at a non-constant sampling rate. Predictions of position between the samples are provided by integrating

acceleration measurements, which are available at a high rate (approximated to be continuous sampling). Estimates with smaller variance are computed by averaging multiple observer copies of position and velocity.

K: Peer-reviewed conference paper
Astrid H. Brodtkorb, Andrew R. Teel and Asgeir J. Sørensen (2016). **Hybrid Observer Combining Measurements of Different Fidelities.** *The 10th IFAC Conference on Control Applications in Marine Systems (CAMS 2016). IFAC-PapersOnLine. vol. 49 (23), pp. 506-511, doi: /10.1016/j.ifacol.2016.10.486*

Contribution: The hybrid observer from Paper J is adapted to the more realistic scenario where there are no velocity measurements, and no angular rate acceleration measurements. The observer is validated through simulations, where the estimates are used in closed-loop control during DP setpoint changes.

The following co-authored papers are not a part of the thesis:

Ulrik D. Nielsen, Roberto Galeazzi, and Astrid H. Brodtkorb (2016). **Evaluation of Shipboard Wave Estimation Techniques Through Model-scale Experiments.** *OCEANS 2016 Shanghai - MTS/IEEE, pp. 1-8, doi: 10.1109/OCEANSAP.2016.7485701.*

Ole Maurice Røste Rabanal, Astrid H. Brodtkorb, and Morten Breivik (2016). **Comparing Controllers for Dynamic Positioning of Ships in Extreme Seas.** *The 10th IFAC Conference on Control Applications in Marine Systems (CAMS 2016). IFAC-PapersOnLine. vol. 49 (23), pp. 258-264, doi: 10.1016/j.ifacol.2016.10.35.*

Ulrik D. Nielsen, Astrid H. Brodtkorb, and Jørgen J. Jensen (2017). **Response Predictions for Marine Vessels Using the Observed Autocorrelation Function.** *Accepted for publication in Marine Structures 2017.*

Ulrik D. Nielsen, and Astrid H. Brodtkorb (2018). **Ship-motion-based Estimation Using a Spectral Residual-calculation.** *Submitted to IEEE International Conference on Acoustics, Speech, and Signal Processing (ICASSP 2018).*

1.4 Thesis Organization and Overview

The first part of the thesis contains an overview of, and background for the research, going into the details of Figure 1.1. The second part contains the papers. Figure 1.2 illustrates the topics of each chapter and paper, and indicates how each publication is related to the others. This section attempts to string the papers together.

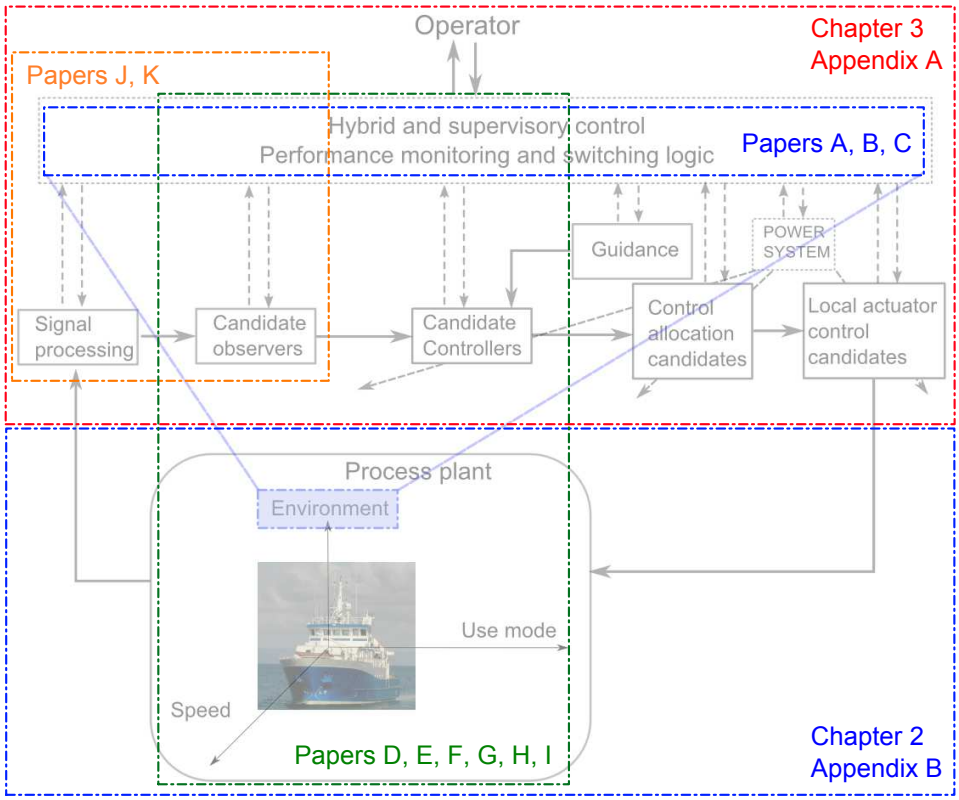

Figure 1.2: Sketch of Figure 1.1 illustrating the thesis overview, with the topics of the chapters and papers indicated.

Part I

Chapter 2 gives an overview of the relevant theory related to mathematical modeling of the marine environment and vessels, as this theory is discussed only briefly in the papers. Special focus is given to modeling of waves in the time-domain and frequency-domain, and describing the differences between vessel models.

Chapter 3 goes into the details of the block diagram in Figure 1.1, giving an overview of the hybrid control system structure, a description of the performance monitoring and switching logic, state-of-the-art observer and controller algorithms,

and applications of hybrid systems to marine control. The hybrid dynamical systems framework applied in this work is introduced, the applicability of hybrid theory to marine systems is discussed, and some methods for control system testing are mentioned.

Chapter 4 concludes the thesis and indicates directions for further work.

Appendix A gives mathematical preliminaries for hybrid dynamical systems that may be useful when reading Papers D-F, J, and K.

Appendix B presents the experimental test platforms Cybership 3 and R/V Gunnerus. Cybership 3 is used in Papers A, D, and J, and R/V Gunnerus is used for Papers B, C, F, H and I.

Part II

The papers look into different parts of the hybrid control system, see Figure 1.2 for indications of how the topics are linked. The contributions from the individual papers may be collected into one hybrid system that performs well in changing environmental conditions and for different speed ranges, use modes and loading conditions.

Papers A-C present two strategies for sea state estimation with computationally efficient implementations. In **Paper A**, the peak frequency is estimated using the fast Fourier transform (FFT) of the heave and pitch response measurements, and in **Papers B** and **C**, the wave spectrum and wave direction are estimated. Detailed knowledge of the sea state, like this, may be used in hybrid performance monitoring and switching logic in order to adjust observer parameters and controller gains, and automatically switch to the *best* suited algorithm amongst the candidates. An example of using the peak frequency estimate to switch between a set of observer and controller candidates is given in **Paper D**, where an earlier version of the peak frequency estimation algorithm from **Paper A** is applied.

Papers E-H investigate improving the transient response of the vessel using reactive control strategies. Two main approaches are presented; one hybrid observer strategy, and one time-varying model-based observer strategy. The performance monitoring functions guiding hybrid switching, and changing of gains, include estimation error and desired turning rate in order to detect transients early, and correct for the response quickly.

Papers J and **K** propose a hybrid observer combining sensor signals with different sampling times for position, velocity and acceleration estimation. The observer concept is hybrid on its own, but can also be a part of the observer set, from which the *best* performing algorithm is chosen.

Certification of stability for the control algorithms presented in the papers is done through one or more of the following; theoretical stability analysis, simulations, model-scale experiments, full-scale experiments, or estimation on model-scale or full-scale data. **Paper I** gives an account of full-scale testing of control algorithms onboard R/V Gunnerus.

Chapter 2

Mathematical Modeling of the Marine Environment and Vessels

This chapter enters deeper into modeling of the marine environment and vessels for control design and testing. The focus of Section 2.1 is on modeling of waves, and state-of-the-art wave estimation techniques, and Section 2.2 presents reference frames, and three models for marine vessels.

2.1 The Marine Environment

When modeling the marine environment for the purpose of marine control system design and testing, the environmental effects are categorized into different frequency regimes. Figure 2.1 shows how the sea environment, in terms of wave, wind and current loads, generally is distributed over frequency. The high-frequency regime consists of ripples and second-order sum-frequency waves, and the wave-frequency regime includes wind-generated waves and swell. The low-frequency regime includes ocean current, mean wind, and second-order difference-frequency wave effects like mean and slowly-varying wave drift. Ocean currents are generated by wind, tides, the Coriolis effect due to the Earth's rotation about itself, sea temperature and salinity differences. The environmental effects that fall into the low-frequency and wave-frequency regimes contain significant amounts of energy, and are important to capture correctly for modeling and control of marine vessels, as discussed in Section 2.2 and Chapter 3.

Wind is usually modeled as a mean, or slowly varying, component and gusts. For ships and offshore structures the slowly varying wind constitutes a lot of the forces on the structure, however the gusts may also be of importance since they can cause resonant oscillations. Gusts usually have durations of less than 20 seconds. The Harris or NORSOK wind spectra[1] are commonly used to describe the wind energy distribution with respect to frequency.

[1] Different wind spectrum formulations are given in 10th ISSC Proceedings (1988). The NORSOK are standards are developed by the Norwegian petroleum industry to ensure adequate safety for petroleum industry developments and operations.

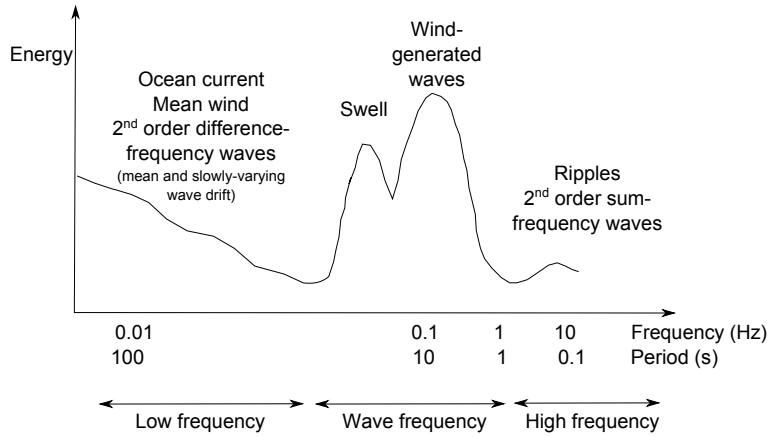

Figure 2.1: Sketch illustrating the marine environment distributed over frequency. The low-frequency, wave-frequency and high-frequency regimes are indicated. Note that the axes are not in scale.

When the wind blows over an open stretch of water (called fetch) for some time without changing direction, waves are created. These are called wind-generated waves. The wave height and period depend on the wind strength, fetch length, and the wind duration, and they can be classified according to their oscillation period. Wind-generated waves generally have periods between 5-20 seconds, and swell has periods of 15-40 seconds. Swell is generated by distant weather systems due to e.g., storms, and travel to other places. Therefore they are not affected by the local wind, and swell often has a different direction than local wind-generated waves. The sea state is said to be *fully developed* when the energy in the sea state is constant, i.e., when the energy transfer from the wind to the sea and the dissipation of energy through breaking waves are of equal magnitude.

Price and Bishop (1974) divided the environmental conditions into different sea states according to the significant wave height H_s (the mean of the 1/3 highest waves, also denoted $H_{1/3}$ in literature) and peak period T_p, and Lee and Bales (1985) also included the wind speed in the sea state codes, see Table 2.1. The probability of occurrence of the different sea states in the northern North Atlantic, including the North Sea, is also given, where sea states 3, 4, and 5 occur the most often. This is also dependent on the season, as rougher sea states occur more often in the winter time. By increasing the operational window of marine vessels from a moderate sea state 4 to a very rough state 6, year-round operations in the North Sea are one step closer. In Arctic areas, sea ice may be more prominent than waves; however, such conditions are not considered in this work.

Table 2.1: Definition of the sea state codes given by significant wave height H_s, peak period T_p (Price and Bishop, 1974), and mean wind speed at 19.5 m above the sea surface V (Lee and Bales, 1985). The percentage probability for the northern North Atlantic is given, and is summarized for sea states 0-2.

Sea State Code	Description of sea	H_s [m]	T_p [s]	V [m/s]	% probability
0	Calm (glassy)	0	-	0	
1	Calm (rippled)	0-0.1	4.87 - 5.66	1.54	6.062
2	Smooth (wavelets)	0.1-0.5	5.66- 6.76	4.37	
3	Slight	0.5-1.25	6.76 - 7.95	6.94	21.57
4	Moderate	1.25-2.5	7.95 - 9.24	9.77	40.99
5	Rough	2.5-4.0	9.24 - 10.47	12.6	21.24
6	Very rough	4.0-6.0	10.47 - 11.86	19.3	7.010
7	High	6.0-9.0	11.86- 13.66	26.5	2.693
8	Very high	9.0-14.0	13.66 - 16.11	30.6	0.4346
> 8	Phenomenal	> 14	> 16.11	> 32.4	0.0035

2.1.1 Modeling of Ocean Wave Systems

Generally the sea surface elevation may be modeled in the time domain as a finite sum of many regular (sinusoidal) wave components with different oscillation frequency ω_j, and amplitude a_j (Faltinsen, 1993). The total wave elevation ζ in a *long-crested*[2] sea state can be expressed as

$$\zeta = \sum_{j=1}^{N} a_j \sin(\omega_j t - k_j x + \epsilon_j), \tag{2.1}$$

where k_j is the wave number, t is the time, $\epsilon_j \in [0, 2\pi)$ is a random phase angle, and the wave propagates with (main) propagation direction along the positive x-axis. Figure 2.2 illustrates how the regular wave components are added to get the total irregular wave elevation, and how the amplitudes of the regular wave components can be related to the wave spectrum $S(\omega)$ as

$$\frac{1}{2} a_j^2 = S(\omega_j)\Delta\omega, \tag{2.2}$$

where $\Delta\omega$ is the constant difference between successive wave frequencies. Since the wave energy is proportional to the wave amplitude squared, the wave spectrum describes the energy present in a sea state. The energy E (per unit width) in a wave component with length λ_j can be written as

$$E = \frac{1}{2}\rho g \lambda_j a_j \tag{2.3}$$

[2]Long-crested waves have one main propagation direction with little directional spread. Short-crested waves have a large directional spread, and the sea surface may often appear chaotic.

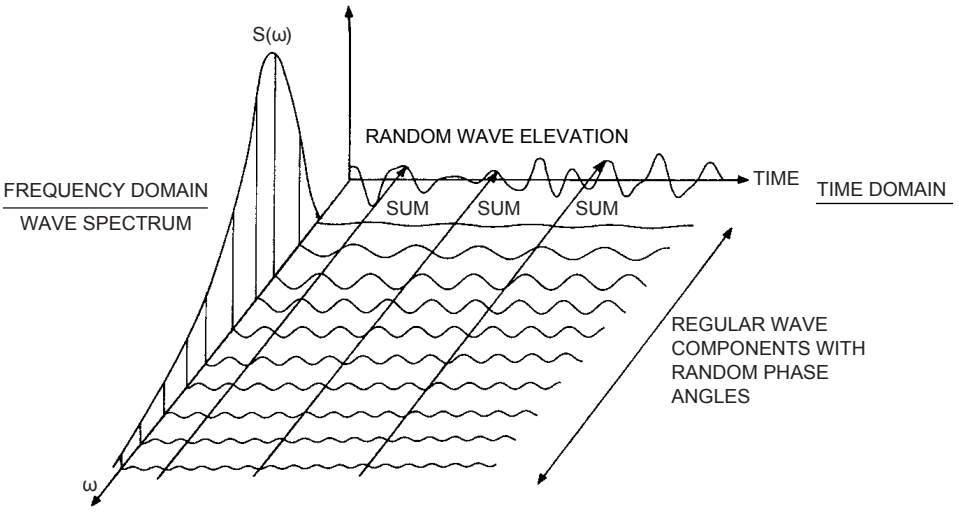

Figure 2.2: Sketch illustrating the connection between frequency-domain and time-domain representation of waves in a long-crested sea state. The regular wave components are summed to give the irregular wave elevation at each time instant. Source: Faltinsen and Timokha (2009).

where ρ is the water density, and g is the acceleration due to gravity. There are many wave spectra with different shapes for describing various sea states, three of which are shown in Figure 2.3. The JONSWAP (Joint North Sea Wave Project) spectrum is used to describe developing seas, when the wind has limited fetch length, and the Pierson-Moskowitz spectrum describes fully developed sea states in the open ocean. These spectra are both single-peaked, with the Pierson-Moskowitz being more broad spectered compared to the JONSWAP spectrum. The Torsethaugen spectrum is a two-peaked spectrum which describes a sea state with swell and wind-generated sea. In some cases, wave spectra without distinct peaks are measured. These are not described by the spectra above, but the frequency ranges where the most wave energy is present is still important for marine operations. The JONSWAP and Torsethaugen spectra are common in the North Sea.

Statistical properties like the significant wave height H_s, and characteristic periods, like the mean or peak period T_p relate to $S(\omega)$ through,

$$H_s := 4\sqrt{m_0}, \quad m_0 := \int_0^\infty S(\omega)d\omega \tag{2.4a}$$

$$T_p := \frac{2\pi}{\omega_p}, \qquad \omega_p := \arg\max_j S(\omega_j). \tag{2.4b}$$

The wave propagation direction is usually described by a mean direction and spread α. The distribution of energy over different directions can be modeled by a

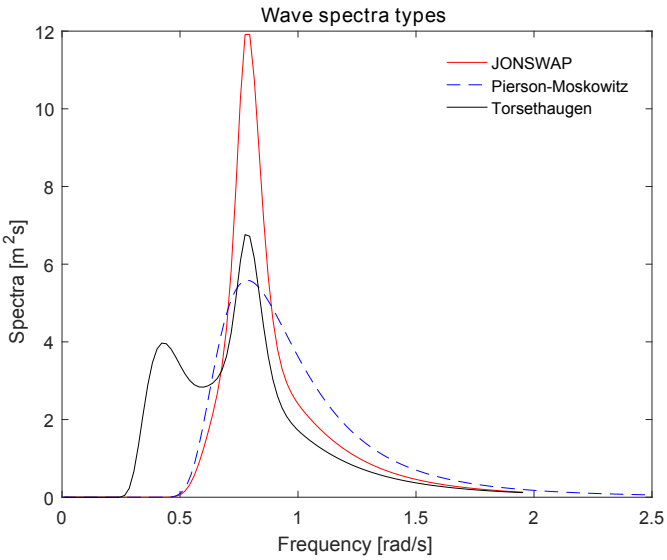

Figure 2.3: Examples of JONSWAP, Pierson-Moskowitz and Torsethaugen wave spectra. The wind-generated peak has $H_s = 7$ m and $T_p = 8$ s for all spectra, and the swell peak in the Torsethaugen spectrum has $H_s = 8$ m and $T_p = 15$ s.

spreading function $f(\alpha)$, for example given as,

$$f(\alpha) = \begin{cases} 2\pi^{-1}\cos^2(\alpha), & \text{for } -\pi/2 < \alpha < \pi/2 \\ 0, & \text{otherwise,} \end{cases} \tag{2.5}$$

with $\alpha = 0$ corresponding to the main propagation direction of the waves (Faltinsen and Timokha, 2009). Other ways of representing the directional distribution may be found in the 10th ISSC Proceedings (1988). For instance expressing the directional spread as a function of frequency $f(\alpha, \omega)$, allows for waves with different lengths to come from different directions, e.g., swell from one direction and first-order wind-generated waves from another direction, which typically occurs. This could be done by having one distribution (2.5) for each dominant wave period. The integral of the energy distribution over all directions is equal to the total energy in the sea state,

$$\int_0^{2\pi} f(\alpha, \omega) d\alpha = 1,$$

so that the directional wave spectrum is the multiplication of the wave spectrum $S(\omega)$ with the directional spread $f(\alpha, \omega)$,

$$S(\omega, \alpha) = S(\omega) f(\alpha, \omega). \tag{2.6}$$

2.1.2 Estimating the Sea State

Knowing what type of environment the vessel is operating in is crucial for a successful operation, either through weather forecasts, on-site wave rider buoys, wave radar systems, or by onboard sea state estimation algorithms. This section provides a literature review of the state-of-the-art methods for wave estimation.

There are many different providers of weather forecasts at sea. Satellite images are used to derive the wind speed and direction, and altimeters measure the wave height. The satellite images cover a large area, so a good overview over the sea state in a region is achieved. However, the local wave parameters are difficult to quantify exactly, and the processed data (the sea state) will not be available in real-time. On the other hand, directional wave rider buoys have a high precision for local areas. The buoys are usually placed along the coastline or near offshore infrastructure. They include inertial measurements units (IMU) with accelerometers, magnetic compass and Global Navigation Satellite System (GNSS), such as GPS (Global Positioning System), for measuring the wave elevation time series, from which statistics like H_s, T_p, direction and spread can be calculated. In order to have good use of a wave buoy, the operation should take place in proximity to the buoy.

Wave radar systems that are installed on ships can estimate the surface elevation up to 2-3 nautical miles (3.70-5.56 km), depending on the radar, which corresponds to looking 4-5 minutes ahead in time, depending on the vessel speed and the encounter direction of the waves. Clauss et al. (2012) discusse a decision support system based on wave radar measurements in directional sea states. The wave length and direction are measured directly from the wave radar images, whereas the wave height is derived from the signal-to-noise ratio. For fixed platforms good agreement for the wave height can be achieved, but for floating vessels the wave height measurements are degraded due to the vessel motion, amongst other factors (Thornhill and Stredulinsky, 2010). To solve this problem, Stredulinsky and Thornhill (2011) fuse wave radar measurements and ship motion measurements to get a more reliable wave height measurement. Another onboard measurement system are bow-fixed altimeters, which may be used to measure the surface elevation at the bow.

Marine vessels are equipped with many sensors that measure and monitor the vessel's response in waves, and hence these measurements can be used to estimate the sea state. Figure 2.4 illustrates the main procedure for calculating a wave spectrum estimate from global ship response measurements. A time series of the measured responses are transformed into the frequency domain. An initial wave spectrum estimate is assumed, and the complex-valued motion transfer functions, are used to calculate a response spectra. Based on the error between the measured and estimated response spectra, adjustments are made to the estimated wave spectrum, before the procedure is repeated. There are a number of methods for estimating the sea state in this way, often referred to as the *wave-buoy analogy*, since the method resembles the way a traditional wave buoy calculates the sea state. The complex-valued motion transfer functions are dependent on the detailed hull geometry, mass distribution, and loading condition, and they are calculated

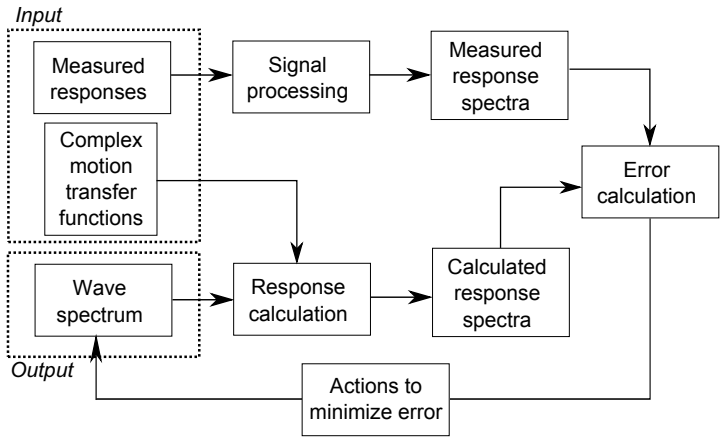

Figure 2.4: Illustration of the fundamental idea behind estimating the sea state using ship responses. Inputs are usually measured responses and complex-valued motion transfer functions, and the output is the wave spectrum.

using panel codes like WAMIT[3] for zero forward speed or strip codes like ShipX[4] for forward speed. Jensen et al. (2004) present a simple semi-analytical way of approximating the motion transfer functions for a box-shaped vessel in heave, roll and pitch, called closed-form expressions, and the phases of the responses are given in Mansour et al. (2004). The closed-form expressions are convenient approximations for the transfer functions of vessels in varying operational conditions, and for vessels where the detailed hull geometry is unknown, or unavailable due to confidentiality.

For a vessel with forward speed in following sea, the Doppler shift of the encounter frequency creates challenges for for ship-motion based sea state estimation because of the 1-to-3 relationship between encounter and absolute wave frequency. The first successful attempt to include the 1-to-3 problem in the wave buoy analogy was made by Iseki and Ohtsu (2000), and since then several works have followed; Nielsen (2006), Iseki (2010), Nielsen et al. (2013), Iseki and Nielsen (2015), Montazeri et al. (2016b), and Montazeri et al. (2016a), Nielsen et al. (2017b) (Paper C). A practical procedure for transforming wave energy spectra from the encounter to the absolute domain is presented in Nielsen (2017b). Estimation methods that consider DP operations only include Tannuri et al. (2003), Simos et al. (2007), Pascoal and Guedes Soares (2009), and Brodtkorb et al. (2017a) (Paper B). Nielsen (2017a) conveniently summarizes some shipboard sea state estimation techniques.

The preceding references study procedures that yield the complete frequency-directional wave energy distribution, however, the procedures may not necessarily be applicable online in a controller due to relatively high computational footprint, with the exception of Brodtkorb et al. (2017a) and Nielsen et al. (2017b). Estimation methods that are designed to run online in a controller that estimate only some

[3] http://www.wamit.com/
[4] http://www.sintef.no/programvare/shipx/

wave parameters, include the time-domain approach by Belleter et al. (2015), that uses an Aranovksii filter (Aranovskii et al., 2007) to estimate the peak frequency of encounter, which is applied in parametric roll resonance detection (Fossen and Neijmer, 2012). Brodtkorb et al. (2015a) (Paper A) presents a frequency-domain peak wave frequency estimation algorithm based on the heave and pitch response, applicable in the wave filter of observers. Nielsen et al. (2015) proposes a time-domain algorithm that estimates a regular wave by first applying an Aranovski filter to estimate the frequency, and then a nonlinear least squares method for estimating the amplitude and the phase. Nielsen et al. (2016) is an extension of this work with experimental results. A different time-domain approach is taken in Udjus (2017), where measurements from multiple IMUs that are distributed along a model-ship hull are fused in order to estimate the wave direction.

Many of the estimation methods are in the frequency domain, so then the response measurements are transformed into the frequency-domain using Fourier transforms. Hence, it is implicitly assumed that the vessel response is in stationary conditions in a stochastic sense, i.e., that the ship course and speed are constant. The Hilbert Huang Transform (HHT) is a method for analyzing nonlinear and nonstationary data using Empirical Mode Decomposition (Huang et al., 1998). A time series is first decomposed into a finite number of intrinsic mode functions, which have well-behaved Hilbert transforms. This results in a frequency-energy-time distribution, which is used for instance for control of wave energy converters (Garcia-Rosa et al., 2017). Efforts are attempting to make the HHT method work in real-time.

2.2 Modeling of Marine Vessels for Control Design and Testing

In this section, three models of marine vessels that are used for observer and controller design and testing are presented. Two of the models are based on the vessel's hydrodynamic parameters, and are essentially different fidelities of the same model type; the process plant model (PPM) and the control plant model (CPM), see Sørensen (2011) and Fossen (2011). The third model introduced is the kinematic model, which relates the acceleration, velocity and position in body-fixed and inertial frame to each other through a rotation matrix and integration, see Bryne et al. (2017a). The reference frames and body motions are introduced first.

2.2.1 Reference Frames

The reference frames that are usually applied for modeling and control of marine vessels are shown in Figure 2.5, and described below.

- The Earth-centered-Earth-fixed (ECEF) reference frame is a global reference frame with origin at the Earth's center. As a consequence of being fixed to the Earth it rotates with the rotational rate of the Earth. It is for instance used for global navigation and control of marine vessels in transit between continents. The position (latitude and longitude) is given in degrees North/South and degrees East/West.

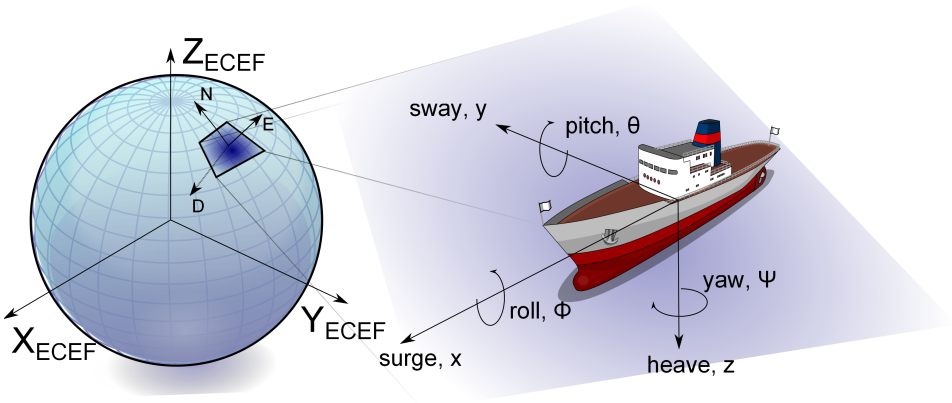

Figure 2.5: Overview of reference frames and ship motions. Ship adapted from Fiestoforo (2017).

- The North-East-Down (NED) reference frame is a local Earth-fixed frame used for local positioning. In marine applications it is often assumed to be inertial (non-rotating). The N-axis points towards the true North, the E-axis points East, and the D-axis points towards the Earth's center.
- The body (xyz) frame is a body-fixed reference frame with origin usually placed along the centerline of the body and in the water plane. The x-axis points forwards (towards the bow), the y-axis points towards starboard, and the z-axis points down.

The reference frames are all right-handed. Figure 2.5 also shows how the linear degrees of freedom (DOF); *surge (x), sway (y)* and *heave (z)*, and the angular DOFs; *roll (ϕ), pitch (θ)* and *yaw* (ψ), are defined. The generalized position η and velocity ν of a marine vessel in 6 DOFs are defined as

$$\begin{aligned} p^n &:= [x, y, z]^\top, & v^b &:= [u, v, w]^\top \\ \Theta &:= [\phi, \theta, \psi]^\top, & \omega^b &:= [p, q, r]^\top \\ \eta &:= [p^{n\top}, \Theta^\top]^\top, & \nu &:= [v^{b\top}, \omega^{b\top}]^\top. \end{aligned} \tag{2.7}$$

η is given in the NED frame, and ν is in the body frame. The relation between linear velocity in the body frame v^b and linear velocity in the NED frame $\dot{p}^n$ is given by a rotation about the (zyx)-axes as

$$\dot{p}^n = R(\Theta)v^b, \tag{2.8}$$

with

$$R(\Theta) := \begin{bmatrix} c\psi c\theta & -s\psi c\phi + c\psi s\theta s\phi & s\psi s\phi + c\psi c\phi s\theta \\ s\psi c\theta & c\psi c\phi + s\phi s\theta s\psi & -c\psi s\phi + s\theta s\psi c\phi \\ -s\theta & c\theta s\phi & c\theta c\phi \end{bmatrix}, \tag{2.9}$$

with $s\cdot$ denoting $\sin(\cdot)$, and $c\cdot$ denoting $\cos(\cdot)$. $R(\Theta)$ in (2.9) is the rotation matrix parametrized by Euler angles Θ. The relation between angular velocity in the body frame ω^b and angular velocity in the NED frame $\dot{\Theta}$ is

$$\dot{\Theta} = T(\Theta)\omega^b, \tag{2.10}$$

with

$$T(\Theta) := \begin{bmatrix} 1 & s\phi t\theta & c\phi t\theta \\ 0 & c\phi & -s\phi \\ 0 & s\phi/c\theta & c\phi/c\theta \end{bmatrix}, \tag{2.11}$$

with $s\cdot$ denoting $\sin(\cdot)$, and $c\cdot$ denoting $\cos(\cdot)$ as before, and $t\cdot$ denoting $\tan(\cdot)$. Another common representation of $R(\Theta)$ and $T(\Theta)$ is given by quaternions, where the singularity in $T(\Theta)$ is avoided for $\theta = \pm 90°$, see Fossen (2011), Chapter 2 for more details. The kinematic relation can be formulated compactly as

$$\begin{aligned} \dot{\eta} &= J(\Theta)\nu, \\ &\Updownarrow \\ \begin{bmatrix} \dot{p}^n \\ \dot{\Theta} \end{bmatrix} &= \begin{bmatrix} R(\Theta) & 0 \\ 0 & T(\Theta) \end{bmatrix} \begin{bmatrix} v^b \\ \omega^b \end{bmatrix}. \end{aligned} \tag{2.12}$$

2.2.2 Process Plant Model

The process plant model (PPM), also called the *simulation model*, is a high-fidelity model which accurately describes the real vessel dynamics in 6 DOFs, see Figure 2.6 for an illustration. It is used in simulators for controller testing and verification, and includes process disturbances, sensor outputs and control inputs, see Sørensen (2011) and Fossen (2011) for details. The low-frequency vessel motion, see Figure 2.6, is described by a nonlinear model given by,

$$M\dot{\nu} + C_{RB}(\nu)\nu + C_A(\nu_r)\nu_r + D(\kappa, \nu_r) + \mu + G(\eta) = \tau_{moor} + \tau_{thr} + \tau_{env}, \tag{2.13}$$

where $M = M_{RB} + M_A \in \mathbb{R}^{6\times 6}$ is the rigid body inertia matrix including added mass, $C_{RB}(\nu) \in \mathbb{R}^{6\times 6}$ and $C_A(\nu_r) \in \mathbb{R}^{6\times 6}$ are the rigid body and added mass Coriolis matrices, $D(\kappa, \nu_r) \in \mathbb{R}^{6\times 6}$ is the damping matrix consisting of a linear second-order wave-induced damping and nonlinear damping, μ represents fluid memory effects (Cummins, 1962), and $G(\eta) \in \mathbb{R}^{6\times 6}$ is the restoring matrix. The hydrodynamic parameters are calculated using hydrodynamic codes like WAMIT or ShipX. $\dot{\nu} \in \mathbb{R}^6$ is the vessel acceleration in the body frame, the generalized position and velocity η and ν are defined in (2.7), and $\nu_r = \nu - \nu_c \in \mathbb{R}^6$ is the relative velocity where ν_c is the current velocity in the body frame. For control purposes current effects are included by considering the velocity of the vessel relative to the water, and this is why the relative velocity appears in $C_A(\nu_r)$ and $D(\kappa, \nu_r)$. The current velocity is often modeled as a mean and a slowly varying component. For surface vessels, modeling the surface current is sufficient, but for marine structures in the water column, the full current depth profile is of importance. τ_{moor} and τ_{thr} are the external forces acting on the ship from the mooring and thrusters. The actual

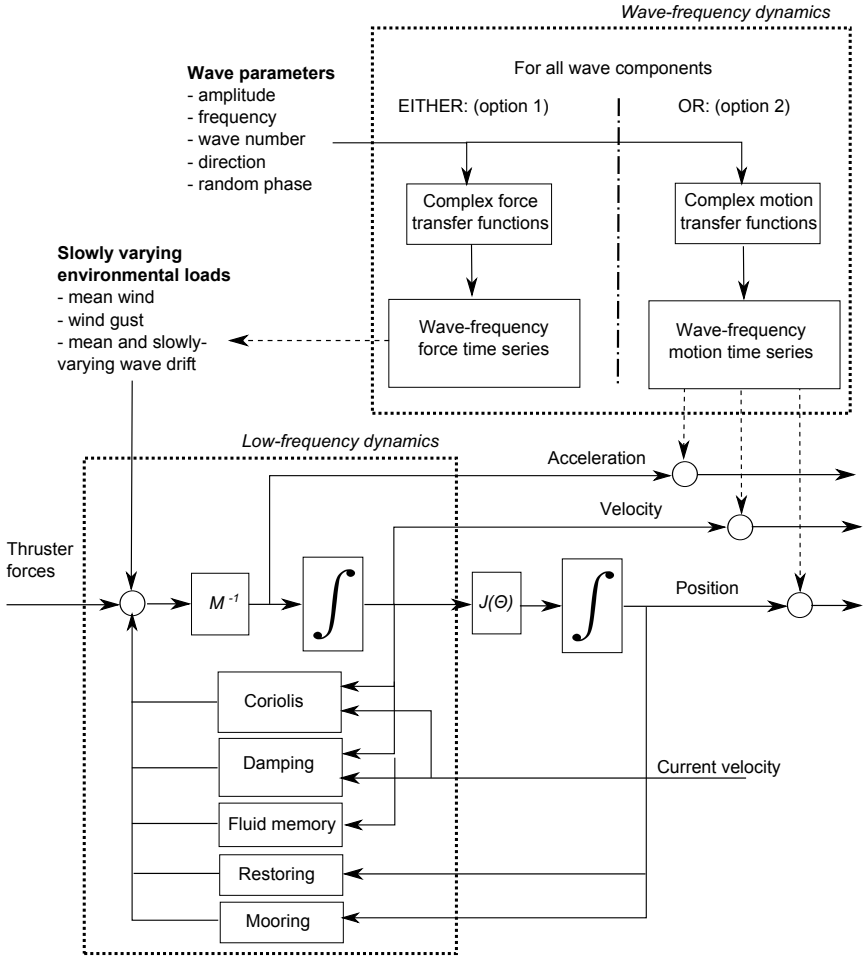

Figure 2.6: Illustration of the 6 DOF process plant model with low-frequency and wave-frequency dynamics. The wave-frequency vessel motion can be calculated in two different ways; by using the complex force transfer functions to get the first-order wave forces, or using complex motion transfer functions to get the wave-frequency motion directly. The rotation matrix $J(\Theta)$ is defined in (2.12).

thrust vector τ_{thr} acting on the vessel is the output from the control allocation, minus thruster losses due to thruster-hull and thruster-thruster interaction, cavitation, ventilation, amongst other effects.

The forces from the environment τ_{env} are from wind and waves, since the current effects are included in the relative velocity. The forces and moments from the wind on the topside (super structure) are modeled as

$$\tau_{wind} = \begin{cases} qC_i(\gamma)A_{p,i} & i = \{x, y, z\} \\ qC_i(\gamma)A_{p,i}l_i & i = \{\phi, \theta, \psi\}, \end{cases} \tag{2.14}$$

where $q = \frac{1}{2}\rho_a V^2$ is the dynamic pressure of the wind, ρ_a is the density of air, and V is the wind speed. C_i are drag coefficients as a function of the wind angle of attack γ relative to the bow, $A_{p,i}$ are projected areas, and l_i are the arms from the center of gravity to the center of the projected area.

Forces and moments from waves τ_w are usually divided into first-order wave-induced forces τ_{w1}, and second-order wave-induced forces τ_{w2}. Relating this the environment illustrated in Figure 2.1, τ_{w1} are due to wind-generated waves and swell, and τ_{w2} are due to mean and slowly-varying wave drift loads. By using the complex force transfer functions, τ_{w1} and τ_{w2} can be computed directly, and are added to the right-hand side of (2.13), as indicated by *option 1* in Figure 2.6. When using the complex motion transfer functions, the wave-frequency motion η_w is calculated directly, so that the total motion of the vessel is $\eta + \eta_w$, as indicated by *option 2* in Figure 2.6. The mean and slowly-varying wave drift loads are not included in the motion transfer functions, so τ_{w2} is calculated using force transfer functions, like before. See for instance Sørensen (2011) and Fossen (2011) for more details on the PPM.

2.2.3 Control Plant Model

The control plant model (CPM), also called the *control design model*, is a simplified vessel model describing only the main physics, see Figure 2.7 for an illustration. It is often the basis for model-based observer and controller design, including stability analysis, and therefore needs to be computationally efficient. The CPM contains a simplified low-frequency motion model based on the PPM, (2.13), a simplified wave-frequency motion model, a bias model for slowly-varying forces, and a coordinate transformation from the body to the NED frame. Depending on the vessel type, environmental conditions, speed ranges, and use modes, different physical effects matter, and hence the CPM takes various forms. For ships the model includes the horizontal plane motions surge, sway and yaw (see below), but for vessels with small waterplane areas, there is a larger coupling between the horizontal plane motions and the vertical plane motions heave, roll and pitch. Therefore for semi-submersibles the CPM includes surge, sway and yaw coupled with roll and pitch (Sørensen and Strand, 2000). ROVs usually have 4 DOF models where the motions in the horizontal plane in addition to heave are modeled, though sometimes pitch is also included.

The wave motion model allows the separation of the wave-frequency motion, due to first-order waves, from the low-frequency motion due to mean wind, current and second-order wave forces, similarly to *option 2* in Figure 2.6. Then the wave frequency motion of the vessel can be eliminated from the low-frequency position and velocity, which is called *wave filtering*, see Figure 2.8 for an illustration. When the wave filtered position and velocity are used in the control law, the commanded thrust will not oscillate with the zero mean wave-frequency motion, and hence the wear and tear on machinery and emissions can be reduced, compared to when using the total motion for control. When the sea state is extreme, some waves can be so long that the first-order wave periods are on the same time scale as swell, mean and slowly-varying wave drift, see Figure 2.1. Then a wave filter that eliminates the first-order wave motion will take away low-frequency components as well. Therefore

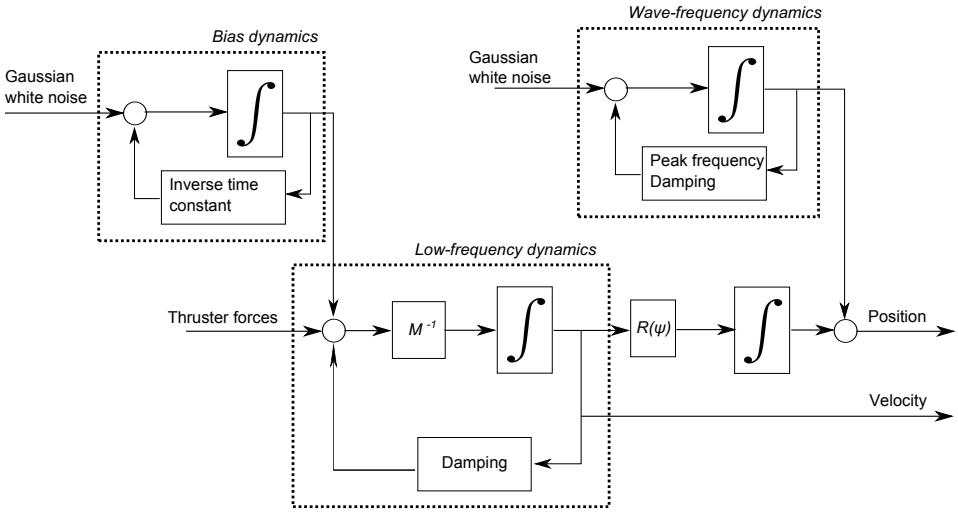

Figure 2.7: Illustration of a 3 DOF control plant model for a ship including low-frequency, wave-frequency and bias dynamics. Notice how the structure is similar to the process plant model in Figure 2.6. The rotation matrix about the (z)-axis is $R(\psi)$, given in (2.16).

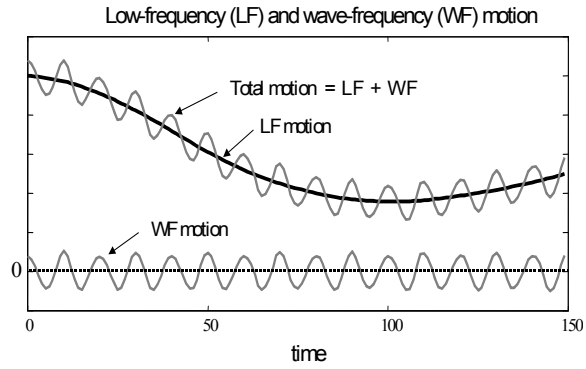

Figure 2.8: Total vessel motion is modeled as the sum of a low-frequency part and a wave-frequency part. Source: Sørensen (2013).

in extreme seas the wave motion model is eliminated so that the total vessel motion is modeled instead (Sørensen et al., 2002).

The bias model takes care of dynamics due to mean wind, current and second-order wave loads, that are slowly varying in the NED frame. However, forces acting from the environment on the vessel, especially for ship-shaped vessels are heading dependent, and therefore, the forces on the hull may change rapidly if the vessel changes heading fast. In such cases, capturing the vessel dynamics may be challeng-

ing. The bias model also captures dynamics that are not modeled in the simplified low-frequency motion model.

The CPM for a starboard-port symmetric ship in 3 DOFs is:

$$\dot{\xi} = A_\omega \xi + E_w w_w \tag{2.15a}$$
$$\dot{\eta} = R(\psi)\nu \tag{2.15b}$$
$$\dot{b} = -T_b^{-1} b + E_b w_b \tag{2.15c}$$
$$M\dot{\nu} = -D_L \nu + R^\top(\psi) b + \tau \tag{2.15d}$$
$$y = \eta + W\xi, \tag{2.15e}$$

where the states of the system are the wave states $\xi \in \mathbb{R}^6$, low-frequency 3 DOF position vector $\eta = [x, y, \psi]^\top$, low-frequency 3 DOF velocity vector $\nu = [u, v, r]^\top$, and the bias force vector $b \in \mathbb{R}^3$. Notice that η and ν include surge, sway and yaw here, as opposed to in Section 2.2.1, where they are 6 DOF. $R(\psi)$ is the rotation matrix about the (z)-axis, given by

$$R(\psi) = \begin{bmatrix} \cos(\psi) & -\sin(\psi) & 0 \\ \sin(\psi) & \cos(\psi) & 0 \\ 0 & 0 & 1 \end{bmatrix}. \tag{2.16}$$

The wave-induced yaw motions are typically less than 5° in extreme sea states (sea state codes 5-10), and less than 1° in normal sea states (sea state codes 1-5) (Fossen and Strand, 1999). Therefore it is often assumed that the wave-frequency yaw angle ψ_w is small, so that $R(\psi+\psi_w) \approx R(\psi)$. The low-frequency part of the vessel motion, is separated from the wave-frequency motion $\eta_w = W\xi$ with $W = [0_{3\times3},\ I_{3\times3}]$ in the measurement $y \in \mathbb{R}^3$. $\tau \in \mathbb{R}^3$ is the control input vector. $A_\omega \in \mathbb{R}^{6\times6}$ is a Hurwitz matrix including peak wave frequency and damping, $M = M^\top \in \mathbb{R}^{3\times3}$ is the inertia matrix including added mass, and $D_L \in \mathbb{R}^{3\times3}$ is the linear damping coefficient matrix including second-order wave-induced damping. $T_b \in \mathbb{R}^{3\times3}$ is a diagonal matrix of bias time constants, E_w, E_b are scaling matrices, and w_w, w_b are zero mean white noise. The bias dynamics (2.15c) accounts for *slowly-varying* environmental disturbances from mean wind, current, and second-order wave loads, as well as unmodeled vessel dynamics. For 3 DOF DP models this includes nonlinear damping, Coriolis, and possible coupling with the horizontal plane motions heave, roll, and pitch. See Sørensen (2011) for more on the CPM.

2.2.4 Kinematic Model

A different type of model that is not based on the PPM, is the kinematic model. It is a 6 DOF model relating the angular rates of the vessel to angles, and the acceleration of the vessel to velocity and position, see Figure 2.9 for an illustration. The kinematic model splits the vessel motion into an angular part and a translational part, and is essentially an expansion of the kinematic relation in (2.12). It is usually formulated in the ECEF frame, but for marine vessels with relatively low speed, the rotation of the Earth can be neglected, and the kinematic model can be

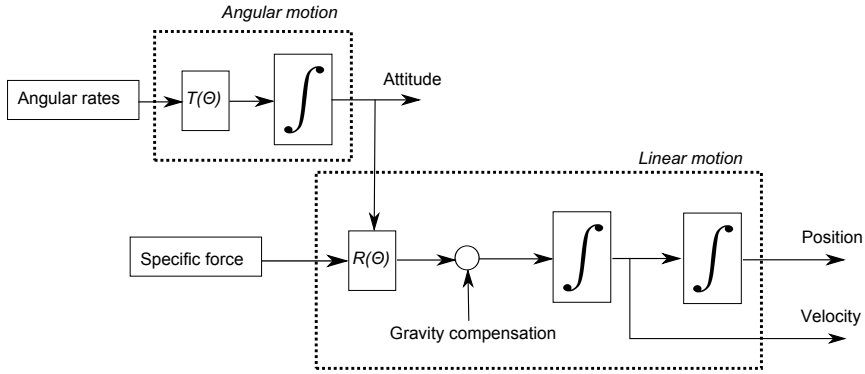

Figure 2.9: Kinematic model consisting of an angular part and a linear part. Angular rates are integrated to obtain the attitude, which are used to rotate the *specific force*, consisting of the linear acceleration of the vessel and acceleration due to gravity, into the ECEF frame. The acceleration due to gravity is constant in the ECEF frame, and therefore efficiently eliminated. The linear acceleration of the vessel is integrated to get velocity and position.

expressed in the NED frame. The equations may be written as

$$\dot{\Theta} = T(\Theta)\omega^b \tag{2.17a}$$

$$\dot{p}^n = v^n \tag{2.17b}$$

$$\dot{v}^n = R(\Theta)f^b + g^n, \tag{2.17c}$$

where the states are the Euler angles Θ, and the NED position and velocity (p^n, v^n) from (2.7). For control purposes we are also interested in the body-fixed velocity vector $v^b := R(\Theta)^\top v^n$. ω^b is the angular rate, and f^b is the specific force, i.e., the *measurable* acceleration including the linear acceleration of the vessel $\dot{v}^b$ and the acceleration due to gravity g^n, with units $[m/s^2]$.

An alternative formulation of the attitude dynamics (2.17a) is

$$\dot{R}(\Theta) = R(\Theta)S(\omega^b), \tag{2.18}$$

where the rotation matrix $R(\Theta)$ given in (2.9) is the state, with

$$S(\omega^b) := \begin{bmatrix} 0 & -r & q \\ r & 0 & -p \\ -q & p & 0 \end{bmatrix}, \quad \omega^b = [p, q, r]^\top. \tag{2.19}$$

For more details on the kinematic model, see for instance Bryne et al. (2017a).

Chapter 3

Hybrid Control of Marine Vessels

Up to now, models for the environment and vessel motions have been introduced, and it is evident that the vessel behavior is fundamentally dependent on the environmental conditions. It is time to look closer at the block diagram in Figure 1.1, which is closely linked to the vessel operational conditions *speed* and *use mode*. This chapter gives an overview of a hybrid marine control system structure, with performance monitoring and switching logic, and mentions previous work on observer, and controller algorithms, as well as applications of hybrid theory to marine systems. The hybrid framework applied in Papers D-F, J and K (Brodtkorb et al., 2014, 2015b, 2016a,b, 2017b) is introduced, some thoughts on the usability of the framework for marine control systems are given, and testing of complex control systems is discussed.

3.1 Vessel Operational Conditions

The use mode and vessel speed are changed by the operator, in order to safely and efficiently perform a set of operations, for instance ocean passage, confined water passage, ROV support, collision avoidance, fleet formation, helicopter landing, drilling, surveying, search and rescue, to name some. Each use mode requires algorithms that satisfy different *control objectives*, for instance stationkeeping (dynamic positioning of various precision, or thruster-assisted position mooring), coursekeeping, motion damping (wave-induced motion damping in roll and pitch, or surge-sway damping for moored vessels), maneuvering control, formation control, and speed control (Perez et al., 2006). Changes in the use mode bring changes in the number of DOFs that are needed to describe the vessel motion in the control plant model (Section 2.2.3). For instance heading control requires modeling of only sway and yaw, whereas drilling operations of a semi-submersible require modeling of surge, sway, and yaw in the horizontal plane, coupled with roll and pitch in the vertical plane. The speed changes hydrodynamic effects like wave-induced damping, viscous damping, and wave encounter frequency. For high-speed vessels lift effects are prominent, causing significant changes in the system restoring and dynamical behavior (Faltinsen, 2005). The environment acts as disturbances on the vessel, inducing undesired motion that reduces the passenger and crew comfort. The wind

often exerts large forces on the topside infrastructure, and waves make the vessel heave, roll and pitch so that the actuators (thrusters, rudders, fins) may exit the water and have reduced efficiency.

Finding one model that can cover all use modes, environmental conditions, vessel speed and loading conditions is difficult, since different physics are important. Therefore there are various control strategies that are suitable in different vessel operational conditions. In the industry switching using different ad-hoc methods for phasing in and out controllers have been used with success for many years. However, when increasing the number of system functions that switch automatically, it is of increasing importance to know that the dynamics triggered by a switch are well behaved. Hybrid systems frameworks can combine continuous-time dynamics with discrete-time logics into one system, and are suitable for describing marine vessel dynamics over all operational regimes with the related control algorithms. A hybrid control system that can evaluate different control strategies, and choose the best one on its own, will improve system reactivity, safety, and performance relative to having an operator change the use mode.

3.2 Control System Structure

The hybrid motion control system from Figure 1.1 is expanded in Figure 3.1 to show observer, controller, control allocation and thruster control candidates that are switched between automatically. The vessel is equipped with instrumentation, providing measurements, with different sampling rates, required for operation. The position reference system, for instance GNSS, hydroacoustic, laser, tautwire or riser angle measurement system, provides measurements of the vessel's position. Other common sensor systems include IMUs with gyros and accelerometers, for measuring angular rate and specific force, gyrocompass and/or magnetic compass for measuring heading, wind sensors, draft sensors, and sensors that are specific to the marine operation, like tension sensors for pipelay operations, or thruster-assisted position mooring. Actuators include propellers, rudders, stabilizing fins, and rotatable thrusters. Each component of the motion control system in Figure 3.1 is described below (Sørensen, 2005, 2011).

- The signal processing software checks the measurement signals for errors and rejects bad signals. It usually includes wildpoint, signal freeze and high variance detection. In most marine motion control systems redundant sensor measurements are weighted or voted.
- Observers, also called state estimators, estimate unmeasured system states, filter out noise and wave-frequency motion, and in the case of signal loss, predict the vessel states, often referred to as dead reckoning. There are different observers amongst the *candidate observers* that have their areas of expertise.
- The guidance system provides smooth references to the controller based on the position of the vessel, waypoints and weather data provided by the operator.
- The controller commands desired generalized forces in surge, sway, and yaw in order to satisfy the control objective, for instance stationkeeping, path following, or maneuvering. The control law usually consists of a feedback part

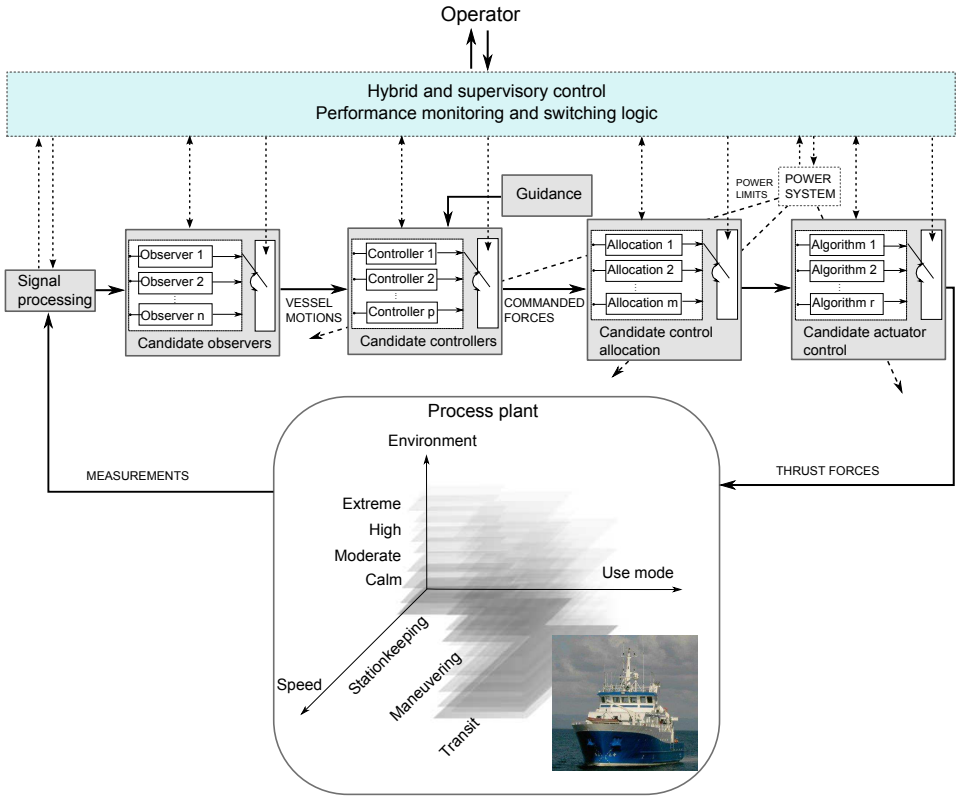

Figure 3.1: Hybrid control system for marine vessels, details. The ship is R/V Gunnerus.

using position and velocity estimates from the observer, and a feedforward part consisting of mean wind forces and reference. There are different controllers amongst the *candidate controllers* for different speed ranges and that satisfy different control objectives.

- The control allocation system takes the commanded forces and moment from the controller, and calculates the desired force and direction for each actuator. Thrusters that can be rotated, called azimuthing thrusters, are commonly used on DP vessels, and the thrust allocation needs to take into account forbidden directional sectors. Optimization based on fuel consumption is also common.
- Local actuator control algorithms control the actuators according to the set-points from the thrust allocation system. Smogeli (2006) proposes thruster control strategies and control allocation for changing operational conditions, featuring *anti-spin* and power/torque control for extreme conditions (Smogeli and Sørensen, 2009; Sørensen and Smogeli, 2009).
- The power system is not a direct part of the motion control system, however power limits are sent to the controllers, thrust allocation system, and local

actuator control in order to prevent a system blackout, as this is one of the most severe failure modes for marine vessels.

- The performance monitoring monitors the performance of the different blocks, and the switching logic chooses which algorithms to use in closed-loop control from the candidates. When necessary the parameters in the different algorithms are altered according to the vessel operational conditions. Relevant information and alarms are sent to the operator, and input from the operator is inserted where needed. Transitions between the different use modes and speed ranges are handled automatically in this block.
- The operator has screens monitoring the system performance, either onboard or remotely. Performance monitoring functions alert the operator by raising alarms and warnings, and provide decision support.

As indicated in Figure 3.1, all the software blocks may have different algorithms to choose from, although only observer and control algorithms are considered in this work. In Section 3.2.1 the *performance monitoring and switching logic* block is discussed further, in Section 3.2.2 relevant literature for observer and control algorithms are given, and in Section 3.2.3 applications of hybrid theory to control of marine vessels are elaborated.

3.2.1 Performance Monitoring and Switching Logic

In order for a hybrid control system to be reliable, good switching criteria that are robust to measurement noise and system errors need to be established for the vessel speed, use modes, and environmental conditions. Figure 3.2 illustrates parts of the functionality that can be found within the performance monitoring and switching block in a hybrid control system. Firstly, the performance monitoring detects and diagnoses, and secondly the switching logic reconfigures the blocks in the hybrid control system, in a similar way to fault-tolerant control (Blanke et al., 2003).

The main tasks of the performance monitoring functions are to decide which of the candidate algorithms to use in closed loop, detect faults, and alert the operator of these, and provide decision support for the operator, in case the system needs human interaction. The performance monitoring takes input from the operator, references, operating conditions, measured position, estimated position, control input, line tension, risk management system, measured wind speed, and more, depending on the operation taking place. Different norms of the inputs can be used as performance measures, for instance the Euclidian norm, p-norm and infinity norm (Desoer and Vidyasagar, 1975). Often, several different parameters need to be considered in order to get a good picture of the overall performance, and here the norms of different inputs may be combined in cost functions. For instance, performance metrics (Rabanal et al., 2016) like the integral of the absolute error over a time window, or combined positioning error and thrust usage, that are commonly used for comparing observer/controller performance in simulations may also be useful in online applications. In some cases the inputs to the performance monitoring functions have large oscillations, due to wave-induced motion or noise. In these cases, averaging the cost functions over a short time may be useful in order to prevent unnecessary switching. Which variables to include, and how to

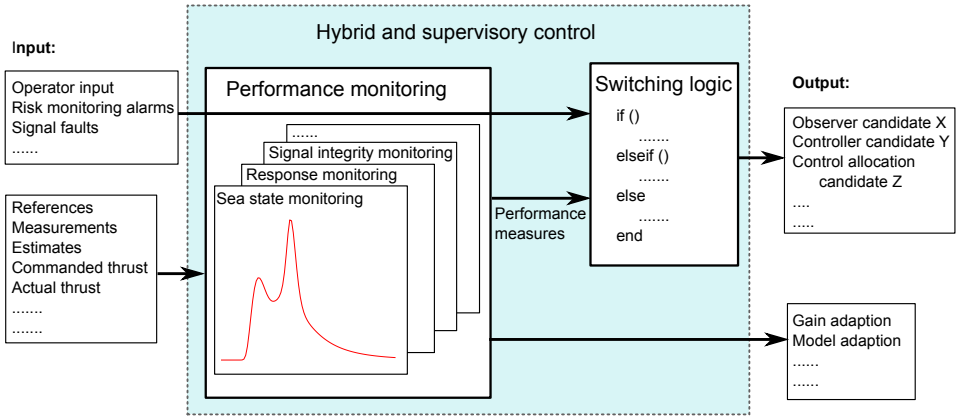

Figure 3.2: Illustration of performance monitoring and switching logic setup. As indicated by the layers in the performance monitoring, there are various functions that monitor different aspects of the vessel performance. Certain inputs, like signal faults, some operator inputs and risk management alarms, will override performance monitoring functions. Based on performance measures, the switching logic chooses algorithms from the candidates to use in closed-loop control.

weight them depends on the operational condition, and as the layers in Figure 3.2 indicate, there are various functions for monitoring different operational aspects. Sea state estimation algorithms like presented in Brodtkorb et al. (2015a, 2017a) and Nielsen et al. (2017b) (Papers A-C) are examples of environmental monitoring functions, and response prediction (Nielsen et al., 2017a) may be another useful monitoring function. Some inputs, like alarms from the risk management software, certain operator inputs, and signal faults, will override performance monitoring.

Fault handling of measurement signals is taken care of by the signal processing software. The performance monitoring can further detect faults due to modeling, implementation, and software/hardware integration errors, by comparing outputs from multiple sources that have different inputs and/or structures in a signal integrity monitoring function. Knowing that measurement signals may fail and remain undetected, it is important to have redundancy in performance measures, and have safe-modes available.

The task of the switching logic is to ensure safe switching to the candidate algorithms indicated by the performance measures. A switch, here also referred to as a *jump*, induces a transient in the continuous-time system, which introduces additional dynamics that are not encountered in purely continuous-time systems. Therefore analyzing the hybrid system behavior is important. A scenario that may occur is that the hybrid system is not allowed enough time to come to steady state after a jump, so that new jumps are triggered based on the transient system behavior. This may lead to instability induced by switching. Another common phenomenon that may occur in systems that switch automatically, is rapid switching back and forth, called chattering. In order to avoid such scenarios, explicit constraints on switching may be achieved through hybrid stability analysis.

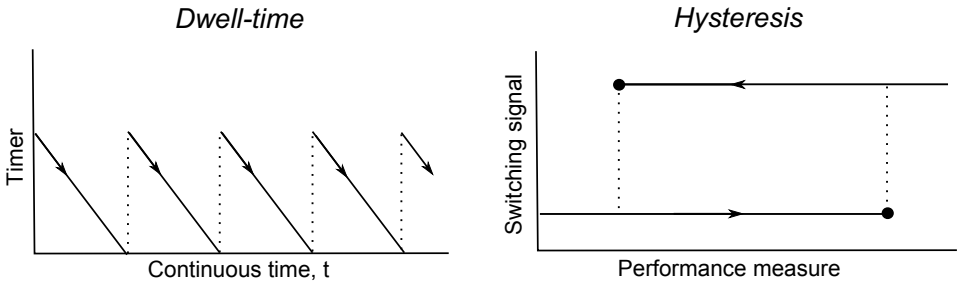

Figure 3.3: Illustration of dwell-time and hysteresis switching constraints, which commonly are included in switching logic. The timer dynamics to the left only allows periodic switches each time the timer reaches zero. The hysteresis on the right switches based on the history of the system state, or performance measure. A jump is indicated by the dotted lines.

Constraining switches can be done though switching logic based on time, such as dwell-time or average dwell-time dynamics, or based on the system variables, such as hysteresis (Hespanha et al., 2003; Hespanha and Morse, 2002). Figure 3.3 shows examples of both dwell-time and hysteresis switching constraints. During dwell-time or average dwell-time switching a timer keeps track of the time from the last switch, and does not allow a new switch until a certain time has passed. Hysteresis switching is based on the history of the variables, allowing switching only if the variable crosses a boundary with a certain direction of change. In many cases it is possible to implement both types of switching logic, however the choice should complement the system dynamics as much as possible.

3.2.2 Observer and Control Algorithms for Different Vessel Operational Conditions

Observers may be grouped into two main categories based on their structure; the *model-based observer* is based on the control plant model, and the *signal-based observer* is based on the kinematic model, see Sections 2.2.3 and 2.2.4, respectively. Model-based observers like the Kalman filter (Fossen and Perez, 2009), or the nonlinear passive observer (NPO) (Fossen and Strand, 1999) are commonly used for state estimation onboard marine vessels. Two features of this observer type is the ability to separate the wave-frequency motion from the low-frequency motion, called wave filtering (see Figure 2.8), and in the case of signal loss predict the states of the system. Model-based observers are tailored to a specific operational speed range; DP, maneuvering, or transit, and for DP observers, capturing the vessel dynamics correctly during transients is typically a challenge due to the slowly-varying nature of the bias force dynamics, see for instance Værnø et al. (2017) (Paper H).

Observers based on the kinematic model are often called signal-based, sensor-based, or kinematic observers. The observer is more sensitive to signal failure than the model-based, but has good performance during transients. The kinematic ob-

server consists of an attitude observer, combined with a translational motion observer into one GNSS and INS (inertial navigation system) integration, see for instance Farrell et al. (2000), Vik and Fossen (2001), Mahony et al. (2008), Grip et al. (2013), and Grip et al. (2015). The observer from Grip et al. (2013) is applied to DP in Bryne et al. (2014), where time-varying gains are introduced. Bryne et al. (2015) introduces a virtual vertical reference in order to improve the down estimates, and Bryne et al. (2017b) adds a wave filter. When measurements from different sensors are combined and compared; commonly called sensor fusion, faulty sensors can be isolated so that higher accuracy measurements are obtained, see for instance Blanke (2006). GNSS and INS integration is one type of sensor fusion.

When designing observers and controllers for marine vessels, the separation principle is often used, which allows design of the observer and the controller independently (Loria et al., 2000). Then the observer dynamics should converge faster than the controlled system dynamics, so that the estimates available to the feedback controller are reasonably accurate (Oppenheim and Verghese, 2010). Åstrøm and Wittenmark (1997) recommends observer dynamics that are 2-10 times faster than the system under state feedback control, depending on the desired dynamics, measurement signal noise ratio, and process disturbances.

As mentioned, there are different control strategies for different types of control objectives and environmental conditions, some of which are referenced here. Marine controllers usually consist of feedback of measured or estimated system states, and the control strategies differ in the way that the feedback terms are calculated. For surface vessels, the wind forces are often large, and therefore the forces and moments due to the wind are predicted, and used in *feedforward* control. For vessels on thruster-assisted position mooring, the mooring force may be fed forward (Strand et al., 1998), and for DP operations in ice, feedforward of acceleration measurements may be beneficial (Kjerstad and Skjetne, 2016) for highly reactive control.

Starting with DP at the lower speed regime, usually between $0-2$ m/s. A typical DP system is evaluated through numerical studies and model-scale experiments in Tannuri and Morishita (2006). Lindegaard (2003) investigates the use of acceleration feedback in DP, Rabanal et al. (2016) compares two control strategies for DP in a harsh sea state, Værnø et al. (2017, 2016) (Papers G and H) looks at improving the transient response of a surface vessel in DP using time-varying model-based observers and a bias rejection scheme, and Hassani et al. (2017) presents a robust DP control strategy using mixed-μ synthesis. Typically *fault tolerance* and *robustness* are system design properties that are sought after (Blanke et al., 2003). When increasing the vessel speed into the maneuvering regime, different dynamics occur. In DP, the vessel is usually over-actuated, implying that the surge, sway and yaw motion can be controlled individually, but when the vessel speed increases, thrusters in the bow region are not efficient anymore due to deflection of the propeller wake, which makes the vessel under-actuated. There is more coupling between sway and yaw during maneuvering both due to hydrodynamics, and fewer efficient actuators, and the nonlinear damping dominates the linear damping, see Skjetne (2005). Maneuvering is also usual in confined waters, where the finite water depth may influence the hydrodynamic parameters. Sometimes operations require collaboration between multiple vessels, above the sea surface or below, in order to satisfy a

control objective. Then, controlling the position of the vessels with respect to each other, called formation control (Ihle et al., 2005), may be of importance. Formation control can also be done while following a specified path (Xidias et al., 2017). Path following control, where the vessel (or vessels) follows a specified path is common for all speed ranges (Belleter et al., 2016; Skjetne et al., 2011).

3.2.3 Applications of Hybrid Theory to Marine Control

The interest for applying hybrid systems theory to the marine area began about 10-15 years ago. A large inspiration for this work is taken from Sørensen et al. (2002), Nguyen et al. (2004), Sørensen et al. (2004), and Nguyen (2006). In the three latter, the hybrid framework of Hespanha and Morse (2002) was used to design hybrid controllers for changing environmental conditions (Nguyen et al., 2007), and for switching automatically between controllers for different speed ranges (Nguyen et al., 2008). In a similar manner as Nguyen et al. (2007), Brodtkorb et al. (2014) (Paper D) proposes a controller for changing environmental conditions, by using the hybrid framework in Goebel et al. (2012) for modeling and analyzing stability.

In Section 3.2.2, several non-hybrid reactive control strategies were mentioned, which can be added amongst the candidate algorithms of a hybrid control system. Some hybrid algorithms that quickly can detect and correct for a disturbance after it is encountered, include resetting strategies (Kjerstad, 2016; Tutturen and Skjetne, 2015), jumping between estimates from different observer types based on performance (Brodtkorb et al., 2016b, 2017b) (Papers E and F), and hybrid signal-based observers (Brodtkorb et al., 2015b, 2016a) (Papers J and K). Supervisory control for thrust allocation was investigated by Ruth (2008), and a slightly different application area for hybrid systems is control of top-tensioned risers (Rustad, 2007).

A reactive control system requires that the power system can deliver a lot of power over a short time frame, and that the thruster system dynamics are fast. Batteries are one type of responsive power source that can support reactive control strategies, by combining them with conventional diesel engines connected to a generator, like presented in Miyazaki et al. (2016). This makes the power generation and thruster system more decoupled, giving better working conditions for both systems. This strategy is also in line with the International Maritime Organization (IMO) emission regulations (IMO, 2011), which encourages the design of new power system solutions.

3.3 Hybrid Dynamical Systems Framework

The hybrid framework applied in this work is called *hybrid dynamical systems*, and is presented in the book by Goebel et al. (2012). The book unifies some of the key developments for hybrid dynamical systems, and introduces the necessary tools for understanding the stability of these systems. The modeling, stability and robustness results are extensions of nonlinear systems theory (Khalil, 2002) to include discrete dynamics and the interconnection of discrete and continuous dynamics into

one system. In general, the hybrid system $\mathcal{H} = (C, F, D, G)$ is written formally as

$$x \in C \quad \dot{x} \in F(x) \tag{3.1a}$$

$$x \in D \quad x^+ \in G(x), \tag{3.1b}$$

where the hybrid state x evolves in continuous time according to the differential inclusion $\dot{x} \in F(x)$ when $x \in C$, and when $x \in D$ the state is allowed to change instantaneously according to the difference inclusion $x^+ \in G(x)$. x^+ represents the value of x after an instantaneous change. Changes that occur according to the differential inclusion are called *flows*, and changes that occur according to the difference inclusion are called *jumps*, and hence C is called the flow set, F is the flow map, D is the jump set, and G is the jump map. The hybrid state can contain a mix of states that change only during continuous time, logic variables, timers, and variables that change both during continuous and discrete time.

Differential and difference inclusions like $\dot{x} \in F(x)$ and $x^+ \in G(x)$ are generalizations of differential and difference equations, like $\dot{x} = f(x)$ and $x^+ = g(x)$. The *set-valued mappings* $F : \mathbb{R}^n \rightrightarrows \mathbb{R}^n$ and $G : \mathbb{R}^n \rightrightarrows \mathbb{R}^n$ relate the input x to one, *or more*, outputs (hence the double arrow), see Figure 3.4 for an illustration. This implies that $F(x)$ and $G(x)$ are *sets* rather than single points. See Rockafellar and Wets (1998) for more on set analysis.

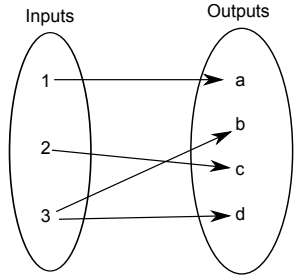

Figure 3.4: Example of a set-valued mapping. Notice that one input can be mapped to multiple outputs.

A solution $\phi(t, j)$ to a hybrid system $\mathcal{H}$, called a *hybrid arc*, is parametrized by continuous time $t \in \mathbb{R}_{\geq 0}$ and discrete time $j \in \mathbb{N}$, and the solution evolves in dom $\phi \subset \mathbb{R}_{\geq 0} \times \mathbb{N}$, called a *hybrid time domain*. A solution can be classified based on the structure of its domain, for instance if dom $\phi \subset \{0\} \times \mathbb{N}$, the solution is *discrete*, and if dom $\phi \subset \mathbb{R}_{\geq 0} \times \{0\}$, the solution is *continuous*. For more on the solution concept, see Appendix A.1 and Goebel et al. (2012), Chapter 2.

For control purposes, analyzing the stability properties of the equilibrium point(s) of a system is desired. For a hybrid system the equilibrium is a set, usually denoted $\mathcal{A}$. Stability analysis provides qualitative information about the solutions to the system, and their long term trends. A useful mathematical property of systems is *well-posedness*, which usually implies that a solution exits, is unique, and that the solution has a reasonable dependence on the initial condition (Hadamard, 1902). A well-posed hybrid system has good robustness properties, and numerous stability

tools may be applied[1]. The systems considered in this thesis are well-posed. Formally, a hybrid system $\mathcal{H} = (C, F, D, G)$ is well-posed if the system satisfies the hybrid basic assumptions.

Assumption 3.1. *Hybrid basic assumptions (Goebel et al., 2012, Assumption 6.5)*

(A1) C and D are closed subsets of $\mathbb{R}^n$;

(A2) The set-valued mapping $F : \mathbb{R}^n \rightrightarrows \mathbb{R}^n$ is outer semi-continuous (OSC) and locally bounded relative to C, $C \subset$ dom F, and $F(x)$ is convex for every $x \in C$;

(A3) The set-valued mapping $G : \mathbb{R}^n \rightrightarrows \mathbb{R}^n$ is OSC and locally bounded relative to D, and $D \subset$ dom G.

A set-valued mapping $H : \mathbb{R}^n \rightrightarrows \mathbb{R}^n$ is OSC if for each convergent sequence $\{(x_i, y_i)\}_{i=1}^{\infty}$ that satisfies $y_i \in H(x_i), \forall i \geq 1$ and the limit denoted (x, y) satisfies $y \in H(x)$ (Goebel et al., 2012, Def. 5.9). If $F : C \to \mathbb{R}^n$ is continuous and C is closed, then F is OSC, or more generally if the graph of a mapping is closed, then the mapping is also OSC.

The main references used for modeling and stability of hybrid systems are, in addition to Goebel et al. (2012); Goebel et al. (2009) for cascaded hybrid systems, Cai and Teel (2009) for input-to-state stability for hybrid systems, and Teel (2013) for hybrid systems with noise entering in the jump map. Appendix A gives an overview over definitions, stability results, and theorems, which may be useful when reading Papers D-F, J and K.

3.4 Discussion of the Hybrid Systems Framework

This section discusses the applicability of hybrid systems frameworks, in particular Goebel et al. (2012), to marine control systems. Table 3.1 summarizes some of the main points of the section.

3.4.1 Modeling and Stability

The main strength of the framework in Goebel et al. (2012) is that it can model many different types of systems; systems with impacts, sampling of continuous-time systems, resetting dynamics, and control of continuous-time systems where the dynamics vary a lot, to name a few. The control system designer has the freedom to include many specialized control schemes into observer, controller, control allocation and thruster control algorithm candidates, in order to manipulate the various vessel dynamics during changing vessel operational conditions. The inclusion of jump dynamics, such as controller logics, into the analysis of any system,

[1] In some cases, there are reasons to consider hybrid systems that are not well-posed, i.e., systems that do not have solutions from some initial conditions, or systems with non-unique solutions (Goebel et al., 2009, pp. 44-47). For instance, for certain classes of switching systems where the flow dynamics are described by set-valued mappings, or systems where the flow and jump sets overlap, the solutions may be non-unique. Stability analysis tools that do not require the hybrid system to be well-posed can be found in Goebel et al. (2012), Chapter 3. A key result from there is stated in Appendix A.2.

inevitably makes it more complex to accurately model the hybrid system for stability analysis. However, when the complexity of a system increases, it is of even greater importance to know that the dynamics are well behaved.

When formulating the hybrid system, it is convenient to have a well-posed system, satisfying the hybrid basic assumptions (Assumption 3.1), which in turn makes achieving stability much less complicated. However, sometimes formulating the system dynamics according to Assumption 3.1 is not straightforward. Stability builds on stability results for sets and nonlinear systems, which makes it convenient to combine existing nonlinear observers and controllers with logics and analyze the hybrid system properties. In many cases one may already know a Lyapunov function candidate for the continuous-time system, and this is a good start to hybrid stability analysis using Lyapunov functions. Many of the classical control design and analysis tools like Lyapunov analysis, invariance principles, robustness, input-to-state stability, and cascaded systems, have been extended to hybrid systems. The modeling frameworks, Goebel et al. (2012) and also others, for deterministic hybrid systems (without noise) are mature. There are a significant number of users of the different hybrid frameworks, though not as many as for nonlinear control theory, for instance. The research interest in the last years has shifted focus to stochastic hybrid systems Hespanha (2005), Teel (2013), and Teel et al. (2014), and this framework is still under development.

Table 3.1: Summary of the discussion regarding applicability of the hybrid systems framework Goebel et al. (2012) to control of marine vessels.

Issue	Summary
Versatility	The framework can model a wide variety of systems with a mixture of continuous and discrete dynamics.
Model complexity	The inclusion of continuous-time and discrete-time dynamics into one system, inevitably increases the model complexity compared to purely continuous-time or discrete-time systems, however choosing the modeling fidelity is to a large extent up to the system designer.
Stability tools	Stability analysis tools are based on nonlinear systems and set mathematics, and many classical stability analysis tools have been extended to hybrid systems.
Maturity	Deterministic hybrid systems frameworks are highly mature, and stochastic hybrid systems theory is under development.
Modularity	The framework promotes modularity in the way the flow and jump maps are defined.
Scalability	Other hybrid systems frameworks may be better suited for large systems, like hierarchical hybrid systems or networked systems.
Autonomy	Hybrid systems frameworks may be a core design and stability analysis tool for marine control systems with high levels of autonomy, in order to guarantee that the control objective is satisfied.

3.4.2 Modularity and Scalability

The framework in Goebel et al. (2012) is powerful for analyzing parts of a marine control system, like an observer, a controller, an output feedback controller, or switching based on a sea state estimate, as done in this work. The inclusion of all components of a marine control system in one large analysis with the same modeling fidelity as considered in this work, is a daunting task. However, as in classical control theory like linear or nonlinear control, the fidelity of the hybrid system model also dictates the complexity of the analysis. For instance, if a system is made up of several modules that have known stability properties, the modules may be simplified in order to analyze the interconnections between the modules. It is important to keep in mind that stability analysis for most systems is usually performed on highly simplified system dynamics, like a control plant model, and as a result, the stability properties are dependent on the validity of the model. If the model does not capture important dynamics of the system, whether a continuous, discrete or hybrid system model is used, the stability properties may not hold in practice.

There are many frameworks that describe hybrid systems. Some are more specialized to a specific system type than others; from local switching control systems (Hespanha and Morse, 2002) to modeling and control of large-scale hybrid systems (Lygeros, 1996). The framework in Goebel et al. (2012) is broad, and covers a wide selection of systems, though for large-scale hybrid systems, like networked systems, other frameworks may be more suited. Lygeros (1996) uses a hybrid dynamical systems formulation, called hierarchical hybrid systems that can be used to model large-scale systems in a modular fashion. A modular control system design will make it easier to get a sufficiently redundant and robust system design that is much simpler to test. Section 3.5 goes more into details of control system testing. For many large hybrid, or networked, systems, the components may be analyzed by using traditional theoretical approaches, like linear, nonlinear, and adaptive approaches, but the interconnections and components as a whole is beyond the reach of these methods. Arcak et al. (2016) propose a way of certifying network properties of subsystems of managable sizes, and combining simple models of the subsystems based on dissipativity, to formulate network level performance and safety guarantees in a compositional fashion.

3.4.3 Hybrid Systems and Autonomy

Higher levels of autonomy in the next generation marine control systems may lead to smarter and more efficient operations in the future. Control systems today have certain functionality that can be characterized as autonomous, from low-level performance switching control, to automatic navigation with collision avoidance schemes, and online risk monitoring. Collision avoidance algorithms identify objects, and plan a new route in order to avoid collision in accordance with marine traffic rules (COLREG, 1972). Generally the components, or modules, of a fully autonomous control system already exist, thus it is the combination of these modules into a safe and reliable system that is the challenge. The risk of a certain module may be known, but the interactions between these risks and other types

of risk, could cause unexpected nonlinear and stochastic behavior. Since there is little operational experience from autonomous operations, it is difficult to model risk for these types of operations, and this poses challenges related to verification of safe performance (Utne et al., 2017).

The autonomous system must be able to determine if it can continue with possible degraded performance by detecting, isolating and handling failures and faults. Performance monitoring and switching logic is an integral part of this, and therefore, hybrid systems theory may become a core design and stability analysis tool for marine control systems with higher levels of autonomy.

3.5 Control System Testing

The motion control system is a complex system with many components. Therefore, there are strict marine industry standards focusing on the system design and testing, both hardware and software, failure mode and effect analysis (FMEA), necessary equipment, operating requirements and documentation (Sørensen, 2013). The aim is to reduce the risk to personnel, the vessel itself, other vessels and structures, subsea equipment, and the environment. The DP system has especially strict class rules, since DP vessels usually operate in close proximity to other infrastructures, see for instance DNV-GL (2017).

Two commonly used software testing methods are software-in-the-loop (SiL) and hardware-in-the-loop (HiL) testing. The SiL testing simulator is based upon the PPM (2.13), a high-fidelity model reconstructing the physical properties of the marine system, so that control algorithms can be tested thoroughly in different environmental conditions. Different failure scenarios can be simulated, for instance; power loss, thruster failure, drive-off, drift-off (signal failure), and a combination of the above. SiL testing can be done in accelerated time, so extensive testing does not take as much time. In HiL testing, the hardware is connected to a high-fidelity simulator that contains models of the vessel motion, thrusters, power generation and distribution, main consumers, sensor system, and position reference system. The HiL simulator is vessel specific and runs in real-time. This enables systematic and comprehensive testing of control system functionality and failure handling without risk to people, equipment, or the environment (Piviano et al., 2015; Skjetne and Egeland, 2006; Smogeli et al., 2014).

Testing and verification of semi- and fully autonomous systems pose a challenge. As mentioned in Section 3.4.2, autonomous marine control systems should have modular designs, so that certification of the system can be done in two steps (Kapinski et al., 2016). First, verification of the modules should be done so that each module has a formal proof of correctness, e.g., stability analysis, for a large set of parameters and inputs. Here, the focus can be on designing control algorithms so that high-level requirements are met, since it is easier to debug and repair code at this point. Classical control theory, like linear, nonlinear, or robust system theory, can be used, as well as hybrid systems theory to provide formal stability proofs for the different system modules. Thereafter, the interconnection between the modules can be checked through extensive simulations. At this time, the focus can be on control implementations, real-time requirements, and the software platform that

Figure 3.5: Model ships, to the left Cybership 3, to the right C/S Inocean Cat 1 Drillship.

physically and functionally interconnects the different modules. Informal stability and performance bounds may be found through simulations, that stress the interconnections between stable modules.

Observer and control algorithms developed in this work have been tested through theoretical analysis, simulations, model-scale experiments, on full-scale field data, and in full-scale experiments. The initial algorithms were developed on paper, using theory to evaluate if the idea was worth pursuing, or if it needed adjustments. The design was implemented in the Matlab/Simulink simulation model Marine Cybernetics Simulator (MCSim) (Sørensen et al., 2003), closely related to the open source MSS Toolbox (Fossen and Perez, 2004). MCSim is a simulation model containing the vessel motion model (2.13) with simplified thruster dynamics, and an environment consisting of wind, waves and current that can change with time. When the algorithm design worked satisfactory in simple simulations, the concept was tested thoroughly in different conditions in simulations, so that bugs were found and fixed before moving on to model-scale experiments in the Marine Cybernetics Laboratory (MCLab). Testing of signal freeze detection was done, but persistent failure mode testing as in SiL was not performed.

The MCLab is a laboratory with a basin equipped with a towing carrige, a wavemaker, and camera positioning systems for over and under water applications. Control systems can be tested on model-scale vessels, see Figure 3.5 where Cybership 3 and C/S Inocean Cat 1 Drillship are depicted. An initial tuning for the observers tested in the lab was found by tuning on experimental data, and the observers were implemented and tuned on the vessel before enabling the thrusters. Safety functions in the lab included emergency disabling of the thrusters and wave flap. Appendix B.1 gives more information about Cybership 3, which was used in multiple experiments. The model C/S Inocean Cat 1 Drillship was used in Brodtkorb et al. (2017b) (Paper F), see Bjørnø (2016) for more details.

In order to validate several DP control algorithms in a realistic environment, the full-scale DP test campaign, AMOS DP Research Cruise 2016 (ADPRC'16) was conducted, see Skjetne et al. (2017) (Paper I). This was a collaboration between

the company Kongsberg Maritime[2] and researchers at the NTNU AMOS. Four researchers coded their algorithms into a test interface in the Kongsberg Maritime DP system of the NTNU-owned and operated R/V Gunnerus. Each code module was first tested for bugs by making sure the inputs and outputs to the functions corresponded, and that the code did as expected when experiencing common failures like signal freeze. Before running the algorithms on the ship itself, they were tested on a sophisticated model of R/V Gunnerus provided by Kongsberg Maritime. Appendix B.2 provides an overview of the main parameters of R/V Gunnerus.

[2] www.km.kongsberg.com

Chapter 4

Conclusions and Further Work

A hybrid control concept for marine vessels was proposed, and some possible strategies for improving the vessel performance in varying conditions was investigated. The research questions guiding this work have been:

1. How can the sea state be characterized and monitored in order to improve operational availability and safety?
2. How can the operational window of a marine control system, subject to a varying sea state, be increased by automatic switching from a bank of observers and controllers based on performance monitoring of the system states and algorithms?
3. How can a theoretical control concept using a hybrid systems framework be developed in order to support 1 and 2?

4.1 Concluding Remarks

Through the course of this work, it was found that hybrid systems theory is a suitable approach for designing marine control systems with higher levels of autonomy for varying vessel operational conditions. Performance monitoring functions for the vessel operational conditions were designed for transient response detection and sea state estimation. The vessel speed, loading condition and use mode were straightforward criteria to base switching upon, and it was shown that the sea state can be estimated with reasonable accuracy. For applications with strict requirements on the redundancy, like high risk operations, care should be taken to implement redundancy in the switching methodology and performance monitoring as well.

From a marine control perspective, the main strength of the framework in Goebel et al. (2012) is that it can model a wide range of systems, including sampling, and control of continuous-time systems where the dynamics vary a lot; noting that variation in the dynamics is a typical feature of many marine applications. Stability builds on stability results for nonlinear systems, so therefore it is convenient to combine existing nonlinear observers and controllers with logics, and analyze the hybrid system properties. The framework is powerful for analyzing parts of a marine control system, like an observer, a controller, an output feedback controller, or switching based on a sea state estimate, as done in this work. The

inclusion of all components of a marine control system in one large analysis with the same modeling fidelity as included in this work, is a daunting task, however, the fidelity of the hybrid system model dictates the complexity of the analysis. In the following, specific conclusions to the present work's three main topics; characterization and monitoring of the environment, improving transient vessel response, and sensor fusion of measurements with different fidelities, are given.

In Paper A, it was found based on model-scale data gathered on Cybership 3 in the MCLab, that the heave and pitch peak frequency followed the peak frequency of the sea state to a larger extent than what the roll peak frequency did. This can be explained by the ship roll motion transfer function shape, where the peak is fairly narrow around the roll natural frequency. The algorithm was later implemented on Cybership 3 and on C/S Incoean Cat 1 Drillship and has provided good operator support, but since the wave flap in the MCLab did not allow for changing sea states, the algorithm has not been tested in closed-loop experiments. An earlier version of the peak frequency estimation method presented in Paper A was run in simulations of a vessel in a sea state that was changing with time (Paper D). The algorithm worked well for tracking the peak frequency of the sea state, and successfully triggered switches in the hybrid controller. The results in Paper D clearly showed the stability problem encountered with the wave filter if used in extreme sea states, and the advantage of using a peak frequency estimation algorithm to switch off the wave filter in extreme sea states.

An efficient and reliable method for estimating the sea state, consisting of the wave spectrum and main direction, was presented in Paper B. The wave spectrum was estimated by solving a set of linear equations through iteration, based on the heave, roll and pitch response of R/V Gunnerus in DP. Paper C generalized the method from Paper B to include short-crested wave conditions, and to also include forward speed. The estimation results were reasonably accurate compared to wave measurements from a wave buoy, generally the significant wave height was estimated within 5% and peak period was estimated within 7%. Moreover, the algorithm presented in Papers B and C calculates the estimation results in just a few seconds, whereas established approaches, like Bayesian modeling and parametric optimization, use minutes to calculate the estimate. This is promising for online applications, for instance in a performance monitoring function for a hybrid controller.

Papers E-H were targeted towards improving the transient response of a vessel in DP during operations with heading and setpoint changes using reactive control strategies. Two approaches were suggested for solving this problem. The method in Papers E and F proposed to switch between a signal-based observer and a model-based observer based on a performance monitoring function detecting transients. This method had redundancy in the software design methodology, so that the two estimates could be used to check for signal faults and implementation errors. Papers G and H proposed a model-based observer with time-varying gains with a performance monitoring function that changed the gains. Using the bias estimate from the model-based observer with time-varying gains as integral action worked well in simulations (Paper G) and in closed-loop experiments with R/V Gunnerus (Paper H). The hybrid method had redundancy in the software design in the sense that two observers based on structurally different models run in parallel, whereas

the time-varying model-based method did not. When that is said, the time-varying model-based approach was simpler to implement, and solved the task with corresponding results. Both for the observer with a signal-based part and a model-based part, and the time-varying model-based observer, the performance monitoring functions included the same measures for detecting transients; the estimation error of the observers, the desired yaw rate from the guidance system, and for practical implementation dead reckoning mode was included.

Using hybrid systems theory to combine measurements of different fidelities in a signal-based observer was successful. The approach in Papers J and K gave estimates of position, velocity and acceleration with smaller variance than the measurements. The observer was tested through simulations of a marine vessel in a simplified scenario where the acceleration of gravity did not appear in the specific force measurements. Additional development is required before the method can be compared with other state-of-the-art signal-based observers.

Hence, summing up regarding the research questions:

1. It was shown that the sea state can be estimated with reasonable accuracy, generally the significant wave height was estimated within 5% and the peak period within 7%. The algorithms proposed in this thesis are computationally efficient, obtaining estimates within a few seconds, and therefore they can be used as performance monitoring for automatic adjustment of model parameters and gains, to engage switching in hybrid controllers, and for operator decision support.
2. The operational window of a marine vessel can be extended by considering many specialized control modules for the various speed ranges, use modes, environmental conditions, and loading conditions, and applying the *best* algorithms in closed-loop control based on performance monitoring and automatic switching. It was shown that using a peak wave frequency estimate for disabling the wave filter in a model-based observer for extreme sea conditions, extended the stable operation region of a vessel in DP. It was also demonstrated, using two different methods, that the transient response of a vessel in DP can be improved by changing gains, or by switching between multiple observers by performance monitoring of the estimation error.
3. A hybrid control concept for marine vessels was proposed for incorporating multiple observers, controllers, control allocation and thruster control algorithms into one system in a structured way. The hybrid systems framework allowed rigorous stability analysis of the hybrid control system, providing formal proof of performance for extended operational windows, improving the overall safety and robustness of the operation. Moreover the system structure is modular, which makes it suitable for control systems with higher levels of autonomy where requirements for redundancy, system testing and certification are high.

4.2 Further Work

Autonomous marine operations are the next wave of development within marine control systems, and this will change the marine and other affected industries. A lot of the technology that is required for autonomous ships is already developed, so the challenge is combining the relevant components into a safe and reliable system that can be tested and certified. Essentially, this thesis has addressed the core element herein; namely making sure switching between different use modes, speed and control strategies is stable for the sampling times that appear in the system, and for changing environmental conditions. Hybrid systems is a well suited framework for this task, and should be considered for theoretical analysis of the next generation marine control systems with high levels of autonomy.

Suggestions for further work related to characterization and monitoring of the environment:

- Perform a sensitivity study for the peakedness of the sea state, number of response measurement samples, steady-state assumption, and vessel size and type for algorithms in Papers B and C.
- Implement the algorithms presented in Papers B and C in a controller, and run experiments to investigate the applicability of the estimates when running online, and the robustness of the method.

Suggestions for further work related to the hybrid observers and controllers:

- Incorporate performance metrics (Rabanal et al., 2016) and response prediction (Nielsen et al., 2017a), in performance monitoring functions of a hybrid controller in order to support proactive control strategies and prevent extreme responses.
- Introduce signal integrity monitoring for processed measurements, estimates, commanded thrust, and more, in order to detect and isolate errors in modeling, implementation and in the signals.
- Investigate how performance monitoring and switching logic can be organized hierarchically for signals with different associated risk.

Suggestions for further work related to sensor fusion using hybrid theory:

- Expand the observer to 6 DOF, and include a gravity elimination procedure in the proposed signal-based observer in order to have realistic specific force measurement inputs.
- Compare the expanded observer against state-of-the-art signal-based observers for various signal-to-noise ratios and sampling times in simulation and on full-scale data.
- Fuse measurements from sensors that are distributed along the hull, e.g., from low-cost IMU sensors, or strain gauges, in order to give higher precision measurements applicable for control and operational performance monitoring.

References

10th ISSC Proceedings (1988). *Proceedings of the Tenth International Ship & Offshore Structures Congress: Lyngby, August 1988. Lyngby, Denmark:*, volume 1. Issued by ISSC '88.

Aranovskii, S.V., Bobtsov, A.A., Kremlev, A.S., and Luk'yanova, G.V. (2007). A robust algorithm for identification of the frequency of a sinusoidal signal. *Journal of Computer and Systems Sciences International*, 46(3), 371–376. doi: 10.1134/S1064230707030045.

Arcak, M., Meissen, C., and Packard, A. (2016). *Networks of Dissipative Systems Compositional Certification of Stability, Performance, and Safety.* Springer, Series: SpringerBriefs in Electrical and Computer Engineering. doi:10.1007/978-3-319-29928-0.

Åstrøm, K.J. and Wittenmark, B. (1997). *Computer-controlled systems, theory and design.* Prentice Hall Information and system sciences series.

Belleter, D.J., Galeazzi, R., and Fossen, T.I. (2015). Experimental verification of a global exponential stable nonlinear wave encounter frequency estimator. *Ocean Engineering*, 97, 48 – 56. doi:10.1016/j.oceaneng.2014.12.030.

Belleter, D., Paliotta, C., Maggiore, M., and Pettersen, K. (2016). Path following for underactuated marine vessels. *IFAC-PapersOnLine*, 49(18), 588 – 593. doi: 10.1016/j.ifacol.2016.10.229.

Bjørnø, J. (2016). *Thruster-Assisted Position Mooring of C/S Inocean Cat 1 Drillship.* Master thesis, Department of Marine Technology, Faculty of Engineering Science and Technology, Norwegian University of Science and Technology, NTNU. Supervisor: Roger Skjetne, NTNU.

Blanke, M. (2006). *Fault-tolerant Sensor Fusion for Marine Navigation.* Elsevier Science.

Blanke, M., Kinnaert, M., Lunze, J., and Staroswiecki, M. (2003). *Diagnosis and Fault-tolerant Control.* Springer.

Branicky, M.S. (1995). *Studies in Hybrid Systems; Modeling, Analysis and Control.* PhD Thesis, MiT, Cambridge, Masachusetts.

Brodtkorb, A.H., Nielsen, U.D., and Sørensen, A.J. (2015a). Sea state estimation using model-scale DP measurements. *MTS/IEEE OCEANS'15 in Washington DC*, 1–7.

Brodtkorb, A.H., Nielsen, U.D., and Sørensen, A.J. (2017a). Sea state estimation using vessel response in dynamic positioning. *Accepted for publication in Applied Ocean Research*.

Brodtkorb, A.H., Sørensen, A.J., and Teel, A.R. (2014). Increasing the operation window of dynamic positioned vessels using the concept of hybrid control. *ASME. International Conference on Offshore Mechanics and Arctic Engineering, 33rd International Conference on Ocean, Offshore and Arctic Engineering (OMAE)*, 1A, V01AT01A046. doi:10.1115/OMAE2014-23601.

Brodtkorb, A.H., Teel, A.R., and Sørensen, A.J. (2015b). Sensor-based hybrid observer for dynamic positioning. *Proceedings of the IEEE Conference on Decision and Control (CDC 2015), Osaka, Japan*, 2015-December, 948–953. doi: 10.1109/CDC.2015.7401995.

Brodtkorb, A.H., Teel, A.R., and Sørensen, A.J. (2016a). Hybrid observer combining measurements of different fidelities. *10th IFAC Conference on Control Applications in Marine Systems (CAMS), September 13-16 2016, Trondheim Norway*, 49(23), 506–511. doi:10.1016/j.ifacol.2016.10.486.

Brodtkorb, A.H., Værnø, S.A.T., Teel, A.R., Sørensen, A.J., and Skjetne, R. (2016b). Hybrid observer for improved transient performance of a marine vessel in dynamic positioning. *10th IFAC Symposium on Nonlinear Control Systems (NOLCOS), August 23-25. 2016, Monterey, California, USA*, 49(18), 245–350. doi:10.1016/j.ifacol.2016.10.189.

Brodtkorb, A.H., Værnø, S.A.T., Teel, A.R., Sørensen, A.J., and Skjetne, R. (2017b). Hybrid controller concept for dynamic positioning of marine vessels with experimental results. *Submitted to Automatica*.

Bryne, T.H., Fossen, T.I., and Johansen, T.A. (2014). Nonlinear observer with time-varying gains for inertial navigation aided by satellite reference systems in dynamic positioning. *2014 22nd Mediterranean Conference on Control and Automation, MED 2014*, 1353–1360. doi:10.1109/MED.2014.6961564.

Bryne, T.H., Fossen, T.I., and Johansen, T.A. (2015). A virtual vertical reference concept for GNSS/INS applications at the sea surface. *10th Conference on Maneouvring and Control of Marine Craft, MCMC August 24-26 2015 Copenhagen, Denmark*, 48, 127–133. doi:10.1016/j.ifacol.2015.10.269.

Bryne, T.H., Hansen, J.M., Rogne, R.H., Sokolova, N., Fossen, T.I., and Johansen, T.A. (2017a). Nonlinear observers for integrated INS/GNSS navigation: Implementation aspects. *IEEE Control Systems Magazine*, 37(3), 59–86. doi: 10.1109/MCS.2017.2674458.

Bryne, T.H., Fossen, T.I., and Johansen, T.A. (2017b). Design of inertial navigation systems for marine craft with adaptive wave filtering aided by triple-redundant sensor packages. *International Journal of Adaptive Control and Signal Processing*, 31(4), 522–544. doi:10.1002/acs.2645.

Cai, C. and Teel, A. (2009). Characterizations of input-to-state stability for hybrid systems. *Systems and Control Letters*, 58(1), 47–53. doi:10.1016/j.sysconle.2008.07.009.

Clauss, G.F., Kosleck, S., and Testa, D. (2012). Critical situations of vessel operations in short crested seas-forecast and decision support system. *Journal of Offshore Mechanics and Arctic Engineering*, 134(3). doi:10.1115/1.4004515.

COLREG (1972). *Convention on the International Regulations for Preventing Collisions at Sea*. International Maritime Organization (IMO).

Cummins, W. (1962). *The impulse response function and ship motions*, volume 1661. Symposium on Ship Theory at the Institut fur Schiffbau der Univeritat Hamburg, 25-27 January 1962.

Desoer, C. and Vidyasagar, M. (1975). *Feedback Systems: Input–Output Properties*. Academic Press.

DNV-GL (2017). *DNV Rules for Classification of Ships, Part 6, Chapter 6: Dynamic Positioning Systems*. DNV-GL service documents, https://rules.dnvgl.com/servicedocuments/dnv.

Faltinsen, O.M. (1993). *Sea Loads on Ships and Offshore Structures*. Cambridge University Press.

Faltinsen, O.M. (2005). *Hydrodynamics of High-Speed Marine Vehicles*. Cambridge University Press.

Faltinsen, O.M. and Timokha, A.N. (2009). *Sloshing*. Cambridge University Press.

Farrell, J.A., Givargis, T.D., and Barth, M.J. (2000). Real-time differential carrier phase GPS-aided INS. *IEEE Transactions on Control Systems Technology*, 8(4), 709–721. doi:10.1.1.20.795.

Fiestoforo (2017). via wikimedia commons, user: Al2 [public domain].

Fossen, T.I. (2011). *Handbook of Marine Craft Hydrodyamics and Motion Control*. Wiley.

Fossen, T.I. and Neijmer (2012). *Parametric resonnance in dynamical systems, Ch. 2: Detection of parametric roll for ships*. Springer-Verlag London.

Fossen, T.I. and Perez, T. (2004). Marine systems simulator (MSS). URL http://www.marinecontrol.org.

Fossen, T.I. and Perez, T. (2009). Kalman filtering for positioning and heading control of ships and offshore rigs. *IEEE Control Systems Magazine*, 29(6), 32–46. doi:10.1109/MCS.2009.934408.

Fossen, T.I. and Strand, J.P. (1999). Passive nonlinear observer design for ships using Lyapunov methods: full-scale experiments with a supply vessel. *Automatica*, 35(1), 3 – 16. doi:10.1016/S0005-1098(98)00121-6.

Garcia-Rosa, P.B., Kulia, G., Ringwood, J.V., and Molinas, M. (2017). Real-time passive control of wave energy converters using the hilbert-huang transform. *20th IFAC World Congress, July 9-14 2017*.

Goebel, R., Sanfelice, R., and Teel, A.R. (2009). Hybrid dynamical systems robust stability and control for systems that combine continuous-time and discrete-time dynamics. *IEEE Control Systems Magazine, April 2009*, 28–93. doi:10.1109/MCS.2008.931718.

Goebel, R., Sanfelice, R.G., and Teel, A.R. (2012). *Hybrid Dynamical Systems, Modelling, Stability and Robustness*. Princeton University Press.

Grip, H.F., Fossen, T.I., Johansen, T.A., and Saberi, A. (2013). Nonlinear observer for GNSS-aided inertial navigation with quaternion-based attitude estimation. *Proceedings of the American Control Conference*, 272–279. doi:10.1109/ACC.2013.6579849.

Grip, H.F., Fossen, T.I., Johansen, T.A., and Saberi, A. (2015). Globally exponentially stable attitude and gyro bias estimation with application to GNSS/INS integration. *Automatica*, 51, 158–166. doi:10.1016/j.automatica.2014.10.076.

Grumman, N. (2017). History of sperry marine, viewed 2017-06-09. URL http://www.sperrymarine.com/corporate-history/sperry-marine.

Hadamard, J. (1902). Sur les problèmes aux dérivés partielles et leur signification physique. *Princeton University Bulletin*, 13, 49–52.

Hassani, V., Sørensen, A.J., Pascoal, A.M., and Athans, M. (2017). Robust dynamic positioning of offshore vessels using mixed-μ synthesis modeling, design, and practice. *Ocean Engineering*, 129, 389 – 400. doi:10.1016/j.oceaneng.2016.10.041.

Henzinger, T.A. (2000). *The Theory of Hybrid Automata*, 265–292. Springer Berlin Heidelberg, Berlin, Heidelberg. doi:10.1007/978-3-642-59615-5_13. URL http://dx.doi.org/10.1007/978-3-642-59615-5_13.

Hespanha, J.P., Liberzon, D., and Morse, A.S. (2003). Hysteresis-based switching algorithms for supervisory control of uncertain systems. *Automatica*, 39(2), 263–272. doi:10.1016/S0005-1098(02)00241-8.

Hespanha, J.P. and Morse, A.S. (2002). Switching between stabilizing controllers. *Automatica*, 38(11), 1905–1917. doi:10.1016/S0005-1098(02)00139-5.

Hespanha, J. (2005). A model for stochastic hybrid systems with application to communication networks. *Nonlinear Analysis: Theory, Methods & Applications*, 62(8), 1353 – 1383. Hybrid Systems and Applications.

Huang, N.E., Shen, Z., Long, S.R., Wu, M.C., Shih, H.H., Zheng, Q., Yen, N.C., Tung, C.C., and Liu, H.H. (1998). The empirical mode decomposition and the hilbert spectrum for nonlinear and non-stationary time series analysis. *Proceedings of the Royal Society of London A: Mathematical, Physical and Engineering Sciences*, 454(1971), 903–995. doi:10.1098/rspa.1998.0193.

Ihle, I.A.F., Jouffroy, J., and Fossen, T.I. (2005). Formation control of marine surface craft using Lagrange multipliers. In *Proceedings of the 44th IEEE Conference on Decision and Control*, 752–758. doi:10.1109/CDC.2005.1582247.

IMO (2011). *International convention for the prevention of pollution from ships (MARPOL) Annex VI.* International Maritime Organization (IMO).

Iseki, T. (2010). Real-time analysis of higher order ship motion spectrum. *Proceedings of the 29th International Conference on Ocean, Offshore and Arctic Engineering (OMAE 2010), June 6-11, Shanghai, China*, 2, 399–405. doi:10.1115/OMAE2010-20521.

Iseki, T. and Nielsen, U.D. (2015). *Study on Short-term Variability of Ship Responses in Waves*, volume 132. Japan Institute of Navigation. doi:10.9749/jin.132.51.

Iseki, T. and Ohtsu, K. (2000). Bayesian estimation of directional wave spectra based on ship motions. *Control Engineering Practice*, 8(2), 215–219. doi:10.1016/S0967-0661(99)00156-2.

Jensen, J., Mansour, A., and Olsen, A. (2004). Estimation of ship motions using closed-form expressions. *Ocean Engineering*, 31, 61–85. doi:10.1016/S0029-8018(03)00108-2.

Kalman, R.E. (1960). A new approach to linear filtering and prediction problems. *Transactions of the ASME–Journal of Basic Engineering*, 82(Series D), 35–45.

Kapinski, J., Deshmukh, J.V., Jin, X., Ito, H., and Butts, K. (2016). Simulation-based approaches for verification of embedded control systems: An overview of traditional and advanced modeling, testing, and verification techniques. *IEEE Control Systems*, 36(6), 45–64. doi:10.1109/MCS.2016.2602089.

Khalil, H.K. (2002). *Nonlinear Systems, 3rd. edition.* Prentice Hall.

Kjerstad, Ø.K. (2016). *Dynamic Positioning of Marine Vessels in Ice.* PhD Thesis 2016:168, Department of Marine Technology, Faculty of Engineering Science and Technology, NTNU. Supervisor: Professor Roger Skjetne, NTNU.

Kjerstad, Ø.K. and Skjetne, R. (2016). Disturbance rejection by acceleration feedforward for marine surface vessels. *IEEE Access*, 4, 2656–2669. doi:10.1109/ACCESS.2016.2553719.

Lee, W. and Bales, S. (1985). Environmental data for design of marine vehicles. *Ship structure symposium '84 New York: Society of Naval Architects and Marine Engineers*, 197–209.

Lindegaard, K.P. (2003). *Acceleration feedback in dynamic positioning.* PhD thesis 2003:4-W, Department of Engineering Cybernetics, Norwegian University of Science and Technology, NTNU. Supervisor: Thor I. Fossen.

Loria, A., Fossen, T.I., and Panteley, E. (2000). A separation principle for dynamic positioning of ships: Theoretical and experimental results. *IEEE Transactions on Control Systems Technology*, 8(2), 332–343. doi:10.1109/87.826804.

Lygeros, J. (1996). *Hierarchical, hybrid control of large scale systems.* PhD Thesis University of California, Berkeley.

Mahony, R., Hamel, T., and Pflimlin, J.M. (2008). Nonlinear complementary filters on the special orthogonal group. *IEEE Transactions on Automatic Control*, 53(5), 1203–1218. doi:10.1109/TAC.2008.923738.

Mansour, A., Jensen, J., and Olsen, A. (2004). Fast evaluation of the reliability of container securing arrangements. *Proceedings of PRADS´04*, 577–585.

Marintek (1988). *Model tests with T-AGOS-1 class vessel, model hull number M1841.* Unpublished report, Marintek A/S (Currently Sintef Ocean).

Minorsky, N. (1922). Directional stability of automatically steered bodies. *Journal of the American Society for Naval Engineers*, 34(2), 280–309. doi:10.1111/j.1559-3584.1922.tb04958.x.

Miyazaki, M.R., Sørensen, A.J., and Vartdal, B.J. (2016). Reduction of fuel consumption on hybrid marine power plants by strategic loading with energy storage devices. *IEEE Power and Energy Technology Systems Journal*, 3(4), 207–217. doi:10.1109/JPETS.2016.2621117.

Montazeri, N., Nielsen, U.D., and Jensen, J.J. (2016a). Selection of the optimum combination of responses for wave buoy analogy - an approach based on local sensitivity analysis. *Proceedings of the 13th International Symposium on PRActical Design of Ships and Other Floating Structures (PRADS' 2016), Technical University of Denmark (DTU).*

Montazeri, N., Nielsen, U.D., and Jensen, J.J. (2016b). Estimation of wind sea and swell using shipboard measurements – a refined parametric modelling approach. *Applied Ocean Research*, 54, 73 – 86. doi:10.1016/j.apor.2015.11.004.

Nguyen, T.D. (2006). *Design of Hybrid Marine Control Systems for Dynamic Positioning.* PhD Thesis, Department of Civil Engineering, National University of Singapore (NUS). Supervisor: Professor Quek Ser Tong, NUS, Co- Supervisor: Professor Asgeir J. Sørensen, NTNU.

Nguyen, T.D., Sørensen, A.J., and Quek, S.T. (2004). Observer for dynamic positioning of floating structures in extreme seas. *The Seventeenth KKCNN Symposium on Civil Engineering, December 13-15, Thailand.*

Nguyen, T.D., Sørensen, A.J., and Quek, S.T. (2007). Design of hybrid controller for dynamic positioning from calm to extreme sea conditions. *Automatica*, 43(5), 768–785. doi:10.1016/j.automatica.2006.11.017.

Nguyen, T.D., Sørensen, A.J., and Quek, S.T. (2008). Multi-operational controller structure for station keeping and transit operations of marine vessels. *IEEE Transactions on Control Systems Technology*, 16(3), 491–498. doi: 10.1109/TCST.2007.906309.

Nielsen, U.D. (2006). Estimations of on-site directional wave spectra from measured ship responses. *Marine Structures*, 19, 33–69. doi:10.1016/j.marstruc.2006.06.001.

Nielsen, U.D. (2017a). A concise account of techniques available for shipboard sea state estimation. *Ocean Engineering*, 129, 352–362. doi:10.1016/j.oceaneng.2016.11.035.

Nielsen, U.D. (2017b). Transformation of a wave energy spectrum from encounter to absolute domain when observing from an advancing ship. *Submitted to Marine Structures*.

Nielsen, U.D., Bjerregård, M., Galeazzi, R., and Fossen, T.I. (2015). New concepts for shipboard sea state estimation. *MTS/IEEE OCEANS 2015 in Washington DC*.

Nielsen, U.D., Brodtkorb, A.H., and Jensen, J.J. (2017a). Response predictions for marine vessels using observed autocorrelation function. *Accepted for publication in Marine Structures, 2017*.

Nielsen, U.D., Brodtkorb, A.H., and Sørensen, A.J. (2017b). A brute-force spectral approach for wave estimation using measured vessel responses. *Submitted to Marine Structures*.

Nielsen, U.D., Galeazzi, R., and Brodtkorb, A.H. (2016). Evaluation of shipboard wave estimation techniques through model-scale experiments. *OCEANS 2016 - Shanghai*, 1–8. doi:10.1109/OCEANSAP.2016.7485701.

Nielsen, U., Andersen, I., and Koning, J. (2013). Comparisons of means for estimating sea states from an advancing large container ship. *Proceedings of the PRADS 2013*.

Oppenheim, A.V. and Verghese, G.C. (2010). *Signals, Systems and Interference*. MIT Class Notes for 6.011: Introduction to Communication, Control and Signal Processing Spring 2010.

Pascoal, R. and Guedes Soares, C. (2009). Kalman filtering of vessel motions for ocean wave directional spectrum estimation. *Ocean Engineering*, 36(6-7), 477–488. doi:10.1016/j.oceaneng.2009.01.013.

Perez, T., Sørensen, A., and Blanke, M. (2006). Marine vessel models in changing operational conditions—a tutorial. *14th IFAC Symposium on Identification and System Parameter Estimation, IFAC Proceedings Volumes*, 39(1), 309 – 314. doi: http://dx.doi.org/10.3182/20060329-3-AU-2901.00044.

Piviano, L., Husteli, N., Mikalsen, J., and Liset, P. (2015). Automated hardware-in-the-loop testing – experience from onboard remote testing with cybersea signature. *Dynamic Positioning Conference, Marine Technology Society, October 13-14*.

Price, W.G. and Bishop, R.E.D. (1974). *Probalistic Theory of Ship Dynamics*. Chapman and Hall, London.

Rabanal, O.M.R., Brodtkorb, A.H., and Breivik, M. (2016). Comparing controllers for dynamic positioning of ships in extreme seas. *10th IFAC Conference on Control Applications in Marine Systems (CAMS), September 13-16 2016, Trondheim Norway*, 49(23), 258–264. doi:10.1016/j.ifacol.2016.10.352.

Rockafellar, R.T. and Wets, R.J.B. (1998). *Variational Analysis*. Springer Berlin Heidelberg, Series: Grundlehren der mathematischen Wissenschaften. doi:10.1007/978-3-642-02431-3.

Rustad, A.M. (2007). *Modeling and Control of Top Tensioned Riser*. PhD Thesis 2007:183, Department of Marine Technology, Faculty of Engineering Science & Technology, NTNU. Supervisor: Professor Asgeir J. Sørensen, NTNU, Co-supervisor: Professor Carl M. Larsen, NTNU.

Ruth, E. (2008). *Propulsion Control and Thrust Allocation on Marine Vessels*, volume 203. PhD Thesis 2008, Department of Marine Technology, Faculty of Engineering Science and Technology, NTNU. Supervisor: Professor Asgeir J. Sørensen, NTNU, Co-supervisors: Dr. Tristan Perez, NTNU and Professor Mogens Blanke, DTU.

Simos, A.N., Sparano, J.V., Tannuri, E.A., and Matos, V.L.F. (2007). Directional wave spectrum estimation based on a vessel 1st order motions: Field results. *Proceedings of the International Offshore and Polar Engineering Conference (ISOPE 2007)*, 1938–1944. doi:ISOPE-I-07-196.

Skjetne, R. (2005). *The Maneuvering Problem*. PhD-thesis 2005:1, Faculty of Information Technology, Mathematics and Electrical Engineering, Department of Engineering Cybernetics, NTNU. Main supervisor: Professor Thor I. Fossen.

Skjetne, R. and Egeland, O. (2006). Hardware-in-the-loop testing of marine control systems. *Journal on Modeling, Identification and Control (MIC)*, 27(4), 239–258.

Skjetne, R., Jørgensen, U., and Teel, A.R. (2011). Line-of-sight path-following along regularly parametrized curves solved as a generic maneuvering problem. *50th IEEE Conference on Decision and Control (CDC) and European Control Conference (ECC)*, 2467–2474. doi:10.1109/CDC.2011.6161364.

Skjetne, R., Kjerstad, Ø.K., Værnø, S.A.T., Brodtkorb, A.H., Sørensen, A.J., Sørensen, M.E.N., Breivik, M., Calabrò, V., and Vinje, B.O. (2017). AMOS DP research cruise 2016: Academic full-scale testing of experimental dynamic positioning control algorithms onboard R/V Gunerus. *Proceedings of the 36th International Conference on Ocean, Offshore and Arctic Engineering (OMAE), Trondheim Norway, June 25-30*, (OMAE2017-62045).

Smogeli, Ø., Vik, B., Haugen, O., and Pivano, L. (2014). Risk management for control system software for the maritime and offshore oil and gas industries. *Proceedings of the IMCA Annual Seminar, London.*

Smogeli, Ø.N. (2006). *Control of Marine Propellers, From Normal to Extreme Conditions.* PhD Thesis 2006:187, Department of Marine Technology, Faculty of Engineering Science and Technology, NTNU. Supervisor: Asgeir J. Sørensen.

Smogeli, Ø.N. and Sørensen, A.J. (2009). Antispin thruster control for ships. *IEEE Transactions on Control Systems Technology*, 17(6), 1362–1375. doi:10.1109/TCST.2008.2009065.

Sørensen, A.J. (2005). Structural issues in the design and operation of marine control systems. *Annual Reviews in Control*, 29(1), 125–149. doi:10.1016/j.arcontrol.2004.12.001.

Sørensen, A.J. (2011). A survey of dynamic positioning control systems. *Annual Reviews in Control*, 35(1), 123–136. doi:10.1016/j.arcontrol.2011.03.008.

Sørensen, A.J. (2013). *Marine Control Systems, Propulsion and Motion Control of Ships and Ocean structures, Lecture Notes.* Department of Marine Technology, Faculty of Engineering Science and Technology, NTNU.

Sørensen, A.J., Nguyen, T.D., and Quek, S.T. (2004). Improved operability and safety of dp vessels using hybrid control concept. *International Conference on Technology & Operation of Offshore Support Vessels (OSV Singapore 2005), Jointly organized by Joint Branch of RINA-IMarEST Singapore and CORE, 20-21 September, Singapore.*

Sørensen, A.J., Pedersen, E., and Smogeli, Ø. (2003). Simulation-based design and testing of dynamically positioned marine vessels. *In Proceedings of International Conference on Marine Simulation and Ship Maneuverability, MARSIM'03, August 25 - 28, Kanazawa, Japan.*

Sørensen, A.J. and Smogeli, Ø. (2009). Torque and power control of electrically driven marine propellers. *IFAC Journal Control Engineering Practice (CEP)*, 17(9), 1053–1064.

Sørensen, A.J. and Strand, J.P. (2000). Positioning of small-waterplane-area marine constructions with roll and pitch damping. *IFAC Journal of Control Engineering in Practice*, 8(2), 205–213. doi:10.1016/S0967-0661(99)00155-0.

Sørensen, A.J., Strand, J.P., and Nyberg, H. (2002). Dynamic positioning of ships and floaters in extreme seas. *In Proceedings of OCEANS'02 MTS/IEEE, Biloxi, Mississippi, US*, 3, 1850–1855. doi:10.1109/OCEANS.2002.1191913.

Steen, S. (2014). *Experimental Methods in Marine Hydrodynamics, Lecture Notes.* Department of Marine Technology, Faculty of Engineering Science and Technology, NTNU.

Steen, S., Selvik, Ø., and Hassani, V. (2016). Experience with rim-driven azimuthing thrusters on the research ship Gunnerus. *10th Symposium on High-Performance Marine Vessels (HIPER'16), October 17-19 2016, Cortona, Italy.*

Strand, J.P., Sørensen, A.J., and Fossen, T.I. (1998). Design of automatic thruster assisted mooring systems for ships. *Journal on Modeling, Identification and Control (MIC)*, 19(2), 61–75. doi:10.4173/mic.1998.2.1.

Stredulinsky, D.C. and Thornhill, E.M. (2011). Ship motion and wave radar data fusion for shipboard wave measurement. *Journal of Ship Research*, 55, 73–85.

Tannuri, E.A. and Morishita, H.M. (2006). Experimental and numerical evaluation of a typical dynamic positioning system. *Applied Ocean Research*, 28(2), 133–146. doi:10.1016/j.apor.2006.05.005.

Tannuri, E., Sparano, J., Simos, A., and Da Cruz, J. (2003). Estimating directional wave spectrum based on stationary ship motion measurements. *Applied Ocean Research*, 25(5), 243–261. doi:10.1016/j.apor.2004.01.003.

Teel, A.R. (2013). Lyapunov conditions certifying stability and recurrence for a class of stochastic hybrid systems. *Annual Reviews in Control*, 37(1), 1–24. doi:10.1016/j.arcontrol.2013.02.001.

Teel, A., Hespanha, J., and Subbaraman, A. (2014). Equivalent characterizations of input-to-state stability for stochastic discrete-time systems. *IEEE Transactions on Automatic Control*, 59(2), 516–522.

Teknikum29 (2017). Scientifical calculators and mini computers, viewed 2017-06-05. URL http://www.technikum29.de/en/computer/early-computers.

Thornhill, E.M. and Stredulinsky, D.C. (2010). Real Time Local Sea State Measurement using Wave Radar and Ship Motions. In *Society of Naval Architects and Marine Engineers (SNAME) annual meeting*. Seattle, WA, USA.

Tutturen, S.A. and Skjetne, R. (2015). Hybrid control to improve transient response of integral action in dynamic positioning of marine vessels. *10th IFAC Conference on Manoeuvring and Control of Marine Craft (MCMC2015)*, 56(7), 1636–1649. doi:10.1016/j.ifacol.2015.10.275.

Udjus, G. (2017). *Force field identification and positioning control of an autonomous vessel using inertial measurement units.* Master's thesis, Department of Marine Technology, NTNU. Supervisor: Roger Skjetne.

Utne, I.B., Sørensen, A.J., and Schjølberg, I. (2017). Risk management of autonomous marine systems and operations. *Proceedings of the 36th Intenational Conference on Ocean, Offshore and Arctic Engineering, OMAE 2017,June 25-30, Trondheim, Norway*, (OMAE2017-61645).

Værnø, S.A., Brodtkorb, A.H., Skjetne, R., and Calabrò, V. (2017). Time-varying model-based observer for marine surface vessels in dynamic positioning. *IEEE Access*, 5, 14787–14796. doi:10.1109/ACCESS.2017.2731998.

Værnø, S.A.T., Brodtkorb, A.H., Skjetne, R., and Sørensen, A.J. (2016). An output feedback controller with improved transient response of marine vessels in dynamic positioning. *10th IFAC Conference on Control Applications in Marine Systems (CAMS), September 13-16 2016, Trondheim Norway*, 49(23), 133–138. doi:10.1016/j.ifacol.2016.10.333.

Vik, B. and Fossen, T.I. (2001). Nonlinear observer design for integration of GPS and intertial navigation systems. *Proceedings of the Conference on Decision and Control (CDC'2001). Orlando, FL.*, 2956–2961. doi:10.1109/CDC.2001.980726.

West, G.S. and Apelt, C.J. (1982). The effects of tunnel blockage and aspect ratio on the mean flow past a circular cylinder with reynolds numbers between 10e4 and 10e5. *Journal of Fluid Mechanics*, 114, 361–377. doi: 10.1017/S0022112082000202.

Witsenhausen, H. (1966). A class of hybrid-state continuous-time dynamic systems. *IEEE Transactions on Automatic Control*, 11(2), 161–167. doi:10.1109/TAC.1966.1098336.

Xidias, E., Paliotta, C., Aspragathos, N., and Pettersen, K. (2017). *Path Planning for Formation Control of Autonomous Vehicles*, 302–309. Springer International Publishing. doi:10.1007/978-3-319-49058-8_33.

Appendices

Appendix A

Preliminaries for Hybrid Dynamical Systems

This appendix gives an overview over definitions and theorems that are preliminary and applied in the hybrid systems description and analysis in Papers D-F, J and K. The solution concept is briefly described in Section A.1, sufficient Lyapunov conditions are found in Section A.2, conditions for stability based on set invariance and convergence are given in Section A.3, and Section A.4 discusses stability of hybrid systems in cascade. The reader is referred to the textbook *Hybrid Dynamical Systems* Goebel et al. (2012) for more details on the hybrid systems framework applied in this work.

A.1 The Solution Concept

Solutions to hybrid systems are called *hybrid arcs*, which are functions that evolve in continuous time $t \in \mathbb{R}_{\geq 0}$ and in discrete time $j \in \mathbb{N}$, where j denotes the number of jumps. Only certain subsets of $\mathbb{R}_{\geq 0} \times \mathbb{N}$ can correspond to evolutions of hybrid systems, and these subsets are called *hybrid time domains*.

Definition A.1. Hybrid time domain (Goebel et al., 2012, Def. 2.3)
A subset $E \subset \mathbb{R}_{\geq 0} \times \mathbb{N}$ is a compact hybrid time domain if

$$E = \bigcup_{j=0}^{J-1} ([t_j, t_{j+1}], j)$$

for some finite sequence of times $0 = t_0 \leq t_1 \leq t_2 \leq ... \leq t_J$. It is a hybrid time domain if for all $(T, J) \in E$, $E \cap ([0, T] \times \{0, 1, ..., J\})$ is a compact hybrid domain.

An example of a hybrid time domain E is shown to the left in Figure A.1, with $0 = t_0 < t_1 < t_2 = t_3 < t_4$. For all $(T, J) \in E$ in Figure A.1, the domain $E \cap ([0, T] \times \{0, 1, ..., J\})$ is a compact hybrid time domain. It follows from Definition A.1 that the points $(0, 1)$ and $(1, 0)$ cannot belong to the same hybrid time domain.

Definition A.2. Hybrid arc (Goebel et al., 2012, Def. 2.4)
A function $\phi : E \to \mathbb{R}^n$ is a hybrid arc if E is a hybrid time domain and if for

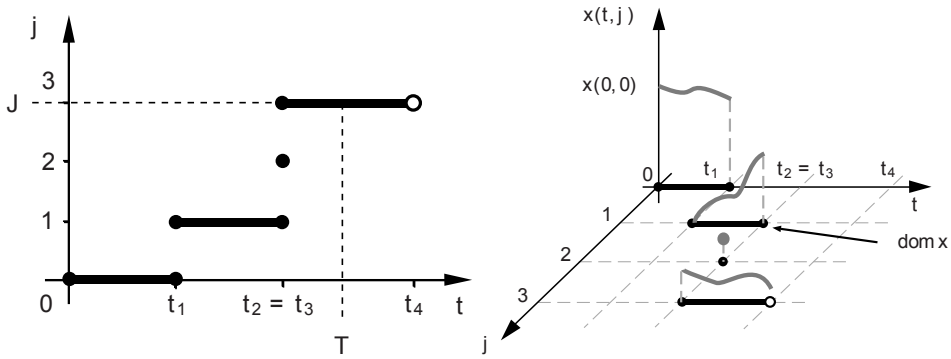

Figure A.1: Example of a hybrid time domain E (left), and example of a hybrid arc ϕ (right). Source: Goebel et al. (2012).

each $j \in \mathbb{N}$, the function $t \mapsto \phi(t, j)$ is locally absolutely continuous on the interval $I^j := \{t : (t, j) \in E\}$.

A function is locally absolutely continuous if the derivative is continuous for almost all time, and the function can be recovered by integrating the derivative. Absolute continuity is a smoothness property of functions that is stronger than continuity and uniform continuity. An example of a hybrid arc is shown to the right in Figure A.1.

Definition A.3. Solution to a hybrid system (Goebel et al., 2012, Def. 2.6)
A hybrid arc ϕ is a solution to a hybrid system $\mathcal{H} = (C, F, D, G)$ if $\phi(0, 0) \in \bar{C} \cup D$, and

(i) for all $j \in \mathbb{N}$ such that $I^j := \{t : (t, j) \in \text{dom } \phi\}$ has nonempty interior

$$\begin{aligned} \phi(t, j) &\in C && \text{for all} && t \in \text{int} I^j, \\ \dot{\phi}(t, j) &\in F(\phi(t, j)) && \text{for almost all} && t \in I^j; \end{aligned} \tag{A.1}$$

(ii) for all $t, j \in \text{dom } \phi$ such that $(t, j + 1) \in \text{dom } \phi$,

$$\begin{aligned} \phi(t, j) &\in D, \\ \phi(t, j + 1) &\in G(\phi(t, j)). \end{aligned} \tag{A.2}$$

$\bar{C}$ denotes the closure of C, and $\text{int} I^j$ denotes the interior of the interval I^j. This is a broad definition that admits solutions of many forms. A solution is said to be complete if the domain of the solution dom ϕ is unbounded, i.e., if length(dom ϕ) $= \infty$. Solutions that cannot be extended are said to be maximal.

Definition A.4. Maximal solutions (Goebel et al., 2012, Def. 2.7)
A solution ϕ to $\mathcal{H}$ is maximal if there does not exist another solution ψ to $\mathcal{H}$ such that dom ϕ is a proper subset of dom ψ and $\phi(t, j) = \psi(t, j)$ for all $(t, j) \in$ dom ϕ.

$\phi \in \mathcal{S}_{\mathcal{H}}(S)$ denotes the set of all maximal solutions to $\mathcal{H}$ with $\phi(0,0) \in S$. Complete solutions are maximal, but the converse statement is not true. In the next sections the term 'pre' allows for the possibility that maximal solutions are not complete, that is, the solutions may exist only for a time interval. For examples of maximal solutions see Goebel et al. (2012), Example 2.9.

A.2 Lyapunov-based Stability Analysis

Lyapunov functions can be used to analyze stability of the equilibrium set $\mathcal{A}$ of hybrid systems. A Lyapunov function candidate is defined in Definition A.5, and conditions for stability are stated in Theorem A.6.

Definition A.5. Lyapunov function candidate (Goebel et al., 2012, Def. 3.16)
A function $V : \text{dom } V \to \mathbb{R}$ is said to be a Lyapunov function candidate for the hybrid system $\mathcal{H} = (C, F, D, G)$ if the following conditions hold:

1. $\bar{C} \cup D \cup G(D) \subset \text{dom } V$;
2. V is continuously differentiable on an open set containing $\bar{C}$;

where $\bar{C}$ denotes the closure of C.

Theorem A.6. *Sufficient Lyapunov conditions (Goebel et al., 2012, Thm. 3.18) Let $\mathcal{H} = (C, F, D, G)$ be a hybrid system and let $\mathcal{A} \subset \mathbb{R}^n$ be closed. If V is a Lyapunov function candidate for $\mathcal{H}$, and there exists $\alpha_1, \alpha_2 \in \mathcal{K}_\infty$, and a continuous positive definite function ρ such that*

$$\textit{i)} \quad \alpha_1(|x|_{\mathcal{A}}) \leq V(x) \leq \alpha_2(|x|_{\mathcal{A}}) \quad \forall x \in C \cup D \cup G(D);$$
$$\textit{ii)} \quad < \nabla V(x), f > \leq -\rho(|x|_{\mathcal{A}}) \quad \forall x \in C, f \in F(x);$$
$$\textit{iii)} \quad V(g) - V(x) \leq -\rho(|x|_{\mathcal{A}}) \quad \forall x \in D, g \in G(x);$$

then $\mathcal{A}$ is uniformly globally pre-asymptotically stable for $\mathcal{H}$.

Sufficient conditions for ii) and iii) are

$$\text{ii}^*) \quad < \nabla V(x), f > \leq -\epsilon V(x) \quad \forall x \in C, f \in F(x);$$
$$\text{iii}^*) \quad V(g) = (1-\epsilon)V(x) \quad \forall x \in D, g \in G(x);$$

with $\epsilon > 0$.

A.3 Stability Based on Set Invariance and Convergence

In some cases it might be difficult to find a Lyapunov function for the system. Proposition A.9 uses the notions of *strong forward invariance* and *uniform attractivity*.

Definition A.7. Strong forward pre-invariance (Goebel et al., 2012, Def. 6.25)
If for every maximal solution ϕ starting in $\mathcal{A}$, the range of ϕ is in a subset of $\mathcal{A}$, then $\mathcal{A}$ is strongly forward pre-invariant.

Definition A.8. Uniformly pre-attractive (Goebel et al., 2012, Def. 6.24)
A compact set $\mathcal{A} \subset \mathbb{R}^n$ is said to be uniformly pre-attractive from a set $S \subset \mathbb{R}^n$ if every $\phi \in \mathcal{S}_{\mathcal{H}}(S)$ is bounded and for every $\epsilon > 0$ there exists a $T > 0$ such that $|\phi(t,j)|_{\mathcal{A}} \leq \epsilon$ for every $\phi \in \mathcal{S}_{\mathcal{H}}(S)$ and $(t,j) \in \text{dom } \phi$ with $t + j \geq T$.

Proposition A.9. *Stability from invariance plus uniform convergence (Goebel et al., 2012, Def. 7.3 and Prop. 7.5)*
(a) Let the hybrid system $\mathcal{H}$ be nominally well-posed.
(b) Suppose that a compact set $\mathcal{A} \subset \mathbb{R}^n$ has the following properties:

i. it is strongly forward pre-invariant;

ii. is it uniformly pre-attractive from a neighborhood of itself, i.e., there exists a $\mu > 0$ such that $\mathcal{A}$ is uniformly pre-attractive from $\mathcal{A} + \mu\mathbb{B}$;

iii. the basin of pre-attraction of $\mathcal{A}$, denoted $\mathcal{B}^p_{\mathcal{A}}$, is all of $\mathbb{R}^n$. $\mathcal{B}^p_{\mathcal{A}}$ is the set of points $\xi \in \mathbb{R}^n$ such that every solution ϕ to $\mathcal{H}$ with $\phi(0,0) = \xi$ is bounded, and if it is complete, then also $\lim_{t+j\to\infty} |\phi(t,j)|_{\mathcal{A}} = 0$.

Then the compact set $\mathcal{A}$ is uniformly globally pre-asymptotically stable.

(a) holds if the hybrid basic assumptions (Assumption 3.1) are satisfied, and $\mathbb{B}$ denotes the unit ball.

A.4 Stability of Cascaded Hybrid Systems

Corollary A.10. *Stability of cascaded hybrid systems (Goebel et al., 2009, Corollary 19.) Consider a hybrid system $\mathcal{H} = (C, F, D, G)$, satisfying the basic assumptions. If the compact set $\mathcal{A}_1$ is globally pre-asymptotically stable for $\mathcal{H}$ and the compact set $\mathcal{A}_2 \subset \mathcal{A}_1$ is globally pre-asymptotically stable for $\mathcal{H}|_{\mathcal{A}_1} := (C \cap \mathcal{A}_1, F, D \cap \mathcal{A}_1, G)$, then $\mathcal{A}_2$ is globally pre-asymptotically stable for $\mathcal{H}$.*

Corollary A.10 may be applied to analyze cascaded hybrid systems $\mathcal{H}$ of the form

$$(x_1, x_2) \in C_1 \times C_2 \quad \left.\begin{array}{l} \dot{x}_1 = f_1(x_1, x_2) \\ \dot{x}_2 = f_2(x_2) \end{array}\right\} = F(x), \tag{A.3a}$$

$$(x_1, x_2) \in D_1 \times D_2 \quad x^+ = G(x), \tag{A.3b}$$

where the hybrid state is $x = (x_1, x_2)$, the flow set is $C = C_1 \times C_2$, the jump set is D, and $\mathcal{H}$ satisfies the hybrid basic assumptions given in Assumption 3.1. The origin of

$$x_2 \in C_2 \quad \dot{x}_2 = f_2(x_2)$$

is globally asymptotically stable, and the origin of

$$x_1 \in C_1 \quad \dot{x}_1 = f_1(x_1, 0)$$

is globally asymptotically stable.

Appendix B

Experimental Platforms

In this appendix more information about the experimental platforms Cybership 3 and R/V Gunnerus are given. As a part of the data validation for Paper A and B, complex-valued transfer functions were calculated for Cybership 3 and for R/V Gunnerus. Details from the oscillation tests for Cybership 3 are given in addition to some details of the setup in the Marine Cybernetics Laboratory (MCLab). The main parameters and hull resistance coefficients are given for R/V Gunnerus.

B.1 Cybership 3

Cybership 3, is a 1:30 scaled model of a platform supply vessel (PSV) made by Marintek A/S (currently Sintef Ocean) in 1988 (Model number 1841). The data for the model given in this section is based on extensive model tests reported in Marintek (1988), as well as Nguyen (2006), Ruth (2008), Kjerstad (2016), and oscillation tests that were performed in June 2015 as part of data validation for Cybership 3. The model hull has not changed since 1988, but the instrumentation and weight distribution of the model has been altered significantly over the years. This has consequences for the vessel mass and damping matrices, and motion transfer functions.

B.1.1 Thruster Configuration

Cybership 3 has two azimuthing thrusters for main propulsion at the stern, and a ducted azimuth thruster in the bow. The thruster motor controllers were changed before Kjerstad (2016) did experiments in 2015, and the tunnel thruster in the bow was disabled. Ruth (2008) used the angle signals from the thrusters for feedback, but the current angle signals from the thruster motor controllers are too noisy to use in feedback control, and therefore the thrusters are set to fixed angles. Below, the thruster details for Cybership 3 are given, and the angles a_i and arms

$l_{ix}, l_{iy},\ i = \{1, 2, 3\}$ are illustrated in Figure B.1.

$$
\begin{aligned}
&a_1 = 30^\circ\ (port) \quad a_2 = -30^\circ\ (starboard) \quad a_3 = 90^\circ\ (bow)\\
&l_{1x} = -0.81m \quad l_{2x} = -0.81m \quad l_{3x} = 0.76m\\
&l_{1y} = -0.11m \quad l_{2y} = 0.11m \quad l_{3y} = 0m\\
&B = \begin{bmatrix} \cos(a_1) & \cos(a_2) & \cos(a_3) \\ \sin(a_1) & \sin(a_2) & \sin(a_3) \\ l_{1x}\sin(a_1) - l_{1y}\cos(a_1) & l_{2x}\sin(a_2) - l_{2y}\cos(a_2) & l_{3x}\sin(a_3) - l_{3y}\cos(a_3) \end{bmatrix}\\
&\tau = Bf
\end{aligned}
$$

$\tau \in \mathbb{R}^3$ is the generalized force vector, $f \in \mathbb{R}^3$ are the forces for each thruster, and $B \in \mathbb{R}^{3\times3}$ is the thrust allocation matrix that relates the two. In this case B is constant, since the angles are fixed. Bollard pull tests were done by Nguyen (2006) and Kjerstad (2016) to map the thruster force, f [N], to the rotational speed, u [rounds per second, rps], of each thruster. Thrust coefficients that were applied in the MCLab are given in Table B.1. Note that these values are slightly different than the values stated in Appendix C of Nguyen (2006), since the thruster motor controllers were exchanged in 2015. The commanded thruster rotational speed u [rps] was calculated as follows:

$$
u = \begin{cases} \sqrt{\frac{f}{K_{Tp} d^4 \rho}}, & \text{if } f \geq 0 \\ -\sqrt{\frac{|f|}{K_{Tn} d^4 \rho}}, & \text{otherwise} \end{cases}
$$

where d is the thruster diameter, K_{Tn} are thrust coefficients for negative rotation rates, and K_{Tp} are thrust coefficients for positive rotation rates from Table B.1, and ρ [kg/m^3] is the density of water.

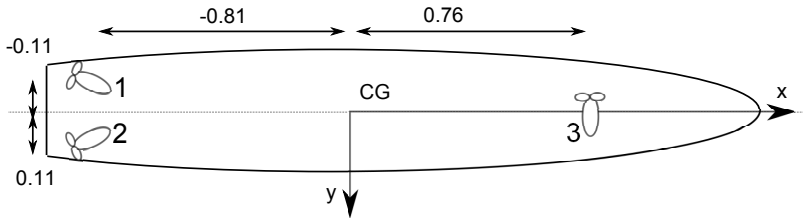

Figure B.1: Cybership 3 thruster configuration, fixed angle stern ±30 degrees and front 90 degrees. The units of the arms l_i is meters.

Table B.1: Cybership 3 thrust coefficients K_T applied in the MCLab in 2015-2017. K_{Tn} are thrust coefficients for negative rotation rates, and K_{Tp} are thrust coefficients for positive rotation rates (Kjerstad, 2016).

Thruster	K_{Tn} [N/rps^2]	K_{Tp} [N/rps^2]	Diameter [m]
1 Port main at 30°	0.2423	0.3507	0.09
2 Starboard main at -30°	0.2402	0.3464	0.09
3 Bow at 90°	0.1790	0.2383	0.05

B.1.2 Structure Mass Distribution

In June 2015 the structure mass distribution was calculated for Cybership 3 for the current instrumentation, including batteries. The model weighed 86.5 kg, and had 0.15° aft trim, i.e., the model was 6 mm deeper than design draught aft and 1 mm deeper than design draft fore. Figure B.2 shows the model on the cradle during oscillation tests in roll. The oscillation tests were done for four heights in roll and pitch, in order to increase the accuracy of the measurements. The three lowest heights seemed to be the most accurate, so these are used to compute the results that are shown in Table B.2, together with the principle hull data and structure mass distribution for the model-scale ship in 1988 and for the full-scale PSV. Note that the principal hull data are the same for the model in 1988 and in 2015. The oscillation test setup for Cybership 3 is shown in Figure B.3, together with some of the results listed in Table B.2.

Figure B.2: Cybership 3 during oscillation tests in roll.

Table B.2: Principle hull data and design structure mass distribution for platform supply vessel, full-scale and model-scale, scale factor, $\lambda = 1/30$ (Marintek, 1988). The structure mass distribution values calculated in 2015 are given in parenthesis. AP = Aft perpendicular, BL= baseline, CL = centerline, CG = center of gravity.

Principle hull data	Model-scale	Full-scale	
Length over all L_{oa}	2.275	68.26	m
Length between perpendiculars L_{pp}	1.971	59.13	m
Breadth moulded, B_m	0.437	13.11	m
Breadth waterline, B_{wl}	0.437	13.11	m
Draught at $L_{pp}/2$, T	0.153	4.59	m
Draught at fore perpendicular, T_{FP}	0.153	4.59	m
Draught at aft perpendicular, T_{AP}	0.153	4.59	m
Depth to main deck D	0.203	6.10	m

Structure mass distribution	Model-scale 1988 (2015)	Full-scale	
Mass	74.7 (86.5)	2 067 300	kg
Waterline	0.153 (0.154)	4.59	m rel. to BL
Trim	0 (0.15)	0	° rel. to BL
Longitudinal center of gravity, LCG	1.005 (0.925)	30.15	m rel. to AP
Transverse center of gravity, TCG	0 (0)	0	m rel. to CL
Vertical center of gravity, VCG	0.1956 (0.1105)	5.87	m rel. to BL
Roll moment of inertia, I_{44}	2.192 (1.584)	$58.74{\cdot}10^6$	kgm^2
Pitch moment of inertia, I_{55}	19.72 (18.939)	$483.2{\cdot}10^6$	kgm^2
Yaw moment of inertia, I_{66}	19.72 (18.939)	$483.2{\cdot}10^6$	kgm^2
Roll radius of gyration, r_{44}	0.1713 (0.135)	5.139	m rel. to CG
Pitch radius of gyration, r_{55}	0.5138 (0.468)	15.41	m rel. to CG
Yaw radius of gyration, r_{66}	0.5138 (0.468)	15.41	m rel. to CG

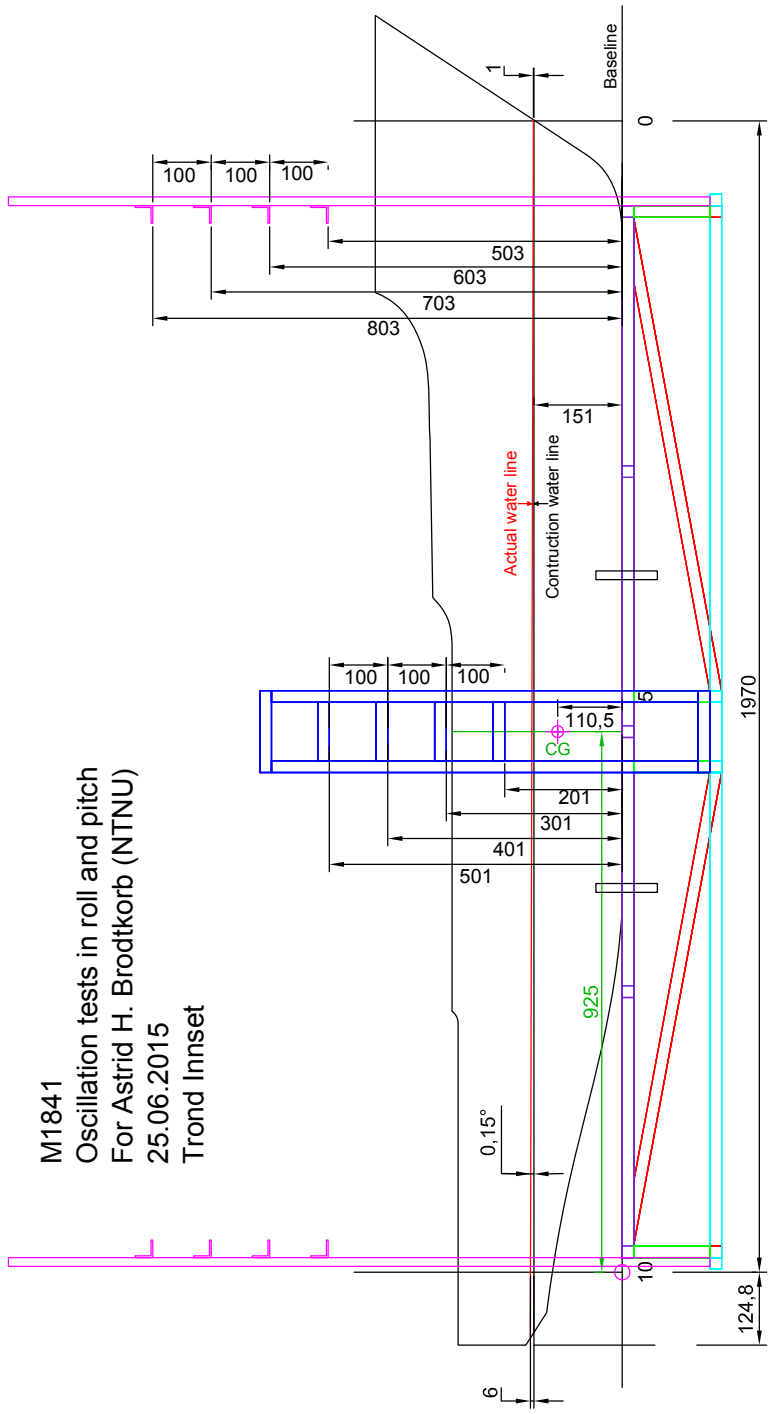

Figure B.3: Figure showing the setup and some results from the oscillation tests in roll and pitch. Units (where not stated) are [mm].

Using the updated structure mass distribution from 2015 in ShipX response analysis, gives the following model-scale parameters:

$$M_{RB} = diag([85.1263, 85.1263, 85.1263, 1.5514, 18.5386, 18.6447]) \tag{B.1}$$

$$M_A = \begin{bmatrix} 4.4204 & 0 & 0 & 0 & 0 & 0 \\ 0 & 25.3496 & 0 & 1.7976 & 0 & 3.0812 \\ 0 & 0 & 169.1854 & 0 & 22.5983 & 0 \\ 0 & 1.7976 & 0 & 0.5566 & 0 & -0.1585 \\ 0 & 0 & 22.5983 & 0 & 39.2569 & 0 \\ 0 & 3.0812 & 0 & -0.1585 & 0 & 5.9068 \end{bmatrix} \tag{B.2}$$

$$D_L = \begin{bmatrix} 4.2151 & 0 & 0 & 0 & 0 & 0 \\ 0 & 24.1719 & 0 & 1.6401 & 0 & 2.6573 \\ 0 & 0 & 21.6093 & 0 & 11.3818 & 0 \\ 0 & 1.6401 & 0 & 0.2119 & 0 & -0.1967 \\ 0 & 0 & 11.3818 & 0 & 14.1326 & 0 \\ 0 & 2.6573 & 0 & -0.1967 & 0 & 6.7726 \end{bmatrix} \tag{B.3}$$

$$B_v = diag([2.3676, 13.5773, 0, 0.0596, 0, 2.8634]) \tag{B.4}$$

M_{RB} is the rigid body mass, $M_A = A(\infty)$ is the added mass for $\omega \to \infty$ for zero forward speed, $D_L = B(\infty)$ is the linear wave radiation damping for $\omega \to \infty$ for zero forward speed, and B_v is approximate viscous damping. Froude scaling has been applied to (B.1)-(B.4) with $\lambda = 1/30$ to ensure correct scaling of hydrodynamic forces and moments.

B.1.3 Notes on Experimental Setup with Cybership 3 and Error Sources

The Marine Cybernetics Laboratory (MCLab) contains a basin with dimensions 40 m by 6.5 m by 1.5 m filled with fresh water, a Qualisys tracking camera system for positioning of surface vessels, a Qualisys underwater tracking system for positioning of underwater vehicles, a towing carriage, and a wave flap. It is a versatile laboratory allowing testing of control algorithms for surface and underwater vehicles, testing of underwater communication systems, hybrid model-tests, identification of hydrodynamic coefficients, and drag tests of slender marine structures, to name a few applications. Figure B.4 shows the DHI[1] wavemaker to the left, and to the right Cybership 3 is on DP, Cybership Enterprise to the front left is on remote control, and a remotely operated vehicle (ROV) that master students designed and built can be seen under water between the two surface models.

[1] www.dhigroup.com

Figure B.4: (left) DHI wavemaker and (right) marine operation in the MCLab featuring Cybership 3 on DP, Cybership Enterprise in front to the left, and a remotely operated vehicle (ROV) Neptunus designed and built by students under water between the surface models.

Control System

Cybership 3 has an onboard computer, a compact rio (cRIO) from National Instruments[2] (NI), which controls the three thrusters. The DP control algorithms, may be made in Matlab/Simulink, and are compiled to a NI Veristand executable file, and then transferred to the cRIO. During tests the user can monitor, change and save parameters online from the workspace, which is customized by the user.

The primary control loop of the cRIO is set to have a sampling time of 0.01 seconds as default, however the system may lag a bit if many custom devices are connected, especially joystick through Raspberry Pi. The user can log the execution time of each of the control loops in the NI software, see http://www.ni.com/product-documentation/13033/en/, and compute an approximate loop time by adding the following times together:

- Time step duration - the duration in microseconds of the last model time step, which is the execution time of the Matlab/Simulink executable file.
- LP loop duration - duration of the data processing loop in nanoseconds.
- HP loop duration - the duration of the primary control loop in nanoseconds.

During multiple experiments in 2015 and 2016, the slightly higher sampling time of 0.0133 seconds when including a joystick, and 0.0121 seconds when not, did not have any noticeable effects on the DP system performance when running. However, if the software includes Fourier analysis or other sample time sensitive algorithms, correcting for this lag is essential.

On a related note, the thrusters on Cybership 3 are over dimensioned relative to the scale of the vessel, and are powerful. Therefore it is recommended to have an emergency solution for disabling the thrusters, and to start with low controller gains.

[2] www.ni.com

Qualisys Camera System

The position and orientation in 6 DOFs are measured by the Qualisys camera system. Three cameras take pictures of the position of the reflector balls on Cybership 3, see Figure 3.5. The way the reflector balls are set up here, the highest one (port side around frame three), is positioned $(x, y, z) = (510, -180, -860)$ mm from the center of gravity (CG). Selecting this marker in the Qualisys trackmanager software, and translating the Qualisys coordinate system by the (x, y, z)-values given above, then the center of the body frame is approximately in the CG of the model. This will give a positive z-reading since the CG is placed just below the waterline, see Figure B.3. In addition, the global reference frame was at this time calibrated so that z=0 was about 5 cm above the water surface.

Signal freeze is relatively common to experience with the Qualisys cameras. Including some simple signal freeze detection in order to enable dead reckoning for a model-based observer was found to be helpful. Depending on how well the Qualisys cameras are calibrated, the signal may jump where there is an overlap between different camera views. The accuracy of optical position measurements is around ± 0.5 mm, and optical angle measurements is around $\pm 0.1^\circ$, and the measurements are sampled at 50 Hz. Realistic noise and sampling of the measurements could be added after signal processing.

Wave Flap

The wave flap is a single hinged flap DHI wavemaker[3] that can produce long-crested regular and irregular waves from a user-specified wave spectrum. The largest spectrum the flap can produce has significant wave height and peak period around $(H_s, T_p) = (0.15\text{m}, 1.5\text{s})$. For Cybership 3 (scale 1:30) $H_s = 0.1m$ corresponds to $H_s = 3m$ in full-scale. However, since the top of Cybership 3 is not watertight, $(H_s, T_p) = (0.04, 0.8)$ is a good place to start. The wave flap does not allow for changing sea states at the time of writing this.

If knowledge of the exact sea state is important for the results, measuring the wave elevation at the center of the basin where the model is placed during experiments is recommended. After the experiments for Paper A the wave elevation was recorded at different positions along the center of the basin, revealing that there are significant wall effects leading to energy dissipation when the waves travel along the basin. A wave probe generally measures with ± 1 mm accuracy.

In addition to this, the transfer function in the wavemaker software relating the wave elevation time series to the flap position time series does not conserve energy. Therefore, in order to have the exact (H_s, T_p) as specified in the basin, the flap should be calibrated before each experiment.

Hydrodynamic Error Sources

The flow of water in a model tank may be affected by the size of the model relative to the tank, the tank dimensions relative to the wave parameters, and many others. Some considerations are named below (Steen, 2014).

[3] www.dhigroup.com

- Blockage effects: The flow past the model may be partially blocked due to the large size of Cybership 3, especially for large heading angles (West and Apelt, 1982). Therefore unwanted hydrodynamic effects may be induced by tank walls and floor.
- Wave reflection and tank wall effects: If the model is stationary, or with forward speed, it generates a transverse wave system that will be reflected on the tank walls. For low towing speed the reflected waves will hit the model, and influence the response of the model. To avoid tank wall interference for head sea make sure the towing speed $U > U_{crit}$, defined as

$$U_{crit} = \frac{g}{2\omega}\left[\sqrt{1 + \frac{2L_M}{B_t}} - 1\right],$$

  where L_M is the model length and B_t is the breadth of the tank. Usually for following seas, interference occurs for models longer than $0.25B_t$, which is the case for Cybership 3.
- Scale effects: If operating close to resonance, the damping of the model is important to capture correctly, especially if the results are used for full-scale design validation.
- Wave parameters and spectral shape: Propagating waves may change downstream, especially in long and narrow model tanks. Waves should therefore be measured along the tank in the center of the basin, as mentioned briefly above.
- Length of records: As a rule of thumb, the length of the time series should be 1000 seconds in full-scale if only wave frequency effects are to be captured. This corresponds to 183 seconds long time series for Cybership 3, after the controller has reached steady state. If low-frequency effects are to be captured, experiments of at least 45 minutes should be performed.

B.2 Research Vessel Gunnerus

R/V Gunnerus is a NTNU-owned and operated ship which was put into operation in the spring of 2005. The vessel is a test platform for biologists, archeologists, marine robotics, and recently for DP and autopilot testing that is reported in Skjetne et al. (2017) (Paper I). In the winter of 2015 the main propulsion was changed from two conventional fixed-pitch propeller-rudder combinations to two Rolls Royce rim-driven azimuthing thrusters (Steen et al., 2016). The main parameters are given at the top of Table B.3. Parameters specific for the loading condition during DP tests in 2013, presented in Brodtkorb et al. (2017a) Paper B are given below the double line. Notice that the draught for this loading condition is smaller than the design draught. The values given in Table B.3 and a hull geometry file were inputs to ShipX for calculation of complex transfer functions. The cruising speed of R/V Gunnerus is 9.4 knots (4.84 m/s).

Table B.3: R/V Gunnerus principle hull data and structure mass distribution.

Principle hull data	
Length over all, L_{oa}	31.25 m
Length between perpendiculars, L_{pp}	28.90 m
Length in waterline, L_{wl}	29.90 m
Breadth middle, B_m	9.60 m
Breadth extreme, B	9.90 m
Depth mld. Main deck D_m	4.20 m
Draught (design), T	2.70 m
Dead weight	107 000 kg
Mast/antenna height	14.85 / 19.70 m
Block coefficient, C_B	0.56 [-]
Waterplane area coefficient, C_{WP}	0.837 [-]
Prismatic coefficient, C_p	0.653 [-]
Mid section area coefficient, C_m	0.855 [-]

Structure mass distribution during 2013 DP tests	
Displacement, Δ	417 000 kg
Wetted surface, S	353.24 m^2
Draught (loading condition), T	2.630 m
Vertical center of buoyancy, KB	1.591 m
Vertical center of gravity, VCG	2.630 m
Longitudinal center of buoyancy, LCB	13.202 m
Longitudinal center of gravity, LCG	13.202 m
Longitudinal metacentric height, GM_L	31.545 m
Transverse metacentric height, GM_T	2.663 m
Roll radius of gyration, r_{44}	3.840 m
Pitch radius of gyration, r_{55}	7.225 m
Yaw radius of gyration, r_{66}	7.225 m
Roll-yaw radius of gyration, r_{46}	0.000 m

B.2.1 Wave Resistance Coefficients

The wave resistance, wave coefficients, sinkage and trim were calculated, and are given in Tables B.4 and B.5. These were not directly used in this work, however they are included for a sense of completion. The calculations are done for the same structure mass distribution as given in Table B.3. An explanation of the parameters in Tables B.4 and B.5 is given below.

- $U_{s,n}$ - forward speed of the ship (knots).
- U_s - forward speed of the ship (m/s).
- F_N - Froude number $F_N = U_s/\sqrt{gL}$.
- C_w - wave resistance coefficient.
- $C_{r,c}$ - residual resistance coefficient (form factor calculated by program). In Table B.4 this coefficient is split into linear, nonlinear and total coefficient.
- $C_{r,u}$ - residual resistance coefficient (form factor input by user).
- C_f - frictional resistance coefficient for ship.
- F_{ds} - increase of wetted surface divided by nominal wetted surface.

The form factor calculated by the program is calculated as follows:

- For $C_B < 0.6$ Holtrop's form factor is applied.
- For $C_B > 0.7$ MARINTEK's form factor is applied.
- For $0.6 < C_B < 0.7$ a transition between the two are applied.

R/V Gunnerus has $C_B = 0.56$ (Table B.3), and hence the Holtrop's form factor was applied. The form factor calculated by the program was $(1 + k) = 1.3892$, and the form factor given by the user was $(1 + k) = 1.2353$.

- C_{33} - heave restoring coefficient.
- C_{55} - pitch restoring coefficient.
- AP - aft perpendicular.
- FP - fore perpendicular.

Table B.4: R/V Gunnerus wave resistance coefficients [-].

$U_{s,n}$ [kn]	U_s [m/s]	F_N	$C_{w,lin}$	$C_{w,nl}$	$C_{w,tot}$	$C_{r,c}$	$C_{r,u}$	C_f	F_{ds}
5.237	2.694	0.157	0.3766E-03	0.0000E+00	0.3766E-03	0.3920E-03	0.3903E-03	0.2192E-02	0.5046E-02
5.892	3.031	0.177	0.5710E-03	0.0000E+00	0.5710E-03	0.5904E-03	0.5883E-03	0.2154E-02	0.6472E-02
6.547	3.368	0.196	0.9830E-03	0.0000E+00	0.9830E-03	0.1007E-02	0.1004E-02	0.2121E-02	0.8156E-02
7.200	3.704	0.216	0.1086E-02	0.0000E+00	0.1086E-02	0.1115E-02	0.1112E-02	0.2091E-02	0.9950E-02
7.855	4.041	0.236	0.1739E-02	0.0000E+00	0.1739E-02	0.1773E-02	0.1770E-02	0.2065E-02	0.1205E-01
8.510	4.378	0.255	0.1724E-02	0.0000E+00	0.1724E-02	0.1765E-02	0.1760E-02	0.2042E-02	0.1426E-01
9.165	4.715	0.275	0.2952E-02	0.0000E+00	0.2952E-02	0.3000E-02	0.2995E-02	0.2020E-02	0.1714E-01
9.818	5.051	0.295	0.3834E-02	0.0000E+00	0.3834E-02	0.3892E-02	0.3886E-02	0.2000E-02	0.2067E-01
10.473	5.388	0.314	0.4184E-02	0.0000E+00	0.4184E-02	0.4248E-02	0.4241E-02	0.1982E-02	0.2329E-01
11.129	5.725	0.334	0.4665E-02	0.0000E+00	0.4665E-02	0.4736E-02	0.4728E-02	0.1965E-02	0.2620E-01

Table B.5: R/V Gunnerus running sinkage and trim, positive sinkage is up, and positive trim is bow up.

$U_{s,n}$ [kn]	C_{33} [kN/m]	C_{55} [kN/rad]	Sinkage [m]	Trim [deg]	Sinkage AP [m]	Sinkage FP [m]
5.237	0.2277E+04	0.1370E+06	-0.0297	-0.0527	-0.0164	-0.0430
5.892	0.2277E+04	0.1370E+06	-0.0381	-0.0671	-0.0212	-0.0551
6.547	0.2277E+04	0.1370E+06	-0.0481	-0.0830	-0.0271	-0.0690
7.200	0.2277E+04	0.1370E+06	-0.0586	-0.1068	-0.0317	-0.0856
7.855	0.2277E+04	0.1370E+06	-0.0710	-0.1240	-0.0397	-0.1023
8.510	0.2277E+04	0.1370E+06	-0.0840	-0.1557	-0.0448	-0.1233
9.165	0.2277E+04	0.1370E+06	-0.1010	-0.1680	-0.0587	-0.1434
9.818	0.2277E+04	0.1370E+06	-0.1218	-0.1358	-0.0876	-0.1561
10.473	0.2277E+04	0.1370E+06	-0.1372	-0.1503	-0.0993	-0.1751
11.129	0.2277E+04	0.1370E+06	-0.1544	-0.1846	-0.1078	-0.2009

Part II

Selected Publications
- Beads On A String -

Paper A:

Sea State Estimation Using Model-scale DP Measurements

Astrid H. Brodtkorb, Ulrik D. Nielsen, Asgeir J. Sørensen

MTS/IEEE OCEANS 2015 - Washington, DC, 2015, pp. 1-7,
doi: 10.23919/OCEANS.2015.7404402.

Note that there is a typing error in Table II in the version available online.
PM1 should have $H_s = 0.05$ m and $T_p = 0.9$ s.
This is corrected here.

Sea State Estimation Using Model-scale DP Measurements*

Astrid H. Brodtkorb[1] and Ulrik D. Nielsen[1,2] and Asgeir J. Sørensen[1]

Abstract— **Complex marine operations are moving further from shore, into deeper waters, and harsher environments. The operating hours of a vessel are weather dependent, and good knowledge of the prevailing weather conditions may ensure cost-efficient and safe operations. This paper considers the estimation of the peak wave frequency of the on-site sea state based on the vessel's motion in waves. A sea state can be described by significant wave height, peak wave frequency, wave direction, and often wind speed and direction are added as well. The signal-based algorithm presented in this paper is based on Fourier transforms of the vessel response in heave, roll and pitch. The measurements are used directly to obtain an estimate of the peak frequency of the waves. Experimental results from model-scale offshore ship runs at the Marine Cybernetics Laboratory (MCLab) at NTNU demonstrate the performance of the proposed sea state estimation algorithm.**

I. INTRODUCTION

Most marine operations are highly dependent on the Captain's experience, and his ability to make correct decisions in stressful situations. In addition it is often difficult for operators to judge the sea state only by visual observations especially from large vessels. A decision support system (DSS) containing detailed information about the on-site sea state contributes to the Captain's decision making process. Developing such decision support tools has seen an increasing interest over the years.

The sea state can for instance be estimated using a wave rider buoy, wave radar, or satellite images of the ocean topology. Traditionally the wave rider buoy has been a provider of such data, contributing greatly to the weather forecasts offshore. However, these are at fixed locations, and most likely not able to provide information of the on-site sea state where the particular operation is taking place. Installing a wave radar is fairly costly, and the system itself requires careful tuning on a daily basis. [1] proposes an algorithm for predicting the short-crested sea state based on wave radar measurements. The algorithm estimates the local sea state, and in special conditions it has been used to recreate actual wave trains. However it is a computationally demanding algorithm which depends fundamentally on the radar measurements to be regularly calibrated, see [2] and [3]. Moreover, the algorithm requires independent radar measurements and, thus two radar systems are needed if navigation and sea state estimation should happen simultaneously. Satellite images are dependent on low cloud cover for quality of the data gathered. Inevitably the cloud cover becomes thicker at times when the sea state estimate may be of greater interest.

Today, the majority of marine vessels are equipped with various sensors to measure operational state and performance such as global wave-induced motions, fuel consumption, hull girder stresses and geographical position. One example is DP ships which typically are installed with motion reference units, gyros and position measurement systems. In this sense, the marine vessels are indirectly equipped with sea state measuring systems, since the sensor measurements can be used to infer about the on-site sea state. Thus, the thought of using ships as wave buoys has been explored quite extensively the last 10-15 years, e.g. [4], [5], [6] and [7]. One proposed method is called the *wave buoy analogy*, where the ship motions in 6 degrees of freedom (DOF), or other global ship responses such as hull girder stresses, are transformed into the frequency domain, and an estimate of the wave spectrum is obtained by means of parametric or Bayesian modeling. This method takes the vessel's motion response amplitude operators (RAOs), also called transfer functions, into account when estimating the wave spectrum and/or associated sea state parameters such as the peak wave frequency ω_p, significant wave height H_s and relative wave direction β. As noted, the estimation method relies on both measurements – the measured signals – and transfer functions to model the theoretical relation between the waves and vessel responses. In this respect, the method is partly signal-based and partly model-based. However, for referencing from here on the term model-based will be used. This term is also useful to distinct the procedure from a signal-based method which is based solely on measured signals.

A signal-based approach has been applied in a hybrid controller which switches between candidate controllers based on an estimate of the peak wave frequency, see [8], [9], and [10]. The method does not consider the vessel's motion RAOs, and hence cannot estimate H_s or β, but it has been shown to track a changing sea state reasonably well. This paper looks further into the properties of this particular algorithm.

Other types of signal-based methods exist, as shown in [11], [12], [13] and, although state-of-the-art techniques allows for peak wave frequency estimation only, theoretical studies have been initiated towards estimation of significant wave height H_s and wave direction β as well, see [14]. The development of a (complete) signal-based method for sea state estimation, including H_s and β would be considered a very important step improving planning and execution of

*This work was supported by the Research Council of Norway through the Centres of Excellence funding scheme, project number 223254 AMOS.

[1]Centre for Autonomous Marine Operations (AMOS), Department of Marine Technology, Norwegian University of Science and Technology (NTNU), Otto Nielsens vei 10, 7491 Trondheim, Norway

[2] DTU Mechanical Engineering, Technical University of Denmark, Kgs. Lyngby, Denmark

marine operations including DP and transit.

This paper presents one signal-based estimation algorithm, and it is applied to measurements from a model-scale vessel controlled by a DP system. The vessel is freely floating, using the thrusters as sole means of keeping a constant position. Model-scale experiments are done of different cases including various relative wave directions β and loading conditions in several sea states.

The paper is organized as follows: Section II gives a brief introduction to DP, as this is a required tool for collecting data to be used in the estimation method. Section III describes the signal-based sea state estimation method including a small example. The experimental setup as well as validation of the experimental results is presented in Section IV, before the estimation results are presented and discussed in Section V. Section VI concludes the paper.

II. Dynamic Positioning of Marine Vessels

A DP control system should control the vessel position and heading to a fixed setpoint or pre-determined track (low speed) solely by using the thrusters of the vessel [15]. This control objective can be expressed as

$$\lim_{t\to\infty} \boldsymbol{\eta}^{LF}(t) - \boldsymbol{\eta}^{*}(t) \to \mathbf{0} \tag{1}$$

where $\boldsymbol{\eta}^{LF}(t)$ is the low frequency vessel position vector, and $\boldsymbol{\eta}^{*}(t)$ is the desired position vector. Normally for a ship in DP the position in surge and sway and the heading angle are controlled. This means that the heave, roll and pitch can be seen as uninfluenced by the control system, and hence these degrees of freedom (DOF) can be used in sea state estimation, as done later in the paper. However, as shown in [16], this may not be the case for semisubmersibles with small water-plane-area where the roll and pitch may be influenced by the DP system. Normally the position measurement at time t can be expressed as

$$\mathbf{y}(t) = \boldsymbol{\eta}^{LF}(t) + \boldsymbol{\eta}^{WF}(t) + \mathbf{v}(t), \tag{2}$$

where $\boldsymbol{\eta}^{LF}(t)$ is the low frequency vessel position vector induced by slowly varying forces from the environment and thrusters, $\boldsymbol{\eta}^{WF}(t)$ is the first order wave frequency motion and $\mathbf{v}(t)$ is the sensor noise vector.

$\boldsymbol{\eta}^{LF}(t)$ is not available directly from (2), so therefore an observer of the type Kalman filter or nonlinear passive observer, is required to provide a state estimate by filtering out the wave frequency motions, sensor noise, and estimating bias from slowly varying environmental forces and unmodeled dynamics. The wave frequency motion is filtered out to reduce unnecessary wear and tear on the propulsion system. Sensor-based observers such as IMU integration filters, see [17], [18] and model-based observers such as the extended Kalman Filter, see [19], [20] or passive nonlinear observers, see [21] are often applied to DP.

The control algorithm takes in the estimated vessel position and velocity vectors $\hat{\boldsymbol{\eta}}^{LF}, \hat{\boldsymbol{\nu}}$ from the observer and compares it with the desired vessel position $\boldsymbol{\eta}^{*}(t)$ to calculate a control input $\mathbf{u}$, here exemplified by a nonlinear PID controller:

$$\begin{aligned}\mathbf{u} = &-\mathbf{R}^{T}(\psi)\mathbf{K}_p(\hat{\boldsymbol{\eta}}^{LF} - \boldsymbol{\eta}^{*}) - \mathbf{K}_d\hat{\boldsymbol{\nu}} \\ &- \mathbf{R}^{T}(\psi)\mathbf{K}_i\int_0^t(\hat{\boldsymbol{\eta}}^{LF} - \boldsymbol{\eta}^{*})dt,\end{aligned} \tag{3}$$

where $\mathbf{K}_p, \mathbf{K}_d, \mathbf{K}_i$ are the nonnegative proportional, derivative and integral gain matrices, respectively. The different parts required for the DP system to fulfill the control objective (1) are described in detail in [22], [23], [24].

III. Signal-Based Sea State Estimation Algorithm

The signal-based method presented in this paper, is solely based on the measurements, i.e. the procedure does not require knowledge of the vessel motion RAOs, and in this way it is a purely signal-based method. This is in contrast to the wave buoy analogy which is model-based; because of the need for RAOs. The present approach is based on Fourier transforms, where N samples of heave, roll and pitch motion in the time domain are transformed to the frequency domain, and an estimate of the peak wave frequency $\hat{\omega}_p$ is computed based on the resulting response spectra of the three motion components heave, roll and pitch.

A. Assumptions on Time Domain Vessel Response

In small to relatively high sea states, linear theory is often sufficient to describe irregular wave-induced motions on marine vessels [25]. The first order wave-induced response $\boldsymbol{\eta}^{WF} \in \mathbb{R}^6$ in irregular waves can be written as a finite sum of sinusoidal components with different amplitudes $\mathbf{a}_j \in \mathbb{R}^6$, frequencies ω_j, wave numbers k_j, relative direction β_j, and random phases $\epsilon_j \in [0,\ 2\pi]$:

$$\boldsymbol{\eta}^{WF} = \sum_{j=0}^{J-1} \mathbf{a}_j \sin(\omega_j t - k_j x\cos(\beta_j) - k_j y \sin(\beta_j) + \epsilon_j + \boldsymbol{\gamma}_j).$$

$\boldsymbol{\gamma}_j \in \mathbb{R}^6$ is the vector of phase of the low frequency position and phase of the RAOs. Here $\beta = 0^\circ$ is head sea, and $\beta = 180^\circ$ is following sea.

The low frequency vessel motion is usually modeled as a mass-damper-spring system subject to forces from current, wind, and mean and slowly varying forces due to wave loads. For a vessel on DP the thrusters will produce mean and slowly varying forces to cancel those from the environment. Slowly varying forces are modeled as sinusoidal components with frequency $(\omega_j - \omega_i)$, and therefore:

$$\boldsymbol{\eta} = \boldsymbol{\eta}^{LF} + \boldsymbol{\eta}^{WF} = \sum_{m=0}^{M-1} \mathbf{A}_m \sin(\omega_m t + \boldsymbol{\Gamma}_m) \tag{4}$$

where ω_m spans both the low frequency and wave frequency regime, $\mathbf{A}_m \in \mathbb{R}^6$ is the vector of low frequency and wave frequency amplitudes, and $\boldsymbol{\Gamma}_m \in \mathbb{R}^6$ is the total phase shift vector relative to the wave elevation.

The Fourier transform approach requires that the response due to any irregular wave train can be described by (4), and that the wave-induced vessel motions are small and in steady

state. The steady state assumption may be relaxed, see for instance [13].

B. Fast Fourier Transform of Vessel Response

The DP measurements (2) are sampled every $T > 0$ seconds, and $N \in \mathbb{Z}_{\geq 1}$ consecutive measurements are stored in a shift register with state $\boldsymbol{\chi} = [\boldsymbol{\chi}_1, ..., \boldsymbol{\chi}_N]^T \in \mathbb{R}^{6N}$, where $\boldsymbol{\chi}_k \in \mathbb{R}^6$, $k \in \{0, \ldots, N-1\}$ are the stored measurements. The state component $\boldsymbol{\chi}_1$ contains the most recent sample, and $\boldsymbol{\chi}_N$ contains the least recent sample.

$$\boldsymbol{\chi}_1^+ = \mathbf{y} \tag{5a}$$
$$\boldsymbol{\chi}_2^+ = \boldsymbol{\chi}_1 \tag{5b}$$
$$\vdots$$
$$\boldsymbol{\chi}_N^+ = \boldsymbol{\chi}_{N-1} \tag{5c}$$

The fast Fourier transform (FFT) is applied to $\boldsymbol{\chi}$ in order to generate the response spectra. The time for each sample is defined as $t_k = Tk$ so that $t_k = \{0, ..., Nk\}$. We want to determine a complex polynomial $\mathbf{q}(\boldsymbol{\chi}) \in \mathbb{R}^6$ with $i = \sqrt{-1}$

$$\mathbf{q}(\boldsymbol{\chi}) = \sum_{n=0}^{N-1} \mathbf{c}_n e^{int_k}, \tag{6}$$

which interpolates $\boldsymbol{\eta}$ in (4), i.e. we need to find the coefficients $\mathbf{c}_0, ..., \mathbf{c}_{N-1}$ so that $\boldsymbol{\eta}_k = \mathbf{q}(\boldsymbol{\chi}_k)$. The coefficients are found by the formula:

$$\mathbf{c}_n = \frac{1}{N} \sum_{k=0}^{N-1} \boldsymbol{\chi}_k e^{-int_k}, \; n = \{0, ..., N-1\}. \tag{7}$$

The real part of the spectral amplitude $\mathbf{S}_\eta(f) \in \mathbb{R}^{6N}$ of the measurements are then given by

$$\mathbf{S}_\eta(f) = Re\left\{\mathbf{F}_N^6 \boldsymbol{\chi}\right\} \tag{8}$$

where $\mathbf{F}_N^6 \in \mathbb{R}^{6N \times 6N}$ is the stacked $N \times N$ Fourier matrix for all 6 DOFs, i.e. all elements of $\mathbf{F}_N$ are multiplied by the 6×6 identity matrix. $\mathbf{F}_N$ has the form

$$\mathbf{F}_N = \begin{bmatrix} 1 & 1 & ... & 1 \\ e^{-it_0} & e^{-it_1} & ... & e^{-it_{N-1}} \\ e^{-i2t_0} & e^{-i2t_1} & ... & e^{-i2t_{N-1}} \\ \vdots & \vdots & \vdots & \vdots \\ e^{-i(N-1)t_0} & e^{-i(N-1)t_1} & ... & e^{-i(N-1)t_{N-1}} \end{bmatrix}.$$

The FFT solves (8) by splitting the problem into even and odd parts, which reduces the number of operations from $O(N^2)$ for normal discrete Fourier transform to $O(N)\log_2 N$. For more on Fourier transforms, see for instance [26].

In this setting it is more convenient to have the spectrum and frequencies related to angular frequency $\omega = 2\pi f$

$$\mathbf{S}_\eta(\omega) = \frac{T}{\pi} \mathbf{S}_\eta(f). \tag{9}$$

The function $\Upsilon : \mathbb{R}^{6N} \to \mathbb{R}_{\geq 0}$ operates on $\mathbf{S}_\eta(\omega)$, returning the peak frequencies in each DOF $\omega_{p,i}$, $i = \{1, ..6\}$. In this paper the estimate of the peak wave frequency is the average of the heave, roll and pitch peak frequencies

$$\hat{\omega}_p = \frac{\omega_{p,3} + \omega_{p,4} + \omega_{p,5}}{3}. \tag{10}$$

In the case where the response has multiple peaks, the frequency corresponding to the largest is utilized. In different sea states the vessel responds little in some DOFs and more in others. To make sure that the algorithm is robust, the estimate is taken as the average of the heave, roll and pitch motions.

Figure 1 shows a time series of heave and the corresponding response spectrum when (8) and (9) are applied to the series. The measured incident wave spectrum is also shown.

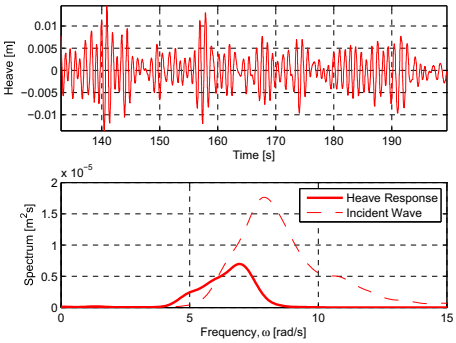

Fig. 1. Signal-based algorithm applied to a time series in heave; time series shown above and spectrum below. The spectrum of the heave response is plotted together with the FFT of the measured incident wave.

The response spectrum in each DOF is here found by using the Matlab toolbox WAFO [27], which is based on the built-in matlab function `fft`. See [10] to see how the estimation algorithm is implemented in a controller.

IV. Experimental Setup and Validation of Measurements

This section gives a brief introduction to the experimental facilities and presents the test cases. A thorough validation of the measurements was done, and it is also discussed.

A. Vessel and Laboratory Facilities

The Marine Cybernetics Laboratory (MCLab) at NTNU, Trondheim was used for the experiments. It includes a basin with dimensions ($L \times B \times D$) 40 m $\times$ 6.45 m $\times$ 1.41 m, a camera positioning system that provides position and orientation measurements to the DP system, and a wave flap[1] for generating sea states from different wave spectra. Figure 2 shows the camera system and the model vessel in action.

The experiments were conducted with Cybership 3, a 1:30 scale model of a platform supply vessel (PSV) with dimensions $L_{pp} = 1.971$ m and $B = 0.437$ m. It is equipped

[1]DHI Wave Synthesizer, www.dhigroup.com.

Fig. 2. Cybership 3 in action. The three cameras measuring position are seen above the bridge structure, and the surface elevation is measured to the far right at the wooden plank.

with three azimuth thrusters, two stern with fixed angles of $\pm 30\,^\circ$ and one in the bow at $90\,^\circ$, see Figure 3. The vessel has eight 12 V batteries supplying power to the thrusters and a National Instruments CompactRio (cRIO) where the DP control system is running. The operator supplies setpoints and specifies controller gains from a laptop, see Figure 4. Communication between the camera system, operator laptop and cRIO is via ethernet.

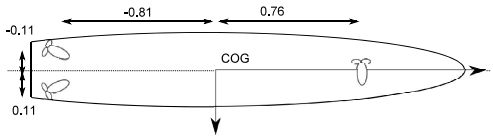

Fig. 3. Thruster configuration of Cybership 3.

B. Experimental Test Cases

Different cases were run with combinations of wave spectra with (H_s, T_p), relative wave direction β and loading conditions (LC), see Table I. The sea state numbers (SSn) are defined in Table II. The values within the parenthesis $\{...\}$ in Table I are the ones changing in the case, e.g. for Case 1-3 the heading is changed for three different JONSWAP spectra J1, J2 and J3. Case a corresponds to $\beta = 0°$, Case b to $\beta = 10°$, and Case c to $\beta = 20°$.

Common wave spectra used in the North Sea include the wind-generated JONSWAP (Joint North Sea Wave Project)

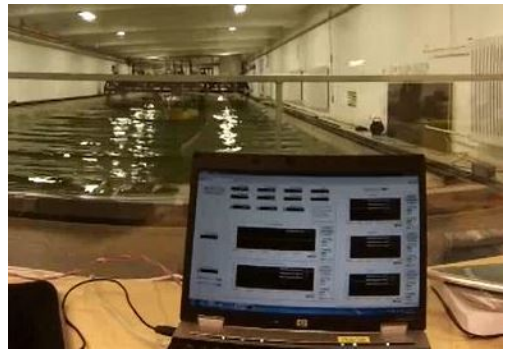

Fig. 4. Operator laptop where DP setpoints and controller gains are specified. The wave flap is also seen directly behind the laptop.

for developing sea states and the Pierson Moskovitz spectra for fully developed sea states, which are both single-peaked spectra. The Torsethaugen spectrum is also widely used to describe sea states in the North Sea. However, this is a double peaked spectrum and is not investigated in this paper. Experimental tests were done with a double-peaked spectrum: Case 4, but these results are omitted here, as further elaboration of the estimation method is needed to handle double-peaked spectra.

TABLE I

THE TEST CASES RUN IN MODEL-SCALE. LC = LOAD CONDITION; LC = 1 NORMAL, LC=2 8.6% EXTRA WEIGHT.

Case no.	SSn	β[°]	LC
1a,b,c	J1	$\{0, 10, 20\}$	1
2a,b,c	J2	$\{0, 10, 20\}$	1
3a,b,c	J3	$\{0, 10, 20\}$	1
5a,b,c	J1	$\{0, 10, 20\}$	2
5d	J4	0	2
6a,b,c	{J1, J2, J3}	180	1
7	J4	0	1
8a,b,c	PM1	$\{0, 10, 20\}$	1
9a,b,c	{J1, J2, J3}	160	1
10a,b	{J1, J2}	30	1

TABLE II

DEFINITION OF THE SEA STATE NUMBER (SSN) WITH SPECTER TYPE, H_s AND T_p.

SSn	Specter type	H_s [m]	T_p [s]
J1	JONSWAP	0.04	0.8
J2	JONSWAP	0.05	0.9
J3	JONSWAP	0.05	1.5
J4	JONSWAP	0.10	1.5
PM1	Pierson Moskovitz	0.05	0.9

C. Validation of Measurements

In this section the measurements of wave elevation and vessel response are validated. Two main issues relating to the measurements were found while processing the results, the first relates to the motion RAOs, and the second involves

the sample time of the cRIO used for DP control and data logging.

1) Motion RAOs: Cybership 3 is a model made by MARINTEK in 1988, with RAO data from this time period as well. Since then the instrumentation onboard has changed, tha actual mass and mass distribution have changed as well. New RAOs were made by first finding the new center of gravity, the gyroradii and moments of inertia giving the mass distribution, waterline and trim. A ship lines plan was made from a rather coarse panel model, and the MARINTEK software Veres ShipX was used to calculate the motion RAOs in the center of gravity. The new motion RAOs have not been verified experimentally, although dedicated studies in this respect should be considered, as the effect of the coarse geometry file is unknown.

The response measurements of the vessel were taken at a point different from the center of gravity, so the new motion RAOs were translated to this point. The measurement point is $r = [x_m, y_m, z_m] = [110, 0, 153]$ mm forward and above the center of gravity.

2) Sample Time of the cRIO: It was found that the cRIO did not manage to log with the specified sample time of $T = 0.01$ s. The reason for the lag is that the model needed to wait for the other system loops in order to execute, and the total loop time of all control loops[2] was $T = 0.0133$ s. As a result all logged measurements have sample time $T = 0.0133$ s. For future tests it is advised to log the loop times of the individual control loops in addition to the system sample time.

Figure 5 shows a typical validation result for the measured surface elevation and pitch response. The top plot shows the wave spectrum specified in the wavemaker (dashed line) and the measured spectrum. The wave spectra have similar shapes and contain similar amounts of energy. The peaks are shifted slightly, and there are several possible reasons for this, for instance that the waves might not have been perfectly long-crested, the surface elevation was not measured at the center of the basin, reflections from the tank walls and wave beach, the tank filling, and calibration of the measurement device.

The middle plot shows the motion RAO for pitch for $\beta = 0°$. Pitch has two prominent resonance peaks at 4.9 and 7.7 rad/s with the lower having the higher amplitude. The resonance frequencies in heave are $6.2 - 6.9$ rad/s for the different headings, and roll has one narrow peak at 6.7 rad/s. The shapes of the RAOs reveal that heave and pitch respond significantly to a broader range of frequencies than roll.

The bottom plot shows the pitch response spectrum obtained by the measured signal with corrected sample time (bold), and the theoretical response calculated based on the new motion RAO. It is observed that the frequency and magnitude of both peaks correspond reasonably well, though

[2]An illustration of the system architecture of the National Instruments Veristand Engine is found here: http://www.ni.com/product-documentation/13033/en/

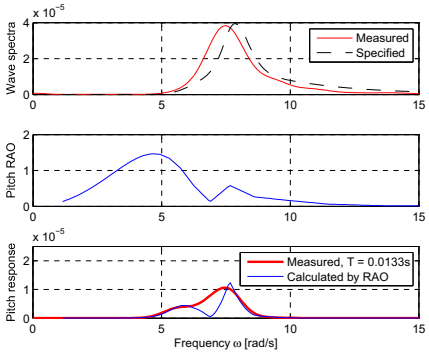

Fig. 5. Validation of the wave elevation from the JONSWAP J1 spectrum and pitch angle measurements for head sea $\beta = 0°$. Above: Measured and specified wave spectra, Middle: Pitch motion RAO for $\beta = 0°$, Below: Theoretical calculated response based on the RAO and the measured response with corrected sample time.

the cancellation effect at around 7 rad/s is not captured in the measurements.

Generally the frequencies of the peaks correspond very well, but the amplitudes are often off. Usually the amplitude of the measured response is higher than the theoretical calculated using RAOs, which means that the energy present at the different frequencies is larger in the experiment.

One explanation for this behaviour is that the DP system keeps the specified heading relative to the waves β with an accuracy of around $\pm 3°$. Since the motion RAO changes in amplitude with β, the theoretical and measured amplitudes do not match up. This is very prominent in roll, where the amplitude of the roll RAO more than doubles for each $10°$ when $\beta \in \{0°, 90°\}$, with a similar decrease for $\beta \in \{90°, 180°\}$. The heave amplitudes generally agree more than illustrated by pitch in Figure 5, though the fit depends highly on the incident sea state. Alongside the DP system, a sea state that is not perfectly long-crested, may have the same effect on the response amplitudes.

In conclusion, the measurements correspond reasonably well with theory, and the observed deviations are justified.

V. Estimation Results and Discussion

In this section the estimation results of the signal-based estimation algorithm applied to the measurements are presented and discussed.

A. Results

An example of typical response spectra is shown in Figure 6. The incident wave spectra (bold red) is from J3 (JONSWAP with $(H_s, T_p) = (0.05, 1.5)$) with $\beta = 20°$, and the response in all DOFs are plotted, even though only heave, roll and pitch are used in the estimation. In the figure, the response peaks are grouped around two main frequencies, the wave, heave, pitch, surge and yaw around 4.2 rad/s and roll, heave and sway around 6.2 rad/s. In the case of

headings $\beta \neq 0°$ there are large couplings. A summary of the estimation results is given in Table III presenting the arithmetic mean and standard deviation for each sea state. The error is the difference between the measured ω_p and each of $\omega_{p,3}, \omega_{p,4}, \omega_{p,5}$ as well as $\hat{\omega}_p$, i.e for heave error $= (\omega_p - \omega_{p,3})/\omega_p$. Negative error means that the peak frequency from the response is higher than the incident peak wave frequency.

The following observations can be made:

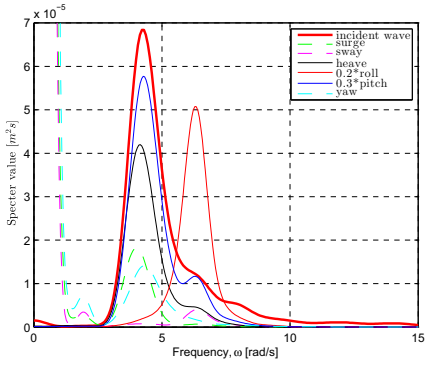

Fig. 6. Measured incident wave and measured response spectra for J3 (JONSWAP with $(H_s, T_p) = (0.05, 1.5)$) with $\beta = 20°$.

- Based on all 45 series: Pitch has the smallest absolute estimation error of 6.8%, closely followed by heave with 7.4%. Both these have fairly small standard deviations on the error, so they are the most reliable. Roll has the largest error and standard deviation of $22.2\% \pm 14.8\%$.
- Roll has the largest errors and standard deviations for all spectra except PM1, where pitch is worse. This behavior can be explained by inspecting the RAO. It is zero for small and high frequencies, and has one narrow peak at 6.7 rad/s . Only wave components with frequency close to the natural frequency are transferred to the response, and hence wave spectra with peaks far away from the natural frequency in roll worsens the estimation, for instance when $T_p = 1.5$ s.
- PM1 and J2 both have $(H_s, T_p) = (0.05, 0.9)$, but $\hat{\omega}_p$ is very different. It is due to the wave spectrum shape; a spectrum with broader bandwidth will excite more frequencies in the response, and then the RAOs amplify a larger part of the incident wave spectrum. If the incident wave spectrum is narrow-banded, the response will naturally have smaller components outside the sea state bandwidth. Running experiments with spectra that have different peakedness would be very interesting.
- Roll estimates better for larger heading angles β, though not as well as heave and pitch. For the studied cases, better estimates would be obtained if roll was excluded. It could be interesting to see what happens for $\beta = 90°$.

TABLE III

SUMMARY OF THE RESULTS FOR $\hat{\omega}_p$ BASED ON $\omega_{p,3}, \omega_{p,4}, \omega_{p,5}$, AND $\hat{\omega}_p$ =MEAN$(\omega_{p,3}, \omega_{p,4}, \omega_{p,5})$ FOR ALL DIRECTIONS AND LOADING CONDITIONS, SORTED BY SEA STATE (SEE TABLE II FOR DETAILS ON THE SEA STATES).

Measured and estimated peak wave frequency [rad/s]

SSn		ω_p	$\omega_{p,3}$	$\omega_{p,4}$	$\omega_{p,5}$	$\hat{\omega}_p$
J1	mean	7.545	6.938	6.444	7.086	6.823
	std	0.037	0.87	0.148	0.402	0.245
	error	-	8.0 %	14.6 %	6.1 %	9.6 %
J2	mean	7.056	6.655	6.332	6.615	6.534
	std	0.000	0.107	0.089	0.213	0.136
	error	-	5.7 %	10.3 %	6.3 %	7.4 %
J3	mean	4.244	4.101	6.209	4.255	4.855
	std	0.036	0.042	0.072	0.045	0.053
	error	-	3.4 %	-46.3 %	-0.3 %	-14.4 %
J4	mean	4.257	4.109	6.199	4.224	4.844
	std	0.038	0.063	0.087	0.025	0.058
	error	-	3.5 %	-45.6 %	0.8 %	-13.8 %
PM1	mean	7.517	6.411	6.334	6.151	6.299
	std	0.153	0.107	0.040	0.337	0.161
	error	-	14.7 %	15.7 %	18.1 %	16.2 %

Measured and estimated ω_p

Case		Meas.	$\omega_{p,3}$	$\omega_{p,4}$	$\omega_{p,5}$	$\hat{\omega}_p$
1a,b,c	mean	7.517	6.978	6.468	7.112	6.853
	std	0.000	0.058	0.113	0.341	0.170
	error	-	7.2 %	13.9 %	5.4 %	8.8 %
5a,b,c	mean	7.593	6.747	6.526	7.093	6.789
	std	0.000	0.100	0.139	0.410	0.216
	error	-	11.1 %	14.1 %	6.6 %	10.6 %

Measured and estimated ω_p

β		$\omega_{p,3}$	$\omega_{p,4}$	$\omega_{p,5}$	$\hat{\omega}_p$
0	abs error	7.3 %	27.1 %	5.2 %	13.2 %
10	abs error	8.1 %	20.2 %	6.4 %	11.6 %
20	abs error	8.6 %	20.3 %	9.8 %	12.9 %
30	abs error	5.8 %	12.4 %	9.7 %	9.3 %
160	abs error	4.6 %	24.4 %	7.9 %	12.3 %
180	abs error	3.9 %	24.6 %	0.7 %	9.7 %

- Pitch is marginally better than heave for head and following seas, and heave is marginally better than pitch for headings of $20, 30, 160°$. This can again be related to the motion RAOs since the amplification in heave is larger when $\beta \in \{30° - 160°\}$ and the opposite is observed in pitch.
- Case 1 and 5 have the same environmental conditions, but Case 5 has a 8.6% increase in mass. The estimation errors are slightly smaller for Case 1 than for Case 5. However, this may be a coincidence, as the difference in the measured peak frequency is large. The same timeseries of the wave elevation was run for these cases, so the difference may be due to measurement errors.
- Inspecting the spectra for surge, sway and yaw, see Figure 6, the influence of the control system at low frequencies is noted, and the spectra do not go towards zero. This is because the thrusters insert energy at these frequencies. In the case where the observer does not filter out the wave frequency motion, the thrusters may

also contribute to energy in the wave-frequency regime.

B. Discussion with a Broader Perspective

A topic that is always worth mentioning when model-scale tests are done is whether or not the findings have validity in full-scale. The vessel itself and the RAOs are scaled using Froude scaling, meaning that gravity forces - like those exerted by non-breaking waves - are in theory scaled correctly. With Froude scaling, the vessel length and water depth are scaled by the ratio $\lambda = L_f/L_m$ (L_f is the full-scale length and L_m is the model-scale length), and time is scaled by $\sqrt{\lambda}$. In particular in the MCLab, the water depth is only 1.5 m, which scaled up to full-scale is 45 m. The waves tested in the lab have full-scale heights of $H_{s,f} = 1.2 - 3$ m and peak periods of $T_{p,f} = 4.38 - 8.21$ s, which puts the waves firmly within the shallow water regime. The thrusters and thrust losses should ideally be scaled by Reynold's scaling to get the viscous forces correct, but this is practically not possible to obtain simultaneously with Froude scaling. Effects from the DP system are probably larger than thrust scaling effects. So, all in all, the model-scale results are believed to be reasonably representative of expected behavior in full-scale.

For a vessel in transit or operation, there may be many frequencies of interest simultaneously: for instance the peak wave frequency, the encounter frequency in the case of forward speed, and the oscillation frequency of the different DOFs. These estimates are e.g. used in detection of parametric roll before it happens so that the vessel speed can be reduced, see [11], [12], active roll and pitch damping for instance in ship-platform gangways, heave compensation in cranes or risers, or directly in DP observers and controllers.

In most observers there is a wave filtering function. The filter contains a simple (synthetic) second order model of the wave motion of the vessel with a peak frequency and a damping ratio. The believed peak frequency of the waves is often applied here, see for instance [23], [22], [28], but perhaps inserting the vessel's oscillatory motions due to waves could yield even better filtering. The same sort of argument may be posed about hybrid controllers [8], [9], [10], where the controller is tuned according to the vessel's motions in a sea state, and not to the sea state directly.

VI. Conclusion

The signal-based sea state estimation algorithm based on Fourier transforms presented in this paper was demonstrated to perform quite well in experiments with the model-scale offshore ship run at the Marine Cybernetics Laboratory (MCLab) at NTNU. It was found to be the most accurate using heave and pitch responses, and for narrow-peaked incident wave spectra.

Proposed further work includes more experiments with beam seas as well as with forward speed, and looking into sea states with different peakedness and double peaks.

ACKNOWLEDGMENT

A special thanks to Torgeir Wahl for helping out with the model experiments, and to Trond Innset and Lars Øien for helping with the calculation of new RAOs.

APPENDIX

TABLE IV

PARAMETERS FOR CYBERSHIP 3 (MODEL-SCALE). "OLD" VALUES ARE FROM 1988, AND "NEW" VALUES ARE FROM 2015.

Parameter		Old	New	Comment
Mass	[kg]	74.7	86.5	
Waterline	[m]	0.153	0.154	Rel. to baseline
Trim	[°]	0	0	
Center	x [m]	1.005	0.925	Rel. to AP
of	y "	0	0	
Gravity	z "	0.1956	0.1105	Rel. to baseline
Moment	J_{xx} [kgm^2]	2.192	1.584	
of	J_{yy} "	19.72	18.939	
Inertia	J_{zz} "	19.72	18.939	
Radius	r_{xx} [m]	0.1713	0.135	Rel. to CoG
of	r_{yy}	0.5138	0.468	
Gyration	r_{zz}	0.5138	0.468	

REFERENCES

[1] G. F. Clauss, S. Kosleck, and D. Testa, "Critical situations of vessel operations in short crested seas-forecast and decision support system," *Journal of Offshore Mechanics and Arctic Engineering*, vol. 134, no. 3, 2012.

[2] D. C. Stredulinsky and E. M. Thornhill, "Ship motion and wave radar data fusion for shipboard wave measurement," *Journal of Ship Research*, vol. 55, pp. 73–85, 2011.

[3] E. M. Thornhill and D. C. Stredulinsky, "Real Time Local Sea State Measurement using Wave Radar and Ship Motions," in *SNAME annual meeting*, Seattle, WA, USA, 2010.

[4] U. D. Nielsen, "Estimations of on-site directional wave spectra from measured ship responses," *Marine Structures*, vol. 19, pp. 33–69, 2006.

[5] T. Iseki and K. Ohtsu, "Bayesian estimation of directional wave spectra based on ship motions," *Control Engineering Practice*, vol. 8, pp. 215–219, 2000.

[6] R. Pascoal and C. Guedes Soares, "Kalman filtering of vessel motions for ocean wave directional spectrum estimation," *Ocean Engineering*, vol. 36, pp. 477–488, 2009.

[7] E. A. Tannuri, J. V. Sparano, A. N. Simos, and J. J. Da Cruz, "Estimating directional wave spectrum based on stationary ship motion measurements," *Applied Ocean Research*, vol. 25, pp. 243–261, 2003.

[8] T. D. Nguyen, A. J. Sørensen, and S. T. Tong Quek, "Design of hybrid controller for dynamic positioning from calm to extreme sea conditions," *Automatica*, vol. 43, no. 5, pp. 768–785, 2007.

[9] T. D. Nguyen, A. J. Sørensen, and S. T. Quek, "Multi-operational controller structure for station keeping and transit operations of marine vessels," *IEEE Transactions on Control Systems Technology*, vol. 16, no. 3, pp. 491–498, 2008.

[10] A. H. Brodtkorb, A. J. Sørensen, and A. R. Teel, "Increasing the operation window of dynamic positioned vessels using the concept of hybrid control," *ASME 2014 33rd International Conference on Ocean, Offshore and Arctic Engineering Volume 1A: Offshore Technology San Francisco, California, USA, June 8–13, 2014*, 2014.

[11] D. J. W. Belleter, D. A. Breu, T. I. Fossen, and H. Nijmeijer, "A globally k-exponentially stable nonlinear observer for the wave encounter frequency," *IFAC Proceedings Volumes (IFAC-PapersOnline)*, vol. 9, no. PART 1, pp. 209–214, 2013.

[12] D. J. W. Belleter, R. Galeazzi, and T. I. Fossen, "Experimental verification of a global exponential stable nonlinear wave encounter frequency estimator," *Ocean Engineering*, vol. 97, pp. 48–56, 2015.

[13] C. Møgster, *Sea state estimation using Bayesian modeling methods*, Department for Marine Teechnology, Norwegian University of Science and Technology (NTNU), 2015.

[14] U. D. Nielsen, M. Bjerregård, R. Galeazzi, and T. I. Fossen, "New concepts for shipboard sea state estimation," *submitted to MTS/IEEE OCEANS'15 in Washington DC*, 2015.

[15] D. N. V. (DNV), *Rules for Classification of SHIPS Newbuildings, Special Equipment and Systems, Part 6 Chapter 7: Dynamic Positioning Systems*. DNV (Det Norske Veritas) AS, Norway, 2010.

[16] A. J. Sørensen and J. P. Strand, "Positioning of small-waterplane-area marine constructions with roll and pitch damping," *Control Engineering Practice*, vol. 8, no. 2, pp. 205–213, 2000.

[17] B. Vik and T. I. Fossen, "Nonlinear observer design for integration of GPS and intertial navigation systems," *Proceedings of the Conference on Decision and Control (CDC'2001). Orlando, FL.*, 2001.

[18] J. A. Farrell, T. D. Givargis, and M. J. Barth, "Real-time differential carrier phase GPS-aided INS," *IEEE Transactions on Control Systems Technology*, vol. 8, no. 4, pp. 709–721, 2000.

[19] E. A. Tannuri and H. M. Morishita, "Experimental and numerical evaluation of a typical dynamic positioning system," *Applied Ocean Research*, vol. 28, no. 2, pp. 133–146, 2006.

[20] V. Hassani, A. J. Sørensen, and A. M. Pascoal, "A novel methodology for robust dynamic positioning of marine vessels: Theory and experiments," *Proceedings of the American Control Conference*, pp. 560–565, 2013.

[21] T. I. Fossen and J. P. Strand, "Passive nonlinear observer design for ships using Lyapunov methods: full-scale experiments with a supply vessel," *Automatica*, vol. 35, no. 1, pp. 3 – 16, 1999.

[22] A. J. Sørensen, *Marine Control Systems, Propulsion and Motion Control of Ships and Ocean structures, Lecture Notes*. Department of Marine Technology, NTNU, 2013.

[23] T. I. Fossen, *Handbook of Marine Craft Hydrodyamics and Motion Control*. Wiley, 2011.

[24] A. J. Sørensen, J. P. Strand, and H. Nyberg, "Dynamic positioning of ships and floaters in extreme seas," *Oceans Conference Record (IEEE)*, vol. 3, pp. 1850–1855, 2002.

[25] O. M. Faltinsen, *Sea Loads on Ships and Offshore Structures*. Cambridge University Press, 1993.

[26] E. Kreyszig, *Advanced Engineering Mathematics, 9. ed.* John Wiley & sons, inc., 2006.

[27] P. A. Brodtkorb, P. Johannesson, G. Lindgren, I. Rychlik, J. Rydén, and E. Sjö, "WAFO - a Matlab toolbox for the analysis of random waves and loads," in *Proc. 10'th Int. Offshore and Polar Eng. Conf., ISOPE, Seattle, USA*, vol. 3, 2000, pp. 343–350.

[28] J. P. Strand and T. I. Fossen, "Nonlinear passive observer design for ships with adaptive wave filtering," vol. 244. Springer London, 1999, pp. 113–134.

Paper B:

Sea State Estimation Using Vessel Response in Dynamic Positioning

Astrid H. Brodtkorb, Ulrik D. Nielsen, Asgeir J. Sørensen

Accepted for publication in Applied Ocean Research 2017.

Sea State Estimation Using Vessel Response in Dynamic Positioning

Astrid H. Brodtkorb[a,*], Ulrik D. Nielsen[a,b], Asgeir J. Sørensen[a]

[a] *Centre for Autonomous Marine Operations (NTNU AMOS), Department of Marine Technology, Norwegian University of Science and Technology (NTNU), NO-7491 Trondheim, Norway*
[b] *DTU Mechanical Engineering, Technical University of Denmark, DK-2800 Kgs. Lyngby, Denmark*

Abstract

This paper presents a novel method for estimating the sea state parameters based on the heave, roll and pitch response of a vessel conducting station keeping automatically by a dynamic positioning (DP) system, i.e., without forward speed. The proposed algorithm finds the wave spectrum estimate from the response measurements by iteratively solving a set of linear equations, and it is computationally efficient. The main vessel parameters are required as input. Apart from this the method is signal-based, with no assumptions on the wave spectrum shape. Performance of the proposed algorithm is demonstrated on full-scale experimental DP data of a vessel in three different sea states at head, bow quartering, beam, stern quartering and following sea waves, respectively.

Keywords: Sea state estimation, Vessel response, Dynamic positioning, Closed-form expressions

1. Introduction

Complex marine operations are moving further from shore, into deeper waters, and harsher environments, see Sørensen [1]. The operating hours of a vessel are weather dependent, and good knowledge of the prevailing weather conditions may ensure cost-efficient and safe operations. In addition, the performance of the DP operation will be improved by fast dynamic tracking of the first order wave induced motions used as input to the wave filter in the DP system. Recently, there has been a lot of focus on increasing the level of autonomy in marine operations, see Ludvigsen and Sørensen [2], and having a fast and reliable method for obtaining a sea state estimate is useful both in the control and in decision support systems to aid the decision making process, with or without the operator onboard the vessel.

Several methods exist for obtaining information about the sea state. Wave rider buoys are present at fixed locations, usually near the coast, providing accurate measurements for specific sites. Some vessels have installed wave radar, see Clauss et al. [3], but these systems may be expensive to install, require frequent calibration [4, 5], and in the case of large vessel motion the measurement quality is degraded. The satellite image quality may be affected if the cloud cover is low, and in general, weather data may lag up to six hours.

Today, the majority of marine vessels are equipped with sensors that gather vast amounts of data regarding the operational state, fuel consumption, hull girder stresses, acceleration, attitude and position, to name a few. In this sense, many marine vessels are inherently equipped with sea state measuring systems, since the sensor measurements can be used to infer about the on-site sea state, in a similar way as is done with traditional wave rider buoys. Estimating the sea state based on vessel motions has been explored extensively over the last 10-15 years, e.g., [6, 7, 8, 9], see Nielsen [10] for an overview of the different methods. One proposed method is called the *wave buoy analogy*, where the ship motions in 6 degrees of freedom, or other global ship responses such as hull girder stresses, are transformed into the frequency domain, and an estimate of the wave spectrum is obtained by means of parametric or Bayesian modeling. The vessel is implicitly assumed to be in stationary conditions if not elaborate procedures are applied [11, 12].

For advanced controller schemes, e.g., hybrid or switching control, sea state parameters estimated using computationally efficient algorithms are sought. In

*Corresponding author at: Centre for Autonomous Marine Operations (NTNU AMOS), Department of Marine Technology, Norwegian University of Science and Technology (NTNU), Otto Nielsens vei 10, NO-7491 Trondheim, Norway.

Email address: astrid.h.brodtkorb@ntnu.no (Astrid H. Brodtkorb)

steady state DP operations, reliable and accurate estimates of the sea state are more important than frequent updates, while in transient operations (i.e., start up, change of heading and similar) fast updates even at the expense of accuracy are favoured. *Online* sea state estimates from rapid schemes, can be used to manipulate parameters in the control law directly [13], or be input to performance monitoring functions and risk assessment models that choose the best algorithms available. There are many computationally efficient schemes for estimating the peak frequency of the waves, however, algorithms for estimating the wave height and direction are rare. Belleter et al. [14] present a time-domain method for estimating the peak frequency of encounter in order to detect parametric rolling, and Brodtkorb et al. [15] use the response spectra in heave and pitch to estimate the peak frequency of the sea state for use in controllers. Nielsen et al. [16] estimate the amplitude, phase and frequency of a regular wave, making a step towards a sea state estimation algorithm that is computationally efficient, *and* provides the wave height and direction estimate, in addition to the peak frequency. On a related note, the vessel response history itself may also be used for predicting the vessel response deterministically up to 30-60 seconds ahead of time using the correlation structure in the time history process, see Nielsen et al. [17].

This paper proposes a computationally efficient and robust sea state estimation algorithm that provides an estimate of the wave spectrum, from which sea state parameters such as the significant wave height H_s, peak period T_p (or other characteristic periods), and the relative wave direction β can be derived. The sea state estimation algorithm is non-parametric, i.e., there are no assumptions on the shape of the wave spectrum, and so the sea state estimate is obtained through solving a set of linear equations relating the wave spectrum to the response measurements via (motion) transfer functions. In this initial study, the transfer functions of a barge (box-shaped vessel) called closed-form expressions, see Jensen et al. [18], with the same main parameters as the actual vessel are used in the estimation procedure. The main reason for this is to make the procedure as simple as possible, so it can be used for vessels where the detailed hull geometry is unknown or unavailable due to non-disclosure issues. For DP vendors, this will be an advantage for i.e., efficient tuning of the DP control system. If the actual transfer functions of the vessel are pre-calculated by advanced computational tools, e.g., by panel codes or strip theory, the approach will just require interpolation in a hyper-dimensional matrix, which is done in other sea state estimation algorithms. The sea state estimation algorithm is demonstrated on the heave, roll and pitch response measurements of the NTNU-owned and operated research vessel (R/V) Gunnerus during DP tests in three different sea states with head, bow quartering, beam, stern quartering and following sea waves.

The paper is organized as follows: An introduction to wave spectra, response spectra, cross spectra and closed-form expressions is given in Section 2, and Section 3 presents the sea state estimation algorithm. In Section 4 the collection and validation of the response measurements, wave elevation measurements, and tuning of the closed-form expressions is discussed, before the estimation results are presented. Section 5 concludes the paper.

2. Vessel modeling

2.1. Vessel response in irregular waves

For control design purposes, the vessel motion is usually modeled as a mass-damper-restoring system subject to the loads from current, wind, and waves. For ships in DP the thrusters will produce mean and slowly varying generalized forces in the horizontal plane to cancel those from the environment. Therefore the DP control system influences the surge, sway and yaw motion of ships, and the *heave (z), roll* (ϕ) and *pitch* (θ) motions are more suited for sea state estimation. The measurements of heave, roll and pitch are recorded in the *body*-frame, which is defined with positive x-axis pointing towards the bow, positive y-axis pointing towards starboard, and with positive z-axis pointing down, see Figure 1b. In DP the vessel has zero or low forward speed, so that the frequency of encounter is assumed to be the same as the incident wave frequency.

In this paper, fully developed wind-generated sea states are considered. It is also assumed that the sea state is stationary in the statistical sense (statistical properties are constant), and that the waves are long-crested, with propagation direction Θ, as defined in Figure 1a. The wave direction relative to the vessel heading is β, with $\beta = 180°$ being head sea, and $\beta = 0°$ being following sea, see Figure 1b.

The relationship between the wave amplitude and the vessel response amplitude (here only heave, roll and pitch are considered) is given by the complex-valued (motion) transfer functions $X_i(\omega,\beta)$, which can be calculated using hydrodynamic software codes. The complex-valued cross-spectra $R_{ij}(\omega)$ can be calculated as:

$$R_{ij}(\omega) = X_i(\omega,\beta)\overline{X_j(\omega,\beta)}S(\omega), \tag{1}$$

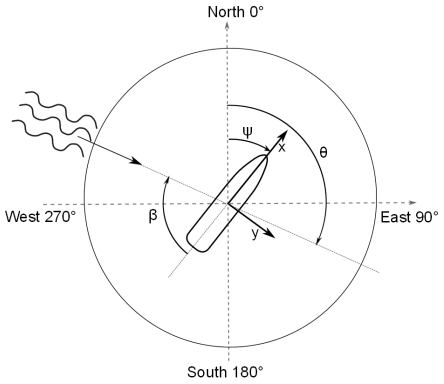

(a) Global wave propagation direction Θ

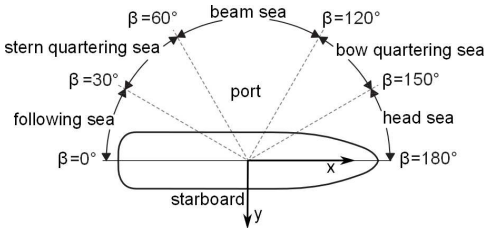

(b) Relative wave direction β

Figure 1: Definition of the wave propagation direction $\Theta \in [0, 360)°$, heading of the vessel ψ, and relative wave direction β. Starboard incident waves have $\beta \in (-180, 0]°$, and port incident waves have $\beta \in [0, 180]°$. The coordinate system x-y represents the *body*-frame with the z-axis pointing down (into the page), and the dashed coordinate frame in (a) is the North-East-Down (NED)-frame, also with the down-axis pointing downward (into the page). Notice that the vessel is symmetric about the x-axis.

where $R_{ij}(\omega)$, $i, j = \{z, \phi, \theta\}$ are the heave, roll, and pitch response spectra, $\overline{X_j(\omega,\beta)}$ is the complex conjugate of the transfer functions in heave, roll and pitch for relative wave direction β, and $S(\omega)$ is the wave spectrum. When $i = j$, $X_i(\omega,\beta)\overline{X_i(\omega,\beta)} = |X_i(\omega,\beta)|^2$, which is the amplitude of the transfer function squared. The cross spectra $R_{ij}(\omega)$ calculated from measured responses for a data set from Run 3 are shown in Figure 2. When $i \neq j$, $R_{ij}(\omega)$ is complex-valued, and when $i = j$ the imaginary part is zero, $\mathcal{I}m(R_{ii}) = 0$. The imaginary parts of the cross spectra pairs have opposite signs, i.e., $\mathcal{I}m(R_{ij}) < 0 \Leftrightarrow \mathcal{I}m(R_{ji}) > 0$, that are dependent on the incident wave direction. This is used later to determine β.

The vessel will act as a *low-pass filter* such that small wave length λ compared to the ship length will hardly result in any response. Hence, limited information about the waves can be obtained from the vessel motion measurements in these cases[1]. Due to the low-pass characteristics, the algorithm will work best for wave length larger than a certain value compared to the ship length and breadth, dependent on the wave direction relatively to the the vessel. For many operations, detailed information about the sea state is in particular of interest for H_s larger that 2-3 m as you get closer to the limitations for e.g., crane operations, off-loading, anchor handling, etc. The procedure implicitly assumes that the wave-induced motions are small so that linear theory is applicable though reasonable good results are obtained for higher sea states. It is also assumed that the vessel response is in steady state, though this may be relaxed, see for instance [11].

2.2. Closed-form expressions

In order to calculate the transfer functions, $X_i(\omega,\beta)$, from the wave amplitude to the response amplitude, of a marine vessel, generally a detailed description of the vessel hull geometry, weight distribution, draught and trim are required for standard as well as advanced computational tools, e.g., the 3D panel code WAMIT [19], or the 2D strip theory code ShipX [20]. In these software codes, the transfer functions are calculated for a pre-specified set of headings, loading conditions and vessel forward speeds (though here only zero forward speed is considered). Jensen et al. [18] present simplified expressions, called closed-form expressions, for the heave, roll and pitch motions of a homogeneously loaded box-shaped vessel with dimensions $L \times B \times T$ (length, breadth, draught), which approximate the transfer functions of a ship. The main reasons for using the closed-form expressions in this procedure, instead of the actual transfer functions of the ship, are:

- To demonstrate that it is possible to obtain a sea state estimate including significant wave height, a characteristic period and direction by using limited knowledge of the vessel hull geometry.
- The use of closed-form expressions offer a convenient way to deal with transfer functions in varying operational conditions without the need to interpolate.

[1] Some studies look at the possibility to infer knowledge about higher frequency wave components by considering the motion of a fixed point on the ship hull relative to the sea surface by installing, for instance, a downward-looking microwave sensor; see e.g., Nielsen [20, 21]

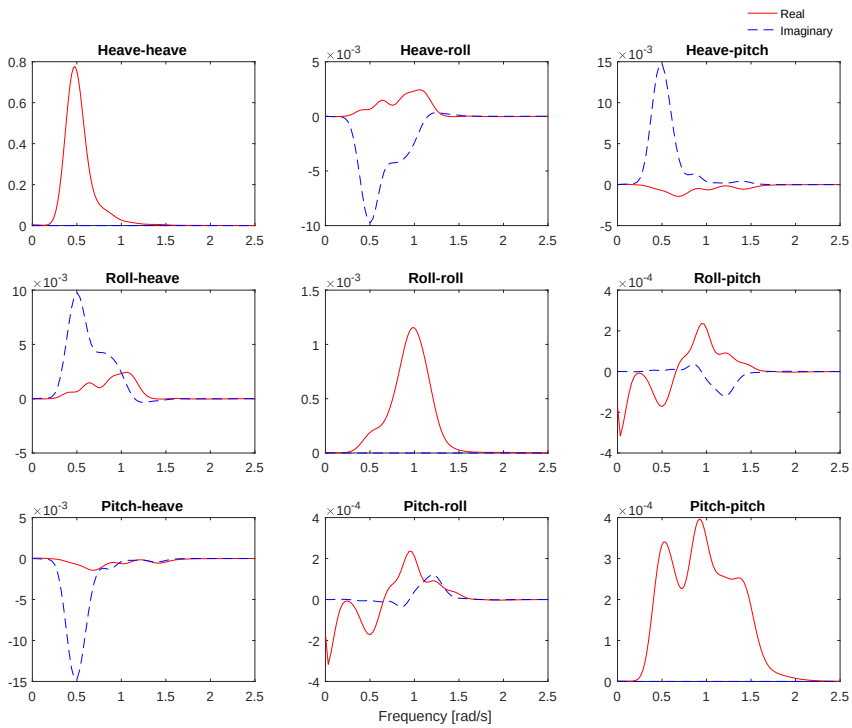

Figure 2: Cross spectra R_{ij} calculated from measured responses in heave, roll and pitch for the data set from Run 3, head seas (see Tables 2 and 3). Frequency [rad/s] on all x-axes.

The closed-form expressions for heave and pitch in Jensen et al. [18] are derived based on the decoupled heave and pitch dynamics of the vessel. This leads to a semi-analytical expression for the transfer functions with inputs L, B, T, block coefficient C_B, and ship forward speed V (although V is set to zero here). For roll, the closed-form expression requires the displacement Δ, water-plane area coefficient C_{WP}, transverse metacentric height GM_T, and roll natural period T_{4n} as additional input. The parameters GM_T and Δ are calculated by ballast programs onboard vessels, usually before the vessel leaves port, in order to ensure sufficient stability of the vessel and avoid capsize. C_{WP} and C_B can be approximated for different hull shapes, and the roll natural period may be approximated by

$$T_{4n} = \frac{2\pi}{\omega_{4n}}, \quad \omega_{4n} = \frac{\sqrt{gGM_T}}{r_x}, \tag{2}$$

where g is the acceleration due to gravity, and the roll radius of gyration used here is $r_x = 0.4B$, see Papanikolaou et al. [21]. Other values of the radius of gyration may also be used.

The roll damping is important to estimate correctly, and is approximated by a linear wave-induced part, and a viscous part. In [18], the linear wave-induced damping is calculated by using two boxes that are rigidly joined, however, here only one box with dimensions $L \times B \times T$ yielded better results. The sectional damping coefficient is determined by an approximation based on the ratio B/T for a wedge-shaped hull, and then multiplied with the length L of the hull. Viscous roll damping is approximated by a factor $0 < \mu \ll 1$ of the critical damping $B^*_{44} = \frac{T_{4n} C_{44}}{\pi}$, where $C_{44} = g\Delta GM_T$ is the roll restoring coefficient. The viscous damping is highly nonlinear, but linearized approximations based on the critical damping are often used both in simplified approaches, and in panel and strip theory codes. The closed-form expressions in heave, roll and pitch are in

the rest of the paper referred to by $\Phi_i(\omega,\beta),\ i = \{z,\phi,\theta\}$.

3. Sea state estimation algorithm

The sea state estimate, consisting of a wave direction estimate and a point-wise wave spectrum estimate, is computed in two main steps, as illustrated by Figure 3. They are described in detail subsequently, but summarized as follows: Firstly, the response spectra in heave, roll and pitch, when $i = j$ $R_{ii}(\omega)$, and the closed-form expressions are used to find an initial estimate of the unknown wave spectrum $S(\omega)$. This is done by solving the following equation through iteration

$$R_{ii}(\omega) = |\Phi_i(\omega,\beta)|^2 S(\omega), \tag{3}$$

which is the relation between the sea state and the vessel response in (1) when $i = j$, $i = \{z,\phi,\theta\}$, with the transfer functions substituted with the closed-form expressions from Section 2.2. $R_{ii}(\omega)$ is the real part of the Fourier transformation of the measured heave, roll and pitch vessel response, respectively.

Secondly, the significant wave heights, computed for each degree of freedom, and for each wave direction are used to find an initial direction estimate. The imaginary parts of the cross spectra $R_{ij}(\omega)$, $i \neq j$ are used to estimate the relative wave direction $\hat{\beta}$, and then the estimates of the peak wave period $\hat{T}_p := \frac{2\pi}{\hat{\omega}_p}$ and significant wave height $\hat{H}_s$ are found.

3.1. Wave spectrum estimate

At first sight, the most obvious method to obtain the wave spectrum estimate is to invert (3). However, because $\Phi_i(\omega,\beta)$, especially for roll and pitch, are small for a large range of frequencies, the inverse squared for the corresponding frequency range is very large. As a result, solving (3) by inversion may be numerically unstable for certain combinations of frequency and directions [22, 23, 24]. In order to circumvent an ill-conditioned system with numerical instabilities, the estimation procedure proposed here is based on the solution of the linear equation (3) using an iterative scheme.

Firstly, the frequencies and directions are discretized into N_ω and N_β parts, respectively, and the discretized direction k, is used to denote directions in the estimation procedure. Since the wave direction is unknown initially, the point-wise wave spectrum estimate needs to be calculated for every direction $k = \{0, ..., 180\}$, and hence the estimated wave spectrum is dependent on the direction as well as frequency, $\hat{S}_i(\omega,k)$. The method does not assume a wave spectrum shape, or parametrize

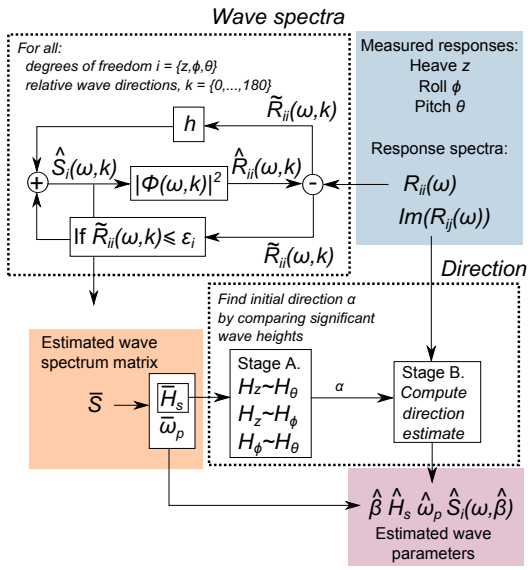

Figure 3: Illustration of the proposed sea state estimation method, in two main steps. Firstly the point-wise wave spectrum estimate matrix $\bar{S}$ is computed by solving (4) through iteration. Secondly, the significant wave heights $\bar{H}_s$ for each of the wave spectra in $\bar{S}$ are compared to find an initial direction α, and the imaginary parts of the cross-spectra $R_{ij}(\omega)$ are used to find the relative direction estimate $\hat{\beta}$. The inputs to the procedure are the measured response spectra in heave, roll, and pitch, and the outputs are estimates of the relative wave direction $\hat{\beta}$, significant wave height $\hat{H}_s$, peak period $\hat{\omega}_p$, and the wave spectra $\hat{S}_i(\omega,\hat{\beta})$.

it in any way, and hence the initial wave spectrum estimate and estimate of the response spectrum are set to zero, $\hat{S}_i(\omega,k) = 0$ and $\hat{R}_{ii}(\omega,k) = 0$. For each degree of freedom $i = \{z,\phi,\theta\}$ and for each direction $k = \{0, ..., 180\}$, repeat the following steps,

$$\tilde{R}_{ii}(\omega,k) = R_{ii}(\omega) - \hat{R}^-_{ii}(\omega,k) \tag{4a}$$

$$\hat{S}_i(\omega,k) = \hat{S}_i(\omega,k) + h\tilde{R}_{ii}(\omega,k) \tag{4b}$$

$$\hat{R}_{ii}(\omega,k) = |\Phi_i(\omega,k)|^2 \hat{S}_i(\omega,k), \tag{4c}$$

until a threshold is reached $|\tilde{R}_{ii}(\omega,k)| \leq \epsilon_i$, for $\epsilon_i > 0$. In (4a), the response spectrum estimation error $\tilde{R}_{ii}(\omega,k)$ is computed by making use of the estimated response spectra from the previous iterate, denoted by $\hat{R}^-_{ii}(\omega,k)$, and the measured response spectra $R_{ii}(\omega)$. In (4b), $\tilde{R}_{ii}(\omega,k)$ is used to make adjustments to the estimated wave spectrum $\hat{S}_i(\omega,k)$, with a small step size $h > 0$, and in (4c) a new response spectrum estimate $\hat{R}_{ii}(\omega,k)$ is calculated. Note that since the transfer functions of a box-shaped vessel are applied, the values for pitch beam

seas and for roll in head and following seas are zero $\Phi_i(\omega, k) = 0$. The iteration is terminated in these cases, giving a wave spectrum estimate of zero, $\hat{S}_i(\omega, k) = 0$

In summary, (4a-c) are one iteration step, which are repeated untill $|\tilde{R}_{ii}(\omega, k)| \leq \epsilon_i$, *for* $\epsilon_i > 0$. *This is done for all degrees of freedom* $i = \{z, \phi, \theta\}$ *and directions* $k = \{0, ..., 180\}$. The output from (4) are three point-wise wave spectrum estimates per direction, yielding a spectrum estimate matrix of dimension $3 \times N_\omega \times N_\beta$.

$$\bar{S} = \begin{bmatrix} \hat{S}_z(\omega, 0) & \dots & \hat{S}_z(\omega, k) & \dots & \hat{S}_z(\omega, 180) \\ \hat{S}_\phi(\omega, 0) & \dots & \hat{S}_\phi(\omega, k) & \dots & \hat{S}_\phi(\omega, 180) \\ \hat{S}_\theta(\omega, 0) & \dots & \hat{S}_\theta(\omega, k) & \dots & \hat{S}_\theta(\omega, 180) \end{bmatrix} \tag{5}$$

Now it remains in this former part to compute the peak frequency and significant wave height for each of the wave spectra in $\bar{S}$. The result is collected in two matrices with dimensions $3 \times N_\beta$.

$$\bar{H}_s = \begin{bmatrix} H_z(0) & \dots & H_z(k) & \dots & H_z(180) \\ H_\phi(0) & \dots & H_\phi(k) & \dots & H_\phi(180) \\ H_\theta(0) & \dots & H_\theta(k) & \dots & H_\theta(180) \end{bmatrix} \tag{6}$$

$$\bar{\omega}_p = \begin{bmatrix} \omega_z(0) & \dots & \omega_z(k) & \dots & \omega_z(180) \\ \omega_\phi(0) & \dots & \omega_\phi(k) & \dots & \omega_\phi(180) \\ \omega_\theta(0) & \dots & \omega_\theta(k) & \dots & \omega_\theta(180) \end{bmatrix} \tag{7}$$

The iteration (4) is a set of $3 \times N_\beta$ linear equations that are computationally efficient to solve. In this paper we have used $N_\beta = 19$ directions, $k = \{0, 10, ..., 180\}$, and $N_\omega = 300$. In the following it is explained how to make the selection of the relative wave direction estimate, considering also the interval $\beta = (-180, 0]$.

3.2. Wave direction estimate

The relative wave direction estimate is found in two stages, as indicated in Figure 3. The initial direction α is found by using the significant wave height matrix $\bar{H}_s$ in (6), and this information is coupled with the imaginary parts of the cross spectra in heave-roll and heave-pitch. The approach for selecting the wave direction is explained in the following.

Stage A: An initial relative wave direction estimate α can be made as either *head/following*, *bow/stern quartering*, or *beam* seas by comparing how much energy is in the different wave spectrum estimates $\bar{S}$, i.e., comparing the elements of $\bar{H}_s$. In Figure 4 the significant wave heights $\bar{H}_s$ from (6) are plotted for the same sea state (Run 3, see Table 3 in Section 4). The vessel is in head seas in (a) and beam seas in (b). The measured significant wave height and correct relative direction are indicated by the red circle in both plots. The wave height estimates $H_\phi(k = 0), H_\phi(k = 180)$ and $H_\theta(k = 90)$ are not included in the plots, since the closed-form expressions are zero in these cases, and the corresponding wave spectrum estimates are set to zero as well.

The estimated significant wave heights from using the heave response and heave closed-form expression vary little over the wave direction, and are close to the measured H_s, see the red dots in Figures 4. This is used as the base case for determining the incident direction of the waves. Since the closed-form expressions for roll and pitch vary a lot over wave direction, the corresponding H_ϕ and H_θ also vary a lot with direction. The angle k where the $\bar{H}_s$ are closest, is chosen as the initial direction α, in the following way:

- $\alpha = 45$: When the sea state is bow or stern quartering, the maximum H_θ and H_ϕ are about the same order of magnitude.
- $\alpha = 0$: When the significant wave height from using pitch for head (or following) $H_\theta(k = 180)$ sea is close to the significant wave height estimate from heave for head (or following) sea $H_z(k = 180)$, the direction is either head or following. From Figure 4a it is ruled out that the waves are approaching from the side, since then $H_\theta(k = 80)$ and $H_\theta(k = 100)$ are a lot larger than H_z for the same directions.
- $\alpha = 90$: When the significant wave height using roll in beam sea $H_\phi(k = 90)$ and using heave $H_z(k = 90)$ are close, the sea state is beam sea. In Figure 4b, H_ϕ for $k = 10°$ and $k = 170°$ are significantly larger than H_z for the same directions, which rules out that the waves are head or following.

In the ideal case, using the actual transfer functions of the ship, the three significant wave height curves in Figure 4 should cross at the same point, and this point should be the actual relative wave direction. However, since the closed-form expressions are used here, the curves are head/following and port/starboard symmetric, and an extra stage is needed.

Stage B: The next stage is to calculate the wave direction estimate $\hat{\beta}$ by using the initial direction α from Stage 1, and the imaginary parts of the heave-pitch and heave-roll cross spectra $\mathcal{I}m(R_{z\phi})$, and $\mathcal{I}m(R_{z\theta})$. The heave response is *symmetric* about the x-axis (body-frame), and the pitch response is *anti-symmetric* about the y-axis, see Figure 5 for an illustration. The symmetric and anti-symmetric properties of the responses, are

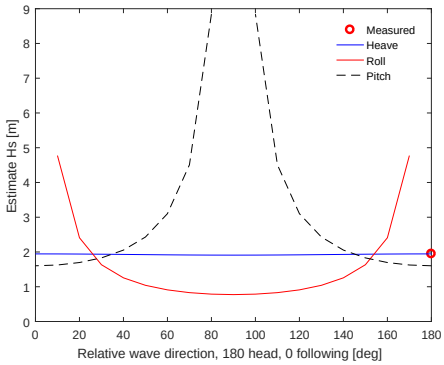

(a) Head sea

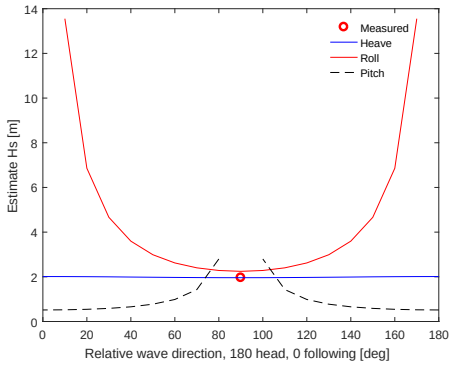

(b) Beam sea

Figure 4: Significant wave height in (6) plotted against relative wave direction. This data set is from Run 3, for actual vessel heading **head** in (a) and **beam** in (b), see Tables 2 and 3 for details. The measured significant wave height and correct relative direction are indicated by the red circles.

reflected in the imaginary part of the heave-pitch cross spectra $\mathcal{I}m(R_{z\theta})$, which has opposite sign for head and following sea. The 'peak' of the imaginary spectra are found by

$$\text{peak}(\mathcal{I}m(R_{ii})) := \{\mathcal{I}m(R_{ii}(\omega_J)) : \omega_J = \arg\max_j |\mathcal{I}m(R_{ii}(\omega_j))|, i = \{z, \phi, \theta\}\}, \quad (8)$$

corresponding to the largest extreme, either maxima or minima. This means that if $\text{peak}(\mathcal{I}m(R_{z\theta})) > 0$, then the vessel is in head sea, and $\hat{\beta} = 180$, and conversely if $\text{peak}(\mathcal{I}m(R_{z\theta})) < 0$, then the vessel is in following sea, and $\hat{\beta} = 0$.

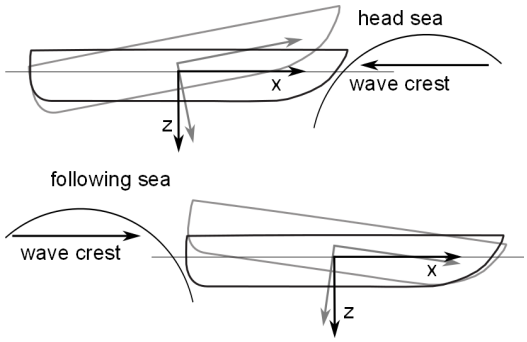

Figure 5: Sketch of the heave and pitch responses to a wave crest for head and following sea for zero forward speed. For head sea, the heave response is upwards, with the bow upwards, and for following sea the heave response is still upwards, but not the bow goes downwards.

For beam seas, $\alpha == 90$, starboard and port seas can be distinguished by using the imaginary part of the heave-roll (or roll-heave) cross spectra $\mathcal{I}m(R_{z\phi})$ in a similar manner. The roll response is *anti-symmetric* about the body x-axis, giving opposite sign for the roll angle when a wave crest approaches from port and starboard side, and the heave response is symmetric about the x-axis. If $\text{peak}(\mathcal{I}m(R_{z\phi})) > 0$ then the vessel is in starboard beam sea and $\hat{\beta} = -90$, and the opposite for port beam sea. When $\alpha == 45$, indicating bow quartering or stern quartering seas, there are four possibilities for the wave direction, because of zero forward-speed and a box-shaped vessel. Then $\mathcal{I}m(R_{z\theta})$ and $\mathcal{I}m(R_{z\phi})$ are used in combination.

It should be realized that the outlined procedure for the wave direction estimate strictly holds only in case of zero-forward speed and for a sea state described by long-crested waves. Without forward speed, waves that are following, will always be *following*, since the vessel will not travel faster than the waves, as can happen in some cases with forward speed. The (geographical) wave propagation direction estimate $\hat{\Theta}$ can be computed by using the heading of the vessel, see Figure 1a.

3.3. Peak frequency and significant wave height estimates

In Brodtkorb et al. [15], it was found through a series of model-scale experiments at zero forward speed, that the best peak wave frequency estimate was achieved by using the mean of the heave and pitch response peak frequencies. Therefore the mean of the peak frequencies following from the wave spectrum estimate for heave

and pitch, for the estimated incident wave direction, are used:

$$\hat{\omega}_p = \frac{\omega_z(\hat{\beta}) + \omega_\theta(\hat{\beta})}{2} \tag{9}$$

The peak frequencies for the estimated wave spectrum were found to be consistent for all directions, and therefore if the wave direction estimate is not found reliable, a peak frequency estimate may still be obtained as the average of the peak frequencies obtained for all directions in heave and pitch. The peak period estimate is $\hat{T}_p = \frac{2\pi}{\hat{\omega}_p}$. In beam seas only the heave estimate is used, since the pitch estimate is set to zero.

The estimate of the significant wave height in heave is consistent for all directions, see Figure 4, and therefore

$$\hat{H}_s = H_z(\hat{\beta}). \tag{10}$$

Again, if the wave direction estimate is not found, the average of the heave significant wave heights can be used instead.

4. Data validation, estimation results and discussion

In this section the data collection setup is described, and the data and closed-form expressions are validated before the estimation results are presented and discussed.

4.1. Data collection

The full-scale DP response measurements were collected during a test campaign in 2013 conducting DP operations of R/V Gunnerus, see Table 1 for main dimensions. The tests were originally done in order to document the effect of a thruster retrofit, where the main propulsion was changed from two conventional fixed pitch propeller-rudder combinations to two Rolls Royce rim-driven azimuthing thrusters, see Steen et al. [25]. The R/V Gunnerus is a test platform for biologists, archeologists, marine robotics, and recently for DP and autopilot algorithms [26]. Table 2 gives an overview over the test cases in three sea states. In the first sea state response data for head, beam, stern quartering and following sea were recorded. The second sea state has measurements for bow quartering sea as well. The third sea state only has two relative directions measured; head and beam seas. The relative directions stated here are the *intentional relative directions*, and are not exactly what was run, since the incident wave direction was judged by sight during the tests. The actual relative directions calculated from the wave buoy direction measurement and the heading of the vessel, are given together with the estimation results in Table 4. The response of the vessel was recorded for 15 minutes in each relative wave direction.

Table 1: R/V Gunnerus main parameters used to calculate closed-form expressions.

Parameter	Value
Length, L_{pp}	28.9 m
Breadth, B	9.6 m
Draught, T	2.7 m
Block coefficient, C_B	0.56 [-]
Waterplane coefficient, C_{WP}	0.837 [-]
Displacement, Δ	417 000 kg
Transverse metacentric height, GM_T	2.663 m

Table 2: Summary of the test cases for Run 1-3.

Run	Relative direction β [deg]
1	{ 0, 45, 90, 180 }
2/2*	{ 0, 45, 90, 135, 180 }
3	{ 90, 180 }

As external information, useful for validation purposes, the sea surface elevation was measured using a directional wave rider buoy that was deployed close to where the DP tests took place. The sea states are in the next sections referred to by run numbers defined in Table 3. The statistical values listed in the table are calculated from the post-processed time series from the wave buoy. The wave elevation time series used to calculate the sea state parameters correspond to the time of the DP tests for the three days. The WAFO toolbox [27] for Matlab® was used to post-process the response and wave measurements.

The sea states in Run 1 and 3 are single-peaked that resemble JONSWAP[2] spectra, and the sea state in Run 2 is double peaked like the Torsethaugen spectrum, with the first values for Run 2 in Table 3 corresponding to wind-generated waves, and the second corresponding to swell. Since the sea state estimation algorithm does not differentiate between multiple peaked spectra at this point, Run 2 is formulated alternatively as Run 2*. The peak period, direction and spread are taken as the values for the highest peak, corresponding to the wind-generated waves. The alternative formulation 2* is used in the discussion of the results. In literature, there exists schemes for partitioning the wave spectra into wind-

[2]Joint North Sea Wave Project

generated waves and swell, see for instance Montazeri et al. [28].

Table 3: Summary of sea states, with most prominent values for the significant wave height H_s, peak period T_p, wave propagation direction Θ, and direction spread, as derived from the wave buoy measurements.

Run	H_s [m]	T_p [s]	Θ [deg]	Spread [deg]
1	2.27	10	160	34.0
2	{ 1.1, 0.9 }	{8, 13.5 }	{ 190.2, 72}	{ 5.3, 10.2 }
2*	1.71	8	190.2	5.3
3	1.92	15.3	72	12.4

4.2. Tuning and validation of closed-form expressions

In this section the closed-form expressions are compared with the ShipX-calculated transfer functions for R/V Gunnerus. Figure 6 compares the transfer functions calculated using ShipX and the closed-form expressions for the tuning found in this section, for encounter directions $\beta = \{90, 100, ..., 180\}^\circ$. The arrow indicates how the amplitude of the transfer functions vary with increasing β. A note of caution worth mentioning is that ShipX uses strip theory to calculate the transfer functions of a vessel. Since R/V Gunnerus has $L/B = 3$, strip theory is not strictly speaking valid for this vessel, however, it is considered accurate enough for validation of the closed-form expressions. Starting with the heave and pitch closed-form expressions. In [18] it is recommended that for block coefficient $C_B < 1$ use BC_B as the breadth of the box, so that the buoyancy of the box and the ship are equal. In this case if the length $L = C_B L_{pp}$ is used instead, both the heave and pitch closed-form expressions are a lot closer to the ShipX transfer functions, and the buoyancy for the ship and the box are still equal. A reason why $L = C_B L_{pp}$ works well may be that R/V Gunnerus is a relatively short vessel compared to its breadth $L/B = 3$, and at the same time it nearly fills a rectangle seen from above, with waterplane area coefficient $C_{WP} = 0.837$.

The roll closed-form expression needs some more attention than the others, because in general, roll is a response that is typically susceptible to larger inaccuracies due to effect of nonlinearities in damping and restoring forces. The roll response of the vessel is centred close to the roll natural frequency, with the level of damping deciding how narrow-peaked the transfer function is. Therefore the measured roll response in one sea state and one heading is used as a tuning case for the roll closed-form expression. The *measured* roll transfer function can be calculated by solving (1) with $i = j$ for the transfer function, $X_\phi^{meas}(\omega, \beta)$. The measured transfer function for Run 2 with $\beta = 45^\circ$ (stern quartering sea) is plotted alongside the amplitude of the closed-form expression in roll in Figure 7. The roll damping and peak frequency were tuned to get similar shapes for the closed-form expression and the measured transfer function.

The sectional wave radiation damping coefficient was found using the wedge hull form, see Jensen et al. [18], as the approximations are in the correct B/T-range (B/T for Gunnerus is $9.6/2.7 = 3.55$). Adding viscous damping of $\mu = 0.3$ of the critical damping made the closed-form expression in roll similar to the measured transfer function. The viscous effects in the ShipX-calculated roll transfer function are underestimated, as seen in Figure 6, since the peak is much higher than the roll closed-form expression. The natural frequency in the roll closed-form expression was approximated by (2) with the GM_T given in Table 1, and the radius of gyration $r_x = 0.4B$, as suggested in [21].

4.3. Data validation

In this section the data gathered by the wave buoy and transfer functions calculated using ShipX are used to validate the closed-form expressions against the measurements of heave, roll and pitch. Notice that this is the reverse process to estimating the sea state, and is only done for validation purposes. The theoretical response is calculated as follows:

$$R_{ii}^{ShipX}(\omega) = |X_i(\omega, \beta)|^2 S_{buoy}(\omega) \tag{11}$$

$$R_{ii}^{CF}(\omega) = |\Phi_i(\omega, \beta)|^2 S_{buoy}(\omega), \tag{12}$$

where R_{ii}^{ShipX}, and R_{ii}^{CF} $i = \{z, \phi, \theta\}$ are the calculated response spectrum in heave, roll and pitch, $X_i(\omega, \beta)$ are the transfer functions calculated using ShipX, $\Phi_i(\omega, \beta)$ are the closed-form expressions, and $S_{buoy}(\omega)$ is the Fourier transform of the wave elevation measured by the wave rider buoy. The direction from the buoy and the heading of the vessel are used to calculate the relative wave direction β. Figure 8 shows the measured and calculated response in heave, roll and pitch for Run 2, for $\beta = 45^\circ$ (stern quartering sea).

The theoretical R_{ii}^{ShipX}, and R_{ii}^{CF}, and measured responses generally correspond well, for heave and pitch. For roll the ShipX transfer functions are overestimated (see Figure 7), and therefore the $R_{\phi\phi}^{ShipX}$ is a lot larger than the others, and is omitted in the plot. The roll closed-form expression performs adequately. It is observed that for beam seas the measured pitch response is generally larger than the theoretical R_{ii}^{CF}, and the same goes for the roll response for close to head and

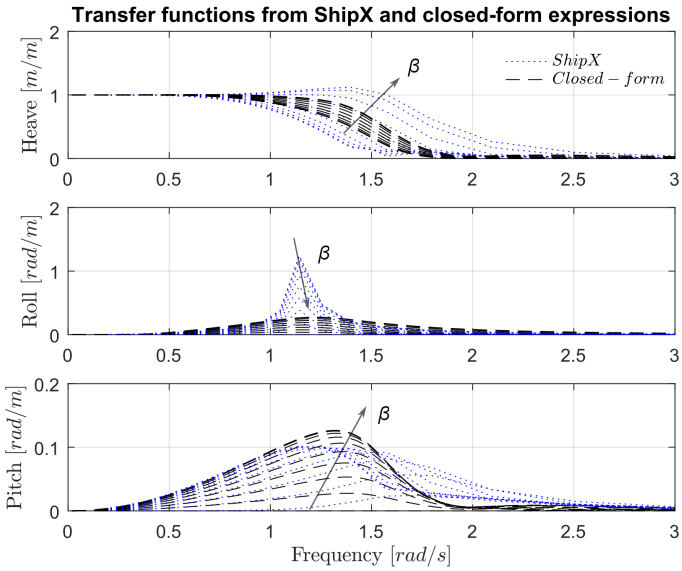

Figure 6: Amplitudes of the ShipX-calculated transfer functions and closed-form expressions in heave, roll and pitch for $\beta \in [90, 180]^\circ$. The arrow indicates how the amplitude varies with increasing β.

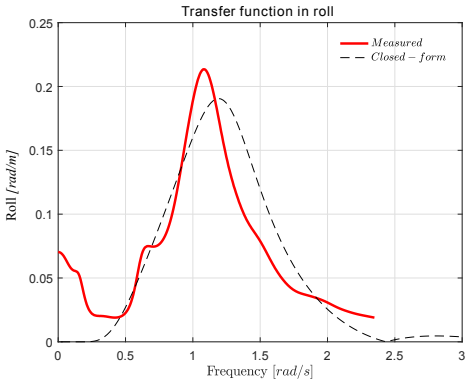

Figure 7: Amplitude of the closed-form expression for roll compared with the *measured* transfer function for Run 2, $\beta = 45^\circ$ (stern quartering sea).

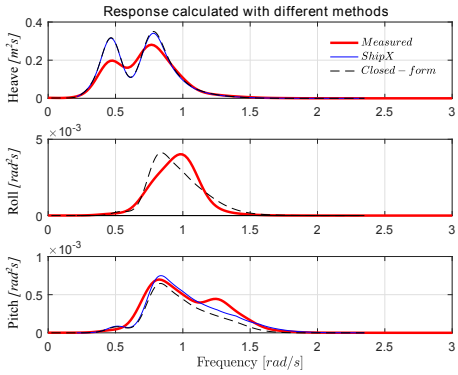

Figure 8: Measured and calculated response spectra using ShipX calculated transfer functions and using the closed-form expressions in Section 2.2. The waves used are Run 2 for 45° (stern quartering sea).

following seas. One reason for this might be that the waves were not completely long-crested since the wave propagation direction had a spread, and waves with different directions than the mean wave direction excite the vessel response.

4.4. Estimation results

The procedure described in Section 3 was applied to all the response measurements available, see Table 2. Figures 9-11 show the estimated wave spectra using the heave and pitch responses for all response time series in

each sea state. A summary of the estimated sea state parameters $\hat{H}_s$, $\hat{T}_p$ and $\hat{\beta}$ and the estimation errors are shown in Table 4. The estimation errors are calculated as

$$\tilde{\beta} = |\beta - \hat{\beta}| \, [^\circ] \tag{13a}$$

$$\tilde{H}_s = 100\frac{|H_s - \hat{H}_s|}{H_s} \, [\%] \tag{13b}$$

$$\tilde{T}_p = 100\frac{|T_p - \hat{T}_p|}{T_p} \, [\%], \tag{13c}$$

with β, H_s and T_p calculated from the wave buoy measurements, see Table 3. Note that the pitch response is zero for beam seas, so no sea state estimate from pitch is obtained for this direction. Inherently, the estimates are in the *encounter domain*, but since the forward speed is zero, this is equivalent to the true domain.

From examining the Figures 9-11, it is observed that generally the estimated wave spectrum based on the heave response is closer to the measured wave spectrum than what the pitch estimates are. The pitch estimate is generally the best when the relative wave direction is bow quartering or following sea. For the estimates in stern quartering sea for Run 1 and 3, and for head sea in Run 3, the pitch response underestimates the peak of the wave spectrum a lot, probably since the approximation of the bow quartering as a box-shape is not accurate. Using the heave estimate for computing the significant wave height yields consistent results, with a mean estimation error for wave height of $\tilde{H}_s$ = 5.79% over all directions, with a standard deviation of

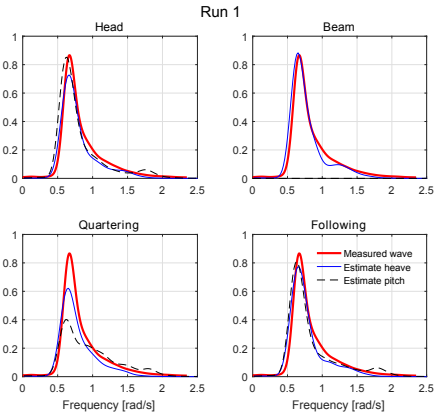

Figure 9: Measured and estimated wave spectra [m^{2}s] using the heave and pitch response; $S(\omega)$, $\hat{S}_z(\omega,\hat{\beta})$, and $\hat{S}_\theta(\omega,\hat{\beta})$, for the sea state in Run 1.

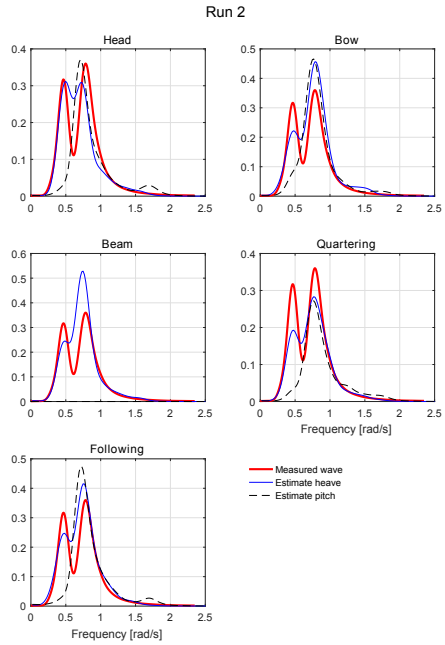

Figure 10: Measured and estimated wave spectra [m^{2}s] using the heave and pitch response; $S(\omega)$, $\hat{S}_z(\omega,\hat{\beta})$, and $\hat{S}_\theta(\omega,\hat{\beta})$, for the sea state in Run 2.

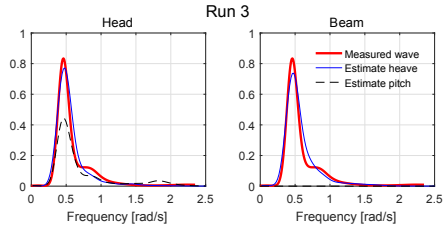

Figure 11: Measured and estimated wave spectra [m^{2}s] using the heave and pitch response; $S(\omega)$, $\hat{S}_z(\omega,\hat{\beta})$, and $\hat{S}_\theta(\omega,\hat{\beta})$, for the sea state in Run 3.

3.78%. The largest estimation error is $\tilde{H}_s$ = 12%, which occurs in Run 1 for stern quartering seas.

For the two-peaked spectrum, Run 2 in Figure 10, the heave response is double-peaked for all the directional estimates, whereas the pitch peak is single-peaked for all estimates. In Table 4 the estimation errors for Run 2*, i.e., for the alternative formulation of Run 2, are stated. According to the wave measurements, there is

Table 4: Measured wave parameters using a directional wave rider buoy, estimated parameters as outlined in Section 3, and the estimation error calculated by (13).

		Measurements			Estimates			Estimation errors		
Run	Heading	β[deg]	H_s [m]	T_p [s]	$\hat{\beta}$ [deg]	$\hat{H}_s$ [m]	$\hat{T}_p$ [s]	$\tilde{\beta}$ [deg]	$\tilde{H}_s$ %	$\tilde{T}_p$ %
1	head	-175.6	2.27	10	-180	2.1044	9.638	4.39	7.56	3.617
1	beam	95.1	2.27	10	90	2.26	9.638	5.1	0.725	3.167
1	stern quartering	50	2.27	10	45	1.999	9.781	5	12.16	2.192
1	following	4.3	2.27	10	0	2.161	9.781	4.3	5.08	2.192
2*	head	179	1.71	8	180	1.6747	10.48	1	1.846	30.03
2*	bow quartering	134.8	1.71	8	135	1.8724	8.091	0.2	9.779	1.133
2*	beam	89.2	1.71	8	90	1.8708	8.402	0.8	9.685	5.02
2*	stern quartering	44.2	1.71	8	45	1.5834	8.192	0.8	7.165	2.398
2*	following	-0.3	1.71	8	0	1.821	8.511	0.3	6.760	6.394
3	head	-171.6	1.925	15.3	-180	1.9451	13.374	8.45	1.03	12.58
3	beam	-79	1.925	15.3	-90	1.961	13.163	11	1.838	14.33

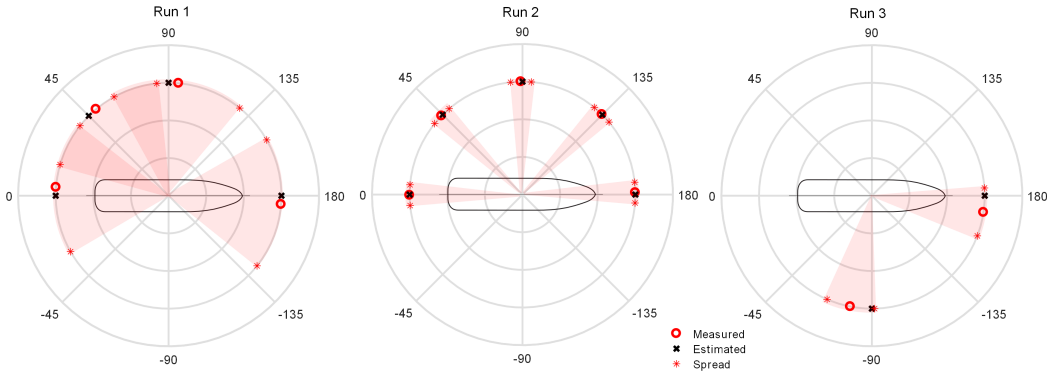

Figure 12: Measured and estimated relative wave direction β, and $\hat{\beta}$ in $[deg]$ for sea states in Runs 1-3. The spread for the sea state in Run 1 is 34°, so the sectors are overlapping for some directions. Keep in mind that the wave propagation direction Θ in the global frame is constant and that the vessel is changing heading.

almost the same amount of energy around the swell peak frequency as around the wind-generated wave peak frequency. However this is not reflected in the estimated wave parameters $\hat{\beta}$, $\hat{H}_s$ and $\hat{T}_p$, which are all (except $\hat{T}_p$ for head seas) estimating the wind-generated wave.

The largest estimation error for the peak period occurs for the sea state in Run 2 for head seas $\tilde{T}_p = 30.0\%$. Here, the two-peaked heave response has a slightly higher peak corresponding to the swell waves, as can also be seen in Figure 10. Coincidentally, the significant wave height estimate for the same case is the best for this sea state, with $\tilde{H}_s = 1.85\%$.

The measured relative wave direction and spread, and the estimated relative wave directions are shown in Figure 12 for all runs. The mean estimation error for the relative wave direction was $\tilde{\beta} = 3.75°$, with a standard deviation of 3.41°. The largest estimation error occurred for Run 3 in beam seas of $\tilde{\beta} = 11°$. However, since the test cases were for $\beta = \{0, 45, 90, 135, 180\}$, and the method is designed to estimate exactly these wave directions, the estimation error $\tilde{\beta}$ is misleading. In general the method identifies a wave direction within 45° intervals, which theoretically gives a maximum estimation error of $\tilde{\beta} = 22.5°$. All relative wave directions in these test cases were identified correctly.

The waves had a relatively large spread in the first sea state of 34°, as seen by the overlapping sectors in Figure 12. It is not easy to detect which effects (if any) this

large spread has had on the estimates. As mentioned, the iteration in (4) does not differentiate between multiple (directional) peaks, but rather makes an indirect energy-directional average, and the procedure outlined in Section 3.2 selects the direction with the best agreement of energy. Therefore the estimated wave direction for the sea state in Run 2 corresponds fairly well for the wind-generated waves, and not at all for the swell.

4.5. General discussion

The procedure for estimating the sea state summarized in Figure 3 works well for the response measurements of R/V Gunnerus in DP. The method requires little tuning in order to work, and is computationally efficient[3], solving $3 \times N_\beta$ linear equations through iteration. Here 15 minutes of response measurements were used for the response spectra, so having some overlap in the samples, a reliable sea state estimate could be available in a controller every 10 minutes, if necessary. Other parameters than the significant wave height, peak period and wave direction may be derived as input to control algorithms as well.

The DP control system kept R/V Gunnerus well in position in these data sets, which is a good basis for sea state estimation. As mentioned in Section 2.1, the size of the vessel compared to the waves influences the quality of the sea state estimates. Usually, the control algorithm in DP filters out the wave-frequency vessel motion from the control law so that first-order wave motions are not compensated for. Hence, it is expected that DP will not actuate in the first order range, but in this case there could be some influence on the controlled surge, sway and yaw motion, since the vessel is relatively small compared to the waves. This is especially a concern for sea state estimation using the roll motion in beam sea, since the maximum roll angles for this relative wave direction are around 10°, and may hence be influenced by the controlled sway and yaw motions. The maximum pitch angles were generally below 5°, so the couplings between the controlled surge motion, and the heave and pitch motions used for estimation, are thought to be small.

The maximum heading deviation from the setpoint was 5.87°, which occurred in beams seas for Run 3, and the average standard deviation of the heading was 1.30°. These are usual values for heading deviation for moderate sea states, which is the case for the relatively small R/V Gunnerus in the data sets examined here [29]. Since the relative wave direction estimate is an energy-directional average found based on a timeseries of measurements, the influence of small oscillations in heading about the setpoint are thought to be small. The influence of the directional spread of the waves is anticipated to be much more significant. Although not shown, examination of the covariance of the response measurements reveals that the vessel is in steady state for most of the time series. However, in some of the data sets the response is not stationary, so the steady-state assumption may be relaxed.

[3]The execution time for the slowest case was 0.1 seconds on an Intel(R)Core(TM)i7-4600U CPU @ 2.10 GHz.

5. Conclusion

The sea state estimation algorithm presented in this paper was a rather direct/brute-force kind of (spectral) approach which was shown to be computationally efficient. The method required little tuning in order to work, and relied only on the vessel responses and main vessel parameters. The method has proved so far to have good estimating performance, with an average significant wave height estimation error of 5.79%, average peak period estimation error of 7.59%, and the relative wave direction was estimated within the correct 45° interval for every data set. Therefore, the method could stand alone but, due to its high computational efficiency, it might also be used as an 'initial sea state estimator' that gives a starting guess for some of the more established sea state estimation techniques based on Bayesian statistics or parametric optimization, e.g., [6, 11, 12, 28]. The fast estimation capabilities will be promising for improving transient performance of the DP system.

This initial study was particularly relevant for DP (no forward speed), but in the meantime the procedure has been generalized to include advance speed and short-crested waves [30]. For future work, a sensitivity study on the number of samples in the FFT of the vessel responses, and the vessel size compared to the wave length, and a comparative study where the method when using the vessel transfer functions instead of the closed-form expressions should be completed.

Acknowledgement

This work was supported by the Research Council of Norway through the Centres of Excellence funding scheme, project number 223254 NTNU AMOS. The data presented in this paper was collected during sea trials in 2013 in connection with the SIMVAL KPN project (grant number 225141/O70). The data collection was financed by Rolls-Royce Marine and the

Norwegian Research Council through grant number 226412/O70. Thanks to Rolls-Royce Marine for permission to publish the results.

References

[1] A. J. Sørensen, A survey of dynamic positioning control systems, Annual Reviews in Control 35 (1) (2011) 123–136.

[2] M. Ludvigsen, A. J. Sørensen, Towards integrated autonomous underwater operations for ocean mapping and monitoring, Annual Reviews in Control 42 (2016) 145–157.

[3] G. F. Clauss, S. Kosleck, D. Testa, Critical situations of vessel operations in short crested seas-forecast and decision support system, in: Journal of Offshore Mechanics and Arctic Engineering, Vol. 134, (2012). doi:10.1115/1.4004515.

[4] D. C. Stredulinsky, E. M. Thornhill, Ship motion and wave radar data fusion for shipboard wave measurement, Journal of Ship Research 55 (2011) 73–85.

[5] E. M. Thornhill, D. C. Stredulinsky, Real Time Local Sea State Measurement using Wave Radar and Ship Motions, in: SNAME annual meeting, Seattle, WA, USA, (2010).

[6] U. D. Nielsen, Estimations of on-site directional wave spectra from measured ship responses, Marine Structures 19 (2006) 33–69.

[7] T. Iseki, K. Ohtsu, Bayesian estimation of directional wave spectra based on ship motions, Control Engineering Practice 8 (2) (2000) 215–219. doi:10.1016/S0967-0661(99)00156-2.

[8] R. Pascoal, C. Guedes Soares, Kalman filtering of vessel motions for ocean wave directional spectrum estimation, Ocean Engineering 36 (6-7) (2009) 477–488. doi:10.1016/j.oceaneng.2009.01.013.

[9] E. Tannuri, J. Sparano, A. Simos, J. Da Cruz, Estimating directional wave spectrum based on stationary ship motion measurements, Applied Ocean Research 25 (5) (2003) 243–261. doi:10.1016/j.apor.2004.01.003.

[10] U. D. Nielsen, A concise account of techniques available for shipboard sea state estimation, Ocean Engineering 129 (2017) 352–362. doi:10.1016/j.oceaneng.2016.11.035.

[11] C. Møgster, Sea state estimation using Bayesian modeling methods, Master's thesis, Department for Marine Technology, (NTNU), Supervisor: Asgeir J. Sørensen (2015).

[12] T. Iseki, Real-time analysis of higher order ship motion spectrum, ASME. International Conference on Offshore Mechanics and Arctic Engineering, 29th International Conference on Ocean, Offshore and Arctic Engineering 2 (2010) 399–405. doi:10.1115/OMAE2010-20521.

[13] T. D. Nguyen, A. J. Sørensen, S. T. Tong Quek, Design of hybrid controller for dynamic positioning from calm to extreme sea conditions, Automatica 43 (5) (2007) 768–785.

[14] D. J. W. Belleter, R. Galeazzi, T. I. Fossen, Experimental verification of a global exponential stable nonlinear wave encounter frequency estimator, Ocean Engineering 97 (2015) 48–56. doi:10.1016/j.oceaneng.2014.12.030.

[15] A. H. Brodtkorb, U. D. Nielsen, A. J. Sørensen, Sea state estimation using model-scale DP measurements, in: MTS/IEEE OCEANS, Washington DC, (2015).

[16] U. D. Nielsen, M. Bjerregård, R. Galeazzi, T. I. Fossen, New concepts for shipboard sea state estimation, in: MTS/IEEE OCEANS, Washington DC, (2015).

[17] U. D. Nielsen, A. H. Brodtkorb, J. J. Jensen, Response predictions for marine vessels using observed autocorrelation function, in: To appear in: Marine Structures, (2017).

[18] J. Jensen, A. Mansour, A. Olsen, Estimation of ship motions using closed-form expressions, Ocean Engineering 31 (2004) 61–85.

[19] WAMIT Inc., WAMIT- State of the art in wave interaction analysis, Massachusetts 02467-2504 USA, `http://www.wamit.com` (2017).

[20] Sintef Ocean, ShipX, Trondheim, Norway, `http://www.sintef.no/programvare/shipx/` (2017).

[21] A. Papanikolaou, E. Boulougouris, D. Spanos, On the roll radius of gyration of ro-ro passenger ships, 7th International Society of Offshore and Polar Engineers (ISOPE) Conference III (1997) 499–507.

[22] J. Hua, M. Palmquist, Wave estimation through ship motion measurement, Technical Report, Naval Architecture, Department of Vehicle Engineering, Royal Institute of Technology.

[23] M. Aschehoug, Scientific paper on the sea state estimation methodology, Technical Report, SIREHNA, France [Paper prepared in the HullMon+ project].

[24] U. D. Nielsen, Estimation of directional wave spectra from measured ship responses, PhD thesis, Section of Coastal, Maritime and Structural Engineering, Department of Mechanical Engineering, Technical University of Denmark, May, 2005.

[25] S. Steen, Ø. Selvik, V. Hassani, Experience with rim-driven azimuthing thrusters on the research ship Gunnerus, in: High-Performance Marine Vessels, Cortona, Italy, (2016).

[26] R. Skjetne, Ø. K. Kjerstad, S. A. T. Værnø, A. H. Brodtkorb, A. J. Sørensen, M. E. N. Sørensen, M. Breivik, V. Calabrò, B. O. Vinje, AMOS DP research cruise 2016: Academic full-scale testing of experimental dynamic positioning control algorithms onboard R/V Gunnerus, in: ASME. International Conference on Ocean, Offshore and Arctic Engineering (OMAE), Trondheim, Norway, (2017).

[27] WAFO-group, WAFO - A Matlab Toolbox for Analysis of Random Waves and Loads - A Tutorial, Math. Stat., Center for Math. Sci., Lund Univ., Lund, Sweden (2000).

[28] N. Montazeri, U. D. Nielsen, J. J. Jensen, Estimation of wind sea and swell using shipboard measurements – a refined parametric modelling approach, Applied Ocean Research 54 (2016) 73 – 86. doi:http://doi.org/10.1016/j.apor.2015.11.004.

[29] T. I. Fossen, J. P. Strand, Passive nonlinear observer design for ships using Lyapunov methods: full-scale experiments with a supply vessel, Automatica 35 (1) (1999) 3 – 16.

[30] U. D. Nielsen, A. H. Brodtkorb, A. J. Sørensen, A brute-force spectral approach for wave estimation using measured vessel responses, in: Submitted to Marine Structures, (2017).

Paper C:

A Brute-force Spectral Approach for Wave Estimation Using Measured Vessel Responses

Ulrik D. Nielsen, Astrid H. Brodtkorb, Asgeir J. Sørensen

Submitted to Marine Structures 2017.

A brute-force spectral approach for wave estimation using measured vessel responses

Ulrik D. Nielsen[a,b], Astrid H. Brodtkorb[b], Asgeir J. Sørensen[b]

[a]*DTU Mechanical Engineering, Technical University of Denmark, DK-2800 Kgs. Lyngby, Denmark*
[b]*Centre for Autonomous Marine Operations, AMOS-NTNU, NO-7491 Trondheim, Norway*

Abstract

The article introduces a spectral procedure for sea state estimation based on measurements of motion responses of a ship in a short-crested seaway. The procedure relies fundamentally on the wave buoy analogy, but the wave spectrum estimate is obtained in a direct - brute-force - approach, and the procedure is simple in its mathematical formulation. The actual formulation is extending another recent work by including vessel advance speed and short-crested seas. Due to its simplicity, the procedure is computationally efficient, providing wave spectrum estimates in the order of a few seconds, and the estimation procedure will therefore be appealing to applications related to realtime, onboard control and decision support systems for safe and efficient marine operations. The procedure's performance is evaluated by use of numerical simulation of motion measurements, and it is shown that accurate wave spectrum estimates can be obtained for all wave directions in short-crested waves, taking the wave system to be composed by both wind generated sea and swell.

Keywords:
Wave spectrum, shipboard estimation, vessel responses, wave buoy analogy, Doppler Shift, spectrum transformation

1. Introduction

The level of autonomy in many aspects of marine operations, including shipping, is increasing, and the trend is believed to continue in the future [1, 2, 3]. One area of autonomy is in this context related to the risk and/or the performance evaluation of the actual operation, where focus may be on, say, cargo and passenger safety on a ship navigating in a seaway, hull girder integrity, fuel performance of the operating marine vessel, exact positioning and deterministic motion prediction of an offshore installation craft, etc. Regardless the type of operation, or whether the concern is on *deterministic* or *statistical* evaluations [4, 5, 6], it will be of an advantage to possess knowledge about the on-site sea state. For instance, statistics of the wave-induced acceleration level at given positions on a cruise ship can be easily calculated for various combinations of advance speed and heading, relative to the incoming waves, if a seakeeping code is coupled with an estimate of the sea state. Hence, it is possible to suggest (or "automatically enforce") the optimum combination of speed and heading in a safety-performance context.

One means to rely on for obtaining an estimate of the sea state at a vessel's exact geographic position is that of the wave buoy analogy, where onboard sensor measurements of wave-induced motion responses are processed to yield the wave energy distribution of the encountered wave system [7, 8, 9, 10, 11, 12]. In the past, various mathematical formulations of the wave buoy analogy have been studied with a main categorisation into A) spectral (frequency-domain) approaches based on Bayesian modelling or parametric optimisation, or B) time-domain approaches based on Kalman filtering or (recursive) nonlinear least squares fitting; an overview of available procedures (A and B) has been given by Nielsen [13]. However, just recently, a new implementation of the wave buoy analogy has been suggested by Brodtkorb et al. [14]. Although the initial work is considering vessels without advance speed, as focus was on ships being dynamically positioned (DP), very promising results have been obtained from full-scale DP experiments assuming long-crested waves.

The present study is a continuation of [14], with the aim to generalise the implementation to include mea-

Email address: udn@mek.dtu.dk (Ulrik D. Nielsen)

surements from a ship with advance speed, *and* letting the seaway be represented by short-crested (directional) waves. It is a central property that the implementation relies on a rather direct or brute-force kind of (spectral) approach that allows for high computational efficiency. The particular approach has, as mentioned, proved so far to have good estimating performance. As such, the approach can therefore stand alone but, due to its high computational efficiency, it might also be used as an 'initial sea state estimator' that gives a starting guess for one of the more - mathematically complex and "consecrated" - sea state estimation techniques based on, say, Bayesian modelling or parametric optimisation [7, 8, 15, 11, 16, 17]. Two characteristics of the present, updated implementation are noteworthy: (1) the implementation is a spectral approach derived in the frequency domain, (2) the given solution applies (initially) to the *encounter*-frequency domain and, thus, a transformation to *absolute* (true) frequency domain is necessary. In its fundamentals, the mathematical formulation is similar to the work by Brodtkorb et al. [14], which also relies on a spectral, brute-force approach, but the details are quite different. The differences are consequences of the generalised setting of the present, updated formulation; taking the speed-of-advance problem *and* short-crested seas into account. Altogether, it means that the governing equations of the two implementations - present work vs. [14] - are the same, but the solution strategies are not. It should be suggested already at this stage to consult available literature on the (practical) complications involved for a ship advancing relative to the incident waves [18, 19, 20, 21].

The simplicity behind the studied procedure is considered as an advantage in relation to many parts of real-time shipboard decision support tools as well as control (DP) applications, where, for instance, advanced controller schemes used in hybrid or switching control algorithms rely on computationally efficient algorithms. Online sea state estimates from rapid schemes, can be used to manipulate parameters in the control law directly, or be input to performance monitoring functions and risk assessment models that choose the best algorithms available [14]. As a further but more general note on the computational efficiency of the present sea state estimation procedure, sea state updates can be made so fast that it will be possible to directly carry out probabilistic assessments of the outcome by integrating the estimation procedure with probabilistic software tools. To date, this has not been possible with the existing sea state procedures [e.g. 7, 8, 15, 11, 16, 17], because of computational times in the order of minutes rather than seconds as is the case for the present work.

The article is composed as follows: After the introduction, Section 2 outlines the theory in terms of the governing equations as well as the solution strategy that includes a subsequent post-process/analysis. The implementation has some restrictions, mentioned in Section 3 together with other practicalities and characteristics. The procedure's performance is investigated through a number of test cases consisting of (artificial) simulations of measurement data, Section 4, and the associated results and discussions are given in Section 5. Finally, Section 6 presents conclusions and suggests further work.

2. Theory

The wave-induced (motion) responses of a ship in an irregular, short-crested seaway are considered. It is assumed that the responses are linear with the incident waves, and the speed and (mean) heading of the vessel relative to the waves are U and $\chi \in [0, 360[$ deg., respectively, with $\chi = 180$ deg. being head sea. The wave energy is distributed according to a directional wave energy spectrum $S(\omega_0, \mu)$ where ω_0 is the *absolute* (wave) frequency and $\mu \in]-180, 180]$ deg. is the angle describing the directional variation of the spectral ordinate relative to an axis parallel with the vessel's centreline. For a given vessel speed, the set of wave frequency and relative heading implies a certain (and unique!) *encounter* frequency ω_e determined by the Doppler Shift,

$$\omega_e = \omega_0 - \omega_0^2 \psi, \ \psi = \frac{U}{g} \cos\chi \tag{1}$$

where g is the acceleration of gravity, and for convenience $\mu = 0$ deg.

The Doppler Shift expresses a mathematical/physical elementary, but it is important to realise that the practical complications related to the Doppler Shift is by no means straight-forward to handle for wave-induced responses of an advancing ship in a seaway, as also mentioned in various textbooks [e.g. 18, 19, 20]. This will be further elaborated on in the following subsections, where the governing equations are specified together with the solution approach, but, at first, a common understanding of *encounter domain* versus *absolute domain* is beneficial. The particular problem-settings imply a solution, i.e. the wave spectrum estimate, obtained in the encounter domain, which is a mapping of the absolute - and true - domain, for an advancing ship. Thus, it is understood that the 'encounter domain' is that one observed from the ship as it advances relative to the inertial frame used for describing the progressing waves.

On the other hand, the 'absolute domain' is the domain any fixed observer without advance speed, relative to the inertial frame, is in. Later, the solution strategy makes direct use of the work by Nielsen [21], which can also be consulted to gain additional insight on the mapping between encounter domain and absolute domain, and vice versa.

2.1. Spectral analysis and fundamental equations

The estimation problem is formulated in the frequency domain through spectral analysis. In principle, this requires data, and the underlying physical process(es), to be stationary in the stochastic sense. Obviously, a truly stationary condition rarely exists for a ship (advancing) in a seaway due to changes in operational and environmental parameters. In a time frame in the order of 15-30 minutes it is however often considered acceptable to take conditions to be stationary, and this assumption will be made throughout, without necessarily stating this at the relevant places.

The linear relationship between waves and wave-induced vessel responses (here only heave, roll and pitch are considered) is given by the complex-valued motion transfer functions* $X_i(\ldots)$, which can be calculated using hydrodynamic software (e.g. strip theory and panel codes) and/or obtained by measurements. In a short-crested, stationary seaway it holds that,

$$R_{ij}(\omega_e) = \int X_i(\omega_e, \mu+\chi)\overline{X_j(\omega_e, \mu+\chi)}S_e(\omega_e, \mu)d\mu \tag{2}$$

where $R_{ij}(\omega_e)$ is the complex-valued cross spectrum for a pair (i, j) taken among the heave (z), roll (ϕ), and pitch (θ) responses $i, j = \{z, \phi, \theta\}$; $\overline{X_j(\ldots)}$ is the complex conjugate of the transfer functions in heave, roll and pitch for wave heading $(\mu + \chi)$ relative to the single waves from direction μ. $S_e(\omega_e, \mu)$ is the wave spectrum ordinate as observed from the advancing ship; note that index 'e' is used to emphasise that the ordinate refers to the encounter domain. As an assumption, $S_e(\omega_e, \mu)$ is represented by the product between a point spectrum $E(\omega_e)$ and a directional spreading function $\varphi(\mu)$,

$$S_e(\omega_e, \mu) = E(\omega_e)\varphi(\mu) \tag{3}$$

*Note, complex-valued motion transfer functions and response amplitude operators (RAOs) are *not* the same, although the terms are sometimes referred to as having similar meanings. Strictly speaking, the RAO is the square of the modulus of $X_i(\ldots)$.

Consequently, Eq. (2) is rewritten,

$$R_{ij}(\omega_e) = E(\omega_e)\int X_i(\omega_e, \mu+\chi)\overline{X_j(\omega_e, \mu+\chi)}\varphi(\mu)d\mu \tag{4}$$

The spreading function [e.g. 18] is taken as

$$\begin{aligned}\varphi(\mu) =& A(s) \times \cos^{2s}\left(\frac{\mu}{2}\right), \\ A(s) =& K \cdot \frac{2^{2s-1}\Gamma^2(s+1)}{\pi\Gamma(2s+1)},\end{aligned} \tag{5}$$

where Γ denotes the Gamma function, and s is the spreading parameter. The spreading function is obliged to fulfill $\int_{\mu_1}^{\mu_2}\varphi(\mu)d\mu \equiv 1$ from which the value of K is determined for a given pair of directions (μ_1, μ_2) that confines the directional spreading. If $(\mu_1, \mu_2) = (-180, 180)$ deg., then $K = 1$.

The cross spectra $R_{ij}(\omega_e)$ can be calculated for sets (i, j) of response measurement time series by using a cross power spectral density function, e.g., `cpsd` in MATLAB®. An example of corresponding sets of cross spectra $R_{ij}(\omega_e)$ calculated from three measured time history recordings is shown in Figure 1 taken from Brodtkorb et al. [14]. From the plots/spectra it is observed that $R_{ij}(\omega_e)$ is complex-valued for $i \neq j$, and that corresponding cross-spectra pairs, or *off-diagonal* pairs, are complex conjugate, i.e. $\mathcal{I}m(R_{ij}) = -\mathcal{I}m(R_{ji})$, which is a property that can be used to infer about the incident wave direction as seen later. The individual off-diagonal complex-valued spectra in Figure 1 can be given as corresponding real-valued pairs of amplitude- and phase-spectra by simply calculating the modulus and phase, respectively, for each frequency component of a given off-diagonal spectrum. For instance, the amplitude spectrum of the coupled motion of heave and roll is,

$$|R_{z\phi}(\omega_e)| = \sqrt{\left[\mathcal{R}e(R_{z\phi}(\omega_e)\right]^2 + \left[\mathcal{I}m(R_{z\phi}(\omega_e)\right]^2} \tag{6}$$

and it is noted that the 'amplitude spectrum' has a similar meaning as the three diagonal spectra of heave, roll, and pitch, respectively, in Figure 1; namely, the amplitude spectrum represents the distribution of 'power' with frequency of the particular (coupled) motion component. Consequently, a total of six independent power (and three phase) spectra can be computed from the three measured motion components heave, roll, and pitch.

Rather than solving Eq. (4) with complex-valued spectra, it is decided (for numerical stability reasons) to solve the equation by introducing instead the six power

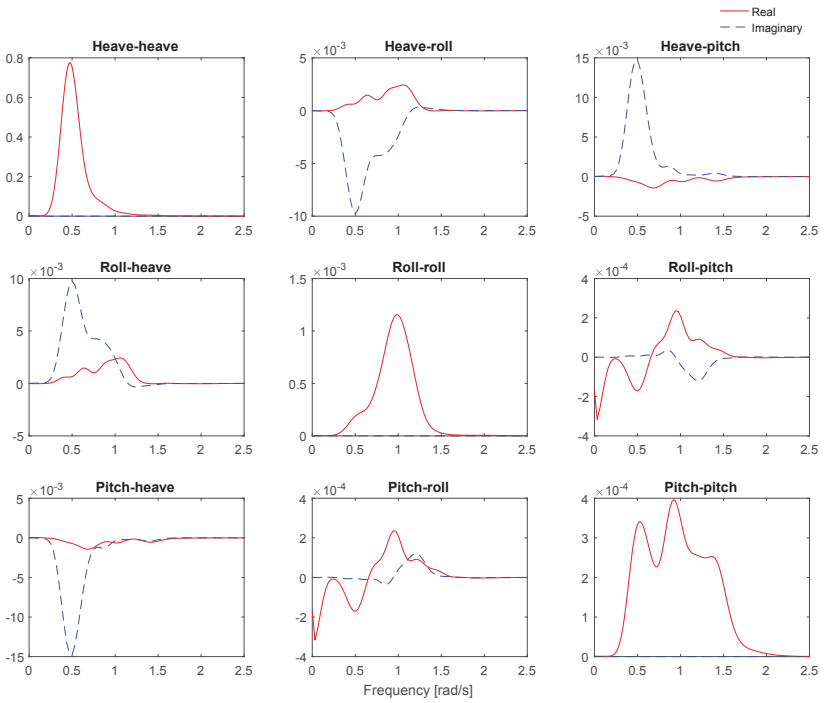

Figure 1: Cross spectra R_{ij} calculated from measured responses in heave [m], roll [rad.] and pitch [rad.] of the research vessel R/V Gunnerus. Brodtkorb et al. [14].

spectra, and to leave phase information/equations out in the first step. Thus, the six governing equations of the estimation problem read,

$$|R_{ij}(\omega_e)| = E(\omega_e) \int \left| X_i(\omega_e, \mu + \chi) \overline{X_j(\omega_e, \mu + \chi)} \right| \varphi(\mu) d\mu \tag{7}$$

formed by the pairs of motion components (i, j), which are (z, z), (ϕ, ϕ), (θ, θ), (z, ϕ), (z, θ), and (ϕ, θ). In Eq. (7), the left-hand side is obtained through measurements while the right-hand side is obtained through theoretical calculations combining available knowledge about the motion transfer functions together with information about the wave energy spectrum.

It is important to note that Eq. (7) is formulated in the encounter-frequency domain (ω_e). However, the motion transfer functions of a vessel are determined for a set of *absolute* wave frequencies (ω_0), and it is therefore necessary to introduce the Doppler Shift, Eq. (1), when solving Eq. (7) for the unknown point-wave energy spectrum $E(\omega_e)$. When a ship advances in following seas*, the Doppler Shift imposes a 1-to-3 mapping between encounter and absolute frequencies, since one encounter frequency may be "clocked" at three different absolute frequencies in certain conditions [21]. Turning to Eq. (7), this means that for any (discrete) encounter frequency - with the 'following sea conditions' fulfilled - the corresponding three absolute frequencies need to be simultaneously considered on the right-hand side of Eq. (7), as the assumption is that the three frequencies, i.e. wave components, will contribute "equally" to form the *encountered* wave component. Symbolically, the corresponding pairs of encounter and absolute frequencies are written as $\{\omega_e \rightleftarrows \omega_{01}\}$ and $\{\omega_e \rightleftarrows \omega_{01}, \omega_{02}, \omega_{03}\}$ for head seas and following seas, respectively; see Nielsen [21] for further details. The final version of the governing equation system is there-

*In this article, the term 'following seas' is at many places used to cover everything from following waves to beam waves (not included), while 'head seas' covers beam waves (included) to head waves.

fore given by,

$$|R_{ij}(\omega_e)| = E(\omega_e)\int |\Phi_{ij}(\omega_{01},\mu+\chi)|^2\varphi(\mu)d\mu \qquad (8)$$
$$+E(\omega_e)\int \left[|\Phi_{ij}(\omega_{02},\mu+\chi)|^2 + |\Phi_{ij}(\omega_{03},\mu+\chi)|^2\right]\varphi(\mu)d\mu$$

where $|\Phi_{ij}(\omega_{0k},\mu+\chi)|^2 = |X_i(\omega_{0k},\mu+\chi)\overline{X_j(\omega_{0k},\mu+\chi)}|$, and it is stressed that the first line of the equation is considered for all conditions, while the second line applies specifically to following seas. However, in following seas, the inclusion of the individual contributions is conditional, depending on the value of the encounter frequency relative to the wave heading and the speed of the vessel. A thorough discussion on these aspects is given by Nielsen [21]. As pointed out, the corresponding set of frequencies, encounter vs. absolute, is given by the Doppler Shift, and solving Eq. (1) for the absolute frequency yields for **head seas**,

$$\omega_{01} = \frac{1-\sqrt{1-4\psi\omega_e}}{2\psi}, \qquad \text{all } \omega_e \qquad (9)$$

and for **following seas**,

$$\omega_{01} = \frac{1-\sqrt{1-4\psi\omega_e}}{2\psi}, \qquad \omega_e < \frac{1}{4\psi} \qquad (10a)$$
$$\omega_{02} = \frac{1+\sqrt{1-4\psi\omega_e}}{2\psi}, \qquad \omega_e < \frac{1}{4\psi} \qquad (10b)$$
$$\omega_{03} = \frac{1+\sqrt{1+4\psi\omega_e}}{2\psi}, \qquad \text{all } \omega_e \qquad (10c)$$

2.2. Stepwise estimation of the wave spectrum

The speed-of-advance problem, introduced through the Doppler Shift, implies that the solution to Eq. (8) is obtained by considering head seas and following seas separately. Irrespectively, the *final* wave spectrum estimate is calculated in two steps: (i) an initial step concerned with the direct, or brute-force, solution of Eq. (8), and (ii) a second step concerned with a wave direction estimate computed through a post-processed solution. The practical details are outlined in the following but it is noteworthy that for the initial step (i) it is relevant only to consider relative wave headings just in the interval $\chi = [0, 180]$ deg., as the brute-force solution is concerned with an equation system, Eq. (8), formulated through power spectra. Thus, calculation of the right-hand side of Eq. (8) gives identical results for, say, $\chi = 70$ deg. and $\chi = 290$ deg. as these headings correspond to incident waves mirrored around the centreline of the ship ($\chi = 180$ deg. is incident waves head on).

(i) Brute-force solution

The brute-force solution does not assume a wave spectrum shape, or parameterise it in any way. Instead, the sea state estimate is based on the direct solution of the linear equation, Eq. (8), which is solved using an iterative scheme, as follows [14]:

$$\tilde{R}_{ij} = R_{ij}(\omega_e) - \hat{R}_{ij} \qquad (11a)$$
$$\hat{E}_{ij}(k) = \hat{E}_{ij}(k) + h\tilde{R}_{ij} \qquad (11b)$$
$$\hat{R}_{ij} = \hat{E}_{ij}(k)\int \sum_{m=1}^{3} |\Phi_{ij}(\omega_{0m},\mu+\chi_k)|^2\varphi(\mu)d\mu \qquad (11c)$$

performed for any pair (i, j) of motion components; herein taken as (z, z), (ϕ, ϕ), (θ, θ), (z, ϕ), (z, θ), and (ϕ, θ), and noting that Eq. (11c) is calculated conditionally with due account for head sea vs. following sea conditions, as addressed in relation with Eq. (8). Furthermore, it should be noted that Eq. (8) is solved for the entire range of (encounter) frequencies considered; in principle, in a frequency-by-frequency approach for the discrete computational settings, see below. Lastly, making a note of a more general character, the formulation of the problem in an iterative scheme, and based on a residual calculation, is a novel idea [14] compared to other existing spectral estimation procedures [e.g. 7, 8, 15, 11, 16, 17]. Indeed, the residual type of solution strategy is what makes the present procedure extremely efficient.

The practical implementation of the iterative scheme, or process, is illustrated using the pseudo script seen in Algorithm 1, which should be read with some supplementary remarks about:

- **Discretisation**. Wave directions and the set of encounter frequencies are discretised into N_χ and N_{ω_e} parts. Since the wave direction is unknown initially, a loop is made over all directions

$$\tilde{\chi}(k) = [0, 180] \text{ deg.}, \qquad k = 1 : N_\chi \qquad (12)$$

- **Initialisation**. The estimate of the (encounter) wave spectrum, and the estimate of the response spectrum are initially set to zero, $\hat{E}_{ij} = 0$ and $\hat{R}_{ij} = 0$. Compute the difference between the measured response spectrum and the estimated response spectrum $\tilde{R}_{ij} = R_{ij}(\omega_e) - \hat{R}_{ij}$.

- **Doppler Shift**. The given frequency is the encounter frequency ω_e, "produced" from the cross-spectral analysis, whereas the absolute frequency ω_0 will be a function of it. The function $f(\omega_e|\chi, U)$ is a result of the Doppler Shift; explicit expressions are seen in Eq. (9) and Eqs. (10a)-(10c).

- **Updates/adjustments**. Use $\tilde{R}_{ij}$ to make adjustments to $\hat{E}_{ij}$ with step size $h > 0$, and calculate the response spectrum estimate $\hat{R}_{ij}$ again. Do this until a threshold is reached $|\tilde{R}_{ij}| \leq \epsilon$, for $\epsilon > 0$.

The output from Algorithm 1 are six wave spectrum estimates per direction, yielding a spectrum estimate (block) matrix of dimension $6 \times (N_\chi \cdot N_{\omega_e})$,

$$\vec{E} = \begin{bmatrix} \hat{E}_{zz}(1,\omega_e) & \hat{E}_{zz}(2,\omega_e) & \dots & \hat{E}_{zz}(N_\chi,\omega_e) \\ \hat{E}_{\phi\phi}(1,\omega_e) & \hat{E}_{\phi\phi}(2,\omega_e) & \dots & \hat{E}_{\phi\phi}(N_\chi,\omega_e) \\ \hat{E}_{\theta\theta}(1,\omega_e) & \hat{E}_{\theta\theta}(2,\omega_e) & \dots & \hat{E}_{\theta\theta}(N_{\chi,\omega_e}) \\ \hat{E}_{z\phi}(1,\omega_e) & \hat{E}_{z\phi}(2,\omega_e) & \dots & \hat{E}_{z\phi}(N_\chi,\omega_e) \\ \hat{E}_{z\theta}(1,\omega_e) & \hat{E}_{z\theta}(2,\omega_e) & \dots & \hat{E}_{z\theta}(N_\chi,\omega_e) \\ \hat{E}_{\phi\theta}(1,\omega_e) & \hat{E}_{\phi\theta}(2,\omega_e) & \dots & \hat{E}_{\phi\theta}(N_\chi,\omega_e) \end{bmatrix} \tag{13}$$

noting that each component in Eq. (13) is a row vector of length N_{ω_e}, i.e. size $\left(\hat{E}_{ij}(k,\omega_e)\right) = 1 \times N_{\omega_e}$.

The matrix in Eq. (13) represents the brute-force solution to the wave estimation problem considered in Eq. (8). However, it is clear that the solution, as is, cannot be directly used, since 1) the solution is ambiguous with several sub-solutions (herein six) depending on the considered response, 2) no estimate of the wave direction, equivalently relative wave heading, is given as sub-solutions exist for all (specified) directions on a half circle [0,180] deg., and 3) the sub-solutions are encounter-wave spectra. Altogether, it is therefore necessary to post-process the brute-force solution, and the means for doing this are explained in the following.

(ii) Post-processed solution

The single wave spectrum estimates in Eq. (13) apply to the encounter domain and, hence, the estimates provide no information about the (true) distribution of wave energy in the absolute domain. Nonetheless, the spectra (Eq. 13) can be used to obtain an estimate of the total energy content of the wave system, since energy preserves irrespectively of the domain. In general, the total energy of a wave system can be given in terms of the significant wave height H_s, calculated from the area under the wave energy spectrum, see e.g. Eq. (22) in Subsection 4.2. Thus, the following $(6 \times N_\chi)$ matrix is obtained

$$\bar{H}_s = \begin{bmatrix} \hat{H}_{s,zz}(1) & \hat{H}_{s,zz}(2) & \dots & \hat{H}_{s,zz}(N_\chi) \\ \hat{H}_{s,\phi\phi}(1) & \hat{H}_{s,\phi\phi}(2) & \dots & \hat{H}_{s,\phi\phi}(N_\chi) \\ \hat{H}_{s,\theta\theta}(1) & \hat{H}_{s,\theta\theta}(2) & \dots & \hat{H}_{s,\theta\theta}(N_\chi) \\ \hat{H}_{s,z\phi}(1) & \hat{H}_{s,z\phi}(2) & \dots & \hat{H}_{s,z\phi}(N_\chi) \\ \hat{H}_{s,z\theta}(1) & \hat{H}_{s,z\theta}(2) & \dots & \hat{H}_{s,z\theta}(N_\chi) \\ \hat{H}_{s,\phi\theta}(1) & \hat{H}_{s,\phi\theta}(2) & \dots & \hat{H}_{s,\phi\theta}(N_\chi) \end{bmatrix} \tag{14}$$

where the single matrix elements are calculated by use of the individual components, i.e. $\hat{E}_{ij}(k,\omega_e)$, of Eq. (13).

In a perfect - purely theoretical - situation there will be one, and just one, column, say, no. k_K in Eq. (14), where all the (six) elements attain the same non-zero value; that is, the average of the values in the column is equal to the values of the single elements. Consequently, the hypothesis is that column no. k_K yields the optimum estimate of the significant wave height and, at the same time, the relative (mean) wave heading will be $\hat{\chi} = \tilde{\chi}(k_K)$, cf. Eq. (12). In practice, it is highly unlikely that the described "perfect" situation happens and, rather, the column (from Eq. 14) with the *smallest variation* in between the significant wave heights can be found. Thus, like for the purely theoretical situation, the given column, i.e. the discrete value of the heading representing the column, can be used as an estimate of the wave heading. In principle, this completes the estimation process, but it should be realised that, to this point, *six* wave spectrum estimates $\hat{E}_{ij}(k_K,\omega_e)$ apply to column k_K; i.e. one for each motion component, cf. Eq. (13). Therefore, the (final) optimum wave spectrum estimate is taken as the average of the six spectrum estimates; noting that the average is calculated frequency-wise,

$$\hat{E}_{final}(\omega_e) = \frac{1}{6}\Big(\hat{E}_{zz}(k_K,\omega_e) + \hat{E}_{\phi\phi}(k_K,\omega_e) + \hat{E}_{\theta\theta}(k_K,\omega_e) + \hat{E}_{z\phi}(k_K,\omega_e) + \hat{E}_{z\theta}(k_K,\omega_e) + \hat{E}_{\phi\theta}(k_K,\omega_e)\Big) \tag{15}$$

The estimation process is illustrated and explained with Figure 2. The two plots in the figure are the (initial brute-force) outcomes of the estimation procedure when it has been applied to artificially generated motion

Algorithm 1 Pseudo script for wave spectrum estimation

for $(i,j) = \{(z,z),(\phi,\phi),(\theta,\theta),(z,\phi),(z,\theta),(\phi,\theta)\}$ **do**
  for $k = 1 : N_\chi$ **do**
    $\hat{E}_{ij}(k) = zeros(1, N_{\omega_e})$
    $\hat{R}_{ij} = zeros(1, N_{\omega_e})$
    $\tilde{R}_{ij} = R_{ij}(\omega_e)$
    $\omega_0 = f(\omega_e|\chi, U)$
    while $|\tilde{R}_{ij}| > \epsilon$ **do**
      $\tilde{R}_{ij} = R_{ij}(\omega_e) - \hat{R}_{ij}$
      $\hat{E}_{ij}(k) = \hat{E}_{ij}(k) + h\tilde{R}_{ij}$
      $\hat{R}_{ij} = \hat{E}_{ij}(k) \int \sum_{m=1}^{3} |\Phi_{ij}(\omega_{0m}, \mu + \chi_k)|^2 \varphi(\mu) d\mu$
    end while
  end for N_χ
end for i

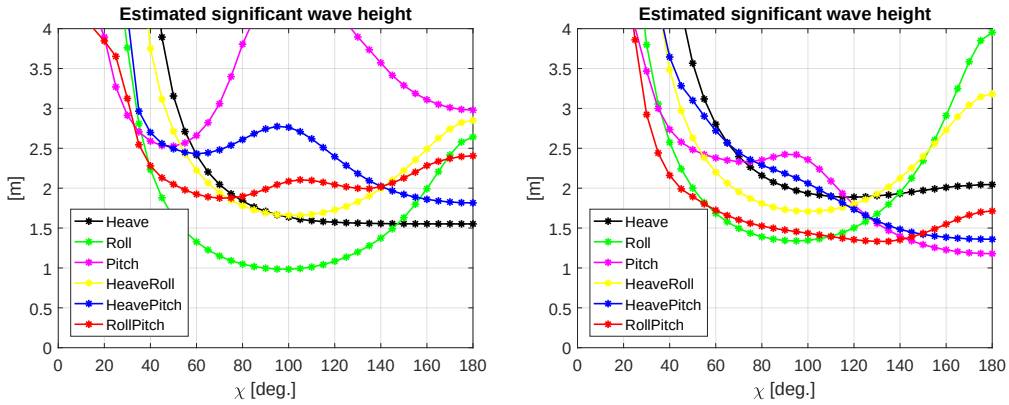

Figure 2: Variation of significant wave height H_s with mean relative wave heading χ using different motion components measured in a short-crested wave system. True parameters are for the left-side plot $\chi = 60$ deg. and $H_s = 2.0$ m, respectively, and for the right-side plot $\chi = 120$ deg. and $H_s = 2.0$ m.

data; the details about the vessel in study, about the time history generation, etc., are given later in Section 4, as the details are of minor importance for this explanatory example. In the given case (Fig. 2), two different sets of time history recordings of {heave,roll,pitch} are used as input to the estimation procedure. The two sets of motion recordings have been obtained/simulated using a short-crested wave system derived from the same type of wave spectrum; herein taken as a Bretschneider spectrum (see Sec. 4) with $H_s = 2.0$ m and $T_m = 6.5$ s. The only difference between the two sets of motion measurements is that the one set applies for a mean wave heading $\chi = 60$ deg. (left-side plot) and the other set for $\chi = 120$ deg. (right-side plot). In accordance with the selection process described above, it is found that the smallest variation between the estimated H_s-values is found for $\hat{\chi} = 55$ deg. and $\hat{\chi} = 125$ deg. for the left- and right-hand side plots, respectively. At these particular headings, the average significant wave heights are $\hat{H}_s = 2.2$ m ($\hat{\chi} = 55$ deg.) and $\hat{H}_s = 1.7$ m ($\hat{\chi} = 125$ deg.), as calculated from the two corresponding optimum wave spectrum estimates, cf. Eq. (15).

On a related note, the 'averaging-approach' has similarities to the study by Nielsen and Stredulinksy [22] that discusses the importance in selecting the best combination of motion measurements. This referred study uses also a mean-value-based solution, where all relevant combinations of motion measurements are considered and used for wave estimation. However, a general discussion about response selection for shipboard sea state estimation is beyond the scope of the present work and, thus, not addressed any further, but another useful study in this context has been given by Nielsen et al. [5].

It is a concern of the selection procedure described above that the obtained wave *heading* estimate will not necessarily be the (correct) optimum, since the selection procedure includes no distinction between incident waves on the port side and on the starboard side. The means to accommodate this problem is to make direct use of the complex-valued off-diagonal spectra, cf. Figure 1. Specifically, the imaginary parts of the off-diagonal elements should be considered, as these parts contain the necessary information because they are measures of the phases between the (coupled) motions. Hence, with reference to the fundamental equation, see Eq. (4), and the derived equation system Eq. (7) considering the six power spectra, three additional equations are considered:

$$\mathcal{I}m\left[R_{ij}(\omega_e)\right] = E(\omega_e)\int \mathcal{I}m\left[X_i(\omega_e,\mu+\chi)\overline{X_j(\omega_e,\mu+\chi)}\right]\varphi(\mu)d\mu \tag{16}$$

formed by the pairs of motion components (i, j), which in this case are (z,ϕ), (z,θ), and (ϕ,θ), respectively. Obviously, Eq. (16) needs to be implemented in the same way as Eq. (8), taking into account the practical complications in following sea. In contrast to the brute-force solution, cf. Algorithm 1, Eq. (16) is not solved for the point-wave spectrum $E(\omega_e)$ as the unknown, but for the wave heading instead. This is done by stepping through a discretised set of headings $\bar{\chi}_\kappa$, $\kappa = 1, 2, ..., \varkappa$ on the

full circle [0,360[deg. and calculating, for each heading, the right-hand side of Eq. (16), using the optimum wave spectrum estimate given by Eq. (15). The calculated right-hand side of Eq. (16) can be subtracted from the left-hand side resulting in an error estimate ε_κ^2 for the particular heading $\tilde{\chi}_\kappa$. The error estimate is defined in the least squares sense using the L_2 norm, and the (final) optimum wave heading is thus found for the heading $\tilde{\chi}_\kappa$ where ε_κ^2 attains its minimum,

$$\min_{\tilde{\chi}_\kappa} \varepsilon_\kappa^2 \equiv \min \|\mathcal{I}m\left[R_{ij}(\omega_e)\right] - f(\tilde{\chi}_\kappa)\|^2 \qquad (17)$$

noting that the right-hand side of Eq. (16) has been written symbolically as $f(\tilde{\chi}_\kappa)$.

Clearly, the estimate of the optimum wave heading is made in a rather brute-force approach. This choice is made to keep the overall estimation procedure consistent and to be of a 'practical engineering' character, although it would be easy to obtain the optimum heading through a strict optimisation formulated through a cost function.

In a summarised form, the estimation process consists of the following points, focusing on the post-processed solution:

1. On the basis of the brute-force solution, i.e. from the block matrix in Eq. (13), calculate the corresponding matrix $\bar{H}_s$ of significant wave heights, cf. Eq. (14).
2. Find the column (k_K) in the matrix $\bar{H}_s$ that has the smallest standard deviation.
3. The six wave spectrum estimates of column k_K are used to determine the optimum (encounter) wave spectrum, calculated as the average of the six spectra in column k_K:

$$\hat{E}_{final}(\omega_e) = \frac{1}{6}\left(\hat{E}_{zz}(k_K,\omega_e) + \hat{E}_{\phi\phi}(k_K,\omega_e) + \hat{E}_{\theta\theta}(k_K,\omega_e) + \hat{E}_{z\phi}(k_K,\omega_e) + \hat{E}_{z\theta}(k_K,\omega_e) + \hat{E}_{\phi\theta}(k_K,\omega_e)\right) \qquad (18)$$

4. Apply the optimum wave spectrum $\hat{E}_{final}(\omega_e)$ to select the optimum wave heading by minimising the error between the left- and right-hand sides of Eq. (16).

2.3. Transformation to absolute domain

Altogether, the outlined estimation procedure results in a point-wave spectrum estimate *and* an estimate of the mean relative heading. The wave spectrum has been estimated for a (particular) set of *encounter* frequencies, and, hence, the significant wave height can be directly obtained from the spectrum. On the other hand, the spectrum reveals no explicit information about the absolute, or true, distribution of wave energy; or equivalently said, knowledge about characteristic *absolute* wave periods such as the mean period (T_m) and peak period (T_p) is unavailable if no action is taken. Consequently, it is needed to further process the solution and to *transform the spectrum from encounter to absolute domain*. Indeed, such a transformation procedure is available, since a dedicated study by Nielsen [21] on the topic/task has been conducted in parallel with the current work. The details of the transformation procedure will not be given here, and it suffices to say that spectrum transformation generally can be uniquely carried out when the ship sails "against" the waves (beam to head sea). In following sea conditions, however, there exists no unique solution to the problem. Instead, a reasonable approach valid for practical engineering must be applied, and the mentioned work [21] outlines one viable approach that can be used to transform a wave spectrum from encounter to absolute domain; which is exactly what is needed in the present study, where an encounter-wave spectrum is available together with knowledge about the relative wave heading. The final result from the estimation procedure is therefore obtained by transforming the optimum wave spectrum estimate $\hat{E}_{final}(\omega_e)$,

$$E(\omega_0) = g(\hat{E}_{final}(\omega_e)|\tilde{\chi}_\kappa, U) \qquad (19)$$

where $g(\ldots)$ is the mapping-function [21] which consistently transforms the estimated wave spectrum from encounter to absolute domain.

3. Practicalities

To this point the estimation procedure has been presented for its fundamental concepts and the associated equations. Thus, it remains as the main task to evaluate the procedure. The evaluation will be performed using perfectly controlled settings in terms of computational simulations. It is, however, important to touch upon some practical aspects of the estimation procedure before its performance is discussed, and these aspects are addressed in the following, where focus will be on limitations, spectral calculations, and on a ship's motion transfer functions and their use in the context of sea state estimation. Moreover, a very brief description of the central point(s) of the wave spectrum transformation algorithm [21] is included.

3.1. Limitations

Due to a solution strategy relying on a residual calculation through an iterative scheme, the estimation pro-

cedure provides a *point spectrum*; initially obtained in the encounter domain and subsequently transformed to the absolute domain with due account for vessel speed and (mean) wave direction. Described by a point spectrum, the wave system is inherently considered as unidirectional, but short-crested waves are "imposed" into the solution by an overlaid directional spreading function. Nonetheless, the solution, or the wave spectrum estimate, is restricted from handling truly crossed-sea conditions where wind waves from one direction occurs at the same time as swells from another (very) different direction. In short, the estimation procedure is limited to deal with mixed seas (wind waves + swells) from the same direction. Or, said equivalently, the procedure facilitates estimation of crossed-seas, but the final estimate will be given as a point spectrum* with no distinction between the directions.

It is considered a strength that the wave spectrum estimate - obtained in the initial study [14] made for ships without forward speed - is completely non-parametric, since typical pre-specified wave spectrum shapes (Bretschneider, JONSWAP, etc.) are not always appropriate. The brute-force and post-processed solution $E(\omega_e)$ obtained in the current, updated work considering vessels with advance speed is also non-parametric. However, the final - and transformed - wave spectrum $E(\omega_0)$ will be only partly non-parametric because the transformation algorithm [21] relies on a procedure introducing parametric wave spectrum shapes.

Like for all other shipboard estimation techniques, the current estimation procedure will be limited to estimate wave components at a certain frequency band. This limitation is due to the general characteristic of a ship being a low-pass filter. Hence, the algorithm will work best for wave lengths larger than some specific value relative to the ship length (and breadth); which obviously are case-specific parameters.

3.2. Spectral calculations

It has already been stressed that stationary conditions are considered/assumed exclusively in this study, which means that spectral analysis of the motion recordings, given as time series, will provide reliable results. In practice, it is difficult to define exactly when conditions are no longer (statistically) stationary, implying that any outcome from spectral analysis will be unreliable. Consequently, it should be interesting to consider, more carefully, in which conditions 'standard' spectral analysis cannot be applied for its particular purpose, i.e. to provide (cross) response spectra, in the context of shipboard sea state estimation. At the same time, it should be mentioned that elaborate means and procedures exist for conducting spectral analysis in nonstationary conditions and, potentially, it should therefore be possible to apply the studied (spectral) estimation procedure even when conditions are not stationary. However, these types of work are beyond the scope of the present study, and herein it suffices to note that several methods/tools are available to carry out the spectral analysis in case of stationary data. The present work uses a built-in function `cpsd` of MATLAB® which can readily be applied to any set of two time history recordings to produce the mutual set of cross-spectra, see Figure 1.

By nature, ocean wave spectra are smooth in their frequency-wise distribution (and as well in their directional-wise distribution), and it is therefore necessary to work with smoothed versions of the set of response spectra. In the numerical studies analysed later, smoothing is imposed by a Parzen window applied with a 50% overlap on the full range of frequencies from the FFT. The resulting spectra are specified on 600 frequencies for a set of lower and higher cut-off frequencies f_{low} = 0.0008 Hz and f_{high} = 1.0 Hz, respectively, and, consequently, the wave spectrum estimate(s) apply to the same range of encounter frequencies. Indeed, it is possible to work with such a fine frequency resolution only because of a highly computationally efficient estimation algorithm. In real-case practices, however, the resolution should be significantly lower in order to optimise computational speed; taking note that, at some point, the wave estimates will be affected if the resolution is too coarse.

3.3. Motion transfer functions

The performance evaluation of the estimation procedure is in this study made exclusively through computational simulation of motion measurements; using the same set of motion transfer functions to both *generate* the measurement time series and to subsequently *estimate* the wave spectrum. As a consequence, details about the transfer functions are of minor importance and just a few words are given here about the applied set of motion transfer functions.

Instead of using the transfer functions of the actual vessel, based on the detailed hull geometry, the transfer functions of a homogeneously loaded barge with the same main dimensions (length, breadth, draught) as the vessel are used in the estimation procedure. In this particular case, a set of closed-form expressions developed

*Likely, the wave spectrum estimate will be fairly accurate if the incident directions of wind waves and swells are not too different. A hypothesis, however, that needs attention in any future work.

by Jensen et al. [23], Mansour et al. [24] yields a good representation/approximation of the transfer functions considering heave, roll, and pitch. Of course, the transfer functions of the real hull geometry, obtained e.g. by strip theory or a panel code, could easily be applied in the sea state estimation algorithm instead of the closed-form expressions. However, the use of closed-form expressions offer a convenient - and highly computational efficient - way to deal with transfer functions in varying operational conditions without the need to interpolate.

3.4. Wave spectrum transformation algorithm

As has already been pointed out, the details of the wave spectrum transformation algorithm outlined in [21] will not be dealt with herein. Anyhow, a few remarks about the algorithm are noteworthy.

Briefly said, the algorithm is based on a scaling approach that assures preservation of energy at corresponding sets of encounter and (true) absolute frequencies. Thus, a set of scaling ratios apply to specific absolute frequencies, obtained through the Doppler Shift of given encounter frequencies, and multiplication between the scaling ratios and the *encounter* wave spectrum ordinate will make the transformed *absolute* wave spectrum available. It happens that spectral ordinates are erroneously transformed from the encounter domain to a high-frequency range of the absolute spectrum; despite 'consistent' multiplication with the spectral ratios. Consequently, the transformation algorithm introduces a tail-fitting which makes sure that for frequencies higher than a user-defined value, the tail of the transformed spectrum follows that of a Bretschneider spectrum. In the particular case studies presented later, this values is taken as 0.25 Hz.

4. Case studies using simulated measurements

The performance of the estimation procedure (Sec. 2) is evaluated using artificial time series data generated through computational simulations. In this setting, exact knowledge is available about the true wave energy spectrum and associated sea state parameters and, hence, it is easy to conduct comparative studies with the corresponding wave spectrum estimate obtained by the estimation procedure.

4.1. Vessel data

Time series simulations of the motion components {heave, roll, pitch} have been performed for an example ship* with data given in Table 1. The example ship was considered in the initial study [14] using DP full-scale data, and it is a scheduled task to also conduct sea state estimation analysis using full-scale data of the vessel at forward speed.

Table 1: Main particulars of the example ship and other necessary data used to calculate the (closed-form) transfer functions.

Length, L_{pp}	28.9 m
Breadth, B	9.6 m
Draught, T	2.7 m
Block coefficient, C_B	0.56 [-]
Waterplane coefficient, C_{WP}	0.84 [-]
Displacement (mass), Δ	417 000 kg
Transverse metacentric height, GM_T	2.66 m

4.2. Wave scenarios (test cases)

Various test cases form the background for the performance evaluation of the estimation procedure. Each test case is represented by a given short-crested input-wave system characterised by a parameterised wave energy spectrum and its associated (true) integrated wave parameters such as significant wave height H_s, mean (wave) period T_m, and peak (wave) period T_p. Thus, the wave elevation and corresponding motion records can easily be generated for a ship advancing in the particular wave system, see Subsection 4.3 below.

An overview of the test cases (A, B, C) is seen in Table 2 which specifies the (absolute) input-wave parameters together with other operational parameters. It is noteworthy that two of the main test cases, A and B, differ only by the selected advance speed being $U = 5.0$ knots and $U = 10.0$ knots, respectively. The actual wave system, on the other hand, is exactly the same for the two cases, and so is the selected sets of mean headings χ_0 relative to the wave system. The main purpose with the subcases of cases A and B is to evaluate the performance of the estimation procedure when the ship advances at different relative (mean) headings specified as $\chi_0 = \{0, 10, \ldots, 350\}$ deg. Notably, the concern is the procedure's ability to correctly estimate the wave system in following seas, and its ability to differentiate between incident waves on the starboard side or the port side. Note, at deep water conditions, the particular choice of mean period $T_m = 6.5$ s corresponds to an absolute wave length $\lambda = \frac{gT_m^2}{2\pi} = 66.0$ m, i.e. $\lambda/L_{pp} \approx 2$. Thus, the wave system is of a wave-length regime where most of the wave energy is concentrated at wave lengths inducing "reasonable" response levels of the considered motion components {heave, roll, pitch}, see Figure 3, which is of relevance due to a ship's inherent low-pass-

*The example ship is *R/V Gunnerus* which is owned and operated by NTNU.

Table 2: Summary of test cases using a Bretschneider wave spectrum overlaid with a spreading function, where the latter has $s = 4$ in every case.

Cases	U [knots]	$T_{m,0}$ [s]	$T_{p,0}$ [s]	$H_{s,0}$ [m]	χ_0 [deg.]
A	5.0	6.5	8.4	2.0	{0:10:350}
B	10.0	6.5	8.4	2.0	{0:10:350}
C	10.0	4.3+9.8 (6.1)	5.6+12.7	2.0+2.0 (2.8)	{0:10:350}

filtering characteristics. The reason to include two vessel speeds is that fewer waves will "overtake" the vessel for the higher vessel speed ($U = 10$ knots) compared to the lower one, when the ship advances in following seas, and this fact may influence the outcome from the estimation procedure, as the physics behind the 1-to-3 relationship is indeed governed by the advance speed of the vessel (together with wave heading).

In addition to cases A and B, one last test case, C, representing a double-peaked wave system, is used to test the estimation procedure's performance in sea states with swells and wind sea occurring at the same time.

The listed wave scenarios in Table 2 are described by a Bretschneider (point) wave spectrum $S_B(\omega_0)$ overlaid with a spreading function $\varphi(\mu)$ (Eq. 5). That is, for the generation of the wave elevation and the corresponding motion records, the input-wave spectrum $\hat{S}(\omega_0, \mu)$, also denoted the *generating spectrum*, is taken as:

$$\hat{S}(\omega_0, \mu) = S_B(\omega_0)\varphi(\mu) \tag{20}$$

$$S_B(\omega_0) = 173\frac{H_s^2}{T^4\omega_0^5}\exp\left[-\frac{692}{T^4\omega_0^4}\right] \tag{21}$$

where the characteristic period T depends on which statistical period is given. The following substitutions apply: $T = T_m$ for the mean period T_m, $T = 0.772T_p$ for the peak period T_p, or by $T = 1.086T_z$ for the zero-upcrossing period T_z. Case C will be taken as the sum of two Bretschneider spectra with parameters as given in Table 2.

The generating spectrum depends on the input parameters (e.g., H_s, T_m) and for quantitative comparisons it is relevant to obtain the corresponding estimates. Thus, integrated/estimated wave parameters can be derived from the n-th order spectral moments of a wave spectrum,

$$m_n = \int_0^\infty \omega_0^n E(\omega_0)d\omega_0 \tag{22}$$

$$H_s = 4\sqrt{m_0},\ T_m = 2\pi\sqrt{\frac{m_0}{m_1}},\ T_p = \frac{2\pi}{\omega_p} \tag{23}$$

where $E(\omega_0)$ is given by Eq. (19), and ω_p is the frequency corresponding to the spectrum peak.

4.3. Time history simulations

The wave elevation and the corresponding vessel motions are considered as Gaussian distributed. Hence, in linear, short-crested waves the time history record $R(t)$ of a wave-induced motion component can be generated using a set of uncorrelated, standard normal distributed variables u_{nm} and $\bar{u}_{nm}$ [e.g. 25],

$$R(t) = \sum_{n=1}^{N}\sum_{m=1}^{M}\left[u_{nm}c_{nm}(t) + \bar{u}_{nm}\bar{c}_{nm}(t)\right] \tag{24}$$

The deterministic coefficients $c_{nm}(t)$ and $\bar{c}_{nm}(t)$ are for an advancing vessel given by,

$$c_{nm}(t) = \sigma_{nm}|\Phi_R(\omega_{0,n}, \mu_m + \chi) \cdot |\cos\left(\omega_{e,nm}t + \epsilon_R(\omega_{0,n}, \mu_m + \chi)\right) \tag{25}$$

$$\bar{c}_{nm}(t) = -\sigma_{nm}|\Phi_R(\omega_{0,n}, \mu_m + \chi)| \cdot \sin\left(\omega_{e,nm}t + \epsilon_R(\omega_{0,n}, \mu_m + \chi)\right) \tag{26}$$

$$\sigma_{nm}^2 = \hat{S}(\omega_{0,n}, \mu_m)\Delta\omega_{0,n}\Delta\mu_m \tag{27}$$

where the modulus (amplitude) and the phase of the motion transfer function are
$|\Phi_R(\omega_{0,n}, \mu_m + \chi)|$ and $\epsilon_R(\omega_{0,n}, \mu_m + \chi)$, respectively, for the particular motion component R. The generating wave energy spectrum $\hat{S}(\omega_0, \mu)$ is discretised at N frequencies and M directions. The present formulation considers time histories of wave-induced motion components observed from the advancing vessel. This means that the encounter frequency ω_e, appearing in the deterministic coefficients, is given by, cf. Eq. (1)

$$\omega_e = \left|\omega_0 - \omega_0^2\psi\right|,\ \psi = \frac{U}{g}\cos\chi \tag{28}$$

for any absolute frequency ω_0.

Based on the parameters of a particular test case, see Table 2, 20 sets of wave and motion measurements are generated. The need for several corresponding records, here 20, of wave and motion components is due to the fact that a statistical evaluation of the estimation procedure's performance is necessary, since a single, finite time history recording is just one out of the infinitely many that comprise the "complete" ensemble. The single time history records are 20 minutes long and

made from $N = 800$ wave components spaced non-equidistantly on the frequency interval $]0, 2\pi]$ at $M = 19$ wave directions using the spreading function (Eq. 5) with $s = 4$. The time history simulations are generated at 10 Hz, and, after adding white noise (SNR = 20), the records are down-sampled to 2 Hz to artificially add measurement noise.

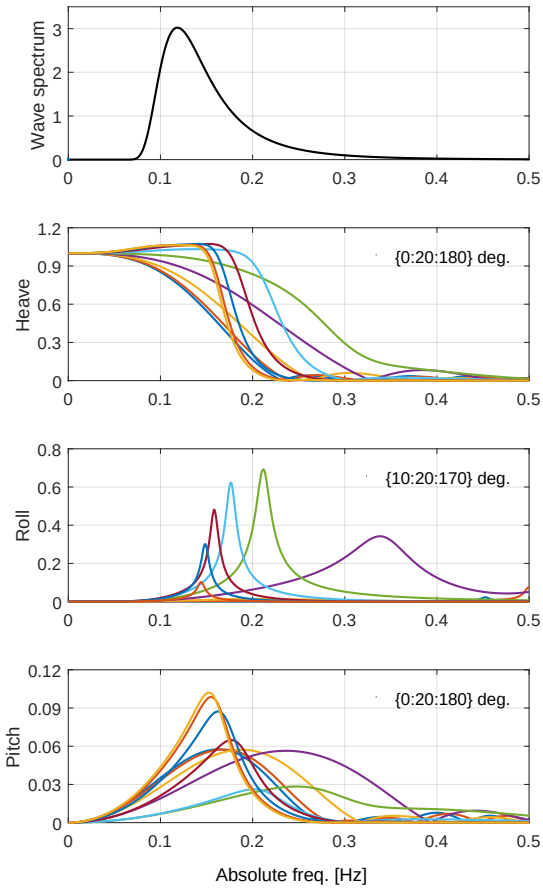

Figure 3: A Bretschneider wave spectrum (uppermost plot) with $T_m = 6.5$ s and $H_s = 2.0$ m is used as the generating spectrum for the time series simulations of {heave, roll, pitch} at forward speed $U = 10$ knots. The modulus (amplitudes) of the motion transfer functions are shown below the wave spectrum, and the results for different relative headings are presented, leaving the detailed legends out since the interest is merely the 'qualitative variation' between the different headings. Units: Wave spectrum [m^2s]; Heave [m/m]; Roll [rad/m]; Pitch [rad/m].

5. Results and discussions

In this section, the performance of the estimation procedure is analysed and discussed. The case studies, see Table 2, have been presented in the preceding section, and the result will simply be the outcome of the estimation procedure when it is applied to the test cases. However, two overall subsets of results are considered, with the main subset reported in the following subsection that studies a situation where perfect knowledge about the hydrodynamic behaviour of the vessel in waves exists. That is, a subset/situation where the motion transfer functions "by default" yield a perfect description of wave-vessel interactions. As another situation, incomplete knowledge about the wave-vessel interactions is introduced as a more realistic scenario. This situation can easily be studied by working with two different sets of motion transfer functions; one set for the time series generation and one set for the wave estimation process.

5.1. Perfect transfer functions

In this part of the evaluation of the estimation procedure, the same set of transfer functions is used for the motion generation/simulation and for the sea state estimation, respectively.

Cases A and B

The specific outcome of the estimation procedure is a (2D) wave spectrum $E(\omega_0)$, and two (arbitrary) selections of estimated spectra taken from cases A and B are shown in Figures 4 and 5, respectively.

In the figures, each plot relates to a specific *true* wave heading, shown in the title of the plot, and the *estimated* wave heading is printed in the plot's legend. It is noteworthy that any plot is the result of just one out of the 20 sets of time history simulations representing the individual subcases/headings reported in Table 2. As such, it should be remembered that the single spectrum estimate may actually be estimating nicely the realised wave elevation process, i.e. its associated energy spectrum, for the specific (stochastic) realisation, although the spectrum estimate and the true generating (deterministic) spectrum are not fully alike for the specific realisation. However, on average, and theoretically speaking, infinitely many realisations should have a mean process/spectrum that will exactly be represented by the (true) generating spectrum. In this study, 'infinitely many' is taken as 20 realisations.

From the plots in Figures 4 and 5, it is evident that there is a good agreement between the true generating spectrum and the estimated one, including wave heading, in all of the considered comparisons. Although this observation is not entirely representative to every single

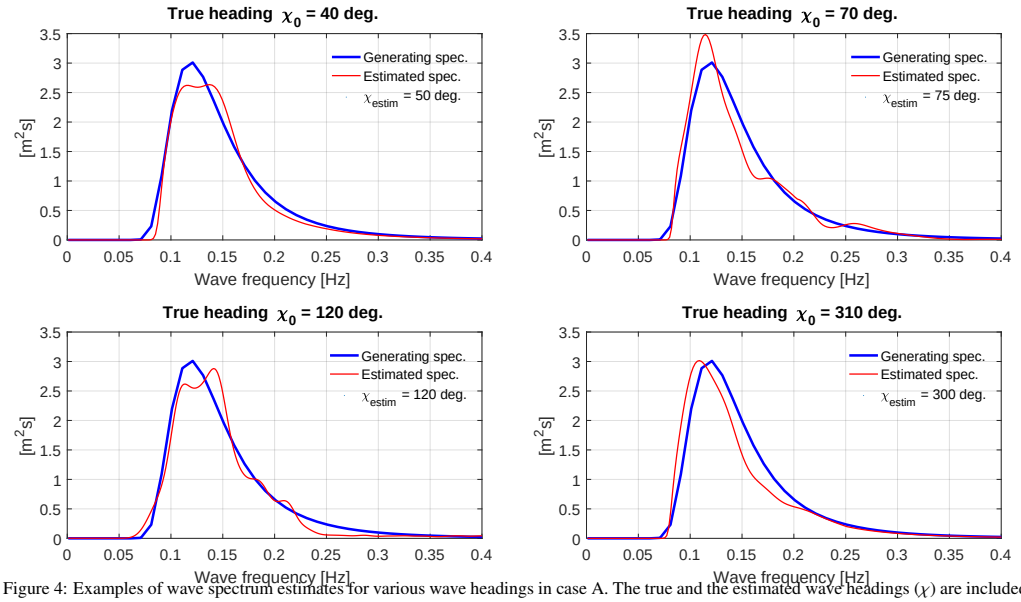

Figure 4: Examples of wave spectrum estimates for various wave headings in case A. The true and the estimated wave headings (χ) are included in the plot titles and legends, respectively.

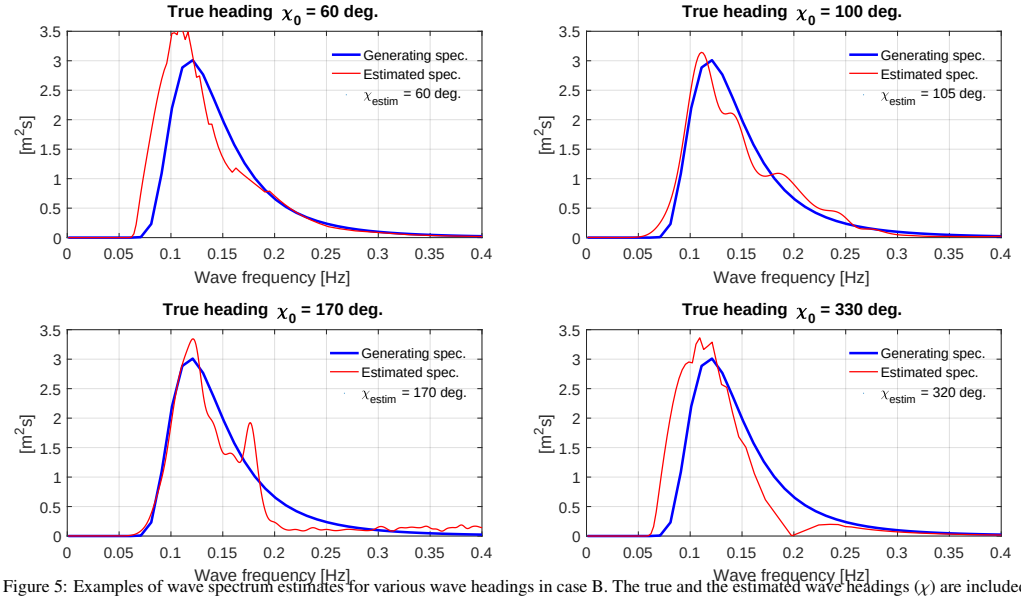

Figure 5: Examples of wave spectrum estimates for various wave headings in case B. The true and the estimated wave headings (χ) are included in the plot titles and legends, respectively.

set of time history recordings for every single (true) subcase of cases A and B, Table 2, the general picture observed from Figures 4 and 5 resembles the overall trend of the spectrum estimates very well.

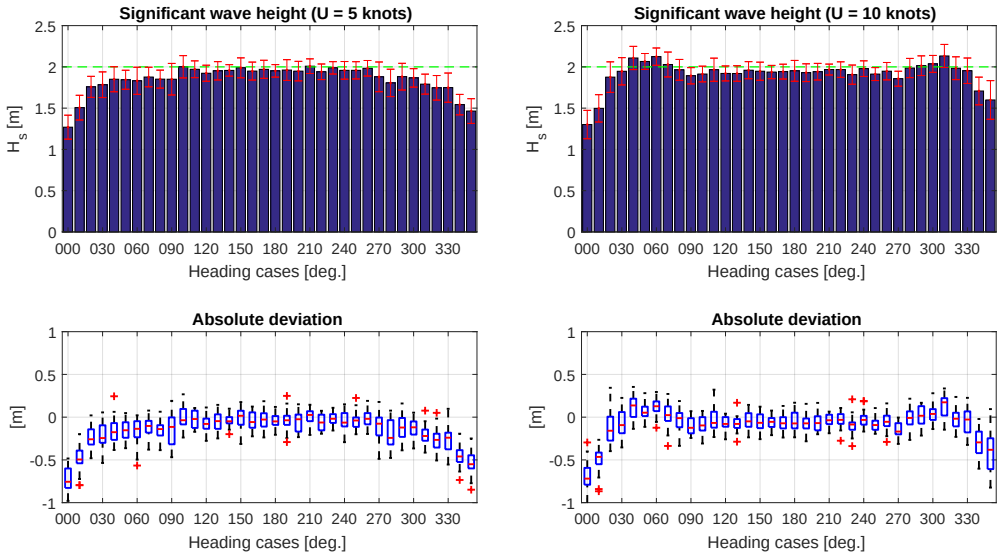

Figure 6: Upper plots: Estimates of **significant wave height** for all subcases (headings) of cases A (left-hand side) and B (right-hand side) with the true value indicated by the green dashed line. Lower plots: Deviations between estimates and true value shown as box plots. On each box, the central mark is the median, and the upper and lower edges of the box are the 25th and 75th percentiles, respectively. The whiskers extend to the most extreme data points which the algorithm considers not to be outliers, and the outliers are plotted individually.

The trend, or the statistics, of the entire set of outcomes for cases A and B can be seen in Figures 6-9. Basically, the four figures contain the same sort of statistical information but relevant for the significant wave height (Fig. 6), the mean period (Fig. 7), the peak period (Fig. 8), and the (mean) relative wave heading (Fig. 9), with results shown for both cases A and B as the left-hand side plots ($U = 5$ knots) and the right-hand side plots ($U = 10$ knots), respectively. The pairs of upper and lower plots in the figures present the same type of comparisons: The upper plot shows the average value of the outcome of estimates of the particular wave parameter considering all headings, and with the average value based on the 20 sets of simulations for each heading. The error bar on the top of each column indicates plus/minus the standard deviation. The lower plot shows the statistics* of the absolute deviation between estimates and the corresponding true value of the particular wave parameter. Irrespectively of the plot/figure it is decided to keep all comparative measures in absolute scale, since relative deviation/scale of wave parameters has, strictly speaking, only a meaning for the significant wave height; which is identical for cases A and B in this study.

Generally, the agreement (Figs. 6-9) between the estimates and the true values are good for all of the considered wave parameters, including the relative wave heading. Thus, it is observed that the average values (and the medians) are close to the true values, with small variations around them although 'outliers' occur here and there; and taking note that the peak period on average is estimated well but being the parameter with the most scatter in the results. The general agreement drops a bit, however, when the ship is exposed to following sea conditions at incident wave angles closely in line with the vessel's centreline ($\chi \approx 0 - 10$ deg. and $\chi \approx 350 - 360$ deg.).

Taking a more detailed look at the statistics, the results for the significant wave height (Fig. 6) reveal that the energy level rather consistently is slightly below the true level; an observation not limited to only following sea conditions. This sort of underestimation is a consequence of the filtering characteristic of a vessel in waves, making the ship less responsive to high-frequency waves, for what reason the observation/underestimation is expected. Indeed, this is one of the inherent and fundamental drawbacks of the wave buoy analogy and, as such, the observation applies to

*Herein, the built-in function `boxplot` of MATLAB® is used.

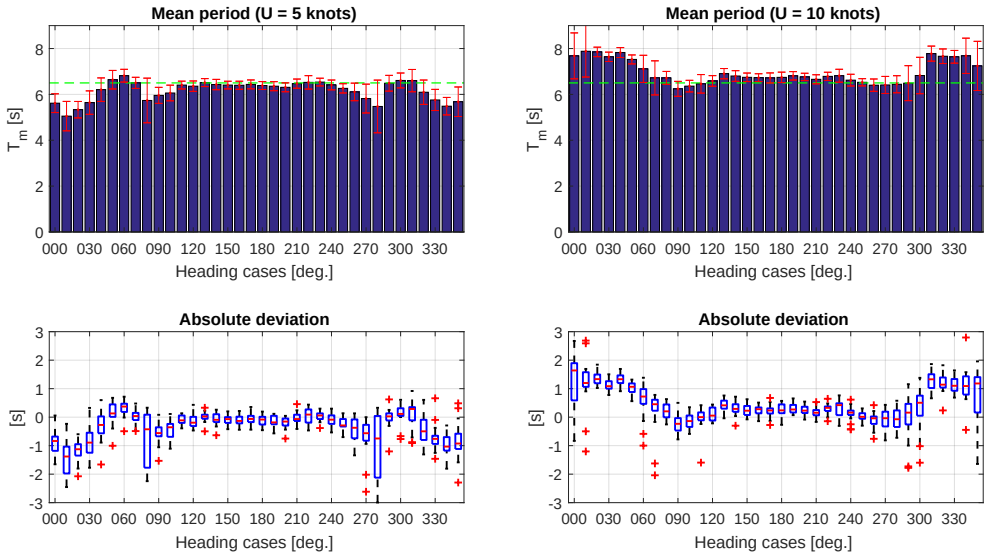

Figure 7: Upper plots: Estimates of **mean period** for all subcases (headings) of cases A (left-hand side) and B (right-hand side) with the true value indicated by the green dashed line. Lower plots: Deviations between estimates and true value shown as box plots; info is given in the caption of Fig. 6.

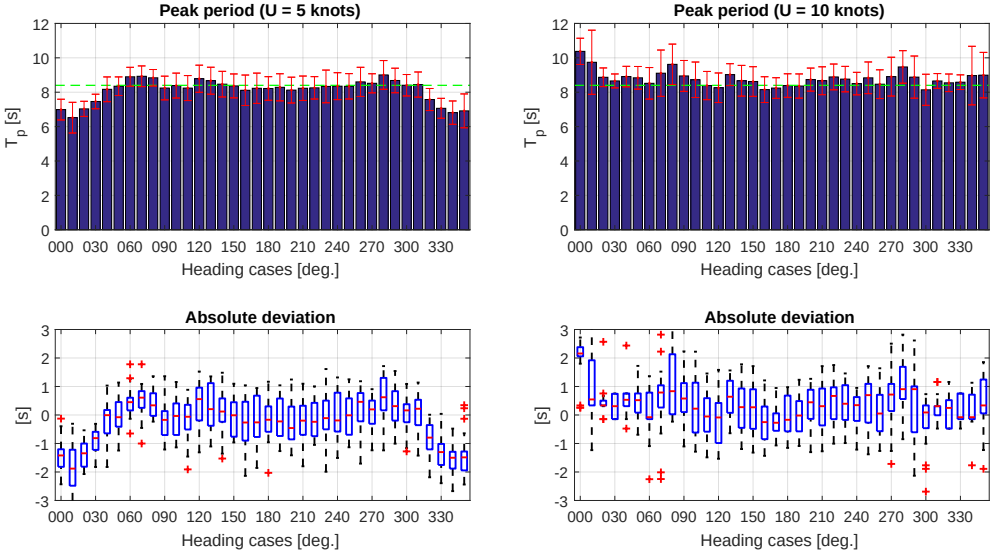

Figure 8: Upper plots: Estimates of **peak period** for all subcases (headings) of cases A (left-hand side) and B (right-hand side) with the true value indicated by the green dashed line. Lower plots: Deviations between estimates and true value shown as box plots; info is given in the caption of Fig. 6.

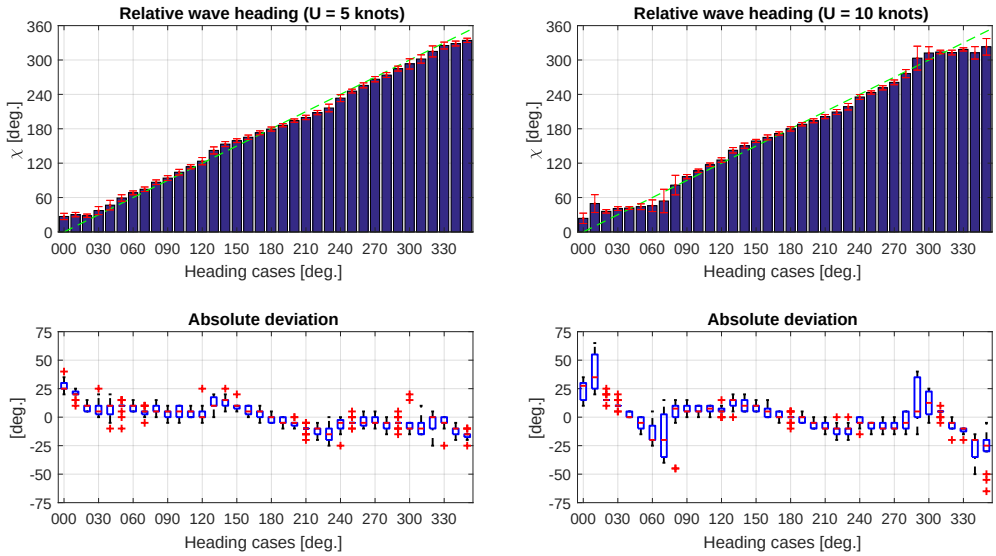

Figure 9: Upper plots: Estimates of (mean) **relative wave heading** for all subcases (headings) of cases A (left-hand side) and B (right-hand side) with the true value indicated by the green dashed line. Lower plots: Deviations between estimates and true value shown as box plots; info is given in the caption of Fig. 6.

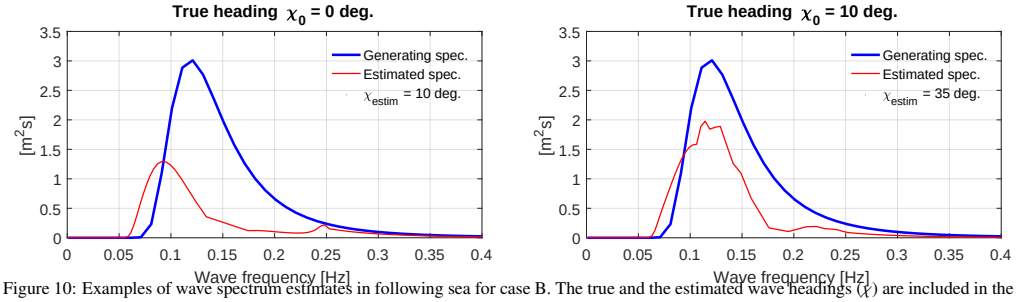

Figure 10: Examples of wave spectrum estimates in following sea for case B. The true and the estimated wave headings (χ) are included in the plot titles and legends, respectively.

any other estimation technique reported in the literature; of course also for cases without forward speed as explained by e.g. Mas-Soler et al. [26]. Generally, the underestimation reduces as the wave period increases, which is a benefit to the wave buoy analogy considering the more severe wave scenarios.

As reported above, the most significant inaccuracies of the estimates occur in strict following sea conditions (stern waves). Two specific outcomes of wave spectrum estimates are shown in Figure 10 for $U = 10$ knots (case B) at $\chi_0 = 10$ deg. $\chi_0 = 10$ deg. true wave headings; noting that the specific spectrum estimates are quite representative for the remaining estimates at the two headings (including $\chi = 350$ deg.); and applies also to the other vessel speed $U = 5$ knots (case A).

Efforts have tried to find the reason for the reduced agreement in stern waves but no clear answer has been found. One plausible explanation could be related to the 1-to-3 relationship, i.e. the Doppler Shift, for following waves, but - interestingly - very similar findings (not shown herein) apply for a situation without advance speed. Not to mention that the 1-to-3 relationship is introduced also at the other headings in following sea conditions, notably $\chi = 20 - 50$ deg., where the esti-

mates are as expected. It is therefore more likely that inaccuracies exist because of the actual hydrodynamic behaviour of the specific vessel, governed by hull geometry*, when it is exposed to stern waves (with or without advance speed), but investigations in this regard are left for future work.

Case C

In the last test case, C (U = 10 knots), swells and wind seas occur at the same time, making the wave spectrum double-peaked. The entire set of statistical plots is included in Figure 11 showing average and median values, including variation, of significant wave height estimates (upper left plot-pair), peak period estimates of swell (upper right plot-pair), peak period estimates of wind sea (lower left plot-pair), and wave heading estimates (lower right plot-pair), respectively. The statistics reveal somewhat similar findings, as were observed in the previous cases (A and B), but generally with a lower agreement between the estimates and the corresponding true values, and substantially larger variation around the average values (and medians). An exception is however the wave heading estimates which are just as good in this case; or in some subcases tending to be even better. It is noteworthy that at true headings χ_0 = 0 deg. and χ_0 = 10 deg., a few estimates are introduced with negative sign. That is, if the particular estimates were, say, 350 deg. the statistics are based on -10 deg. Some additional points to note from the plots are the following: The significant wave height is for all cases, except at wave headings slightly behind beam, lower than the true values, which is a result of the filtering characteristic of the ship in waves. The "inconsistent" result at headings just behind beam is not easily explained since it is not (necessarily) a result of fully correct spectrum estimates, which will be presented further below. The statistics concerning the peak periods of the swell and wind sea parts show an acceptable agreement, although the results are associated with rather large scatter. Moreover, it appears that at headings behind beam the peak periods are estimated closer together; i.e. the peak period of swell is too low and that of wind sea is too high. This observation is realised because the actual spectrum estimates are more blurred with a difficulty to distinctly detect (correctly) the two peaks of the wave system.

The findings mentioned above can be studied/confirmed by inspecting some of the actual spectrum estimates. Thus, for (true) wave headings χ_0 = 60 deg. and χ_0 = 180 deg. all 20 sets of realisations are included in Figure 12. Generally, the plots show a reasonable agreement between the spectrum estimates and the corresponding (generating) spectrum, capturing the most important part of the wave energy distribution. However, it is clear that the spectrum estimates are not as good as the findings were for cases A and B; notably problems occur for some of the 'behind-beam' sea conditions (around $\chi_0 = 60 - 90$ deg.) to detect the two individual peaks of the generating spectrum. It is also evident that the high-frequency part of the (true) wave energy distribution is not estimated correctly, which is a result of the filtering characteristic of the ship in waves.

5.2. Imperfect transfer functions

In this subsection, an *imperfect* set of motion transfer functions for the wave estimation process is imposed. More precisely, the transfer functions are calculated for a changed loading condition of the vessel, as "incomplete" knowledge is introduced simply by doing the calculations using as draught, $T_{new} = 1.1 \cdot T_0$, as displacement, $\Delta_{new} = 1.1 \cdot \Delta_0$, and as transverse metacentric height, $GM_{T,new} = 0.9 \cdot GM_{T,0}$, where the 0-index relates to the original parameter values seen in Table 1. It must be emphasised, however, that the new set of transfer functions is used only in the wave estimation part, while the time history simulations are made using the original set of motion transfer functions, based on the input in Table 1. Otherwise, the operational conditions, including wave system and vessel speed, are exactly as case B, studied in the previous subsection, see also Table 2.

The statistical outcomes of the entire set of spectrum estimates are presented in Figure 13. Indeed, the plots show that the estimates are still good, and by comparison to the right-hand side plots in Figures 6-9 the differences are barely visible. Basically, there are two (interrelated) ways to interpret this finding: 1) The estimation procedure is robust to changes in the applied motion transfer functions; 2) The particular example ship does not behave (very) differently when its loading condition is changed (slightly); or, strictly speaking, the calculated transfer functions [23, 24] exhibit little sensitivity to a change in the input parameters. Making a note here that, obviously, an estimation procedure cannot be robust/reliable if the used motion transfer functions are significantly off relative to the vessel's real hydrodynamic behaviour. However, it should be clear that the more (mathematically) complex the estimation procedure is, the more sensitive its results/estimates will be to changes.

*At this point, the particular set of motion transfer functions obviously plays a significant role.

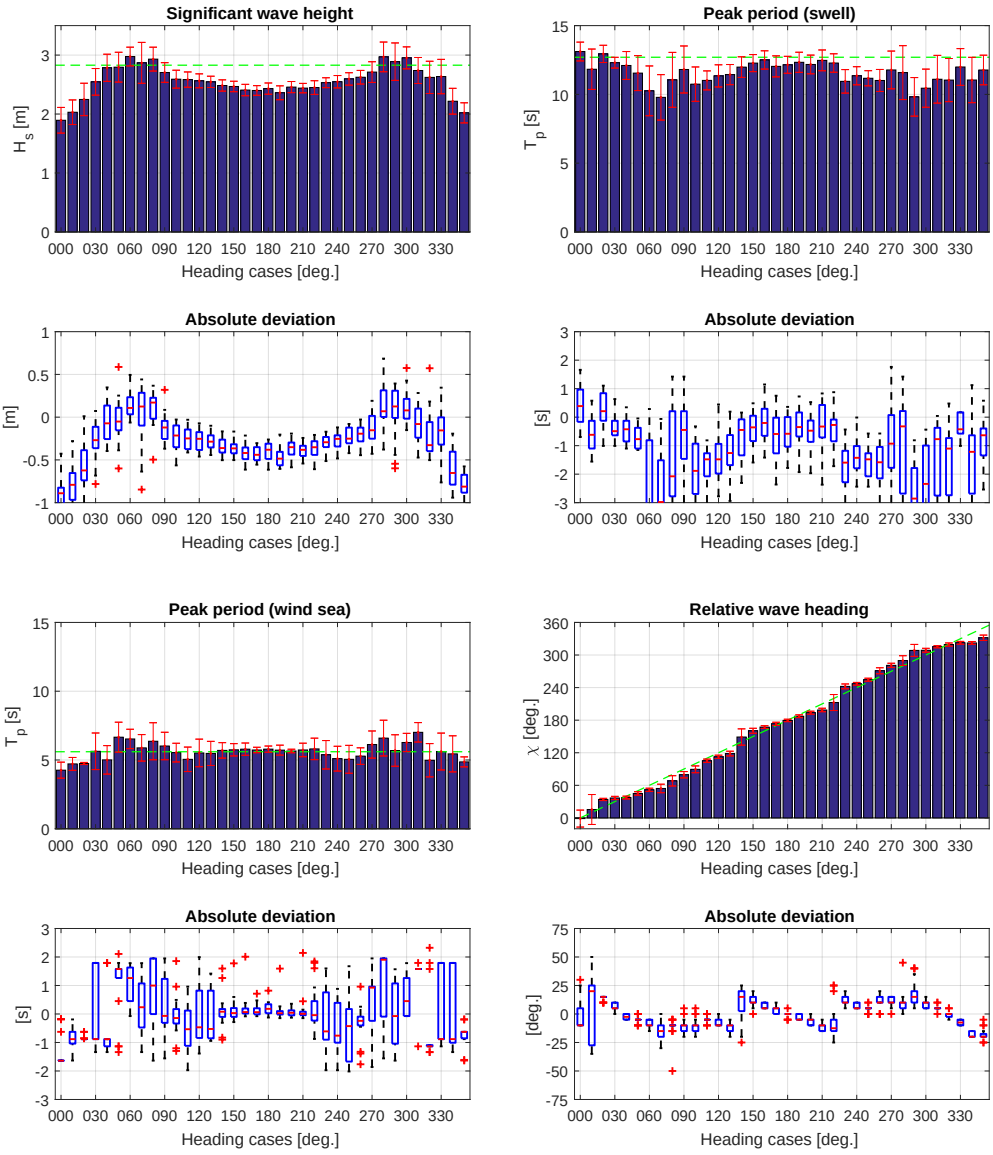

Figure 11: Estimates and deviations of significant wave height, peak periods for wind sea and swell, and relative wave heading, respectively, for all subcases (headings) of cases C with the true value indicated by the green dashed line. Deviations between estimates and true value shown as box plots. On each box, the central mark is the median, and the upper and lower edges of the box are the 25th and 75th percentiles, respectively. The whiskers extend to the most extreme data points which the algorithm considers not to be outliers, and the outliers are plotted individually.

The findings for the imperfect set of motion transfer functions should actually be viewed in a wider perspective than merely as indications of robustness; either it be of the estimation procedure itself, or whether it

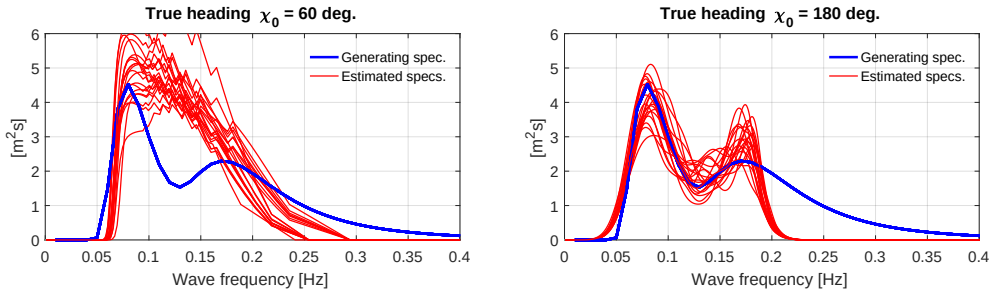

Figure 12: The entire set of wave spectrum estimates (total of 20) for headings χ_0 = 60 deg. and χ_0 = 180 deg. as the left- and right-hand side plots, respectively. The estimated wave headings were, in most cases, close to the true values (see Fig. 11).

means that the particular vessel and its associated hydrodynamic behaviour, represented by its motion transfer functions, exhibits little sensitivity to variations in the hull geometry and/or loading condition. Rather the key point is that, in real-case applications, it is useful to provide sea state estimates where an uncertainty measure, i.e. a "likeliness", is associated to the actual spectrum estimate, or to the corresponding integrated wave parameters. Means to accomplish this has (conceptually) been discussed in the literature [e.g. 5, 27, 28] and a deeper discussion of the means is beyond the scope of the present article. Instead, it suffices to say that probabilistic calculations in this respect will require *several* sea state estimates - for the very same condition, i.e governed by the exact same set of measurements, but using different sets of motion transfer function, where the input parameters are changed. Obviously, this means that the computational efficiency of the sea state estimation algorithm(s) must be very high. Indeed, this is so for the presented estimation procedure, since it is possible to obtain estimates in about 2-3 seconds*, all parts included and also the cross spectral analysis of the time history recordings. And, this calculation time is without doing anything to speed-up the computation or, in other ways, optimise for computational speed. Merely, the efficiency is a consequence of the brute-force approach, which the presented estimation procedure relies upon.

6. Conclusions and further work

It has been shown that the estimation procedure performs well and makes accurate prediction of the on-site sea state; this goes for the integrated wave parameters but also for the more 'delicate' frequency-wise distribution of wave energy, including the mean wave direction (relative heading). In this respect, the present *brute-force wave estimation procedure* has a performance comparable to many of the other shipboard estimation techniques relying on the wave buoy analogy. However, the computational efficiency of the present procedure is significantly improved with estimation speed in the order of a few seconds in contrast to minutes for the other well-tested estimation procedures based on Bayesian modelling or parametric optimisation. On the first hand, this makes the present procedure useful for realtime onboard control and decision support tools, where computational efficiency is vital. Secondly, the high computational speed means that it will be possible to integrate, in realtime, probabilistic calculations directly in the sea state estimation computations; something that cannot be made with other estimation techniques as they require too long computational time for the single spectrum estimates.

In the future, important and suggested work on the presented estimation procedure may be considering points on the following list, which by no means is exhaustive and does not necessarily include (sub)work already mentioned in the main text:

- Application to experimental data, including model-scale and full-scale, where motion measurements obtained on various types of ships (without and with advance speed) are analysed.

- Sensitivity studies taking many forms to examine, for instance, the influence of spectrum discretisation used in the cross spectral analysis; or to examine if certain response combinations will provide better spectrum estimates than others, depending on the operational and/or the wave conditions.

*Intel(R) Core(TM) i7-4600U CPU @ 2.10GHz

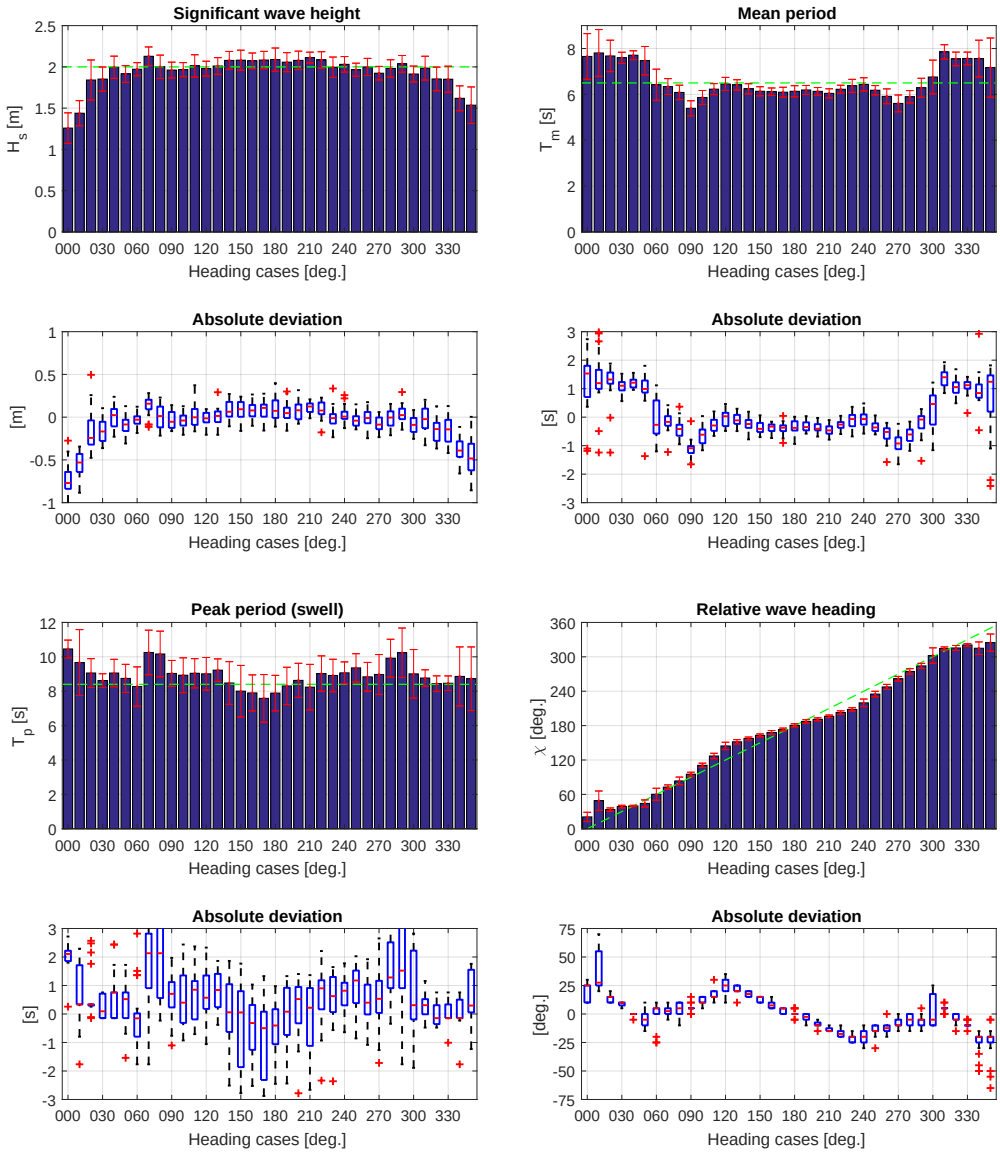

Figure 13: Estimates and deviations of significant wave height, mean periods, peak period, and relative wave heading, respectively, for all subcases (headings) of cases B using an imperfect set of motion transfer functions.

- To have the estimation procedure optimised for computational speed.
- Is it possible to extend the brute-force approach to work for wave systems composed by subsystems from different (mean) directions?

Acknowledgement

The first author would like to acknowledge his long-time colleague and friend Professor Emeritus Jørgen Juncher Jensen. It is interesting that Jørgen many years ago initiated a study introducing an (unpublished) idea for sea state estimation somewhat in line with the brute-force solution presented in this article.

This work was supported by the Research Council of Norway through the Centres of Excellence funding scheme, project number 223254 NTNU AMOS.

References

[1] M. Ludvigsen, A. Sørensen, Towards integrated autonomous underwater operations for ocean mapping and monitoring, Annual Reviews in Control 42 (2016) 145–157.

[2] T. Perez, Ship Seakeeping Operability, Motion Control, and Autonomy - A Bayesian Perspective, IFAC-PapersOnLine 48-16 (2015) 217–222.

[3] R. Veal, M. Tsimplis, The integration of unmanned ships into the lex maritima, Lloyd's Maritime & Commercial Law Quarterly (in press) .

[4] U. D. Nielsen, J. J. Jensen, A novel approach for navigational guidance of ships using onboard monitoring systems, Ocean Engineering 38 (2011) 444–455.

[5] U. D. Nielsen, Z. Lajic, J. J. Jensen, Towards fault-tolerant decision support systems for ship operator guidance, Reliability Engineering and System Safety 104 (2012) 1–14.

[6] U. D. Nielsen, A. H. Brodtkorb, J. J. Jensen, Response predictions using the observed autocorrelaton function, Marine Structures (under review) .

[7] T. Iseki, K. Ohtsu, Bayesian estimation of directional wave spectra based on ship motions, Control Engineering Practice 8 (2000) 215–219.

[8] E. A. Tannuri, J. V. Sparano, A. N. Simos, J. J. D. Cruz, Estimating directional wave spectrum based on stationary ship motion measurements, Applied Ocean Research 25 (2003) 243–261.

[9] R. Pascoal, C. G. Soares, A. J. Sørensen, Ocean Wave Spectral Estimation Using Vessel Wave Frequency Motions, Journal of Offshore Mechanics and Arctic Engineering 129 (2007) 90–96.

[10] R. Pascoal, L. P. Perera, C. G. Soares, Estimation of Directional Sea Spectra from Ship Motions in Sea Trials, Ocean Engineering 132 (2017) 126–137.

[11] U. D. Nielsen, Estimations of on-site directional wave spectra from measured ship responses, Marine Structures 19 (2006) 33–69.

[12] U. D. Nielsen, Introducing two hyperparameters in Bayesian estimation of wave spectra, Probabilistic Engineering Mechanics 23 (2008) 84–94.

[13] U. D. Nielsen, A concise account of techniques available for shipboard sea state estimation, Ocean Engineering 129 (2017) 352–362.

[14] A. H. Brodtkorb, U. D. Nielsen, A. J. Sørensen, Sea State Estimation Using Vessel Response in Dynamic Positioning, Applied Ocean Research (accepted for publication) .

[15] R. Pascoal, C. G. Soares, Non-parametric wave spectral estimation using vessel motions, Applied Ocean Research 30 (2008) 46–53.

[16] U. D. Nielsen, The wave buoy analogy - estimating high-frequency wave excitations, Applied Ocean Research 30 (2008) 100–106.

[17] N. Montazeri, U. D. Nielsen, J. J. Jensen, Estimation of wind sea and swell using shipboard measurements - A refined parametric modelling approach, Applied Ocean Research 54 (2016) 73–86.

[18] R. Bhattacharyya, Dynamics of Marine Vehicles, John Wiley & Sons, 1978.

[19] R. Beck, W. Cummins, J. Dalzell, P. Mandel, W. Webster, Vol. III: Motions in Waves and Controllability, in: E. Lewis (Ed.), Principles of Naval Architecture, Second Revision, SNAME, 1–188, 1989.

[20] J. Journée, W. Massie, Offshore Hydromechanics, lecture notes in course offered at TU Delft, 2001.

[21] U. D. Nielsen, Transformation of a wave energy spectrum from encounter to absolute domain when observing from an advancing ship, Applied Ocean Research (submitted for posible publication) .

[22] U. D. Nielsen, D. C. Stredulinksy, Sea state estimation from an advancing ship - A comparative study using sea trial data, Applied Ocean Research 34 (2012) 33–44.

[23] J. J. Jensen, A. E. Mansour, A. S. Olsen, Estimation of ship motions using closed-form expressions, Ocean Engineering 31 (2004) 61–85.

[24] A. Mansour, J. Jensen, A. Olsen, Fast Evaluation of the Reliablity of Container Securing Arrangements, in: Proceedings of PRADS'04, Travemünde, Germany, 577–585, 2004.

[25] J. J. Jensen, J. Capul, Extreme response predictions for jack-up units in second order stochastic waves by FORM, Probabilistic Engineering Mechanics 21 (2006) 330–338.

[26] J. Mas-Soler, A. N. Simos, E. A. Tannuri, Estimating on-site wave spectra from the motions of a semi-submersible platform: An assessment based on model scale results, Ocean Engineering (under review) .

[27] T. Iseki, An improved stochastic modeling for bayesian wave estimation, in: Proc. of OMAE 2012, ASME, Rio de Janeiro, Brazil, 2012.

[28] I. M. V. Andersen, G. Storhaug, Dynamic Selection of Ship Responses for Estimation of on-site Directional Wave Spectra , in: Proc. 31st OMAE, Rio de Janeiro, Brazil, 2012.

Paper D:

Increasing the Operation Window of Dynamic Positioned Vessels Using the Concept of Hybrid Control

Astrid H. Brodtkorb, Asgeir J. Sørensen, Andrew R. Teel

Proceedings of the ASME 2014 33rd International Conference on Ocean, Offshore and Arctic Engineering, OMAE 2014,
Volume 1A: Offshore Technology: V01AT01A046.
doi: 10.1115/OMAE2014-23601.

Is not included due to copyright

Paper E:

Hybrid Observer for Improved Transient Performance of a Marine Vessel in Dynamic Positioning

Astrid H. Brodtkorb, Svenn A. Værnø, Andrew R. Teel, Asgeir J. Sørensen, Roger Skjetne

NOLCOS 2016, 10th IFAC Symposium on Nonlinear Control Systems,
IFAC-PapersOnLine. vol. 49 (18) 2016, pp 245-250,
doi: 10.1016/j.ifacol.2016.10.189.

Available online at www.sciencedirect.com

ScienceDirect

IFAC Papers Online
CONFERENCE PAPER ARCHIVE

IFAC-PapersOnLine 49-18 (2016) 345–350

Hybrid observer for improved transient performance of a marine vessel in dynamic positioning ⋆

Astrid H. Brodtkorb * **Svenn A. Værnø** * **Andrew R. Teel** **
Asgeir J. Sørensen * **Roger Skjetne** *

* *Centre for Autonomous Marine Operations (NTNU AMOS), Department of Marine Technology, Norwegian University of Science and Technology (NTNU), Otto Nielsens vei 10, 7491 Trondheim, Norway (e-mails: astrid.h.brodtkorb@ntnu.no, svenn.are.varno@ntnu.no, asgeir.sorensen@ntnu.no, roger.skjetne@ntnu.no).*
** *Department of Electrical and Computational Engineering, University of California Santa Barbara, CA USA (e-mail: teel@ece.ucsb.edu)*

Abstract: Dynamic positioning (DP) systems are used on marine vessels for automatic station keeping and tracking operations solely by use of thrusters. Observers are key components of DP systems, and two main types are proposed in this paper. The model-based type is used in steady state conditions since it is especially good at filtering out first order wave induced motions and predicting states in the case of signal loss, and the signal-based type typically has superior performance during transients. In this paper a hybrid observer including a signal-based part and a model-based part with a performance monitoring function is proposed. The observer part that provides the best estimate of the vessel position and heading is used in closed-loop control, thereby allowing for improved transient response while maintaining good steady-state performance. The contributions of this paper include the design of a hybrid signal-based and model-based observer with performance monitoring, stability analysis of the vessel with hybrid estimates in output feedback control, and simulations of a platform supply vessel during a setpoint and heading change.

Keywords: Dynamic positioning, observers, hybrid systems, output feedback control

1. INTRODUCTION

Marine operations are moving further from shore and into harsher environments, and with it requirements for the DP vessel's operational window, safety functions and energy-efficiency become stricter. Vessels that are doing operations with longer duration experience changing sea states with varying wind and wave directions, with suboptimal heading at times. Large forces and moments act on the vessel, making quick and precise control essential, especially when operating close to other offshore infrastructures.

There are many unknown factors at sea that may cause transients in the vessel response depending on the type of operations: wave trains, ice loads, mooring line break, etc. However, many transients are triggered by the operator, which makes them easier to account for with proactive control strategies, e.g. heading and setpoint changes, pipelay operations, well intervention operations, the lowering of a jack-up vessel from jacked-up to floating, etc. In this work the transient response of a DP vessel is improved by combining two observers.

⋆ This work was supported by the Research Council of Norway through the Centres of Excellence funding scheme, project number 23254 - AMOS, and in part by NSF grant number ECCS-1508757 and AFOSR grant number FA9550-15-1-0155.

The model-based observer, like the Extended Kalman filter (Tannuri and Morishita, 2006), (Hassani et al., 2013), or the nonlinear passive observer (Fossen and Strand, 1999), are commonly used in DP systems. The model-based observer uses noisy position and heading angle measurements to estimate the low frequency position, heading, and velocity of the vessel. A key feature of this observer type is the wave filter, which eliminates the wave frequency vessel motion from the output feedback control law. This reduces the wear and tear on the machinery as well as reducing the energy consumption.

The signal-based observer, also referred to as a kinematic, or sensor-based observer, is based on the kinematic equations, see for instance Mahony et al. (2008), Hua (2010), Grip et al. (2012), and Bryne et al. (2015). It is especially well suited during transients, as it uses linear acceleration measurements to predict velocity and position. In this implementation no wave filter was included in this observer, but it is ongoing work by Bryne et al. (2016). As a result this observer estimates the total vessel motion, including low frequency and wave frequency motion. When inserted into the control law it gives an oscillatory thrust command.

Earlier hybrid control theory has been applied to dynamic positioning in a changing sea state, see Nguyen et al.

2405-8963 © 2016, IFAC (International Federation of Automatic Control) Hosting by Elsevier Ltd. All rights reserved.
Peer review under responsibility of International Federation of Automatic Control.
10.1016/j.ifacol.2016.10.189

(2007) and Brodtkorb et al. (2014), and for changing operational modes (Nguyen et al., 2008). These all consist of a bank of controllers and observers with a supervisory mechanism that monitors performance and chooses the best controller/observer pair. Dwell-time and hysteresis switching were applied to avoid chattering. In this paper we apply an output feedback DP controller, using analysis from Loria et al. (2000). Related to this, Prieur and Teel (2011) looks at output feedback control using a hybrid controller with a nonlinear globally stabilizing part, and a linear locally stabilizing part.

The main contributions of this paper includes the design, analysis, and simulation of a hybrid observer with a model-based part and a signal-based part for improving the transient vessel response in an uncertain marine environment. A performance monitoring function keeps track of the mean estimation error over a time period for the observers, and the estimates from the better-performing observer are used in closed-loop output feedback control using a nonlinear proportional, integral, derivative (nPID) controller. Hysteresis is applied in order to limit the number of jumps for the system, and this is important for the stability of the system.

The organization of the paper is as follows: In Section 2 typical instrumentation for DP vessels is discussed, and two mathematical models of marine DP vessels are presented. A model-based and a signal-based observer are introduced in Section 3, and Section 4 presents the output feedback control algorithm. The hybrid signal-based and model-based observer in closed loop control is modeled in Section 5, and stability is discussed in Section 6. Simulation results for a platform supply vessel doing a setpoint change are presented and discussed in Section 7. Section 8 concludes the paper.

2. MARINE VESSEL MODELING AND DYNAMIC POSITIONING

Two reference frames are used in this paper: the North-East-Down (NED) reference frame which is a local Earth-fixed frame, and the body frame, which is body-fixed.

2.1 Instrumentation

DP vessels have statutory class requirements on the onboard instrumentation, and system redundancy. Vessels have positioning systems, e.g. GNSS, acoustics, or laser, a compass measuring heading angle, and an inertial measurement unit (IMU) that combines gyroscopes for measuring angular rates and accelerometers for measuring linear acceleration. The measurements are taken at different sampling rates ranging from 0.1-2 Hz for acoustics, 0.5-4 Hz for GNSS position measurements, to 100-200 Hz for IMU angular velocity and acceleration measurements. The measurements are in this paper assumed to be of the form

$$p^n = [N, E]^\top \tag{1a}$$
$$\psi_c = \psi \tag{1b}$$
$$\omega^b_{imu} = \omega^b + b_g \tag{1c}$$
$$f^b_{imu} = R(\Theta)(\dot{v}^n - g^n), \tag{1d}$$

where the measurements in the NED frame have superscript n, and measurements in the body frame have superscript b. $p^n \in \mathbb{R}^2$ is the measured position in north and east. A heave measurement may also be obtained through GNSS, but it is typically of low quality and is not used here. $\psi_c \in \mathbb{R}$ is measured heading angle (ψ is used in the remainder of the paper), $\omega^b_{imu} \in \mathbb{R}^3$ is measured angular rate ω^b, $f^b_{imu} \in \mathbb{R}^3$ is measured linear acceleration, $\Theta = [\phi,\ \theta,\ \psi]^\top \in \mathbb{R}^3$ is the orientation in roll, pitch and yaw, $R(\Theta) \in \mathbb{R}^{3\times3}$ is the rotation matrix about the z, y, x axes, $g^n \in \mathbb{R}^3$ is acceleration due to gravity, and $b_g \in \mathbb{R}$ is the gyro bias. Measurement noise is disregarded in the stability analysis, but inserted in simulations.

2.2 Marine vessel modeling

Two models of the same system are presented.

Control plant model The control plant model for a vessel is a simplification of the real vessel dynamics. It is different for the various vessel types, operational and environmental conditions, and the design problem under consideration (e.g. observer design or feedback control design); see Fossen (2011) or Sørensen (2013). A surface vessel in DP with starboard/port symmetry, $M = M^\top$, has largest motions in the horizontal plane (surge, sway, and yaw), so the heave, roll, and pitch dynamics are neglected. The control plant model in this case is:

$$\dot{\xi} = A_w \xi + E_w w_w, \tag{2a}$$
$$\dot{\eta} = R(\psi)\nu, \tag{2b}$$
$$\dot{b} = -T_b^{-1} b + E_w w_b \tag{2c}$$
$$M\dot{\nu} = -D\nu + R^\top(\psi) b + u, \tag{2d}$$
$$y = \eta + W\xi + v_y; \tag{2e}$$

where the states of the system include the 3 DOF North, East position and heading $\eta := [N, E, \psi]^\top$ and body-fixed velocity ν in surge, sway and yaw. In normal operational conditions we want to control only the low frequency part of the vessel motion, and the wave filter in (2a) allows us to separate the motion into a wave frequency part, and a low frequency part. The wave filter has a state $\xi \in \mathbb{R}^6$ and system matrix $A_w \in \mathbb{R}^{6\times6}$ that contains the peak wave frequency and damping. It is driven by zero mean white noise w_w. (2b-d) are the low frequency dynamics of the vessel. (2b) is the 3 DOF kinematics that transforms velocity from the body to the NED frame; $R(\psi)$ is the rotation matrix about the z-axis,

$$R(\psi) = \begin{bmatrix} \cos(\psi) & -\sin(\psi) & 0 \\ \sin(\psi) & \cos(\psi) & 0 \\ 0 & 0 & 1 \end{bmatrix}. \tag{3}$$

The wave frequency part of the heading angle, ψ_w, is assumed to be small, $R(\psi+\psi_w) \approx R(\psi)$. (2c) is a bias force model with state $b \in \mathbb{R}^3$, accounting for *slowly-varying* environmental disturbances from mean wind, current, and second-order wave loads and unmodeled vessel dynamics. T_b is the Markov time constant, and w_b zero mean white noise. Note that the bias force model does not capture rapidly varying disturbances. In (2d) $M \in \mathbb{R}^{3\times3}$ is the inertia matrix including added mass for asymptotic values of wave frequency equal to zero, $D \in \mathbb{R}^{3\times3}$ is the linear damping coefficient matrix, and $u \in \mathbb{R}^3$ is the control input. (2e) is the measurement $y = [(p^n)^\top\ \psi]^\top \in \mathbb{R}^3$ of

position and heading including low frequency motion η, wave frequency motion $W\xi$ with $W = [0_{3\times3},\ I_{3\times3}]$, and measurement noise v_y.

Kinematic model The kinematic model is based on fundamental principles of inertia, relating position, velocity and acceleration of the vessel in 6 DOF. It represents the same vessel as in (2), but now the acceleration and angular velocities are inputs as well as the position and heading. The dynamics are split into a translational part and an angular part. The translational part is written as

$$\dot{p}^n = v^n \tag{4a}$$
$$\dot{v}^n = R(\Theta) f^b_{imu} + g^n. \tag{4b}$$

p^n is the north, east and down (heave) position and v^n is the NED velocity. The acceleration measurements from the IMU are rotated directly to the NED frame. The orientation of the vessel is Θ in roll, pitch, and yaw angles, and $R(\Theta)$ is the 6 DOF rotation matrix about the z, y, x-axes. Gravity is also acting on the vessel. The attitude part is written as

$$\dot{\Theta} = T(\Theta)\omega^b \tag{5}$$

with the velocity transformation matrix $T(\Theta)$ and angular rate ω^b.

Relating the two models, we have that

$$\eta = [p^n(1),\ p^n(2),\ \psi]^\top,$$
$$\nu = R(\psi)^\top [v^n(1),\ v^n(2),\ \omega^b(3)]^\top. \tag{6}$$

3. OBSERVERS USED IN DYNAMIC POSITIONING

The two observers are briefly presented in this section. The reader is referred to Fossen and Strand (1999), Fossen (2011) for details on the model-based observer, and to Grip et al. (2012), Grip et al. (2013), Bryne et al. (2014), and Bryne et al. (2015) for details on the signal-based observer.

3.1 Model-based observer

We have chosen to work with the nonlinear passive observer (Fossen and Strand, 1999) since it is an intuitive observer to tune, and it has global stability results. This is based on the control plant model (2) taking in position and heading measurements, and commanded thrust u from the controller (see Section 4). It is a 3 DOF observer, and the algorithm can be written as

$$\dot{\hat{\xi}} = A_\omega \hat{\xi} + K_{1,\omega}\tilde{y} \tag{7a}$$
$$\dot{\hat{\eta}} = R(\psi)\hat{\nu} + K_2\tilde{y} \tag{7b}$$
$$\dot{\hat{b}} = T_b^{-1}\hat{b} + K_3\tilde{y} \tag{7c}$$
$$M\dot{\hat{\nu}} = -D\hat{\nu} + R^\top(\psi)\hat{b} + u + R^\top(\psi)K_4\tilde{y} \tag{7d}$$
$$\hat{y} = \hat{\eta} + C_\omega\hat{\xi}, \tag{7e}$$

where $\hat{\xi}, \hat{\eta}, \hat{v}, \hat{b} \in \mathbb{R}^3$ are the estimates of the states in (2), $\tilde{y} = y - \hat{y}$ is the measurement estimation error and $K_{1,\omega} \in \mathbb{R}^{6\times3}_{>0}, K_2, K_3, K_4 \in \mathbb{R}^{3\times3}_{>0}$ are observer gains chosen to satisfy the Kalman-Yakubovich-Popov (KYP) lemma (Khalil, 2002). The wave filter contains estimates of the peak wave frequency and damping in $A_\omega \in \mathbb{R}^{6\times6}$, and $C_\omega = W$ from (2). The key feature in this observer is the wave filter. This means that the wave frequency motion $W\xi$ is separated from the low frequency motion η, and the output from this observer is the *low frequency motion* estimate of the vessel: $\hat{\eta}_1 := \hat{\eta}$ and $\hat{\nu}_1 := \hat{\nu}$.

Define the estimation errors as $\tilde{(\cdot)}:=(\cdot)$ - $\hat{(\cdot)}$, and collect them in the state $x_1 := [\tilde{\nu}^\top,\ \tilde{\eta}^\top,\ \tilde{\xi}^\top,\ \tilde{b}^\top]^\top$. The error dynamics of (2) and the model-based observer (7) is written compactly as

$$\dot{x}_1 = F_1(x_1, p^n, \psi). \tag{8}$$

3.2 Signal-based observer

The signal-based observer is a 6 DOF observer, and is based on the kinematic relations (4) and (5). The attitude is represented using quaternions, q.

Attitude observer Write the attitude observer dynamics as

$$\dot{\hat{q}} = T(\hat{q})(\omega^b_{imu} - \hat{b}_g + \hat{\sigma}) \tag{9a}$$
$$\dot{\hat{b}}_g = Proj(\hat{b}_g, -k_I\hat{\sigma}), \tag{9b}$$

with the correction term

$$\hat{\sigma} = k_1 c^b \times R(\hat{q})^\top c^n + k_2 f^b_{imu} \times R(\hat{q})^\top \hat{f}^n \tag{10}$$

where $\hat{q}$ is the attitude estimate, $T(\hat{q})$ is the velocity transformation matrix, $\hat{b}_g$ is the gyro bias estimate, and a bias compensated angular rate estimate is provided as well $\hat{\omega}^b$. The projection function used is found in (Grip et al., 2012, Appendix). The symbol $\times$ represents the cross product, $c^b = [\cos(\psi),\ -\sin(\psi),\ 0]^\top$, ψ is measured by the compass, and $c^n = [1,\ 0,\ 0]^\top$ is a reference vector. f^b_{imu} is the measured acceleration and $\hat{f}^n$ is the estimated acceleration in NED. Choose the gains $k_1 \geq k_P,\ k_2 \geq k_P$, with $k_P > 0$ sufficiently large.

Translational Observer The translational observer is based on (4). The equations are taken from Bryne et al. (2015), as we use a virtual vertical reference in heave in stead of the low quality GNSS measurement. The algorithm is

$$\dot{\hat{p}}^n_I = \hat{p}^n_z + k_{pipi}\tilde{p}_I \tag{11a}$$
$$\dot{\hat{p}}^n = \hat{v}^n + \theta^2 \begin{bmatrix} 0_{2\times1} & K_{pp} \\ k_{ppi} & 0_{1\times2} \end{bmatrix} \begin{bmatrix} \tilde{p}_I \\ \tilde{p} \end{bmatrix} \tag{11b}$$
$$\dot{\hat{v}}^n = \hat{f}^n + g^n + \theta^3 \begin{bmatrix} 0_{2\times1} & K_{vp} \\ k_{vpi} & 0_{1\times2} \end{bmatrix} \begin{bmatrix} \tilde{p}_I \\ \tilde{p} \end{bmatrix} \tag{11c}$$
$$\dot{\hat{\xi}}_f = -R(\hat{q})S(\hat{\sigma})f^b_{imu} + \theta^4 \begin{bmatrix} 0_{2\times1} & K_{\xi p} \\ k_{\xi pi} & 0_{1\times2} \end{bmatrix} \begin{bmatrix} \tilde{p}_I \\ \tilde{p} \end{bmatrix} \tag{11d}$$
$$\hat{f}^n = R(\hat{q})f^b_{imu} + \xi_f. \tag{11e}$$

The driving errors are defined as: $\tilde{p} = p^n - \hat{p}^n \in \mathbb{R}^2, \tilde{p}_I = p_I - \hat{p}_I = 0 - \hat{p}_I \in \mathbb{R}$. $R(\hat{q})$ is the rotation matrix in roll, pitch, and yaw represented with quaternion estimates from (9). ξ_f is a correction term on the acceleration estimate. $K_{pp}, K_{vp}, K_{\xi p} \in \mathbb{R}^{2\times2}_{>0}$, and $k_{pipi}, k_{ppi}, k_{vpi}, k_{\xi pi} \in \mathbb{R}_{>0}$. $\theta \geq 1$ is a high gain. The equation (11a) includes only the virtual heave part of the position estimate, i.e. it is scalar.

The estimation error state can be written compactly as $x_2 := [\tilde{q}^\top, \tilde{b}_g^\top, \tilde{p}_I, \tilde{p}^\top, \tilde{v}^\top, \tilde{f}^\top]^\top$, with estimation errors defined as before, $\tilde{(\cdot)}:=(\cdot)$ - $\hat{(\cdot)}$. The error dynamics can be written compactly as

$$\dot{x}_2 = F_2(x_2, p^n, \psi, \omega^b_{imu}, f^b_{imu}). \tag{12}$$

The signal-based estimation error dynamics (12) has the origin uniformly locally exponentially stable (ULES) with almost global attractivity (Grip et al. (2012) and Bryne et al. (2015)). The attractivity is almost global but not global; hence, the convergence rate from points near the boundary of the basin of attraction, particularly those corresponding to yaw estimation error equal to 180 degrees, is slow.

The output from the signal-based observer is transformed so it has the same form as the output from the model-based observer using (6)

$$\begin{aligned}\hat{\eta}_2 &:= [\hat{p}^n(1),\ \hat{p}^n(2),\ \hat{\psi}_2]^\top \\ \hat{\nu}_2 &:= R(\hat{\psi}_2)^\top [v^n(1),\ v^n(2),\ \hat{\omega}^b(3)]^\top \end{aligned} \tag{13}$$

where $\hat{\psi}_2$ is the heading angle estimate we get when converting from quaternions $\hat{q}$ to Euler angles, and the velocity output is transformed from the NED frame to the body frame. Because this observer relies on acceleration measurements and does not include a bias force estimation model, it reacts fast and accurately to transients. The downside to this is that the estimates are not wave filtered, so $\hat{\eta}_2$ and $\hat{\nu}_2$ will cause an oscillatory control input.

4. CONTROLLER

The control objective is to control the vessel to the desired time-varying setpoint $\eta_d(t)$ with the desired velocity trajectory $\nu_d(t)$:

$$\begin{aligned}\lim_{t\to\infty} \eta(t) - \eta_d(t) &= 0 \\ \lim_{t\to\infty} \nu(t) - \nu_d(t) &= 0.\end{aligned}$$

We write the tracking error dynamics as $x_0 := [\nu - \nu_d,\ \eta - \eta_d,\ \zeta - K_i^{-1} b]$, with the integral state in the controller ζ defined below.

The control objective is achieved by combining feedforward of the desired trajectory and output feedback using a nonlinear proportional, integral, derivative (nPID) algorithm. The algorithm is

$$\dot{\zeta} = (\hat{\eta}_s - \eta_d) \tag{14a}$$

$$u = -K_p R^\top(\psi)(\hat{\eta}_s - \eta_d) - K_d(\hat{\nu}_s - \nu_d) \tag{14b}$$

$$- K_i R^\top(\psi)\zeta + M\dot{\nu}_d + D\nu_d. \tag{14c}$$

$u \in \mathbb{R}^3$ is the commanded thrust, $K_p, K_d, K_i \in \mathbb{R}^{3\times 3}$ are the proportional, derivative and integral gains, and $\hat{\eta}_s$ and $\hat{\nu}_s$ are the estimates from the model-based observer when $s = 1$, and from the signal-based observer when $s = 2$. ζ compensates for the unknown bias force in (2d), which is commonly assumed constant for control design. The integral action error is $\zeta - K_i^{-1} b$. K_i should be picked so it can commute with the rotation matrix, i.e. $K_i R(\psi) = R(\psi) K_i$. The last two terms in (14b) are feedforward terms of the desired acceleration times inertia and desired velocity times damping.

Loria et al. (2000) showed that the feedback control law (14) using model-based estimates renders the closed-loop vessel and output feedback controller UGAS.

Following a similar approach for the other observer renders the closed-loop vessel and output feedback controller using signal-based estimates uniformly locally asymptotically stable (ULAS). We conclude local because the desired behavior of the observer error dynamics (12) is predicated on the derivative of the tracking error, $\dot{x}_0$, being bounded. It is not clear whether the region of attraction for the origin of the signal-based output feedback controller and vessel is almost global. The simulations in Section 7 indicate that the basin of attraction when the signal-based estimates are used in feedback is fairly large, but further research on this problem is required to make rigorous statements about the basin of attraction of the origin for (12), (14), (4) and (5).

5. HYBRID SIGNAL-BASED AND MODEL-BASED OBSERVER IN CLOSED-LOOP CONTROL

The observers flow in parallel in the hybrid observer design, and the position and velocity in surge, sway, and yaw from the observer that performs best is used in output feedback with (14). The estimation errors are monitored, and switching is limited by hysteresis.

5.1 Plant, controller, and observer

The flow dynamics of the hybrid system constitutes the marine vessel, controller, and observer dynamics is

$$\dot{\eta} = R(\psi)\nu, \tag{15a}$$

$$M\dot{\nu} = -D_L\nu + R^\top(\psi)b + u \tag{15b}$$

$$\dot{\zeta} = \hat{\eta}_s - \eta_d \tag{15c}$$

$$\begin{aligned} u = &-R^\top(\psi)K_p(\hat{\eta}_s - \eta_d) - K_d(\hat{\nu}_s - \nu_d) \\ &- R^\top(\psi)K_i\zeta + M\dot{\nu}_d + D\nu_d \end{aligned} \tag{15d}$$

$$\dot{x}_1 = F_1(x_1, p^n, \psi) \tag{15e}$$

$$\dot{x}_2 = F_2(x_2, p^n, \psi, \omega^b_{imu}, f^b_{imu}) \tag{15f}$$

$$\dot{s} = 0, \tag{15g}$$

with $\eta, \nu, \hat{\eta}_s, \hat{\nu}_s \in \mathbb{R}^3$. (15a-b) are the vessel dynamics, (15c-d) is the control algorithm with output feedback and reference feedforward, (15e) is the model-based observer (7), and (15f) is the signal-based observer from (9) and (11). $s \in \{1, 2\}$ is a logic variable that indicates if the model-based or signal-based estimates are used in closed-loop control. $s = 1$ is model-based and $s = 2$ is the signal-based estimates, as decided by the performance monitoring and switching logic.

5.2 Performance monitoring and switching logic

The performance monitoring function computes the estimation errors of the two observers in position and heading over a time period to make sure the system does not switch unnecessarily often. In order to make a fair comparison, the total (low frequency and wave frequency) estimates are compared with the measured position and heading where north and east positions are measured in meters and heading in degrees. The model-based estimate, including wave frequency components, is $\hat{y}_1 := \hat{y}$ from (7), and the signal-based position and heading estimates are $\hat{y}_2 := \hat{\eta}_2$.

We sample y, $\hat{y}_1$, and $\hat{y}_2$ every $T > 0$ seconds and $N \in \mathbb{Z}_{\geq 1}$ consecutive measurements are stored in the state of three different shift registers with states $\chi_k \in \mathbb{R}^{3N}$, $k = \{0, 1, 2\}$. $\chi_{k,i} \in \mathbb{R}^3$, $i \in \{1, \ldots, N\}$ are the stored measurements and estimates. The state component $\chi_{k,1}$ contains the most recent samples, and $\chi_{k,N}$ contains the least recent samples; see (17a-f).

Let $\ell \in \mathbb{R}$ be a counter that triggers a performance check of the observer. This happens every LT seconds where $L \in \mathbb{Z}_{\geq 1}$. Let us define the *shift register mean value* for the measurements: $\bar{\chi}_0 := \frac{1}{N}\sum_{i=1}^{N} \chi_{0,i}$, model-based: $\bar{\chi}_1 := \frac{1}{N}\sum_{i=1}^{N} \chi_{1,i}$, and signal-based: $\bar{\chi}_2 := \frac{1}{N}\sum_{i=1}^{N} \chi_{2,i}$. We switch to the other observer if it performs better than the one currently in feedback with a hysteresis margin of $\varepsilon > 0$; see (17g-i).

The jumps for these variables are allowed when

$$(x_0, x_1, x_2, \chi_k, \tau, \ell, s) \in D \tag{16}$$

$D := \mathbb{R}^9 \times \mathbb{R}^{15} \times \mathbb{R}^{16} \times \mathbb{R}^{3Nk} \times \{T\} \times \{0, \ldots, L\} \times \{1, 2\}$

x_0 is the tracking error defined in Section 4. The jumps satisfy

$$\chi_{0,1}^{+} = y \tag{17a}$$
$$\chi_{1,1}^{+} = \hat{y}_1 \tag{17b}$$
$$\chi_{2,1}^{+} = \hat{y}_2 \tag{17c}$$
$$\chi_{k,2}^{+} = \chi_{k,1}, \quad k = \{0, 1, 2\} \tag{17d}$$
$$\vdots \tag{17e}$$
$$\chi_{k,N}^{+} = \chi_{k,N-1}, \ k = \{0, 1, 2\} \tag{17f}$$
$$\tau^{+} = 0 \tag{17g}$$
$$\ell^{+} = \begin{cases} \ell + 1 & \ell \in \{0, \ldots, L-1\} \\ 0 & \ell = L \end{cases} \tag{17h}$$
$$s^{+} \in \begin{cases} s & \ell \in \{0, \ldots, L-1\} \\ 3 - s & \ell = L, \ |\bar{\chi}_0 - \bar{\chi}_{3-s}| \leq |\bar{\chi}_0 - \bar{\chi}_s| - \varepsilon \\ s & \ell = L, \ |\bar{\chi}_0 - \bar{\chi}_{3-s}| \geq |\bar{\chi}_0 - \bar{\chi}_s| - \varepsilon. \end{cases} \tag{17i}$$

All the states introduced in this section remain constant during flows, except for τ that satisfies $\dot{\tau} = 1$. Flows are allowed when

$$(x_0, x_1, x_2, \chi_k, \tau, \ell, s) \in C \tag{18}$$

$C := \mathbb{R}^9 \times \mathbb{R}^{15} \times \mathbb{R}^{16} \times \mathbb{R}^{3Nk} \times [0, \ T] \times \{0, \ldots, L\} \times \{1, 2\}.$

6. STABILITY

The stability results used to analyze the set are based on invariance and uniform convergence according to Proposition 7.5 of Goebel et al. (2012). Consider the set

$$\mathcal{A} := \{0\} \times \{0\} \times \{0\} \times \Psi \times [0, \ T] \times \{0, \ldots, L\} \times \{1, 2\}, \tag{19}$$

with $\Psi := \{\chi_{0,ss}\} \times \{\chi_{1,ss}\} \times \{\chi_{2,ss}\}$ and $\chi_{k,ss}$, $k = \{0, 1, 2\}$ are the steady-state values of the shift register with saved measurements and estimates of the total vessel motion. The set $\mathcal{A}$ is compact because its components are closed and bounded sets.

Theorem 1. The set $\mathcal{A}$ defined in (19) is uniformly locally asymptotically stable (ULAS) for the hybrid system defined in (15)-(18).

Proof: The set $\mathcal{A}$ is:

(i) strongly forward invariant. If the solution starts inside the set $\mathcal{A}$, the observer in closed loop, regardless of which, will keep the solution within $\mathcal{A}$ during flows. During jumps the solution still remains in $\mathcal{A}$ since jumping from the set of values $\mathcal{A} \cap D$, will yield a solution that still is in $\mathcal{A}$.

(ii) uniformly attractive from a neighborhood of itself. Since each observer is converging, at least locally, it follows from the switching condition in (17i) that the number of switches will be uniformly bounded, at least from initial conditions sufficiently close to the set $\mathcal{A}$, and that the last switching time can also be uniformly bounded. That is there exists a T such that

$$|\bar{\chi}_0(t) - \bar{\chi}_1(t)| + |\bar{\chi}_0(t) - \bar{\chi}_2(t)| \leq \varepsilon \quad \forall t \geq T,$$

and there will be no more switching. Then, because of uniform attractivity in the absence of switching, we also have uniform attractivity with the switching. □

7. SIMULATION RESULTS AND DISCUSSION

Simulations are done in Matlab/Simulink with a platform supply vessel in a marine environment with waves, wind and current. The high fidelity simulation model is based on the MSS GNC toolbox (Fossen and Perez, 2010) with realistic measurement noise and sample time. The sea state is very rough with significant wave height 4 meters, peak frequency 0.6 rad/s taken from the JONSWAP [1] spectrum, with mean incident wave heading 150° in the North-East frame (Price and Bishop, 1974). The current speed is 0.5 m/s with direction 180°, and the wind speed and direction are taken as expectation values based on the wave parameters.

The case simulated is a setpoint change where the vessel moves 20 meters North and East, and changes heading from $\psi = 0°$ to $\psi = -90°$. The change happens at 2500 seconds so the observer parts have ample time to converge to steady state first. Figure 1 shows the estimation error for the signal-based and model-based observer parts after the initialization phase. The switching variable s indicates which observer estimates are used in closed loop.

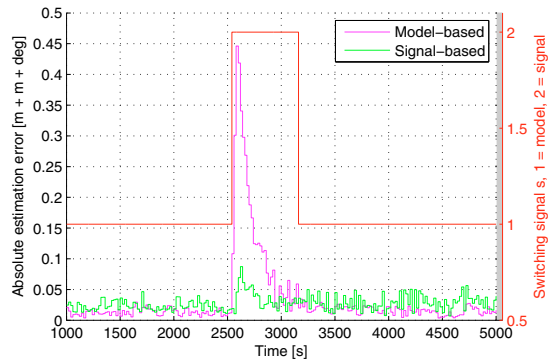

Fig. 1. Estimation error for the signal-based and model-based parts. The estimates used in closed-loop s is indicated, with axis to the right.

At initialization the model-based observer is chosen in feedback, as it takes time for the gyro bias estimate $\hat{b}_g$ in the signal-based observer to converge. The bias force estimate $\hat{b}$ in the model-based observer converges after about 500 seconds. When the vessel changes heading,

[1] Joint North Sea Wave Project.

the forces on the hull due to current, wind and waves changes rapidly. This induces a transient in the model-based part since the bias force estimate takes time to converge to the new value. 40 seconds after the vessel starts the setpoint change, the signal-based observer performs better and is used in feedback. 700 seconds later the model-based bias force estimate $\hat{b}$ has converged to the new value and is used in feedback once more. While performing better during the setpoint change, the signal-based part has higher estimation error during steady state, as seen clearly in the figure. The simulation results indicate that the basin of attraction for the signal-based estimates in output feedback control is fairly large, since it includes points from where we end up switching.

The vessel response is more oscillatory when the signal-based observer is used in closed-loop. This is because the signal-based observer does not include a wave filter and has oscillatory estimates. It therefore induces some wave frequency motion on the system through the control law, approximately ± 1 meter. This motion is insignificant compared with the motion due to the 4 meter waves, however, the vessel uses more energy and in a real system the wear and tear on the machinery would be increased.

8. CONCLUSION

The hybrid observer with a signal-based and a model-based part was shown to have good performance in simulations of a DP vessel in a rough sea state. The observer used in output feedback with a nonlinear PID tracking controller, was shown uniformly locally asymptotically stable.

REFERENCES

Brodtkorb, A.H., Sørensen, A.J., and Teel, A.R. (2014). Increasing the operation window of dynamic positioned vessels using the concept of hybrid control. *ASME 2014 33rd International Conference on Ocean, Offshore and Arctic Engineering Volume 1A: Offshore Technology San Francisco, California, USA, June 813, 2014*.

Bryne, T.H., Fossen, T.I., and Johansen, T.A. (2014). Nonlinear observer with time-varying gains for inertial navigation aided by satellite reference systems in dynamic positioning. *2014 22nd Mediterranean Conference on Control and Automation, MED 2014*, 1353–1360.

Bryne, T.H., Fossen, T.I., and Johansen, T.A. (2015). A virtual vertical reference concept for GNSS/INS applications at the sea surface. *10th Conference on Maneouvring and Control of Marine Craft, MCMC August 24-26 2015 Copenhagen, Denmark*.

Bryne, T.H., Fossen, T.I., and Johansen, T.A. (2016). Design of inertial navigation systems for marine craft with adaptive wave filtering by triple-redundant sensor packages. *To appear in: International Journal of Adaptive Control and Signal Processing*.

Fossen, T.I. (2011). *Handbook of Marine Craft Hydrodyamics and Motion Control*. Wiley.

Fossen, T.I. and Perez, T. (2010). Marine systems simulator, viewed 27.01.2016. URL `http://www.marinecontrol.org`.

Fossen, T.I. and Strand, J.P. (1999). Passive nonlinear observer design for ships using lyapunov methods: full-scale experiments with a supply vessel. *Automatica*, 35(1), 3 – 16.

Goebel, R., Sanfelice, R.G., and Teel, A.R. (2012). *Hybrid Dynamical Systems, Modelling, Stability and Robustness*. Princeton University Press.

Grip, H.F., Fossen, T.I., Johansen, T.A., and Saberi, A. (2013). Nonlinear observer for gnss-aided inertial navigation with quaternion-based attitude estimation. *Proceedings of the American Control Conference*, 272–279.

Grip, H., Fossen, T., Johansen, T., and Saberi, A. (2012). Attitude estimation using biased gyro and vector measurements with time-varying reference vectors. *IEEE Transactions on Automatic Control*, 57(5), 1332–1338. doi:10.1109/TAC.2011.2173415.

Hassani, V., Sørensen, A.J., and Pascoal, A.M. (2013). A novel methodology for robust dynamic positioning of marine vessels: Theory and experiments. *Proceedings of the American Control Conference*, 560–565.

Hua, M.D. (2010). Attitude estimation for accelerated vehicles using GPS/INS measurements. *Control Engineering Practice*, 18(7), 723 – 732. Special Issue on Aerial Robotics.

Khalil, H. (2002). *Nonlinear Systems, Second Edition*. Prentice Hall,.

Loria, A., Fossen, T.I., and Panteley, E. (2000). A separation principle for dynamic positioning of ships: Theoretical and experimental results. *IEEE Transactions on Control Systems Technology*, 8(2), 332–343. doi: 10.1109/87.826804.

Mahony, R., Hamel, T., and Pflimlin, J.M. (2008). Nonlinear complementary filters on the special orthogonal group. *IEEE Transactions on Automatic Control*, 53(5), 1203–1218.

Nguyen, T.D., Sørensen, A.J., and Quek, S.T. (2008). Multi-operational controller structure for station keeping and transit operations of marine vessels. *IEEE Transactions on Control Systems Technology*, 16(3), 491–498.

Nguyen, T.D., Sørensen, A.J., and Tong Quek, S.T. (2007). Design of hybrid controller for dynamic positioning from calm to extreme sea conditions. *Automatica*, 43(5), 768–785.

Price, W.G. and Bishop, R.E.D. (1974). *Probalistic Theory of Ships*. Chapman and Hall, London.

Prieur, C. and Teel, A. (2011). Uniting local and global output feedback controllers. *IEEE Transactions on Automatic Control*, 56(7), 1636–1649. doi: 10.1109/TAC.2010.2091436.

Sørensen, A.J. (2013). *Marine Control Systems, Propulsion and Motion Control of Ships and Ocean structures, Lecture Notes*. Department of Marine Technology, NTNU.

Tannuri, E.A. and Morishita, H.M. (2006). Experimental and numerical evaluation of a typical dynamic positioning system. *Applied Ocean Research*, 28(2), 133–146.

Paper F:

Hybrid Controller Concept for Marine Vessels with Experimental Results

Astrid H. Brodtkorb, Svenn A. Værnø, Andrew R. Teel, Asgeir J. Sørensen, Roger Skjetne

Submitted to Automatica 2017.

Hybrid Controller Concept for Dynamic Positioning of Marine Vessels with Experimental Results ⋆

Astrid H. Brodtkorb [a] Svenn A. Værnø [a] Andrew R. Teel [b] Asgeir J. Sørensen [a] Roger Skjetne [a]

[a] *Centre for Autonomous Marine Operations, Department of Marine Technology, Norwegian University of Science and Technology (NTNU AMOS), 7491 Trondheim, Norway (e-mails: astrid.h.brodtkorb@ntnu.no, svenn.are.varno@ntnu.no, asgeir.sorensen@ntnu.no, roger.skjetne@ntnu.no).*

[b] *Department of Electrical and Computational Engineering, University of California Santa Barbara, CA 93106-9560 USA (e-mail: teel@ece.ucsb.edu)*

Abstract

The next generation marine control systems will, as a step towards increased autonomy, have more automatic functionality in order to cope with a set of complex operations in unknown, challenging environments while maintaining safety and keeping operational costs low. In this paper a hybrid control strategy for stationkeeping and maneuvering of marine vessels is proposed. The proposed hybrid concept allows a structured way to develop a control system with a bank of controllers and observers improving dynamic positioning (DP) performance in stationary dynamics, improving transient performance, and giving robustness to measurement errors. In this paper a novel method improving the transient response of a vessel in DP is developed. DP systems are used on marine vessels for automatic stationkeeping and tracking operations solely by use of the thrusters. The performance of the hybrid control system, including two observer candidates and one controller candidate, is demonstrated in model-scale experiments and on full-scale field data. The hybrid system has global stability properties.

Key words: Marine control systems, hybrid systems, dynamic positioning, observers, output feedback control

1 Introduction

Marine operations are moving into harsher environments, and as a consequence, requirements for the vessel's operational window, safety functions, and energy-efficiency become stricter (Sørensen, 2011). During marine operations, both variations in stationary dynamics and transient behavior are important to account for in an all-year operation philosophy subject to changing weather, sea loads, and modes of operation. There are many unknown factors that may cause transients in the vessel response, both from the environment (e.g., wave trains and wind gusts) and triggered by the operation taking place (e.g., heading changes or crane operations of heavy goods). A block diagram of a hybrid control system for a marine vessel is shown in Figure

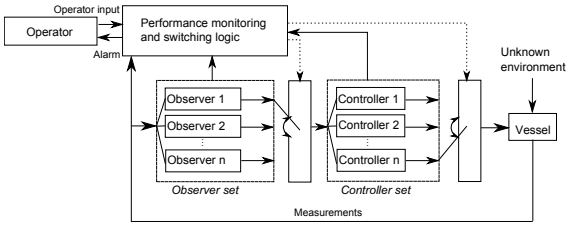

Fig. 1. Block diagram for a hybrid control system for a marine vessel in an unknown environment consisting of wind, waves and current. Here two observers and one controller are used.

1. The observers and controllers in the sets have their areas of expertise, based upon various structures and assumptions. In addition to handling different operational conditions and changing sea states (Nguyen et al., 2007), the proposed setup ensures redundancy in the (software) *design methodology* so that faults (Blanke et al., 2003) may be detected early and alarms may be raised to operators, who are either on-site or remote. The performance monitoring and switching logic block

⋆ This work was supported by the Research Council of Norway through the Centres of Excellence funding scheme, project number 223254 - NTNU AMOS, and in part by NSF grant number ECCS-1508757 and AFOSR grant number FA9550-15-1-0155.

includes monitoring of the environment, power system, observer performance, position precision, signal health, and more. The focus of this paper is on detecting and improving the transient performance of the DP control system using the framework Goebel et al. (2012).

The main scientific contribution of this paper is the development of a hybrid control concept for proper switching of candidate observers and controllers, customized for transient and steady-state behavior of DP vessels. For particular observer candidates, this work combines a model-based observer (Fossen and Strand, 1999), a signal-based observer (Grip et al., 2015), a controller, and a switching logic into a hybrid system with the goal to improve the transient response. The model-based observer, including wave filtering and bias force estimation, is especially suited in steady state, while the signal-based observer is more reactive during transients, even though it is more sensitive to signal noise. Stability analysis of the hybrid system applies results from Goebel et al. (2009). Performance of the proposed concept is demonstrated experimentally through model-scale experiments with the hybrid observer estimates used in closed-loop output feedback control, and through estimation on full-scale field data. The paper is a continuation of Brodtkorb et al. (2016), with the signal-based observer exchanged with one that has global stability properties, enhanced performance monitoring and switching logic, and new hybrid stability analysis.

The paper is organized as follows: The measurements and notation is introduced in Section 2, and the candidate observers and control algorithms are presented in Section 3. The hybrid system is assembled in Section 4, and stability is discussed in Section 5. The experimental setup and results are shown in Section 6. Section 7 concludes the paper.

2 Preliminaries

Common instrumentation in DP vessels includes position reference systems (typically GNSS [1]), compass, and inertial measurement units (IMU). The measurements, denoted with subscript m, are in this paper assumed to be of the form

$$p^n_m = [N, E]^\top \tag{1a}$$
$$\psi^n_m = \psi \tag{1b}$$
$$\omega^b_m = \omega^b + b_g \tag{1c}$$
$$f^b_m = R^\top_\Theta(\dot{v}^n - g^n), \tag{1d}$$

where the measurements in the NED frame (an Earth-fixed local reference frame assumed to be inertial) have superscript n, and measurements in the body-fixed frame have superscript b. As the design is deterministic, measurement noise is disregarded in the analysis. For the purpose of stability analysis, the system is assumed to be deterministic such that noise is disregarded. This follows similar approaches as Fossen and Strand (1999) and Nguyen et al. (2007). The vector $p^n_m \in \mathbb{R}^2$ is the measured position in North and East. A vertical measurement may also be obtained through GNSS, but it is typically of low quality, and is not used here; see Section 3.2. The measured angle $\psi^n_m \in \mathbb{R}$ includes the low frequency yaw angle ψ and the wave-induced heading oscillations ψ_w, which are assumed to be small (Fossen and Strand, 1999). The angular velocity ω^b, which takes values in $\mathbb{R}^3$, is continuous and bounded, and the gyro bias is constant with a known bound $||b_g|| \leq M_b$. The vector $f^b_m \in \mathbb{R}^3$ is the measured specific force [2], including the acceleration of the vessel $\dot{v}^n$ and the acceleration due to gravity $g^n \in \mathbb{R}^3$. $R_\Theta \in \mathbb{R}^{3\times3}$ is the rotation matrix about the z, y, x-axes (Fossen, 2011, Ch. 2). We assume f^b_m is non-biased, bounded $||f^b_m|| \leq M_f$, and the derivative of the actual specific force $\dot{f}^b$ is continuous and bounded. Furthermore, there exists a constant $c_{obs} > 0$ such that $||c^b \times f^b_m|| > c_{obs}$, $c^b = [\cos(\psi^n_m), -\sin(\psi^n_m), 0]^\top$.

3 Candidate Observers and Controllers

Two observers based on two philosophically different models of the same vessel are presented in the next sections. The relationship between them are as follows:

$$\eta + \eta_w \equiv [p^n_{(1,1)}, p^n_{(2,1)}, \Theta_{(3,1)}]^\top \tag{2a}$$
$$\nu + \nu_w \equiv [v^b_{(1,1)}, v^b_{(2,1)}, \omega^b_{(3,1)}]^\top, \tag{2b}$$

with the subscript (i, j) denoting the elements of the corresponding vectors. On the left-hand side we have the position vector $\eta + \eta_w \in \mathbb{R}^3$ (North, East, yaw) and velocity vector $\nu + \nu_w \in \mathbb{R}^3$ (surge, sway, yaw) split into low-frequency and wave-frequency components. η and ν will later be estimated in the model-based observer and marked with a hat. On the right-hand side we have the low-frequency and wave-frequency position $p^n_{(1:2)} \in \mathbb{R}^2$ (North, East) and heading $\Theta_{(3,1)}$, and velocity $v^b_{(1:2)} \in \mathbb{R}^2$ (surge, sway) and yaw $\omega^b_{(3,1)}$. Two consecutive elements of a vector are denoted with subscript $(1:2)$. p^n and $v^n := R_\Theta v^b$ are estimated in the signal-based observer and marked with a hat. Note that $\Theta_{(3,1)} \equiv \psi + \psi_w \approx \psi$.

3.1 Model-based observer

We have chosen to work with the nonlinear passive observer (Fossen and Strand, 1999) since it is an intuitive

[1] Global Navigation Satellite System

[2] Specific force is the physical acceleration experienced by an object, consisting of the acceleration of the object and the acceleration due to gravity, i.e., it is the *measurable* acceleration, with unit $[m/s^2]$.

observer to tune, and it has global stability properties. This observer is based on the DP control plant model (Sørensen, 2011), which is a simplification of the real vessel dynamics. The inputs to the observer are the measurement $y = [p_m^{n\top}, \psi_m^n]^\top \in \mathbb{R}^3$ and the control input $\tau \in \mathbb{R}^3$. The 3 degree of freedom (DOF) model-based observer algorithm for a ship-shaped vessel in DP can be written as (Fossen and Strand, 1999)

$$\dot{\hat{\xi}} = A_\omega \hat{\xi} + K_{1,\omega}\tilde{y} \tag{3a}$$
$$\dot{\hat{\eta}} = R(\psi_m^n)\hat{\nu} + K_2\tilde{y} \tag{3b}$$
$$\dot{\hat{b}} = -T_b^{-1}\hat{b} + K_3\tilde{y} \tag{3c}$$
$$M\dot{\hat{\nu}} = -D_L\hat{\nu} + R^\top(\psi_m^n)\hat{b} + \tau + R^\top(\psi_m^n)K_4\tilde{y} \tag{3d}$$
$$\hat{y} = \hat{\eta} + W\hat{\xi}, \tag{3e}$$

where $\hat{\xi} \in \mathbb{R}^6, \hat{\eta}, \hat{\nu}, \hat{b} \in \mathbb{R}^3$ are the state estimates. The wave states $\xi \in \mathbb{R}^6$, low frequency position vector η and velocity vector ν, and the bias force vector $b \in \mathbb{R}^3$. $\tilde{y} := y - \hat{y}$ is the measurement estimation error, and $K_{1,\omega} \in \mathbb{R}^{6\times3}, K_2, K_3, K_4 \in \mathbb{R}^{3\times3}_{>0}$ are the observer gain-matrices. $A_\omega \in \mathbb{R}^{6\times6}$ is a Hurwitz matrix containing wave parameters, $R(\psi) \in \mathbb{R}^{3\times3}$ is the rotation matrix about the z-axis (Fossen, 2011, Ch. 2), $M = M^\top \in \mathbb{R}^{3\times3}$ is the inertia matrix including added mass, $D_L \in \mathbb{R}^{3\times3}$ is the linear damping coefficient matrix including second-order wave-induced damping, and $T_b \in \mathbb{R}^{3\times3}$ is a diagonal matrix of bias time constants. The first-order model (3c) accounts for *slowly-varying* environmental disturbances from mean wind, current, and second-order wave loads, as well as unmodeled vessel dynamics.

(A1) The bias force dynamics (3c) are assumed to account for only slowly-varying loads (Fossen and Strand, 1999).

This is a good assumption in steady state, but does not capture rapid variations in the bias force due to transients, e.g., heading changes or wave trains. Wave filtering is achieved by separating the wave-frequency motion estimate $\hat{\eta}_w = W\hat{\xi}$, $W = [0_{3\times3}, I_{3\times3}]$ from the low frequency estimate $\hat{\eta}$, giving the output $\hat{\eta}_1 := \hat{\eta}$ and $\hat{\nu}_1 := \hat{\nu}$. The model-based estimation error dynamics, can be written compactly as

$$\dot{e}_1 = F_1(e_1), \tag{4}$$

with state vector $e_1 := x_1 - \hat{x}_1 = [(\xi - \hat{\xi})^\top, (b - \hat{b})^\top, (\eta - \hat{\eta})^\top, (\nu - \hat{\nu})^\top]^\top \in \mathbb{R}^{15}$.

Claim 1: Under Assumption (A1), the origin of the estimation error dynamics (4) is uniformly globally exponentially stable (UGES). □

Proof: See Fossen and Strand (1999). □

3.2 Signal-based observer

Grip et al. (2015) propose a nonlinear observer, for GNSS-aided inertial navigation with biased gyro measurements. It is based on the kinematic model (Fossen, 2011) with an angular and a translational part, relating the position, velocity, and acceleration of the vessel in 6 DOF. The inputs to the signal-based observer are p_m^n, ψ_m^n, ω_m^b, and f_m^b from (1). The rotation matrix R_Θ (about the z, y, x-axis) is estimated directly, giving

$$\dot{\hat{R}}_\Theta = \hat{R}_\Theta S(\omega_m^b - \hat{b}_g) + \sigma L_p \hat{J} \tag{5a}$$
$$\dot{\hat{b}}_g = \mathrm{Proj}_{M_b}(\hat{b}_g, -L_I \mathrm{vex}(\mathbb{P}_a(\hat{R}_{\Theta s}^\top L_P \hat{J}))), \tag{5b}$$

where $\hat{R}_\Theta$ is the rotation matrix estimate, $\hat{b}_g$ is the gyro bias estimate, and the angular rate estimate is $\hat{\omega}^b := \omega_m^b - \hat{b}_g$. The projection function $\mathrm{Proj}_{M_b}(\cdot,\cdot)$ (Grip et al., 2015, Appendix) ensures that $||\hat{b}_g|| \leq M_{\hat{b}}$, and the $S(\cdot)$, $\mathrm{vex}(\cdot)$, and $\mathbb{P}_a(\cdot)$ operators are defined in the footnote [3]. $\hat{R}_{\Theta s}$, appearing in (5b), is saturated elementwise with bound 1; $\hat{R}_{\Theta s} := \mathrm{sat}_1(\hat{R}_\Theta)$. The gain-matrices are $L_P \in \mathbb{R}^{3\times3}_{>0}, L_I \in \mathbb{R}^{3\times3}_{>0}$, and $\sigma \geq 1$ is a scaling factor that is tuned to achieve stability. $\hat{J}$ is a stabilizing term (Grip et al., 2015, (3) and (5)) that takes ψ_m^n measured by the compass, and the specific force measurement f_m^b as input. The translational observer algorithm is

$$\dot{\hat{p}}_I = \hat{p}^n_{(3,1)} + k_{pipi}\tilde{p}_I \tag{6a}$$
$$\dot{\hat{p}}^n = \hat{v}^n + C_p e \tag{6b}$$
$$\dot{\hat{v}}^n = \hat{f}^n + g^n + C_v e \tag{6c}$$
$$\dot{\xi}_f = -\sigma L_p \hat{J} f_m^b + C_\xi e \tag{6d}$$
$$\hat{f}^n = \hat{R}_\Theta f_m^b + \xi_f, \tag{6e}$$

with estimates $\hat{p}_I, \hat{p}^n, \hat{v}^n$ and $\hat{f}^n$, $\hat{R}_\Theta$ is from (5), and ξ_f is a correction term on the specific force estimate. (6b-e) are standard kinematic observer equations, and (6a) is an addition from Bryne et al. (2015) that comes instead of using the vertical GNSS position measurement height, as mentioned in Section 2.

(A2) The mean vertical position of the vessel over time is assumed to be zero.

This gives the *virtual vertical reference* $p_I = 0$. For a marine vessel in normal operation, (A2) is a sound assumption. In (6a) the vertical position estimate $\hat{p}^n_{(3,1)}$ is integrated to give $\hat{p}_I$. For more details, see Bryne et al. (2015). The driving error is $e := [\tilde{p}_I, \tilde{p}^\top]^\top \in \mathbb{R}^3$ with $\tilde{p} := p_m^n - \hat{p}^n \in \mathbb{R}^2$, $\tilde{p}_I := p_I - \hat{p}_I = 0 - \hat{p}_I \in \mathbb{R}$. The

[3] For a vector $x \in \mathbb{R}^3$, $S(x)$ denotes a skew-symmetric matrix so that for any $y \in \mathbb{R}^3$, $S(x)y = x \times y$, where $\times$ denotes the cross product. The skew-symmetric part of a matrix X is denoted by $\mathbb{P}_a = \frac{1}{2}(X - X^\top)$. The linear function $\mathrm{vex}(X)$, with X skew symmetric is defined so that $S(\mathrm{vex}(X)) = X$ and $\mathrm{vex}(S(x)) = x$.

correction gains-matrices are
$C_p = \begin{bmatrix} 0_{2\times1} & K_{pp} \\ k_{ppi} & 0_{1\times2} \end{bmatrix}$ $C_v = \begin{bmatrix} 0_{2\times1} & K_{vp} \\ k_{vpi} & 0_{1\times2} \end{bmatrix}$ $C_\xi = \begin{bmatrix} 0_{2\times1} & K_{\xi p} \\ k_{\xi pi} & 0_{1\times2} \end{bmatrix}$.
The North and East gain components are $K_{pp}, K_{vp}, K_{\xi p} \in \mathbb{R}^{2\times2}_{>0}$, and the down gains are $k_{pipi}, k_{ppi}, k_{vpi}, k_{\xi pi} \in \mathbb{R}_{>0}$. The signal-based estimation error dynamics are written compactly as

$$\dot{e}_2 = F_2(e_2), \tag{7}$$

with state vector $e_2 := x_2 - \hat{x}_2 = [(r - \hat{r})^\top, (b_g - \hat{b}_g)^\top, (p_I - \hat{p}_I), (p^n - \hat{p}^n)^\top, (v^n - \hat{v}^n)^\top, (f^n - \hat{f}^n)^\top]^\top \in \mathbb{R}^{22}$, $r := [R_{\Theta(1,:)}, R_{\Theta(2,:)}, R_{\Theta(3,:)}]^\top \in \mathbb{R}^9$, and $\hat{r}$ defined accordingly. ':' denotes all elements of the row/column.
Claim 2: Under Assumption (A2), with inputs as described in (1), the origin of the signal-based estimation error dynamics (7) is UGES. □
Proof: See Grip et al. (2015) and Bryne et al. (2015).□
The output from the signal-based observer is written using (2), so that $\hat{\eta}_2 := [\hat{p}^n_{(1,1)}, \hat{p}^n_{(2,1)}, \hat{\Theta}_{3,1}]^\top$, $\hat{\nu}_2 := [\hat{v}^b_{(1,1)}, \hat{v}^b_{(2,1)}, \hat{\omega}^b_{(3,1)}]^\top$, where the heading angle estimate $\hat{\Theta}_{(3,1)}$ is extracted from $\hat{R}_\Theta$, and $\hat{v}^b = \hat{R}^\top_\Theta \hat{v}^n$. Because this observer relies on the specific force measurements instead of estimating the bias force, it reacts fast and accurately to transients. Here, no wave filter is included so $\hat{\eta}_2$ and $\hat{\nu}_2$ capture the combined low-frequency and wave-frequency motion. For shorter periods of time this may be acceptable, which is the case during transients.

3.3 Controller

The control objective is to control the vessel to the desired time-varying trajectory $\eta_d(t)$ with the desired velocity trajectory $\nu_d(t)$. The proposed control law is

$$\begin{aligned} \dot{\zeta}_s &= \hat{\eta}_s - \eta_d \\ \tau &= -K_p R^\top(\psi^n_m)(\hat{\eta}_s - \eta_d) - K_d(\hat{\nu}_s - \nu_d) \\ &\quad - K_i R^\top(\psi^n_m)\zeta_s + M\dot{\nu}_d + D_L\nu_d. \end{aligned} \tag{8}$$

$\tau \in \mathbb{R}^3$ is the commanded thrust vector, $K_p, K_d, K_i \in \mathbb{R}^{3\times3}_{\geq0}$ are gain-matrices, and $\hat{\eta}_s$ and $\hat{\nu}_s$ are the estimates from the model-based observer when $s = 1$, and from the signal-based observer when $s = 2$. ζ_s compensates for the unknown bias force vector b with dynamics $\dot{b} = -T_b^{-1}b$. The last two terms in (8) are feedforward terms of the desired acceleration and desired velocity. For the stability analysis of the controller, it is assumed that:

(A3) The yaw rate $\omega^b_{(3,1)}$ (also denoted $\nu_{(3,1)}$) is bounded, $|\omega^b_{(3,1)}| < r_{max}$, and K_i and T_b commute with $R(\psi)$ [4].

[4] $K_i = \text{diag}([k_1, k_1, k_2])$, $T_b = \text{diag}([t_1, t_1, t_2])$ are used. The North and East gains/time constants are equal, which for a marine vessel is justified, since the environmental changes have roughly the same dominating frequencies in surge and sway.

(Lindegaard and Fossen, 2003).

The following result is proven in Lindegaard and Fossen (2003).
Claim 3: If Assumption (A3) holds, and the controller gains are chosen so that the system matrix A_c (see below) is Hurwitz, the origin of the tracking error dynamics consisting of the control plant model using control input with *state feedback*, (8) inserted the real states η, ν, is UGES. □
We note, for later use, that the tracking error dynamics have the form $\dot{e}_0 = T^\top(\psi)A_cT(\psi)e_0$ with
$e_0 = [\xi^\top, b^\top, (\eta - \eta_d)^\top, (\nu - \nu_d)^\top, \zeta^\top]$,

$$A_c = \begin{bmatrix} A_\omega & 0 & 0 & 0 & 0 \\ 0 & -T_b^{-1} & 0 & 0 & 0 \\ 0 & 0 & 0 & I & 0 \\ 0 & I & -M^{-1}K_p & -M^{-1}(D_L+K_d) & -M^-K_i \\ 0 & 0 & I & 0 & 0 \end{bmatrix}, \text{ and}$$

the block diagonal matrix $T(\psi) = \text{blkdiag}([I, R^\top(\psi), R^\top(\psi), I, R^\top(\psi)])$, and a Lyapunov function of the form $V_0(e_0, \psi) := e_0^\top T^\top(\psi)PT(\psi)e_0$ with $P = P^\top > 0$, where P satisfies the linear matrix inequality (LMI) $PA_c + A_c^\top P < 0$, that verifies the UGES property asserted in Claim 3.

4 Hybrid system

In this paper we propose a new hybrid strategy for DP systems in order to cope with both stationary and transient dynamics. In general, a hybrid system $\mathcal{H} = (C, F, D, G)$ is written formally as

$$x \in C \quad \dot{x} \in F(x) \tag{9a}$$
$$x \in D \quad x^+ \in G(x), \tag{9b}$$

where x is the hybrid state, C is the flow set, F is the flow map, D is the jump set, and G is the jump map. When x is in C, then the states are allowed to flow, and when x is in D the states are allowed to jump (Goebel et al., 2012). In this section the hybrid DP control system is assembled, starting with the jump dynamics that choose the appropriate estimates to use in output feedback with (8). In order to evaluate the performance of the observers, we choose to compute the difference in estimation error in North and East $(p^n_m - \hat{\eta}_{2(1:2)}) - (p^n_m - \hat{\eta}_{1(1:2)}) = (\hat{\eta}_{1(1:2)} - \hat{\eta}_{2(1:2)})$, and take the Euclidean norm of this difference. This signal may oscillate a lot, so we take the average of n of the past values that are saved in a shift register of size n with state $m \in \mathbb{R}^n$, i.e., $\bar{m} = \frac{1}{n}\sum_{i=1}^n m_i$. We call $\bar{m}$ the performance monitoring signal. m does not change during flows. Inserting for the steady-state observer estimates we have that $\hat{\eta}_{1(1:2)} = \eta_{(1:2)}$ (Claim 1), and $\hat{\eta}_{2(1:2)} = p^n_{(1:2)}$ (Claim 2). During steady state, the performance monitoring states m_i, $i = \{1, ..., n\}$, are

$$m_i = \left(||\eta_{(1:2)} - p^n_{(1:2)}||\right)_{i-1} = \left(||\eta_{w(1:2)}||\right)_{i-1}, \tag{10}$$

corresponding to the norm of the wave-frequency motion $\eta_w = W\xi$ in North and East, for each sample i in the shift register. The wave states ξ go to zero during steady state, since A_ω in (3a) is Hurwitz. In this case $\bar{m}$ is also zero, and we would like to use the model-based observer estimates in output feedback with (8). This is because these estimates are wave filtered, and hence reduce the wear and tear on the propulsion system. During a transient, the observers do not agree, and then $\bar{m}$ is larger. Since the signal-based observer presumably performs better in transients, these estimates are used in closed loop during these times. The performance monitoring and switching logic dynamics can be written as:

$$\dot{m}_i = 0, \qquad i = \{1, ..., n\} \tag{11a}$$
$$\dot{t}_m = -1 \tag{11b}$$
$$\dot{s} = 0 \tag{11c}$$
$$m_i^+ = \begin{cases} ||\hat{\eta}_{1(1:2)} - \hat{\eta}_{2(1:2)}||, & \text{for } i = 1 \\ m_{i-1}, & \text{for } i = \{2, ..., n\} \end{cases} \tag{11d}$$
$$t_m^+ = T \tag{11e}$$
$$s^+ = \begin{cases} 1, & \text{if } \bar{m} \leq \epsilon_{ss} \\ 2, & \text{if } \bar{m} \geq \epsilon_{tr} \\ 2, & \text{if } \nu_{d(3,1)} \geq \delta \\ s, & \text{otherwise,} \end{cases} \tag{11f}$$

where m are monitoring states, t_m is a timer, and s is the switching signal. The dynamics for m (11a,d) are discussed above. During flows, t_m decreases with unitary rate (11b), and is reset to T during jumps. A new jump is triggered when a new position measurement is available, when $t_m = 0$, so the position measurement has sample time T. The jump map for the switching signal s, including performance and heading change monitoring is (11f), where $\epsilon_{ss} \geq 0$ is the estimation difference we expect to see in steady state, and $\epsilon_{tr} \geq 0$ is the estimation difference we expect to see during a transient. Choose $\epsilon_{tr} > \epsilon_{ss}$ with some margin to provide hysteresis that suppresses unnecessary switching back and forth. The signal-based observer is chosen in closed loop if the desired yaw rate $\nu_{d(3,1)}$ is larger than a threshold $\delta \geq 0$, as we know that the forces on the hull will change rapidly in this situation. s does not change during flows (11c).

The control plant model and the kinematic model represent, with some overlap, the same underlying dynamics being the motion of the vessel. We assume that:

(A4) The solutions to the control plant model and kinematic model dynamics are forward complete [5].

Then the solutions exist for all positive time. The tracking error analysis in Lindegaard and Fossen (2003) (Claim 3) makes sure that x_1 behaves as it is meant to, i.e., η converges to η_d and ν converges to ν_d. From the relation between the control plant model and kinematic model (2), we have that $[p^{n\top}_{(1:2)}, \Theta_{(3,1)}]^\top$ goes to η_d, and $[v^{b\top}_{(1:2)}, \omega^b_{(3,1)}]^\top$, goes to ν_d. The heave, roll, and pitch states in the kinematic model are not controlled, and hence do not converge to a reference. Therefore the kinematic model with state x_2 is not included in the hybrid analysis. We define the state vector of the hybrid system as

$$x := (x_1, \zeta_s, \hat{x}_1, \hat{x}_2, m, t_m, s) \in \mathbb{R}^{15} \times \mathbb{R}^3 \times \mathbb{R}^{15} \times \mathbb{R}^{22} \times \mathbb{R}^n \times [0, T] \times \{1, 2\}, \tag{12}$$

consisting of the control plant model state x_1, the integral state in the control law ζ_s, the model-based observer estimates $\hat{x}_1$, the signal-based observer estimates $\hat{x}_2$, the performance monitoring states m, the timer t_m, and the switching signal s. The flow dynamics of the hybrid system constitutes the vessel described by the control plant model, controller, observer, and timer dynamics. The states $x_1, \zeta_s, \hat{x}_1$, and $\hat{x}_2$ do not change during jumps, i.e., $x_1^+ = x_1$, $\zeta_s^+ = \zeta_s$, and so on. The dynamics for m, t_m, and s are given by (11). Flows are allowed when $x \in C$, and jumps are allowed when $x \in D$ defined by

$$C := \mathbb{R}^{55+n} \times [0, T] \times \{1, 2\} \tag{13}$$
$$D := \mathbb{R}^{55+n} \times \{0\} \times \{1, 2\}. \tag{14}$$

5 Stability

We are analyzing stability of the set

$$\mathcal{A} := C \cap (\{x_{1d}\} \times \{0\} \times \{x_{1d}\} \times \{x_2\} \times \{0\} \times [0, T] \times \{1, 2\}). \tag{15}$$

This corresponds to the vessel tracking the desired trajectory, with $x_{1d} = [0, 0, \eta_d^\top, \nu_d^\top]^\top$, and the controller integral state ζ_s converging to zero. The model-based estimates are equal to the control plant model state x_1, which goes to x_{1d}, and the signal-based estimates are equal to the kinematic model state x_2. The performance monitoring states m go to zero, as discussed around (10), and the timer t_m and the switching signal s stay within $\mathcal{A}$ by design.

Theorem 1 *Under Assumptions (A1-A4) the set $\mathcal{A}$ given by* (15) *is GAS for the hybrid system given by the control plant model, the observers* (3), (5)-(6)*, the controller* (8)*, the performance monitoring and switching logic* (11)*, and the flow and jump sets* (13)-(14). □

Proof: The proof follows from Goebel et al. (2009), Corollary 19. By splitting the control law (8) into a state feedback part and a part that is due to estimation error,

[5] A solution with an unbounded time domain is called complete, (Goebel et al., 2009, p. 41).

the tracking error dynamics and observer error dynamics can be written in a cascaded structure,

$$\dot{e}_0 = F_0(e_0) + g(e_0, e_s) \tag{16a}$$
$$\dot{e}_1 = F_1(e_1) \tag{16b}$$
$$\dot{e}_2 = F_2(e_2) \tag{16c}$$
$$e_0^+ = e_0,\ e_1^+ = e_1,\ e_2^+ = e_2 \tag{16d}$$

(16a) is the tracking error dynamics with tracking error $e_0 = [\xi^\top, b^\top, (\eta - \eta_d)^\top, (\nu - \nu_d)^\top, \zeta^\top]^\top$ and estimation errors e_s, with $s = 1$ model-based estimation error, and $s = 2$ signal-based estimation error. $g(e_0, e_s)$ is the additional control input due to estimation error, where $g(e_0, e_s) = K_p R^\top(\psi_m^n)(\eta - \hat{\eta}_s) + K_d(\nu - \hat{\nu}_s) + K_i R^\top(\psi_m^n)(\zeta - \zeta_s)$. The switching signal s decides which observer perturbs the tracking error dynamics. (16b,c) are the model-based and signal-based estimation error dynamics. The rest of the observer error dynamics are given by (11). The flow and jump sets for (11) and (16) are:

$$C' := \mathbb{R}^{55+n} \times [0, T] \times \{1, 2\} \tag{17}$$
$$D' := \mathbb{R}^{55+n} \times \{0\} \times \{1, 2\} \tag{18}$$

To prove Theorem 1, it is sufficient to prove global asymptotic stability (GAS) of the set

$$\mathcal{A}' := \{0_{55+n}\} \times [0, T] \times \{1, 2\} \tag{19}$$

for the hybrid system $\mathcal{H} := (C', F, D', G)$ given by (11) and (16)-(18). This is done in two steps.

1. We prove GAS of $\mathcal{A}'$ for $\mathcal{H}_\beta := (C_\beta, F, D_\beta, G)$, which is $\mathcal{H}$ with the flow and jump sets intersected with $\beta\mathbb{B} \times \mathbb{R}^{37+n}$ for $\beta > 0$ and unit ball $\mathbb{B} \in \mathbb{R}^{18}$; $C_\beta := C' \cap (\beta\mathbb{B} \times \mathbb{R}^{37+n})$ and $D_\beta := D' \cap (\beta\mathbb{B} \times \mathbb{R}^{37+n})$. Firstly, the compact set

$$\mathcal{A}_1 := \{\beta\mathbb{B}\} \times \{0_{37+n}\} \times [0, T] \times \{1, 2\}, \tag{20}$$

is GAS for $\mathcal{H}_\beta$. This follows from the analysis in Fossen and Strand (1999), Bryne et al. (2015) and Grip et al. (2015) resulting in UGES origin of the observer error dynamics (Claim 1 and 2). Secondly, we prove GAS of $\mathcal{A}'$ for $\mathcal{H}|_{\mathcal{A}_1} := (C' \cap \mathcal{A}_1, F, D' \cap \mathcal{A}_1, G)$. When the solution is in $\mathcal{A}_1$, we have state feedback so that (16a) is $\dot{e}_0 = F_0(e_0)$, since $e_s = 0$, and $g(e_0, 0) = 0$. The analysis in Lindegaard and Fossen (2003) give UGES origin of the tracking error dynamics with state feedback (Claim 3). Applying Corollary 19 in Goebel et al. (2009), we have that the compact set $\mathcal{A}_1$ is GAS for $\mathcal{H}_\beta$, and that the compact set $\mathcal{A}' \subset \mathcal{A}_1$ is GAS for $\mathcal{H}|_{\mathcal{A}_1}$. Then $\mathcal{A}'$ is GAS for $\mathcal{H}_\beta$.

2. We use this preliminary result to prove GAS of $\mathcal{A}'$ for $\mathcal{H}$ without restrictions on e_0 in the flow and jump sets. The solutions of $\mathcal{H}$ are the solutions of $\mathcal{H}_\beta$ when $e_0 \in \beta\mathbb{B}$. The only thing left to prove is that the basin of attraction is the entire space, so that for each solution, β can be chosen large enough so that the $\beta\mathbb{B}$ intersection has no effect. The observer solutions e_s can be bounded by $||e_s(t)|| \leq \lambda_1 ||e_s(t_0)|| e^{-\lambda_2(t-t_0)}$ for $\lambda_1, \lambda_2 > 0$ that are dependent on initial condition $e_s(t_0)$. Integrating $e_s(t)$ over time, we get

$$\int_{t_0}^{\infty} ||e_s(t, t_0, e_s(0))|| dt \leq \phi(||e_s(t_0)||), \quad \forall t_0 \geq 0,$$

with $\phi(||e_s(t_0)||) = \frac{\lambda_1}{\lambda_2}||e_s(t_0)||$. $g(e_0, e_s)$ can be bounded in terms of e_s by $||g(e_0, e_s)|| \leq \gamma ||e_s||$, $\gamma \geq ||[K_p,\ K_d,\ K_i]^\top||$. Then, the only state that can grow unbounded is e_0, but this is ruled out by the following. The Lyapunov function $V_0(e_0, \psi)$, defined below Claim 3, for (16a) with $g(e_0, e_s) = 0$ and $F_0(e_0) = T^\top(\psi) A_c T(\psi) e_0$ satisfies

$$\left|\left|\frac{\partial V_0(e_0, \psi)}{\partial e_0}\right|\right| ||e_0|| \leq c_1 ||e_0||^2, \quad \forall ||e_0|| \geq \mu \tag{21a}$$
$$\left|\left|\frac{\partial V_0(e_0, \psi)}{\partial e_0}\right|\right| \leq c_2, \quad \forall ||e_0|| \leq \mu \tag{21b}$$

with $c_1 = 2\lambda_{max}(P)$ and $c_2 = 2\lambda_{max}(P)\mu$, with $\lambda_{max}(P)$ being the largest eigenvalue of P. (21b) holds for all headings ψ. (21) ensures that e_0 stays bounded (Fossen, 2011, Ch. 13), so that each solution of $\mathcal{H}$ has to converge to $\mathcal{A}'$ because it is a solution to the system $\mathcal{H}_\beta$ for large enough β and the solutions of $\mathcal{H}_\beta$ converge. Hence, $\mathcal{A}'$ in (19) is GAS for the hybrid system $\mathcal{H}$ given by (11) and(16)-(18), which concludes the proof. □

When applying Assumption (A1) we assume that the control plant model is an exact deterministic model of the real vessel dynamics. Then there may only be switching due to reference changes and due to transients during initialization. However, as shown through experiments in Section 6, switching based on performance is triggered because Assumption (A1) of slowly-varying bias loads does not hold during transients.

6 Experimental setup, results and discussion

The model-scale experiments were conducted with C/S Inocean Cat I Drillship, a 1:90 scale model with dimensions (length, beam) = (2.578 m, 0.44 m) in the Marine Cybernetics Laboratory (MCLab) at NTNU. The full-scale DP data was collected during the AMOS DP Research Cruise (ADPRC) 2016 onboard R/V Gunnerus, see Skjetne et al. (2017) for details. The model-based observer was in both cases tuned using tuning rules in Fossen (2011), Ch. 11, for good steady state, and adequate transient performance. The same IMUs were used in model-scale and full-scale, showing that the proposed hybrid observer setup is robust to large variations in noise-to-signal ratio. In full-scale, the tuning from Bryne

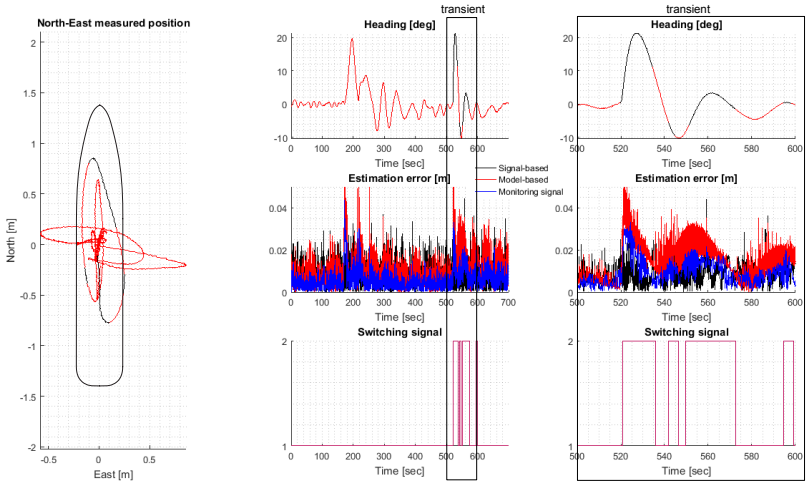

Fig. 2. Closed-loop control: C/S Inocean Cat I Drillship is pushed off position using a boat-hook at time 170 s and 520 s. North-East position track (left),heading, estimation error, monitoring signal and switching signal (middle), details of the second transient (right). Position and heading trajectories are red when model-based estimates are used in closed loop, and black for signal-based estimates. Environmental conditions corresponding to rough full-scale sea state with $H_s = 3.6$ m,$T_p = 10.4$ s, head sea, no wind, $\epsilon_{tr} = 0.02, \epsilon_{ss} = 0.005, \delta = 0.05$.

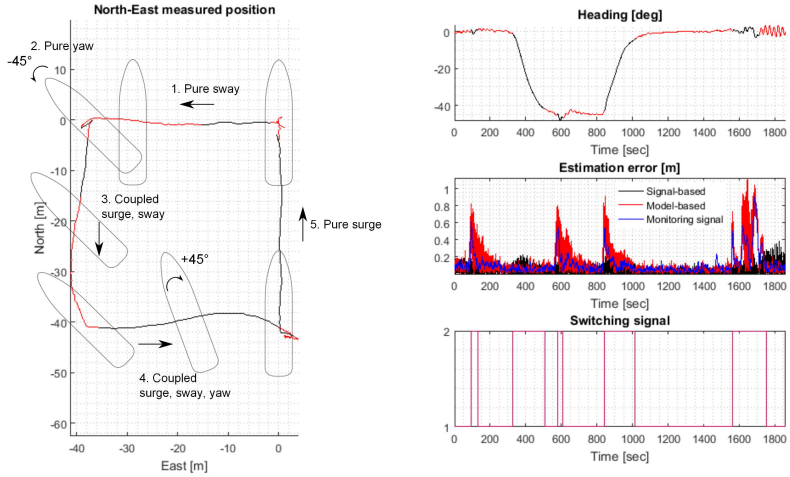

Fig. 3. Estimation: The North-East position (left), heading, observer estimation error and monitoring signal, and switching signal (right) for a DP 4 corner maneuver, starting in (0,0) and moving as indicated by the arrows, for R/V Gunnerus. The position and heading trajectories are red when the model-based estimates should be used in closed loop, and black when the signal-based estimates should be used in closed loop. Environmental conditions: current 0.3 m/s, 290°, wind 7 m/s, 260°, and waves with $H_s = 0.2$ m, $T_p = 13.6$ s, 260°. $\epsilon_{tr} = 0.5, \epsilon_{ss} = 0.03, \delta = 0.2$.

et al. (2015) was tweaked to work better for R/V Gunnerus, but in the MCLab the tuning was found from scratch. Tuning of the controller in the MCLab was found using standard PID tuning rules (Fossen, 2011, Ch. 12), which were tweaked to work well with both observer estimates in feedback. The algorithms were coded in Matlab/Simulink and run in NI Veristand [6] software.

[6] The Bogacki-Shampine solver (Matlab ode23) was used with fixed step 0.01 s, www.ni.com/veristand/.

6.1 Model-scale experiments

Wind loads constitute a lot of the mean forces on the hull, and since wind is not available in the MCLab, the directional dependence of the bias force that is seen in full-scale applications was less prominent in the lab. Hence, switching based on observer performance was triggered by pushing the model off setpoint using a boat-hook, inducing an unknown, rapid transient, see Figure 2. The model is pushed off setpoint twice; at time 170 s and 520 s. In the first transient, the observer is fixed with the model-based observer in closed loop. The vessel spends a long time coming back to the setpoint, since the estimates from the model-based observer (especially the velocity estimate) is off during the transient. In the second transient the observer is allowed to switch based on performance, and chooses the signal-based observer in closed loop for most of the transient, although there is some switching back and forth. The heading reaches steady state somewhat faster when the signal-based observer is in closed loop, *although comparison of the two pushes can be seen only as indications of performance since the conditions were not identical*[7] . Switching during heading changes, based on desired yaw rate, worked well in the MCLab. How large δ is chosen should be dependent on the vessel size and the maximum desired yaw rate. The thrust usage when the model-based or the signal-based observer estimates were used in closed loop was not significantly different, though the signal-based estimates made the thrust more oscillatory.

6.2 Estimation based on full-scale measurements

Figure 3 shows full-scale R/V Gunnerus data from a DP 4 corner test, and that the hybrid observer switches due to transients. If the third and fourth parts of the maneuver were to be done close to other offshore infrastructure, R/V Gunnerus may have been required to either reduce the speed, or choose another control strategy in order to stay on the desired straight-line segments of the square. In the fifth maneuver, a pure surge motion should not induce much transients, however in this dataset the heading oscillates $\pm 3^\circ$, and therefore the signal-based observer is chosen for most of the leg. Depending on the vessel size, propulsion system, and instrumentation, a smarter choice of controller could make the vessel stay on the desired path with a higher speed, reducing the vessel operation time.

7 Conclusion

A general hybrid control strategy for marine control systems providing a redundant design methodology for robustness to system errors was proposed in this paper, and an example of a such control system improving the transient vessel response in dynamic positioning was given. Performance was shown through model-scale experiments, and estimation on full-scale field data.

[7] See Brodtkorb et al. (2016) for comparison of performance in simulations.

Acknowledgements

Thanks to Vincenzo Calabrò and the rest of the Kongsberg Maritime team, Øivind Kjerstad, Mikkel E. Sørensen and Martin Heyn for collaboration during AD-PRC, and to Torgeir Wahl for assistance in the MCLab.

References

Blanke, M., Kinnaert, M., Lunze, J., and Staroswiecki, M. (2003). *Diagnosis and Fault-tolerant Control*. Springer.

Brodtkorb, A.H., Værnø, S.A., Teel, A.R., Sørensen, A.J., and Skjetne, R. (2016). Hybrid observer for improved transient performance of a marine vessel in dynamic positioning. *NOLCOS, USA*.

Bryne, T.H., Fossen, T.I., and Johansen, T.A. (2015). A virtual vertical reference concept for GNSS/INS applications at the sea surface. *MCMC, Denmark*.

Fossen, T.I. (2011). *Handbook of Marine Craft Hydrodyamics and Motion Control*. Wiley.

Fossen, T.I. and Strand, J.P. (1999). Passive nonlinear observer design for ships using lyapunov methods: Full-scale experiments with a supply vessel. *Automatica*, 35(1), 3 – 16.

Goebel, R., Sanfelice, R., and Teel, A.R. (2009). Hybrid dynamical systems robust stability and control for systems that combine continuous-time and discrete-time dynamics. *IEEE Control Systems Magazine, April 2009*, 28–93.

Goebel, R., Sanfelice, R.G., and Teel, A.R. (2012). *Hybrid Dynamical Systems, Modelling, Stability and Robustness*. Princeton University Press.

Grip, H.F., Fossen, T.I., Johansen, T.A., and Saberi, A. (2015). Globally exponentially stable attitude and gyro bias estimation with application to GNSS/INS integration. *Automatica*, 158–166.

Lindegaard, K.P. and Fossen, T.I. (2003). Fuel-efficient rudder and propeller control allocation for marine craft: experiments with a model ship. *IEEE Transactions on Control Systems Technology*, 11(6), 850–862.

Nguyen, T.D., Sørensen, A.J., and Quek, S.T. (2007). Design of hybrid controller for dynamic positioning from calm to extreme sea conditions. *Automatica*, 43(5), 768–785.

Skjetne, R., Kjerstad, Ø.K., Værnø, S.A.T., Brodtkorb, A.H., Sørensen, A.J., Sørensen, M.E.N., Breivik, M., Calabrò, V., and Vinje, B.O. (2017). AMOS DP research campain. *OMAE, Norway*.

Sørensen, A.J. (2011). A survey of dynamic positioning control systems. *Annual Reviews in Control*, 35(1), 123–136.

Paper G:

An Output Feedback Controller with Improved Transient Response of Marine Vessels in Dynamic Positioning

Svenn Are T. Værnø, Astrid H. Brodtkorb, Roger Skjetne, Asgeir J. Sørensen

10th IFAC Conference on Control Applications in Marine Systems (CAMS 2016), Trondheim, Norway.
IFAC-PapersOnLine. vol. 49 (23), 2016.
doi: 10.2016/j.ifacol.2016.10.333.

Available online at www.sciencedirect.com

ScienceDirect

IFAC Papers Online CONFERENCE PAPER ARCHIVE

IFAC-PapersOnLine 49-23 (2016) 133–138

An Output Feedback Controller with Improved Transient Response of Marine Vessels in Dynamic Positioning ⋆

Svenn Are T. Værnø * **Astrid H. Brodtkorb** * **Roger Skjetne** * **Asgeir J. Sørensen** *

* *Centre for Autonomous Marine Operations (NTNU AMOS), Department of Marine Technology, Norwegian University of Science and Technology (NTNU), Otto Nielsens vei 10, 7491 Trondheim, Norway (e-mail: svenn.are.varno@ntnu.no,astrid.h.brodtkorb@ntnu.no, roger.skjetne@ntnu.no,asgeir.sorensen@ntnu.no)*

Abstract: An output feedback controller for dynamic positioning (DP) of marine surface vessels is developed. The proposed algorithm has good performance during transients as well as good steady state performance. The method achieves this by a flexible injection gain in the bias estimation dynamics in the observer. In addition, the traditional integral action is replaced by a filtered bias estimate from the observer. Both these elements combined provide good DP performance in transients, as well as calm behavior in steady state. A simulation study is performed showing the benefit of the proposed output feedback controller, and a stability analysis is performed to show uniform asymptotic stability.

Keywords: Dynamic positioning; Observers; Output feedback; Integral action

1. INTRODUCTION

A surface vessel performing dynamic positioning (DP) has to keep position and orientation (stationkeeping) or do low speed tracking while compensating for the slowly-varying loads that affect the vessel. These loads are typically due to current, mean wind loads, and second order wave loads. The sum of these loads together with unmodeled dynamics, is lumped into the bias load vector. For model-based observer designs it is important to estimate this bias in order to achieve good estimation of the velocity, and thereby the position of the vessel. In addition, this bias load needs to be compensated in the controller to keep the desired position. This is typically achieved through integral action in the control law.

In standard model-based observer designs (Fossen, 2011), the tuning of the bias observer is set low to ensure good performance of the observer in steady state. Since the bias is typically slowly-varying, low tuning will lead to less oscillations in the bias estimate, and therefore also less oscillations in the velocity and position estimates. However, when there is a significant transient in the bias force, for instance by a heading change, a wave train, or a mooring line that breaks (for position mooring), the bias estimate will take some time to converge to the new value. This is problematic for transient performance of the DP system, since the velocities will not be estimated correctly over the course of the transient.

The objective of this paper is to construct a model-based observer and controller with good performance in both transients as well as in steady state. This will be achieved by two changes from the standard model-based design. The first is to allow for a flexible bias estimation in the observer. The injection gain in the bias dynamics will be allowed to take values ranging from a nominal gain matrix to higher gains and a more aggressive tuning. The second contribution is to add a lowpass-filtered bias estimate which has a less oscillatory and smoother characteristics than the direct bias estimate. This filtered estimate will be used to compensate for the bias in the controller. There are two reasons for this implementation. From the literature, the two existing options for compensating the bias is to either use the bias estimate from the observer (Loría and Panteley, 1999), or to add integral action in the controller (Sørensen, 2011). The integral action in the controller finds the bias estimate based on the tracking errors. Since the control performance depends on the convergence of the observer, it is reasonable to believe that the bias estimate in the observer will always be faster than the integral action based on tracking errors (with reasonable tuning).

However, if we use a filtered version of the bias estimate, we allow for fast bias convergence in the observer, without having to send this noisy estimate directly to the controller. At the same time the bias compensation term in the controller is oscillating less than the direct bias estimate itself, and this is most likely faster than integral action based on tracking errors. This is a similar idea as used in L1 adaptive control (Hovakimyan and Cao, 2010).

In addition, there is a tuning benefit of using the bias estimate from the observer, both because tuning an ob-

⋆ Research partly funded by the Research Council of Norway (RCN) project no. 223254: CoE NTNU AMOS, and partly by RCN project no. 237929: CRI MOVE.

10.1016/j.ifacol.2016.10.333

server does not require the system to be in closed loop, and because tuning of integral action (on tracking errors) heavily depends on how fast the observer estimates converge. This is especially beneficial in the current design, since the proposed observer have time-varying gains.

Similar use of time-varying gains is present in the literature. See for instance Tutturen and Skjetne (2015) where hybrid integral action for DP of marine vessels is proposed, and Lekkas and Fossen (2014) where the authors propose to use a time-varying lookahead distance as a function of the cross track error in a line-of-sight algorithm. In Belleter et al. (2013, 2015) a wave encounter frequency estimator is proposed, where the frequency adaption law has a time-varying gain. In Bryne et al. (2014) time-varying gains are proposed for an inertial observer (aided by GNSS) for DP, in order to improve convergence and suppress sensor noise.

2. PROBLEM FORMULATION

In the following we will separate between a simulation model and a control design model. The simulation model has higher fidelity and is used for simulation and verification of observer and control designs. Because of the low-speed nature of the dynamic positioning operations, the control design models typically neglect centripetal and Coriolis terms, as well as nonlinear damping; see (Sørensen, 2005, 2011), and (Fossen, 2011). The control design model considered here is a horizontal motion 3 degree of freedom (DOF) model, with the dynamics

$$\dot{\xi} = A_w \xi + E_w w_w \tag{1a}$$
$$\dot{\eta} = R(\psi)\nu \tag{1b}$$
$$\dot{b} = w_b \tag{1c}$$
$$M\dot{\nu} = -D\nu + R(\psi)^\top b + u \tag{1d}$$
$$y = \eta + C_w \xi + v_y, \tag{1e}$$

where $\xi \in \mathbb{R}^6$ is the state of a synthetic white noise-driven model of the vessel motion due to the 1st order wave loads. In normal operating conditions it is beneficial to counteract the low frequency part of the wave motion only, and the model therefore consists of a wave model (1a) and a low frequency part (1b) - (1d), which consists of the low frequency position in north and east, as well as the heading angle, $\eta := [N, E, \psi]^\top \in \mathbb{R}^3$, the velocities in surge, sway, and the yaw rate, $\nu := [u, v, r]^\top \in \mathbb{R}^3$, the slowly varying NED-fixed bias force $b \in \mathbb{R}^3$ that constitutes the sum of all slowly-varying perturbation loads, such as current, mean wind, 2nd order waves, and unmodeled dynamics. In (1b) the kinematic relation is described by the 3 DOF rotation matrix from the body to the NED frame $R(\psi) \in \mathbb{R}^{3\times 3}$,

$$R(\psi) = \begin{bmatrix} \cos(\psi) & -\sin(\psi) & 0 \\ \sin(\psi) & \cos(\psi) & 0 \\ 0 & 0 & 1 \end{bmatrix}, \tag{2}$$

and the time derivative of $R(\psi)$ is given by $\dot{R} = rS$, where

$$S = \begin{bmatrix} 0 & -1 & 0 \\ 1 & 0 & 0 \\ 0 & 0 & 0 \end{bmatrix}, \tag{3}$$

and $r = \dot{\psi} \in \mathbb{R}$ is the yaw rate. In (1d), $M \in \mathbb{R}^{3\times 3}$ is the inertia matrix including added mass, $D \in \mathbb{D}^{3\times 3}$ is the linear damping matrix, and $u \in \mathbb{R}^3$ is the control input vector. The measurements $y \in \mathbb{R}^3$ in (1e) measure the actual position of the vessel, that is, the sum of the low frequency and wave frequency position, where $C_w = [0\ I] \in \mathbb{R}^{3\times 6}$, and $v_y \in \mathbb{R}^3$ is the measurement noise.

The control objective of the paper is to construct an output feedback tracking controller for DP, that has good performance in both steady state as well as in transients. This output feedback controller will track a reference trajectory given by an open-loop reference system (Sørensen, 2011).

Below are some assumptions relevant for the observer and control design.

Assumption 1. Starboard/port symmetry, $M = M^\top > 0$, and $\dot{M} = 0$. The damping matrix satisfies $D + D^\top > 0$.

Assumption 2. Because of physical limitations of the thrusters, the yaw rate is bounded, by $|r| \leq r_{max} < \infty$.

3. OUTPUT FEEDBACK DESIGN

3.1 Model-based observer

The model-based observer considered is similar to the traditional "nonlinear passive observer" presented in Fossen and Strand (1999) with an additional state $\hat{b}_f$, which is a lowpass-filtered version of $\hat{b}$. By copying the dynamics of (1), neglecting the noise terms, and adding injection terms we get the observer dynamics as

$$\dot{\hat{\xi}} = A_w \hat{\xi} + K_{1,\omega} \bar{y} \tag{4a}$$
$$\dot{\hat{\eta}} = R(\psi)\hat{\nu} + K_2 \bar{y} \tag{4b}$$
$$\dot{\hat{b}} = K_3 \bar{y} \tag{4c}$$
$$\dot{\hat{b}}_f = -T_f^{-1}[\hat{b}_f - \hat{b}] \tag{4d}$$
$$M\dot{\hat{\nu}} = -D\hat{\nu} + R(\psi)^\top \hat{b} + u + K_4 R(\psi)^\top \bar{y} \tag{4e}$$
$$\hat{y} = \hat{\eta} + C_w \hat{\xi}, \tag{4f}$$

where $\hat{\xi} \in \mathbb{R}^6, \hat{\eta}, \hat{b}, \hat{b}_f, \hat{\nu} \in \mathbb{R}^3$ are the state estimates, $K_{1,\omega} \in \mathbb{R}^{6\times 3}, K_2, K_3, K_4 \in \mathbb{R}^{3\times 3}$ are non-negative gain matrices, and $\bar{y} = y - \hat{y}$ is the measurement error. The underlying assumptions for the observer are:

Assumption 3. (a) $R(\psi + \psi_w) \approx R(\psi)$. That is, the heading angle due to wave-induced motion is small.
(b) The frequency used in the wave filter does not change. It corresponds to the peak frequency of the wave spectra of the incoming sea state.

By defining the estimation error states $\bar{\eta} := \eta - \hat{\eta}$, $\bar{\nu} := \nu - \hat{\nu}$, $\bar{b} := b - \hat{b}$, $\bar{b}_f := b - \hat{b}_f$, and subtracting the observer equations (4) from the control design model (1), we get the observer error system,

$$\dot{\bar{\xi}} = A_w \bar{\xi} - K_{1,\omega} \bar{y} \tag{5a}$$
$$\dot{\bar{\eta}} = R(\psi)\bar{\nu} - K_2 \bar{y} \tag{5b}$$
$$\dot{\bar{b}} = -K_3 \bar{y} \tag{5c}$$
$$\dot{\bar{b}}_f = -T_f^{-1}[\bar{b}_f - \bar{b}] \tag{5d}$$
$$M\dot{\bar{\nu}} = -D\bar{\nu} + R(\psi)^\top \bar{b} - K_4 R(\psi)^\top \bar{y}. \tag{5e}$$

3.2 Varying bias gain

To improve the transient response, we want the injection gain K_3 in (4c) to vary. In steady-state it is desired that K_3 stays close to a nominal gain such that the bias estimate is calm. Whenever the vessel experiences transients, K_3 should increase to make the bias estimate more reactive, and when the vessel again reaches steady state, the gain should return to the nominal gain. To solve this, K_3 is allowed to take a range of values within $K_3(t) \in [K_{3,min}, K_{3,max}],\ \forall t \geq 0$. We let $K_3(t) := \kappa(t) K_{3,min}$, where $\kappa(t) \in [\kappa_{min}, \kappa_{max}],\ \forall t \geq 0$. The update law for κ is given by

$$\kappa = \max\{1, \beta\}, \tag{6a}$$

$$\beta = \min\{\varepsilon_{r_d}|r_d(t)| + \varepsilon_\eta|\bar{\eta}_f| + \kappa_{max} e^{-\varepsilon_t t}, \kappa_{max}\}, \tag{6b}$$

$$\dot{\bar{\eta}}_f = -T_{\eta_f}^{-1}\{\bar{\eta}_f - \bar{y}\}. \tag{6c}$$

The first term in (6b) contains a constant $\varepsilon_{r_d} \geq 0$ and the desired yaw rate $r_d(t) \in \mathbb{R}$, related to a heading change. The second term is a performance term that triggers a higher gain when the observer error is large, and the third term only makes κ large during the initial transient. In (6c) T_{η_f} is a positive definite diagonal matrix with filter time constants, and these time constants and the size of $\varepsilon_\eta \geq 0$ are tuned such that κ approach κ_{min} at steady state.

In order to have a convenient expression for K_3 in the further analysis we introduce $\lambda \in [0, 1]$ and write $K_3 := K_{3,\lambda}$ as

$$K_{3\lambda} := \lambda K_{3,min} + (1 - \lambda) K_{3,max}. \tag{7}$$

3.3 Output feedback tracking control

The control law consists of a reference feedforward term and a feedback term. The feedback part consists of a nonlinear PD-term, and a bias rejection term, which is the filtered bias estimate from (4d),

$$u = u_{FB} + u_{FF} \tag{8}$$

$$u_{FF} = M\dot{\nu}_d(t) + D\nu_d(t) \tag{9}$$

$$\begin{aligned} u_{FB} &= -K_p R(\psi)^\top(\hat{\eta} - \eta_d(t)) - K_d(\hat{\nu} - \nu_d(t)) - R(\psi)^\top \hat{b}_f \\ &= -K_p R(\psi)^\top(\tilde{\eta} - \bar{\eta}) - K_d(\tilde{\nu} - \bar{\nu}) - R(\psi)^\top(b - \bar{b}_f). \end{aligned} \tag{10}$$

where $\eta_d(t)$, $\nu_d(t)$, $\dot{\nu}_d(t)$ are the desired references generated by a reference generator. By defining the tracking error states $\tilde{\eta} := \eta - \eta_d(t)$, $\tilde{\nu} := \nu - \nu_d(t)$, the kinematics in (1b) along with the kinetics in (1d) inserted for (8) gives the tracking error system,

$$\dot{\tilde{\eta}} = R(\psi)\tilde{\nu} \tag{11a}$$

$$M\dot{\tilde{\nu}} = -(D + K_d)\tilde{\nu} - K_p R(\psi)^\top \tilde{\eta} \tag{11b}$$

$$+ K_d\bar{\nu} + K_p R(\psi)^\top \bar{\eta} + R(\psi)^\top \bar{b}_f \tag{11c}$$

4. STABILITY ANALYSIS

We collect all error states in $x := col(x_c, x_o)$, where $x_c := col(\tilde{\eta}, \tilde{\nu})$, $x_o := col(\bar{\xi}, \bar{\eta}, \bar{b}, \bar{b}_f, \bar{\nu})$ and combining (5), (7), and (11) the total error dynamic becomes

$$\dot{x} = A_\lambda(\psi)x \tag{12}$$

where

$$A_\lambda(\psi) = \begin{bmatrix} A_c(\psi) & B_{co}(\psi) \\ 0_{18\times 6} & A_{o,\lambda}(\psi) \end{bmatrix}, \tag{13}$$

and

$$A_c := \begin{bmatrix} 0 & R(\psi) \\ -M^{-1}K_p R(\psi)^\top & -M^{-1}(D + K_d) \end{bmatrix}, \tag{14a}$$

$$B_{co} := \begin{bmatrix} & 0_{3\times 18} & \\ 0_{3\times 6} & M^{-1}K_p R(\psi)^\top \ 0_{3\times 3} & M^{-1}R(\psi)^\top \ M^{-1}K_d \end{bmatrix}, \tag{14b}$$

$$A_{o,\lambda} := \begin{bmatrix} A_w - K_{1,\omega}C_w & -K_{1,\omega} & 0 & 0 & 0 \\ -K_2 C_w & -K_2 & 0 & 0 & R(\psi) \\ -K_{3,\lambda}C_w & -K_{3,\lambda} & 0 & 0 & 0) \\ 0 & 0 & T_f^{-1} & -T_f^{-1} & 0 \\ -M^{-1}K_4 R(\psi)^\top C_w & -M^{-1}K_4 R(\psi)^\top & M^{-1} & 0 & -M^{-1}D \end{bmatrix}. \tag{14c}$$

The dynamics (12) can be written (Lindegaard, 2003),

$$\dot{x} = T(\psi)^\top A_\lambda(0) T(\psi) x, \tag{15}$$

if the matrices $K_{1,\omega}$, K_2, $K_{3,\lambda}$, and T_f^{-1} commute with the rotation matrix $R(\psi)$. The transformation matrix $T(\psi)$ is given as

$$T(\psi) = \text{diag}\{T_c(\psi), T_o(\psi)\} \tag{16a}$$

$$T_c(\psi) = \text{diag}\{R(\psi)^\top, I\} \tag{16b}$$

$$T_o(\psi) = \text{diag}\{R(\psi)^\top, \ldots, R(\psi)^\top, I\}. \tag{16c}$$

By inserting (7) we can write

$$A_\lambda(0) = \lambda A_{min} + (1 - \lambda) A_{max}, \tag{17}$$

where A_{min} contains $K_{3,min}$ and A_{max} contains $K_{3,max}$.

Proposition 1. The equilibrium $x = 0$ of (12,) where $K_{3,\lambda}$ can arbitrarily take any value in $[K_{3,min}, K_{3,max}]$, is uniformly asymptotically stable under the following conditions:

- The matrices $K_{1,\omega}$, K_2, $K_{3,\lambda}$, and T_f^{-1} commute with the rotation matrix $R(\psi)$.
- The following LMI's are satisfied,

$$A_{min}^\top P + P A_{min} + r_{max}(S_T P - P S_T) < -Q \tag{18a}$$

$$A_{min}^\top P + P A_{min} - r_{max}(S_T P - P S_T) < -Q \tag{18b}$$

$$A_{max}^\top P + P A_{max} + r_{max}(S_T P - P S_T) < -Q \tag{18c}$$

$$A_{max}^\top P + P A_{max} - r_{max}(S_T P - P S_T) < -Q, \tag{18d}$$

  where $S_T = \text{diag}\{S, 0, S, \ldots, S, 0\}$, and P and Q are symmetric positive definite matrices.

Proof. Consider the transformation $z = T(\psi)x$ given by (16), and notice that $T(\psi)^{-1} = T(\psi)^\top$. From (15) we get

$$\begin{aligned} \dot{z} &= T(\psi)T(\psi)^\top A_\lambda(0) z + \dot{T}(\psi)T(\psi)^\top z \\ &= A_\lambda(0) z - r S_T z \end{aligned} \tag{19}$$

where r is the yaw rate. We introduce a quadratic Lyapunov function $V(z) = z^\top P z$, and from (19) we define $f(z) := A_\lambda(0)z$ and $g_r(z) := -rS_T z$ such that (19) becomes

$$\dot{z} = f(z) + g_r(z), \tag{20}$$

where $f(z) := \lambda f_{min}(z) + (1-\lambda) f_{max}(z)$. From (18a)-(18d) and $r \in [-r_{max}, r_{max}]$ we have

$$\langle \nabla V(z), f_{min}(z) + g_r(z) \rangle \leq -\alpha(|z|) \tag{21a}$$

$$\langle \nabla V(z), f_{max}(z) + g_r(z) \rangle \leq -\alpha(|z|), \tag{21b}$$

where $\alpha(|z|)$ is a positive definite function. Finally, we get

$$\begin{aligned} &\langle \nabla V(z), \lambda f_{min}(z) + (1-\lambda) f_{max}(z) + g_r(z) \rangle \leq \\ &\lambda \langle \nabla V(z), f_{min}(z) + g_r(z) \rangle + (1-\lambda) \langle \nabla V(z), f_{max}(z) + g_r(z) \rangle \\ &\leq -\lambda\alpha(z) - (1-\lambda)\alpha(z) \leq -\alpha(z), \end{aligned} \tag{22}$$

and this concludes the proof.

Table 1. Supply vessel, main parameters

Parameters	Value
Length between perp.	80 m
Breadth	17.4 m
Draft	5.6 m
Displacment	6150 tons

If the observer and controller gains are set such that A_{min} and A_{max} are Hurwitz, and if the ratio of $\kappa_{max}/\kappa_{min}$ is not very large (in practice, up to 5), it is easy to satisfy (18) for a maximum yaw rate far above "normal" yaw rates.

5. SIMULATION RESULTS AND DISCUSSION

The simulations are performed in MATLAB/Simulink on a high fidelity model based on building blocks from the MSS Toolbox (MSS, 2010). The case simulated is a platform supply vessel in an environment consisting of waves, wind, and current. See Table 1 for the main parameters of the vessel. The sea state is very rough with significant wave height of 6 meters, and a peak frequency of 0.53 rad/s taken from the JONSWAP [1] spectrum. The mean incident wave heading is 190° in the north-east frame (Price and Bishop, 1974). The current has a speed of 0.5 m/s and direction of 180°, and the wind has a mean velocity of 5 m/s with a direction of 160°. A first order model for the thrust dynamics is included, and the time constants for thrust force is set to 5 seconds. The GPS measurements have realistic noise properties, and are sampled at 1 Hz, and the measurements are processed by a zero-order hold element before they are sent to the observer.

Three different output feedback controllers are compared to illustrate the benefit of changing the gain K_3 in (4c). The only difference between the three setups is a variation of allowed values for κ from (6a). For two of the output feedback controllers the κ-value is fixed, where the "nominal" controller has $\kappa = \kappa_{min}$ for steady conditions, while the "aggressive" controller has $\kappa = \kappa_{max}$ for transient conditions. The last controller is our proposed algorithm in (6) where $\kappa \in [\kappa_{min}, \kappa_{max}]$, called the "flexible" controller. Even though the difference between these three systems is in the observer we often just write "controller" to describe the system. However, when just the observer performance is discussed, "observer" is used.

At the beginning of the simulation, the position and orientation of the vessel is at $\eta = [0, 0, 0]^\top$. At 1000 seconds there is a setpoint change 20 meters north, 20 meters east, and to heading -90°. Due to the ship hull shape this maneuver will change the bias force experienced by the vessel in the body frame, as well as in the NED frame. After 3000 seconds the direction of the current changes to 90°, to see how the vessel responds to a sudden change in bias force that is not known in advance. The current direction changes as a first order filtered step with time constant 30 seconds.

In Figure 1 the cumulative low-frequency position tracking error of the vessel is shown for the three controllers. The left part starts from the instance of the heading change, and the right part is a zoom-in on the steady period 2000-3000 seconds. The top plots show the combined error in north and east, and the bottom plots show the error in yaw. From the left part it can be observed that the aggressive and flexible controller perform much better than the nominal controller in the transient regime, that is, just after 1000 seconds, and just after 3000 seconds. From the right part of Figure 1 it can be observed that after the system reaches steady state, the flexible and nominal controller perform better than the aggressive controller, and this is due to lower oscillations of the bias and velocity estimates from the observer. This implies that since the flexible and aggressive controllers have similar performance in transients, the flexible controller will eventually perform better.

From the left part of Figure 1 it is observed that already around 2000 seconds the flexible controller has a lower cumulative position deviation. This is because the heading change is a transient known in advance, and the flexible controller can react fast, and go to a higher value for κ quickly. This is observed from Figure 4, where κ for the flexible controller is shown ($\kappa_{max} = 2.5$). In addition, we can observe from Figure 4 that at 3000 seconds it takes a bit more time for κ to go to κ_{max} than at 1000 seconds. This is natural since this increase is based on the estimation error in the observer, and not a command in the reference system as with the heading change. Even though κ will be slower for the "unknown" transients, we see from Figure 1 that the flexible controller has a similar performance to the aggressive controller, and will eventually outperform the aggressive controller if the steady state conditions persist.

In Figure 2 the cumulative bias estimation error (in the body frame) from the observer is plotted for the entire simulated case study. The combined error of surge and sway is shown in the top plot, and the yaw error is shown in the bottom plot. Here we see the same trend as in Figure 1, but the trend is even clearer. The flexible observer is superior to both the aggressive and nominal observer. Even the nominal observer performs better than the aggressive observer after 5000 seconds for the error in surge and sway.

In Figure 3 the bias in surge is plotted, along with the observer estimate, and the filtered bias estimate for the flexible controller. It is observed that the bias estimate (and the filtered estimate) converge to their new bias values quite fast, and within 200 seconds after a transient steady state conditions are reached.

6. CONCLUSION

The proposed output feedback controller was shown to have good closed-loop properties in both transients and steady state. Both the flexible bias estimation, and the filtering of the bias estimate used in the control law, contributed to a good overall performance for the system.

For the flexible bias estimation, the lowest tuning should be quite responsive to ensure good overall responsiveness. There are a couple of reasons for this. If we failed to detect a transient, or the detection was slow, a moderate nominal tuning vastly improved the performance in the transient compared to a very low nominal tuning. That is, if excellent positioning capabilities is the goal, the tuning should have a fairly high minimum. In the presented

[1] Joint North Sea Wave Project

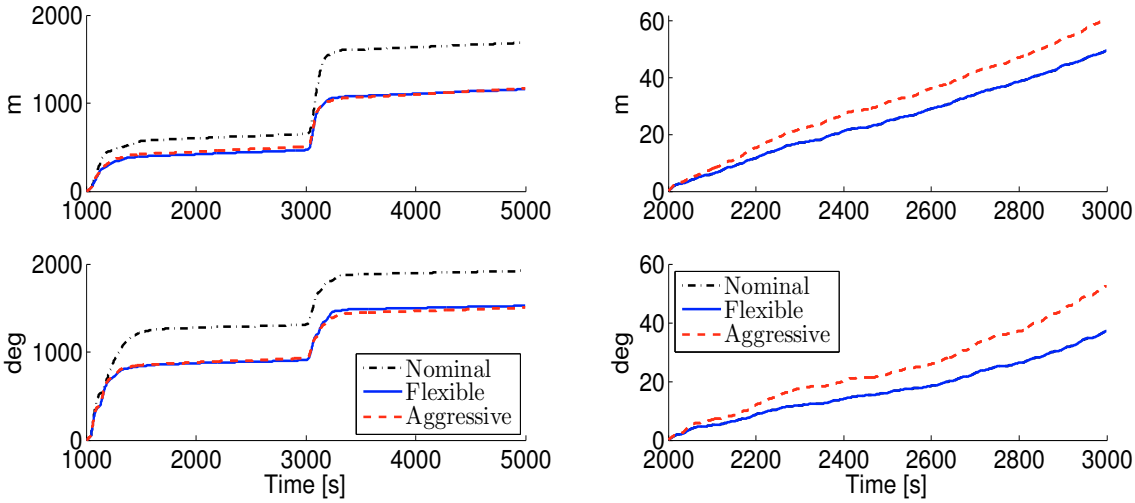

Fig. 1. Cumulative low frequency position tracking error in north and east combined (top plots), and yaw (bottom plots). The right plot is a zoom-in on the steady period 2000-3000s (the flexible and nominal controllers overlap because of steady state conditions).

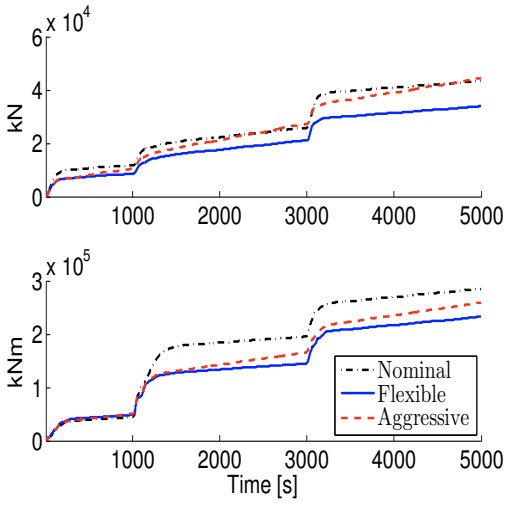

Fig. 2. Cumulative bias estimation error in surge and sway combined (top), and yaw (bottom).

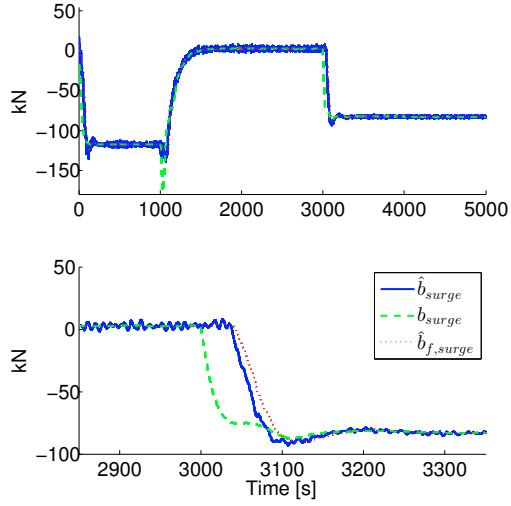

Fig. 3. Bias estimate (blue, solid), actual bias (green, dashed), and filtered bias estimate (red, dotted), all in surge. For the entire simulation (top) and zoom-in (bottom).

simulation case study all the bias estimate tunings were quite fast, and they all converged within 300 seconds.

REFERENCES

(2010). Mss. marine systems simulator. `http://www.marinecontrol.org`. Accessed: 2015-02-24.

Belleter, D.J., Breu, D.A., Fossen, T.I., and Nijmeijer, H. (2013). A globally k-exponentially stable nonlinear observer for the wave encounter frequency. *IFAC Proceedings Volumes*, 46(33), 209–214.

Belleter, D.J., Galeazzi, R., and Fossen, T.I. (2015). Experimental verification of a global exponential stable nonlinear wave encounter frequency estimator. *Ocean Engineering*, 97, 48–56.

Bryne, T.H., Fossen, T.I., and Johansen, T.A. (2014). Nonlinear observer with time-varying gains for inertial navigation aided by satellite reference systems in dynamic positioning. In *Control and Automation (MED), 2014 22nd Mediterranean Conference of*, 1353–1360. IEEE.

Fossen, T.I. (2011). *Handbook of marine craft hydrodynamics and motion control*. John Wiley & Sons.

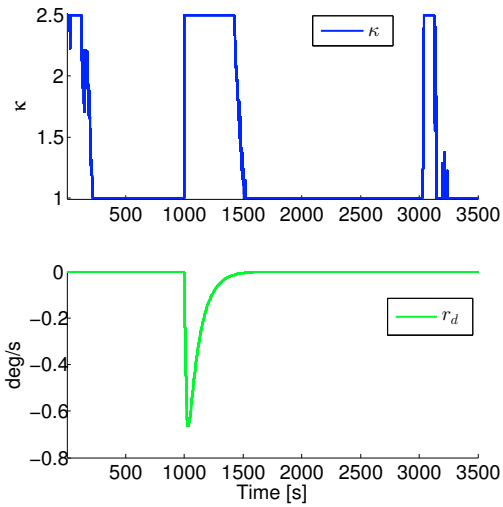

Fig. 4. Plot of κ (top) and desired yaw rate (bottom).

Fossen, T.I. and Strand, J.P. (1999). Passive nonlinear observer design for ships using lyapunov methods: full-scale experiments with a supply vessel. *Automatica*, 35(1), 3–16.

Hovakimyan, N. and Cao, C. (2010). *L1 adaptive control theory: guaranteed robustness with fast adaptation*, volume 21. Siam.

Lekkas, A.M. and Fossen, T.I. (2014). Integral los path following for curved paths based on a monotone cubic hermite spline parametrization. *IEEE Transactions on Control Systems Technology*, 22(6), 2287–2301.

Lindegaard, K.P. (2003). Acceleration feedback in dynamic positioning.

Loría, A. and Panteley, E. (1999). A separation principle for a class of euler-lagrange systems. In *New Directions in nonlinear observer design*, 229–247. Springer.

Price, W.G. and Bishop, R.E.D. (1974). *Probabilistic theory of ship dynamics*. Halsted Press.

Sørensen, A.J. (2005). Structural issues in the design and operation of marine control systems. *Annual Reviews in Control*, 29(1), 125–149.

Sørensen, A.J. (2011). A survey of dynamic positioning control systems. *Annual reviews in control*, 35(1), 123–136.

Tutturen, S.A. and Skjetne, R. (2015). Hybrid control to improve transient response of integral action in dynamic positioning of marine vessels. *IFAC-PapersOnLine*, 48(16), 166–171.

Paper H:

Time-varying Model-based Observer for Marine Surface Vessels in Dynamic Positioning

Svenn Are T. Værnø, Astrid H. Brodtkorb, Roger Skjetne, Vincenzo Calabrò

IEEE Access, vol. 5, pp. 14787-14796,
doi: 10.1109/ACCESS.2017.2731998

IEEE Access
Multidisciplinary | Rapid Review | Open Access Journal

Received July 5, 2017, accepted July 13, 2017, date of publication July 26, 2017, date of current version August 14, 2017.

Digital Object Identifier 10.1109/ACCESS.2017.2731998

Time-Varying Model-Based Observer for Marine Surface Vessels in Dynamic Positioning

SVENN ARE VÆRNØ[1], ASTRID H. BRODTKORB[1], ROGER SKJETNE[1], AND VINCENZO CALABRÒ[2], (Member, IEEE)

[1]Centre of Autonomous Marine Operations and Systems, Department of Marine Technology, Norwegian University of Science and Technology, 7491 Trondheim, Norway

[2]Kongsberg Maritime AS, 3616 Kongsberg, Norway

Corresponding author: Svenn Are Værnø (svenn.are.varno@ntnu.no)

This work was supported in part by the Research Council of Norway, through the Centre of Excellence NTNU AMOS, under Project 223254, and through the Centre for Research-based Innovation MOVE, under Project 237929.

ABSTRACT This paper deals with the problem of transient events in model-based observers for dynamic positioning of marine surface vessels. Traditionally, model-based observers experience a deterioration of performance during transients, and there is a give or take relationship between transient and steady state performance. To remedy this problem, we propose to use time-varying gains for a model-based observer. The gains are aggressive during transients to improve transient performance, and relaxed in steady state to lower the oscillations of the estimates. The proposed observer is analyzed with regard to stability. Its performance is verified in both a high-fidelity simulation model, and on experimental data with the research vessel (R/V) Gunnerus. In addition, a partial closed-loop validation with R/V Gunnerus has been performed.

INDEX TERMS Dynamic positioning, Marine control systems, Observers.

I. INTRODUCTION

A dynamically positioned (DP) vessel means a unit or a vessel which automatically maintains its position (fixed location or predetermined track) exclusively by means of thruster force [1]. As dynamic positioning operations are moving into harsher conditions or doing more complex operations, better transient performance of the DP system is required. A bias term is used as integral action to model slowly-varying environmental loads and unmodeled dynamics, and for good model-based observer performance it is important to estimate this bias accurately. Integral action is typically based on the assumption that this bias is constant. The bias load is, however, slowly-varying in steady state, but can vary rapidly in transient events. A major obstacle in transient performance of DP is how to handle rapid changes in this bias load.

In model-based observers for DP, the environmental loads are typically modeled as a constant force vector in the North-East-Down-frame (NED), that is, the following kinetic equation is typically used, $M\dot{\nu} = -D\nu + R(\psi)^\top b + \tau$, where b is this constant load (bias) vector in the NED-frame and R(·) is a rotation matrix mapping into the body-frame of the vessel; see Section II-A for more details about the modeling, as well as [2], [3]. There are instances when the bias loads change significantly over a short time period, where this assumption does not hold. In Figure 1 we investigate, as an example, how the current and wave drift loads vary in the NED-frame over a heading change. The figure shows a high-fidelity simulation of a surface vessel performing two maneuvers; first, a position setpoint change, and afterwards, a combined setpoint change of position and heading. In the top plot of Figure 1 the low-frequency North position and heading angle are shown. In the bottom plot the combined current and wave-drift loads are shown in North and yaw. We observe that the loads experienced by the vessel in the NED-frame changes significantly, even though the current and wave parameters are constant in the NED-frame. This is because the forces experienced by the vessel vary due to ship hull geometry, which is not accounted for in the simple (but effective) bias model. Consequently, for some time after a transient event, the bias load estimate of a model-based observer will be off, leading to poor velocity and position estimates. This example clearly illustrates that if the vessel changes heading, the common slowly-varying assumption of the bias model in the NED-frame does not apply in transients; see also [4] for a discussion on this for AUVs (Autonomous Underwater Vehicles) exposed to currents. Other common occurrences of rapid bias load changes include wave trains, rotational currents, sea-ice loads, or during mode changes in the operation of the DP system.

Even with the knowledge that the slowly-varying bias assumption is not good in transients, it is difficult to device better ways of handling this. One non-model based option

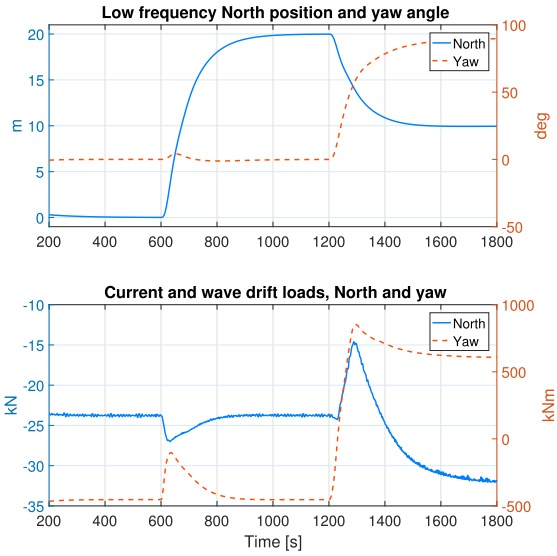

FIGURE 1. Low-frequency North position and heading angle (top), and current and wave-drift loads in North and yaw experienced by the vessel (bottom).

is to measure accelerations to estimate the forces in a direct fashion as suggested in [5]. Another option that does not require more instrumentation is to use a more complex model of the hydrodynamic loads, but this would also give a more complex control algorithm that could be more difficult to parameterize and analyze with respect to stability. Moreover, depending on the type of environment, there will always be uncertainty in such models.

There exists other time-varying observer schemes for DP in the literature. See for instance [6], where an inertial observer for DP is proposed that uses time-varying gains to improve convergence and suppress sensor noise. In [7] and [8] a wave encounter frequency observer is proposed, where time-varying gains are used in an adaption law, and in [9] hybrid gains are used in integral action for DP.

The main contribution of this paper is to construct a model-based observer with time-varying gains that performs well in transients as well as in steady state. In state-of-the-art fixed gain model-based observer design for DP [2], there is a tradeoff in tuning the observer for either good steady state performance or good transient performance, and in commercial systems there are typically three gain settings; low, medium, and high, which the DP operator can select from. As an extension of the observer design from [10], we propose in this paper to use time-varying bias and velocity injection gains. The paper includes a comprehensive analysis and thorough selection of gains, and an observer verification based on experimental data. Another contribution is a full-scale closed-loop validation of the observer when conducting a DP experiment on the AMOS DP Research Cruise 2016 [11]. Demonstration of the observer performance through full-scale closed-loop experiments on an academic research cruise is, to the author's knowledge, not done before.

Notation and Terminology: In UGES, G stands for Global, U for uniform, E for exponential, and S for Stable. The smallest and largest eigenvalues of a matrix $A \in \mathbb{R}^{n\times n}$ is $\lambda_{min}(A)$ and $\lambda_{max}(A)$, respectively, and $\mathbb{R}_{>0}$ denotes positive real numbers. The $\mathcal{L}_\infty$ signal norm is $\|x\|_\infty = \text{ess sup}\{|x(t)| : t \geq 0\}$.

II. PROBLEM FORMULATION

In the following we separate between the *simulation model*, which is a high-fidelity model used for control and observer verification, and the *control design model*, which is a simplified model intended for control and observer design. The control design model typically only includes the parts relevant for the operational regime of the observer or controller. For low-speed applications such as DP, this implies that the Coriolis and centripetal forces are neglected, and the nonlinear damping is typically neglected as well. See [3], and [2] for DP modeling details, and [12], [13], [14] for other insightful DP literature.

Two reference frames are used: The North-East-Down frame (NED) is a local Earth-fixed frame assumed non-rotating, with x-axis pointing North, y-axis pointing East, and z-axis pointing down to the center of the Earth. The body-frame is a local frame, centered along the center line and in the water plane of the vessel. The x-axis points in the direction of the the bow, y-axis starboard, and z-axis down.

A. CONTROL DESIGN MODEL

The control design model is a 3 degree of freedom (DOF) model,

$$\dot{\xi} = A_w \xi + E_w w_w \tag{1a}$$
$$\dot{\eta} = R(\psi)\nu \tag{1b}$$
$$\dot{b} = -T_b^{-1} b + w_b \tag{1c}$$
$$M\dot{\nu} = -D\nu + R(\psi)^\top b + \tau \tag{1d}$$
$$y = \eta + C_w \xi + v_y, \tag{1e}$$

where there is a separation between the first order wave-induced motion in (1a) and the low-frequency motion of the vessel in (1b) - (1d) [2]. When controlling the vessel, we are typically only interested in the low-frequency part of the motion. Controlling the total motion causes extra wear and tear on the thrusters, and in most cases it is not possible to counteract the first order wave-induced motion. The wave-induced motion $\xi \in \mathbb{R}^5 \times \mathbb{S}^1$ is modeled by a second order mass-spring-damper model, where A_w is a Hurwitz matrix that contains the peak frequency of the sea state and the damping ratio of the wave motion model, $w_w \in \mathbb{R}^3$ is zero mean white noise, and $E_w = \begin{bmatrix} 0_{3\times 3} & I_{3\times 3} \end{bmatrix}^\top$. The vector $\eta := \text{col}\,(\eta_N, \eta_E, \psi) \in \mathbb{R}^2 \times \mathbb{S}$ contains the low-frequency North/East position and heading angle of the vessel, and the bias load $b := \text{col}\left(b_N, b_E, b_\psi\right) \in \mathbb{R}^3$ is a NED-fixed vector that contains the slowly-varying loads affecting the vessel due to wave drift, mean and slowly-varying currents, mean wind

loads, as well as unmodeled dynamics from inaccurate mass and added mass, unmodeled hydrodynamic effects, and errors in thrust modeling. The bias load dynamics are modeled by a Markov process, where T_b is a diagonal matrix of time constants, and $w_b \in \mathbb{R}^3$ is the white noise vector [2]. The vector $\nu = \text{col}\,(u, v, r) \in \mathbb{R}^3$ contains the low-frequency surge/sway velocity and yaw rate in the body frame of the vessel, $M \in \mathbb{R}^{3\times3}$ and $D \in \mathbb{R}^{3\times3}$ are the mass (inertia and added mass) and linear damping matrices, respectively. $\tau \in \mathbb{R}^3$ is the control vector. The measurement vector $y \in \mathbb{R}^3$ is a sum of the low-frequency North/East position and heading η, and the wave frequency North/East and heading $C_\omega \xi$, where $C_\omega = \begin{bmatrix} 0_{3\times3} & I_{3\times3} \end{bmatrix}$, and the measurement noise vector $v_y \in \mathbb{R}^3$. The rotation matrix $R(\psi)$ rotates a 3 DOF vector from the body to the NED frame. It satisfies $R(\psi)R(\psi)^\top = I$ and $\det(R(\psi)) = 1$, and its time derivative is $\dot{R} = R(\psi)Sr$, where

$$R(\psi) = \begin{bmatrix} \cos(\psi) & -\sin(\psi) & 0 \\ \sin(\psi) & \cos(\psi) & 0 \\ 0 & 0 & 1 \end{bmatrix}, \quad S = \begin{bmatrix} 0 & -1 & 0 \\ 1 & 0 & 0 \\ 0 & 0 & 0 \end{bmatrix}; \tag{2}$$

see [2] and [15] for details.

B. ASSUMPTIONS

Since the wave-induced heading angle is typically less than 1° for normal sea states and less than 5° for extreme sea states, we assume as in [16] that:

(A1) $R(\psi + \psi_w) \approx R(\psi)$, that is, the heading angle due to wave-induced motion, ψ_w, is small.

We also make the following assumptions:

(A2) The added mass part of M and the wave-induced damping of D are set to the values when the wave frequency approaches infinity, and therefore they are constant. In addition, starboard/port symmetry is assumed, $M = M^\top > 0$, and that the damping matrix satisfies $D + D^\top > 0$.

(A3) $w_w = w_b = 0$. Since the presented observers are deterministic, both the wave and the bias estimates in the observers are driven by the estimation error [16].

(A4) In the stability analysis, no measurement noise is considered, $v_y = 0$. However, simulation and experimental data include it.

The last two assumptions are common for a deterministic observer design, but in practice we will see that the resulting observer has good filtering properties of these noise inputs.

C. PROBLEM STATEMENT

We consider the case where the bias b is constant or slowly varying in long periods of time, but then sporadically experiences rapid changes due to some transient condition. The problem is thus to design an observer for (1) that accurately estimates the states during both steady and transient conditions. The performance of the observer shall be compared to a conventional design basis through a performance index.

III. OBSERVER DESIGN

The proposed observer is based upon the "nonlinear passive observer" initially presented in [16]. Time-varying injection gains for the velocity and the bias dynamics are proposed to capture slowly-varying dynamics in steady state, and fast dynamics during transients. The observer is designed by copying the control design model (1) and adding injection terms, that is,

$$\dot{\hat{\xi}} = A_w \hat{\xi} + K_1 \tilde{y} \tag{3a}$$
$$\dot{\hat{\eta}} = R(\psi)\hat{\nu} + K_2 \tilde{y} \tag{3b}$$
$$\dot{\hat{b}} = -T_b^{-1}\hat{b} + K_3(t)\tilde{y} \tag{3c}$$
$$M\dot{\hat{\nu}} = -D\hat{\nu} + R(\psi)^\top \hat{b} + \tau + K_4(t)R(\psi)^\top \tilde{y} \tag{3d}$$
$$\hat{y} = \hat{\eta} + C_w \hat{\xi}, \tag{3e}$$

where $\hat{\xi} \in \mathbb{R}^5 \times \mathbb{S}^1$, $\hat{\eta} \in \mathbb{R}^2 \times \mathbb{S}$, $\hat{b} \in \mathbb{R}^3$, and $\hat{\nu} \in \mathbb{R}^3$ are the state estimates, $K_1 \in \mathbb{R}^{6\times3}$, $K_2, K_3(t), K_4(t) \in \mathbb{R}^{3\times3}$ are non-negative gain matrices, and $\tilde{y} = y - \hat{y}$ is the measurement error. The gains K_1 and K_2 depend on the peak frequency of the wave spectrum as in [16]. The observer in (3) was preliminarily presented in [10] with only $K_3(t)$ varying with time. Further analysis shows that an appropriate choice of values for K_3 and K_4 are important for good transient observer performance, so here a scheme for time-varying K_3 and K_4 is proposed.

As discussed in Section I, the transient changes of the bias load experienced by the vessel pose challenges for the model-based observer in (3). To illustrate this, consider the following case: When the vessel is pushed off setpoint due to a rapid external load b, the DP controller will try to decelerate and stop the movement, and bring the vessel back to setpoint. The observer has information about this control action τ and position deviation $\tilde{y}$, whereas the bias observer state $\hat{b}$ underestimates the actual bias load. While the position deviation is helpful for the observer, the control action's "push back" to position is seen as an indication that the vessel is moving in the direction of the control action, which initially is opposite of the actual motion of the vessel. Therefore, including feedback control action deteriorates the observer performance in the initial phase of a transient.

Therefore, in order to achieve good transient observer performance, the injection gain $K_4(t)$ in the velocity dynamics (3d) must be high enough to dominate the feedback control action. In addition, the injection gain $K_3(t)$ in (3c) must be high enough in order for the bias estimate to more accurately track the bias load value during the transient. Keeping these gains high all the time will, however, result in oscillatory estimates of the bias and velocity in steady state.

$K_3(t)$ and $K_4(t)$ are proposed to stay within the range

$$K_i(t) \in [K_{i,min}, K_{i,max}], \quad i = 3, 4\ \forall t \geq t_0.$$

The values of $K_{i,max}$ should be set such that they give a good transient performance of the observer, and $K_{i,min}$ such that the observer performs well in steady state. The steady state tuning is purposely set low, providing calmer estimates to the controller, as is normal tuning practice for conventional DP observers. The time-varying gains should react quickly to transient events by approaching their maximum values rapidly.

The equation for $K_3(t)$ and $K_4(t)$ is thus proposed as

$$K_i(t) = \kappa(t)K_{i,max} + (1-\kappa(t))K_{i,min}, \quad i = 3, 4, \tag{4}$$

where $\kappa(t) \in [0, 1]$, $\forall t \geq 0$. Whenever there is a transient event, κ should approach 1, and whenever the vessel is in steady state, κ should stay close to 0.

Three transient events are considered. The first is an operator-executed heading change, which is easily detected through the desired yaw rate from the guidance system. The second is a change in the environmental disturbances. This is detected through a deterioration of the observer performance. The final transient is the error due to initialization of the observer. The proposed dynamics for κ is

$$\kappa(t) = \max\{0, \beta(t) - 1\}\} \tag{5a}$$
$$\beta(t) = \min\{\varepsilon_{r_d}|r_d(t)| + \varepsilon_\eta|\tilde{\eta}_f(t)|, 2\} \tag{5b}$$
$$\dot{\tilde{\eta}}_f = -T_{\eta_f}^{-1}\{\tilde{\eta}_f - \tilde{y}\}, \tag{5c}$$

where $\varepsilon_{r_d} \in \mathbb{R}_{>0}$ and the desired yaw rate $r_d(t) \in \mathbb{R}$ are related to a heading change. The second term $\tilde{\eta}_f$ in (5b) is the lowpass filter (5c) that tracks the observer output error performance, where $T_{\eta_f} \in \mathbb{R}^{3\times3}$ is a diagonal matrix of filter time constants. If the observer performance deteriorate, $|\tilde{\eta}_f|$ will grow. The time constants and $\varepsilon_\eta \in \mathbb{R}_{>0}$ are tuned such that κ approaches zero at steady state. To incorporate the effect of a transient at observer startup, $\tilde{\eta}_f$ is initialized with non-zero values. The value of β in (5b) takes a value between zero and two. The maximum function in (5a) defines a threshold such that κ will not go above zero before β is larger than one. This will reduce the amount of switching back and forth.

IV. STABILITY ANALYSIS

By defining the estimation error states $\tilde{\xi} := \xi - \hat{\xi}$, $\tilde{\eta} := \eta - \hat{\eta}$, $\tilde{\nu} := \nu - \hat{\nu}$, and $\tilde{b} := b - \hat{b}$, and subtracting the observer equations (3) from the control design model (1), we get the observer error dynamics,

$$\dot{\tilde{\xi}} = A_w\tilde{\xi} - K_1\tilde{y} \tag{6a}$$
$$\dot{\tilde{\eta}} = R(\psi)\tilde{\nu} - K_2\tilde{y} \tag{6b}$$
$$\dot{\tilde{b}} = -T_b^{-1}\tilde{b} - K_3(t)\tilde{y} \tag{6c}$$
$$M\dot{\tilde{\nu}} = -D\tilde{\nu} + R(\psi)^\top\tilde{b} - K_4(t)R(\psi)^\top\tilde{y}. \tag{6d}$$

The stability analysis follows the same structure as in [10]. However, the following proof removes the assumption of a maximum yaw rate. We collect all the observer error states from (6) in a vector $x := \text{col}(\tilde{\xi}, \tilde{\eta}, \tilde{b}, \tilde{\nu}) \in \mathbb{R}^{15}$ and write the observer error dynamics from (6) compactly as

$$\dot{x} = A(\psi, t)x, \tag{7}$$

where the equation can be derived, as shown at the bottom of this page.

The dynamics (7) can be written as [17],

$$\dot{x} = T(\psi)^\top A(0, t)T(\psi)x, \tag{8}$$

where

$$T(\psi) = \text{diag}\{R(\psi)^\top, R(\psi)^\top, R(\psi)^\top, R(\psi)^\top, I\}, \tag{9}$$

if the matrices K_2, $K_3(t)$, and T_b commute with $R(\psi)$, and $K_1\ R = \text{diag}\{R, R\}K_1$. Note that the nonlinearity $R(\psi)$ is replaced by $R(0) = I$ in $A(0, t)$. Moreover, it can be shown that we can write $A(0, t)$ as

$$A(0, t) = \kappa(t)A_{max} + (1-\kappa(t))A_{min}, \quad \kappa(t) \in [0, 1]. \tag{10}$$

where $A_{min} = A(0, 0)$ and $A_{max} = A(0, 1)$.

Proposition 1: The equilibrium $x = 0$ of (7) where $K_i(t)$, $i = 3, 4$, is given by (4), and

$$\kappa(t) \in [0, 1] \quad \forall t \geq 0,$$

is uniformly globally exponentially stable (UGES) if the following holds:

(1) The matrices K_2, $K_3(t)$, and T_b commute with the rotation matrix $R(\psi)$, and $K_1\ R = \text{diag}\{R, R\}K_1$.
(2) The linear matrix inequalities (LMIs) below are satisfied,

$$A_{min}^\top P + PA_{min} < -Q \tag{11a}$$
$$A_{max}^\top P + PA_{max} < -Q \tag{11b}$$
$$PS_T - S_TP \text{ is skew-symmetric}, \tag{11c}$$

where $S_T = \text{diag}\{S, S, S, S, 0\}$, and $P \in \mathbb{R}^{15\times15}$ and $Q \in \mathbb{R}^{15\times15}$ are symmetric positive definite matrices. □

Proof 1: Consider the transformation $z = T(\psi)x$ given by (9), and notice that $T(\psi)^{-1} = T(\psi)^\top$. From (8) we get

$$\begin{aligned}\dot{z} &= T(\psi)T(\psi)^\top A(0, t)z + \dot{T}(\psi)T(\psi)^\top z \\ &= A(0, t)z - rS_Tz,\end{aligned} \tag{12}$$

$$A(\psi, t) := \begin{bmatrix} A_w - K_1C_w & -K_1 & 0 & 0 \\ -K_2C_w & -K_2 & 0 & R(\psi) \\ -K_3(t)R(\psi)^\top C_w & -K_3(t)R(\psi)^\top & -T_b^{-1} & 0 \\ -M^{-1}K_4(t)R(\psi)^\top C_w & -M^{-1}K_4(t)R(\psi)^\top & -M^{-1}R(\psi)^\top & -M^{-1}D \end{bmatrix}.$$

where r is the yaw rate. We introduce a quadratic Lyapunov function $V(z) = z^\top Pz$ with P from (11), and take the time derivative of V along (12), which gives

$$\begin{aligned}\dot{V} &= z^\top\{PA(0,t) + A(0,t)^\top P - r(PS_T - S_T P)\}z \\ &= 0.85z^\top\{\kappa(t)(PA_{max} + A_{max}^\top P) \\ &\quad + (1-\kappa(t))(PA_{min} + A_{min}^\top P)\}z \\ &\leq -q_m|z|^2 \end{aligned} \tag{13}$$

where q_m is the smallest eigenvalue of Q from (11).

V. SETUP, RESULTS, AND DISCUSSION

The observer in (3) has been tested on the high-fidelity simulation model and on full-scale experimental data, described in sections V-A and V-B, respectively. For the experimental data we only have data sets with negligible waves, so the observer tested does not apply the wave filter. Hence, the observer used is (3b)-(3d) with $\hat{y} = \hat{\eta}$. In addition, the data series for the full-scale experiments contain a lot of transients, but little steady state. Therefore, the simulation study has a wider discussion of performance than the observer results on the experimental data.

After a presentation of the setup, we start with presenting a closed-loop verification of the observer from [10] onboard the R/V Gunnerus. This serves as a verification of the time-varying observer design, which is relevant for the observer presented in this paper, as the observers have similar structure and scheme for selecting the time-varying gains.

A. DP SIMULATION MODEL

The simulation model is a 6 DOF high-fidelity model of a platform supply vessel with main parameters shown in Table 1. The model includes nonlinear damping, Coriolis, centripetal forces, and linear damping, based on building blocks from the MSS Toolbox [18]. Wave drift and current forces are calculated using lookup tables, which give a realistic variation of the bias loads with vessel heading. Realistic noise is added to the measurement signals from the GPS and compass, with sampling rates of 1 Hz and 10 Hz, respectively.

TABLE 1. Simulation, platform supply vessel, and main parameters.

Parameters	Value
Length between perp.	80 m
Breadth	17.4 m
Draft	5.6 m
Displacment	6150 tons

The simulated sea state is very rough with significant wave height of 6 meters, and a peak frequency of 0.53 rad/s taken from the JONSWAP[1] spectrum. The mean incident wave heading is 190° (head waves) in the North/East frame [19]. The simulation also includes current with a speed of 0.5 m/s with direction of 160° (bow).

[1] Joint North Sea Wave Project

FIGURE 2. The NTNU-owned research vessel R/V Gunnerus.

TABLE 2. R/V Gunnerus, main parameters.

Parameters	Value
Length over all	31.3 m
Length between perp.	28.9 m
Breadth middle	9.6 m
Draft	2.7 m
Dead weight	107 tons

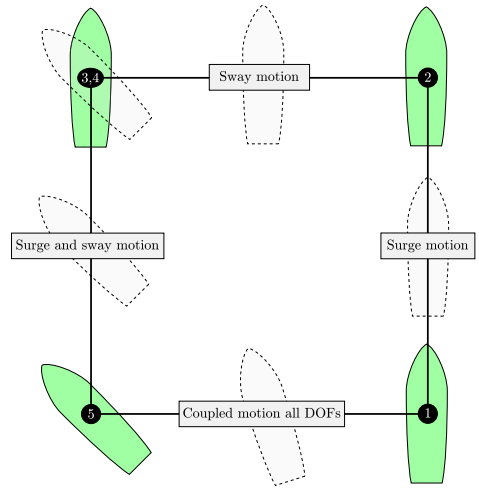

FIGURE 3. The 4-corner DP test. Courtesy: Øivind K. Kjerstad.

B. AMOS DP RESEARCH CRUISE 2016

Full-scale experimental data were collected during the AMOS DP Research Cruise (ADPRC) 2016 [11] with R/V Gunnerus, a 31-meter long research vessel owned and operated by NTNU, as seen in Figure 2, and with main parameters in Table 2. In addition, a closed-loop verification of the observer from [10] onboard the R/V Gunnerus was tested on the cruise. For the experimental data we only have data sets with negligible waves.

The data sets from the full-scale experiment with R/V Gunnerus are all from the vessel performing a box maneuver,

here called *DP 4-corner test*, as shown in Figure 3. The vessel starts at North and East position $(N, E) = (0, 0)$ with heading zero degrees, and the test steps are:

1) Position change to $(N, E) = (40m, 0)$ with zero heading (pure surge motion).
2) Position change 40 meter to $(N, E) = (40m, -40m)$ with zero heading (pure sway motion).
3) Heading change to $\psi = -45$ degrees (pure rotation).
4) Position change to $(N, E) = (0, -40m)$ keeping heading at -45 degrees (combined surge and sway motion).
5) Position change to $(N, E) = (0, 0)$ and heading $\psi = 0$ degrees (coupled motion with all DOFs).

C. PERFORMANCE EVALUATION

To compare performance of the different observer algorithms, we will apply the following cost functions as performance indicators,

$$J_\eta = \int_{t_0}^{t_f} \{|\eta_N - \hat{\eta}_N| + |\eta_E - \hat{\eta}_E| + \frac{180}{\pi}|\psi - \hat{\psi}|\}dt \quad (14a)$$

$$J_v = \int_{t_0}^{t_f} \{|u - \hat{u}| + |v - \hat{v}| + \frac{180}{\pi}|r - \hat{r}|\}dt \quad (14b)$$

$$J_b = \int_{t_0}^{t_f} \{\frac{|b_N - \hat{b}_N|}{\|b_N\|_\infty} + \frac{|b_E - \hat{b}_E|}{\|b_E\|_\infty} + \frac{|b_\psi - \hat{b}_\psi|}{\|b_\psi\|_\infty}\}dt, \quad (14c)$$

where t_0 and t_f are the initial and final time of the interval.

D. DERIVATIVE FREE OPTIMIZATION FOR TUNING

When comparing observers, a fair tuning is important. We would like to find the tuning based on optimization. Due to the absence of information about the gradient, Hessian, or higher derivatives of a typical cost function, a classic gradient descent-like method is not applicable. Therefore, derivative free optimization (DFO) will be used as a guide to tune the observers, and the MATLAB® function *fminsearch* has been adopted.

To illustrate how derivative free optimization works, let us consider a variable of interest, $x \in \mathbb{R}$. The goal is to establish a cost function to minimize the error $\tilde{x} = x - \hat{x}$ given a certain parameter $K \in \mathbb{R}$ and a simulation time of t_f seconds. We consider a cost function $J(K, t_f)$, where for each value of K a new simulation is performed and the cost function is evaluated. The derivative free optimization method explores the solution set around the current iteration result to compute a new solution point which minimizes the cost function. In our case this means to find a new value for K that gives a lower cost for J than the one before. There is a chance of getting stuck in a local minimum, and therefore several initial conditions for K are needed.

E. OBSERVER OF [10]: TIME-VARYING $K_3(t)$ ONLY, WITH FULL-SCALE CLOSED-LOOP VERIFICATION

The time-varying observer from [10] was tested in closed loop on the ADPRC 2016. The observer is similar to (3), with a time-varying bias injection gain $K_3(t)$, but K_4 was kept constant. However, since the waves were negligible while performing the closed-loop trials, the observer used in closed-loop was (3b)-(3d) with $\hat{y} = \hat{\eta}$.

The control law τ used for the full-scale experiments had a feedback term τ_{FB}, and a reference feedforward term τ_{FF}, where the feedback term consisted of a nonlinear PD (proportional, derivative) tracking term and a bias load rejection term,

$$\tau = \tau_{FB} + \tau_{FF} \quad (15a)$$

$$\tau_{FF} = M\dot{v}_d(t) + Dv_d(t) \quad (15b)$$

$$\tau_{FB} = -K_p R(\psi)^\top(\hat{\eta} - \eta_d(t)) - K_d(\hat{v} - v_d(t)) - R(\psi)^\top \hat{b}_f, \quad (15c)$$

where K_p and K_d are positive definite gain matrices, and $\eta_d(t)$, $v_d(t)$, $\dot{v}_d(t)$ are the desired references generated by a guidance system. The state $\hat{b}_f$ is a lowpass-filtered state of the bias estimate $\hat{b}$,

$$\dot{\hat{b}}_f = -T_f^{-1}(\hat{b}_f - \hat{b}), \quad (16)$$

where T_f is a diagonal matrix of the filter time constants. This filter was used instead of the bias estimate directly, to achieve a calmer control signal; see [10] for more details. The tuning for the observer and controller gains were found through trial and error.

1) EXPERIMENTAL CLOSED-LOOP RESULTS

The vessel followed the DP 4-corner maneuver described in Section V-B, and Figure 4 shows the response of the vessel for two different runs. The left side of the figure shows the North/East position of the target and the two runs, and the right side of Figure 4 shows the heading setpoint and the vessel heading for the two runs. The figure indicates that the observer worked well in closed loop, and vessel followed the maneuver well. The best performance was in surge, and when the degree of coupling between surge, sway, and yaw increased, tracking the reference was harder.

The two runs had similar environmental conditions, with current of velocity 0.3 m/s and direction 300°, and with wind speed of 6 m/s and direction 250°. For both runs the observer gains were the same, but the filter time constant for the bias was four times higher for run 2. As seen from Figure 4, both runs were quite similar in performance, but run 2 was more oscillatory, at least on the last part of the maneuver. This is probably due to the higher bias filter time constant. The closed-loop results indicate that the observer worked well in closed loop, and managed to control the vessel to a satisfactory degree.

F. OBSERVER WITH TIME-VARYING BIAS AND VELOCITY INJECTION GAINS

We now present the results for the time-varying observer in (3), where both $K_3(t)$ and $K_4(t)$ are time-varying. In addition, the results of the observer in [10] with only $K_3(t)$ time-varying is presented, with $K_4 = K_{4,min}$. Two benchmarks are included to compare the performance of the observers. The first benchmark is an observer that always uses $K_{3,min}$

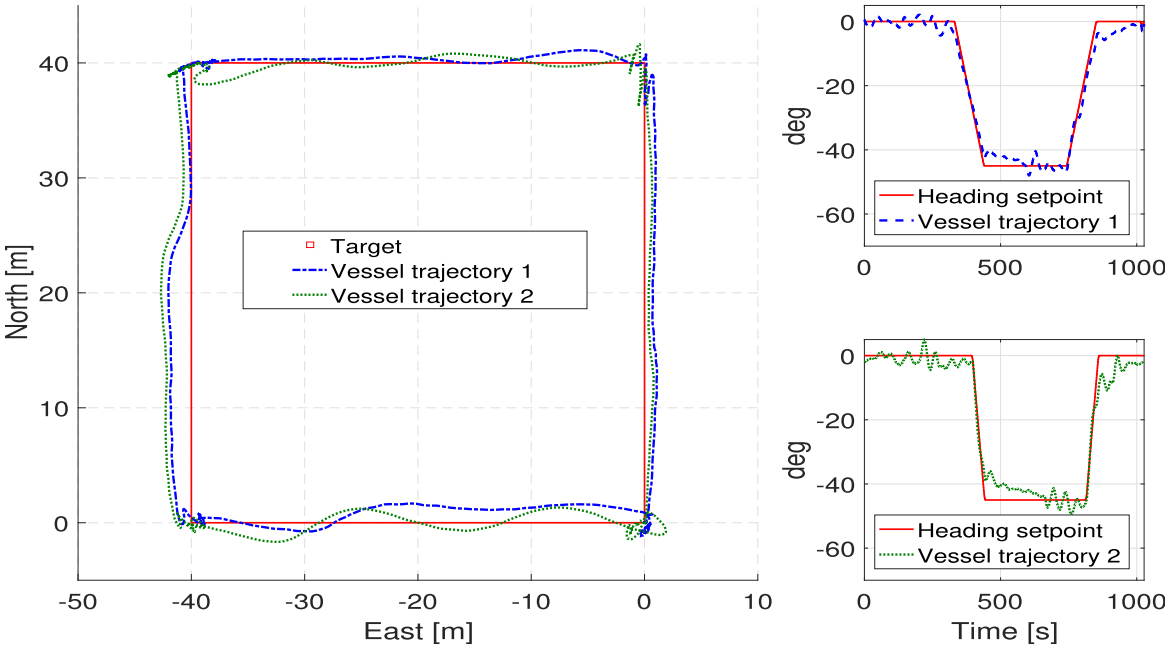

FIGURE 4. Full-scale experimental verification on R/V Gunnerus of the algorithm from [10]. The left plot shows the four corner target and results of two different runs. The right side shows the heading setpoint and the response of the two different runs.

and $K_{4,min}$ in (4), named the *baseline* observer, working well in steady state. This is the "nonlinear passive observer" presented in [16], with normal tuning, and is typical in the literature. The second benchmark is an observer called the *aggressive* observer that always uses $K_{3,max}$ and $K_{4,max}$, working well in transients.

1) TUNING

To find the tuning for the observers, derivative free optimization, as discussed in Section V-D, was used with the cost function

$$J = J_\eta + c_v J_v, \tag{17}$$

where J_η and J_v are defined in (14a) and (14b), and c_v is a scaling factor to weight the relative contributions for position and velocity.

For the simulated data in Section V-F.2, a maneuver with many transients has been used. The data set has both a change of the current direction and a heading change combined with a North/East position change, with short time intervals between the transients. The resulting tuning was adjusted to accommodate the stability requirements in (11), and this was used as a guide to tune the transient observer gains, that is, the maximum values of $K_3(t)$ and $K_4(t)$.

In order to find values for $K_{3,min}$ and $K_{4,min}$, several tests have been conducted. We tried to select maximum gains higher than the gains from the tuning found from DFO and combined this with a low minimum tuning, but this did not yield good results. This makes sense as the DFO tuning is found over a lot of transients, and thus is very aggressive already.

Thereafter, using the DFO tuning as the maximum values, we searched though several variations for the minimum tuning. Setting the minimum gains to $60-70\%$ of the maximum gains yielded the best results. However, since we needed to adjust $K_{3,max}$ to satisfy the stability requirements in (11), we selected the highest feasible $K_{3,max}$ that in combination with minimum gains $K_{i,min} = 0.7\ K_{i,max}$ that satisfied (11). This gave $K_{3,max} = 0.5\ K_{3,max}^{DFO}$.

For the full-scale experimental data, a similar approach was used where the DP 4-corner maneuver seen in Figure 3 was used to find the transient tuning. To find the gains by using DFO, the post-processed position measurement and velocities were used. The velocities were found by differentiating the North/East position and heading using a finite impulse response (FIR) filter. A search over possible ratios between the maximum and minimum tuning was performed, where 0.7 performed well, satisfying (11) with $K_{3,max} = 0.5\ K_{3,max}^{DFO}$.

2) ESTIMATION BASED ON SIMULATED DATA

For the simulated data the vessel is controlled by (15) and (16) that operate on the estimated states, i.e. the observers operate in closed loop.

In the data series, the current changes direction at $t = 500$ seconds, and at $t = 1000$ seconds there is

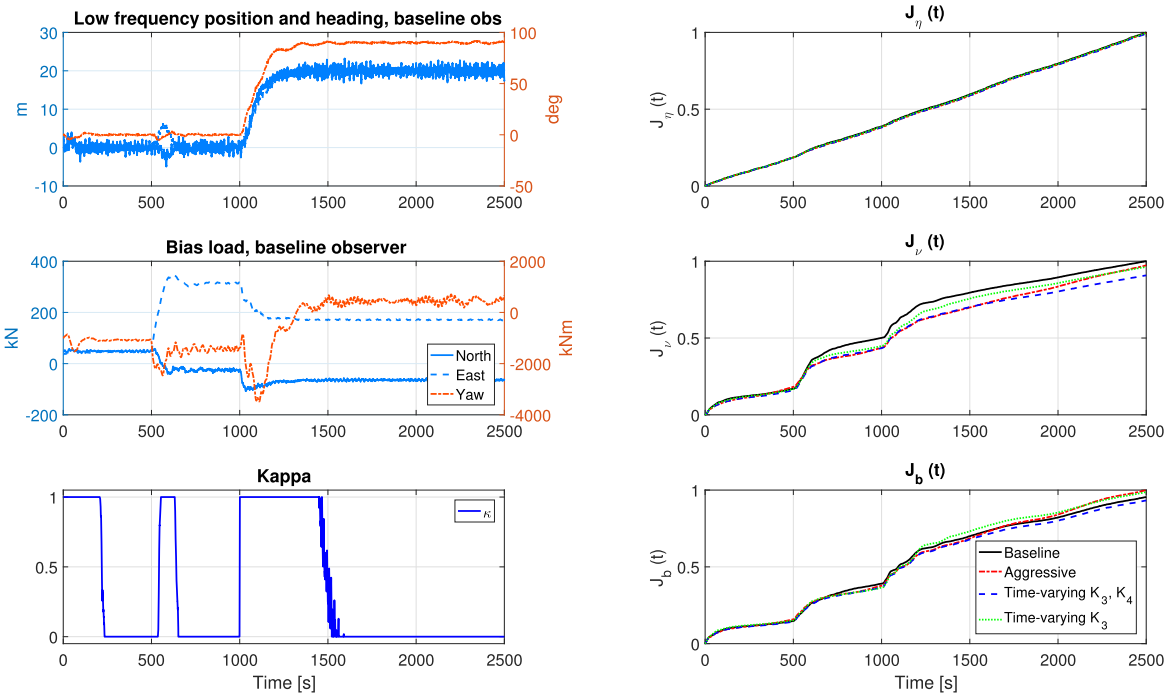

FIGURE 5. Simulation results of observer in closed-loop.

TABLE 3. Performance indices for the estimation error, simulation data.

Time:	0-1500 s			2000-3500 s		
Observer	J_η	J_ν	J_b	J_η	J_ν	J_b
Baseline	2125.2	96.4	666.8	2125.6	36.3	355.0
Aggressive	2098.8	84.7	653.2	2141.8	50.0	446.9
Time-varying K_3 and K_4	2099.3	85.1	646.2	2125.6	36.3	351.3
Time-varying K_3	2117.2	91.7	697.1	2125.6	36.4	352.4

a setpoint change of both North/East position and heading. Figure 5 shows the results of the four observers. The left side shows the low-frequency North/East position and heading of the baseline observer in the top plot, the middle plot shows the bias load of the baseline observer, found by solving (1d) for b, and the lower left plot shows the κ variable of the observer with time-varying $K_3(t)$ and $K_4(t)$ from (4). The right side shows the performance indices J_η, J_ν, and J_b in (14) from top to bottom, respectively. The same performance index values for 0 to 1500 seconds and for the steady-state time interval 2000 to 3500 are listed in Table 3. Note that the steady-state time interval 2500 to 3500 seconds is not shown in Figure 5.

Looking at the left side of Figure 5 we see that the bias loads change a lot, both at the current direction change at 500 seconds, and at the setpoint change at 1000 seconds. The κ-value starts at 1 due to high initialization of $\tilde{\eta}_f(t)$ in (5b) in order to handle initial transients before settling at $\kappa = 0$. At the heading change at 1000 seconds, κ reacts quickly and jumps to 1 due to the non-zero desired yaw rate. The current direction change at 500 seconds has to be detected through deterioration of the observer performance and the subsequent rise in $|\tilde{\eta}_f(t)|$. Therefore it takes κ longer to reach 1 during the current direction change.

On the right side of Figure 5 and in Table 3 we see that all observers perform similarly for J_η. In both the estimation of the velocity and bias loads, the time-varying observer proposed in this paper performs the best, especially in velocity. It outperforms the aggressive observer due to effect of lower oscillations in steady state, and it outperforms the baseline due to faster reaction over the transients. The time-varying observer with only K_3 time varying performs worse than the observer with both K_4 and K_3 time varying, but it performs better than the baseline observer in transients. As seen from Table 3, the baseline and time-varying observers are slightly better than the aggressive observer in steady state for position estimation, and considerable better for bias and velocity estimation.

If the noise variance of the measurements is increased, the time-varying observer performs better relative to the aggressive, due to lower tuning in steady state. To make the time-varying setup better handle large measurement noise, we could make ε_η in (5) depend on the variance of the noise. In this way the time-varying observer could adopt lower gains if the measurement noise increases.

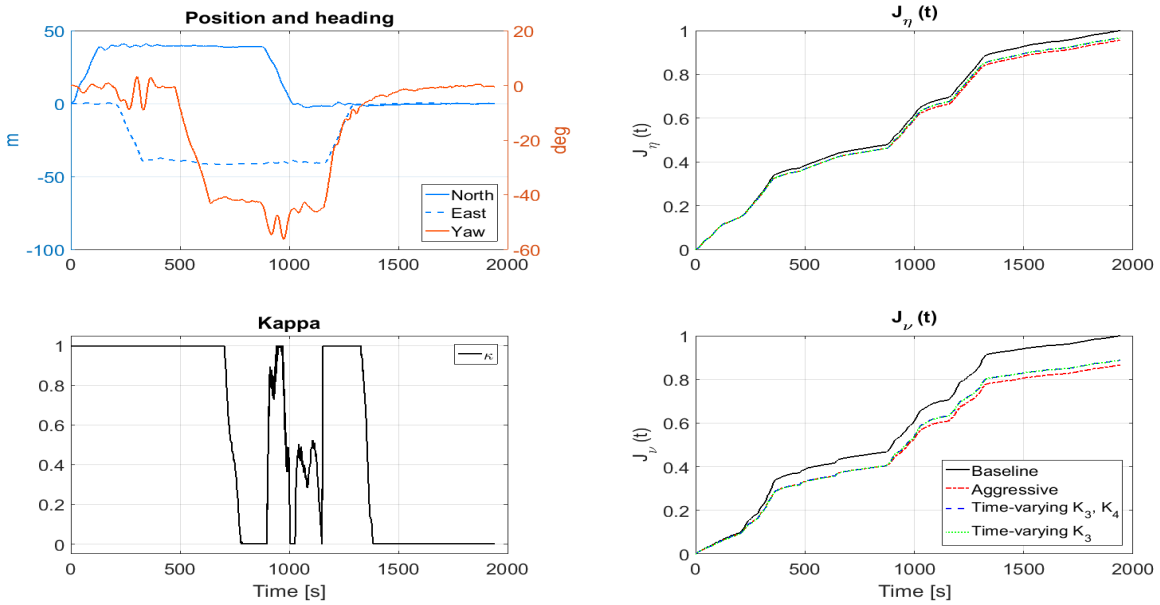

FIGURE 6. Observer results on full-scale experimental data from a DP 4-corner maneuver with R/V Gunnerus.

TABLE 4. Performance indices for the estimation error, full-scale exp. data.

Time:	0-1500 s		1500-1940 s	
Observer	J_η	J_ν	J_η	J_ν
Baseline	142.09	144.02	10.97	8.95
Aggressive	135.27	123.35	11.02	9.05
Time-varying K_3 and K_4	137.00	126.94	10.97	8.95
Time-varying K_3	138.83	126.97	10.97	8.95

3) ESTIMATION BASED ON FULL-SCALE MEASUREMENTS

Figure 6 shows the results of the four observers on data from R/V Gunnerus from ADPRC 2016. In the data set presented, the vessel is exposed to a current roughly estimated to 0.6 m/s and direction 170°, and with wind speed 5 m/s and direction 150°. The left side of the plot shows the measured North/East position, and heading in the top plot. The bottom left plot shows the κ variable. Notice that κ is 1 for most of the four corner maneuver, and after 1500 a steady state is reached.

Since the four corner maneuver has a lot of transients, and not too much steady state, it is harder to show a difference between the different observers. The right side of Figure 6 shows the performance indices J_η and J_ν in (14), and all four observers perform similarly for J_η, but for J_ν the baseline observer is significantly worse than the other three, due to all the transients. However, the performance between the observer with only time-varying K_3 to that of the other time-varying observer is smaller than for the closed-loop simulation results. The values for J_η and J_ν for the transient and steady state periods are given in Table 4, and the trend is similar to that of the closed-loop simulation results, although the differences in steady state are smaller. This is natural as the steady state in simulation is actually steady, and here the environment is changing, and there is less time to settle into steady state conditions.

VI. CONCLUSION

A time-varying model-based observer with good performance in both transients as well as steady state has been proposed. The observer is shown to be UGES, and performance is shown through a simulation study and on full-scale experimental data. In addition, a full-scale closed-loop verification is presented, and this shows that the observer works to a satisfactory degree in closed loop. Satisfactory transient tuning for the observer is found through derivative free optimization. The time-varying observer shows a marginal benefit over a well-tuned transient observer, depending on variations in measurement noise and environmental conditions. Especially, if there are large periods of steady state in between transients the time-varying observer is a tractable solution over the conventional DP observer. In addition, the added complexity of implementation for the time-varying gains is very small.

ACKNOWLEDGEMENTS

The authors would like to thank the crew of R/V Gunnerus and the personel from Kongsberg Maritime for their help and support during the sea trials. Especially, they would like to thank Rune Skullestad and Øystein Lurås from Kongsberg Maritime for help with code implementation and the simulation platform to test our code. Also, they would like to thank the NTNU research team, Øivind K. Kjerstad, Asgeir J. Sørensen, Mikkel E. N. Sørensen, Zhengru Ren, and

Morten Breivik. Finally, MSc. student Alexander Mykland deserves a thanks for writing the test log.

REFERENCES

[1] International Maritime Organization. "Guidelines for vessels with dynamic positioning systems," International Maritime Organization, London, U.K., Tech. Rep. MSC/circ.645, 1994.
[2] T. I. Fossen, *Handbook Marine Craft Hydrodynamics Motion Control*. Hoboken, NJ, USA: Wiley, 2011.
[3] A. J. Sørensen, "A survey of dynamic positioning control systems," *Annu. Rev. Control*, vol. 35, no. 1, pp. 123–136, Apr. 2011.
[4] J. E. G. Refsnes, "Nonlinear model-based control slender body AUVs," Ph.D. dissertation, Dept. Marine Technol., Norwegian Univ. Sci. Technol., Trondheim, Norway, 2007.
[5] O. K. Kjerstad and R. Skjetne, "Disturbance rejection by acceleration feedforward for marine surface vessels," *IEEE Access*, vol. 4, pp. 2656–2669, 2016.
[6] T. H. Bryne, T. I. Fossen, and T. A. Johansen, "Nonlinear observer with time-varying gains for inertial navigation aided by satellite reference systems in dynamic positioning," in *Proc. 22nd Medit. Conf. Control Autom. (MED)*, Jun. 2014, pp. 1353–1360.
[7] D. J. Belleter, D. A. Breu, T. I. Fossen, and H. Nijmeijer, "A globally k-exponentially stable nonlinear observer for the wave encounter frequency," in *Proc. IFAC Conf. Control Appl. Marine Syst.*, 2013, vol. 46. no. 33, pp. 209–214.
[8] D. J. W. Belleter, R. Galeazzi, and T. I. Fossen, "Experimental verification of a global exponential stable nonlinear wave encounter frequency estimator," *Ocean Eng.*, vol. 97, pp. 48–56, Mar. 2015.
[9] S. A. Værnø and R. Skjetne, "Hybrid control to improve transient response of integral action in dynamic positioning of marine vessels," in *Proc. IFAC Conf. Manoeuvring Control Marine Craft*, 2015, vol. 48. no. 16, pp. 166–171.
[10] S. A. Værnø, A. H. Brodtkorb, R. Skjetne, and A. J. Sørensen, "An output feedback controller with improved transient response of marine vessels in dynamic positioning," in *Proc. IFAC Conf. Control Appl. Marine Syst.*, 2016, vol. 49. no. 23, pp. 133–138.
[11] R. Skjetne *et al.*, "Amos dp research cruise 2016: Academic full-scale testing of experimental dynamic positioning control algorithms onboard RV gunnerus," in *Proc. ASME 36th Int. Conf. Ocean, Offshore Arctic Eng.*, 2017, pp. 1–4.
[12] P. Fung and M. J. Grimble, "Dynamic ship positioning using a self-tuning Kalman filter," *IEEE Trans. Autom. Control*, vol. 28, no. 3, pp. 339–350, Mar. 1983.
[13] M. Katebi, I. Yamamoto, M. Matsuura, M. Grimble, H. Hirayama, and N. Okamoto, "Robust dynamic ship positioning control system design and applications," *Int. J. Robust Nonlinear Control*, vol. 11, no. 13, pp. 1257–1284, 2001.
[14] E. Tannuri and H. Morishita, "Experimental and numerical evaluation of a typical dynamic positioning system," *Appl. Ocean Res.*, vol. 28, no. 2, pp. 133–146, 2006.
[15] A. J. Sørensen, "Marine control systems—Lecture notes," Dept. Marine Technol., Dept. Marine Technol., Norwegian Univ. Sci. Tech., Trondheim, Norway, 2013.
[16] T. I. Fossen and J. P. Strand, "Passive nonlinear observer design for ships using Lyapunov methods: Full-scale experiments with a supply vessel," *Automatica*, vol. 35, no. 1, pp. 3–16, Jan. 1999.
[17] K.-P. Lindegaard, "Acceleration feedback dynamic positioning," Ph.D. dissertation, Dept. Eng. Cybern., Norwegian Univ. Sci. Technol., Trondheim, Norway, 2003.
[18] T. I. Fossen and T. Perez. (2010). *Mss. Marine Systems Simulator*, accessed on Feb. 2015. [Online]. Available: http://www.marinecontrol.org
[19] W. G. Price and R. E. D. Bishop, *Probabilistic Theory of Ship Dynamics*. New York, NY, USA: Halsted, 1974.

SVENN ARE VÆRNØ was born in Norway in 1990. He received the M.Sc. degree in marine technology from the Norwegian University of Science and Technology, Trondheim, Norway, in 2014, where he is currently pursuing the Ph.D. degree with the Norwegian Centre of Excellence Autonomous Marine Operations and Systems. His research include marine motion control systems and dynamic positioning.

ASTRID H. BRODTKORB received the M.Sc. degree in marine technology from the Norwegian University of Science and Technology, Trondheim, in 2014, where she is currently pursuing the Ph.D. degree in marine control systems with the Norwegian Centre of Excellence Autonomous Marine Operations and Systems. Her main research interests are hybrid control theory, observers, and sea state estimation applied to dynamic positioning systems for marine vessels.

ROGER SKJETNE received the M.Sc. degree in control engineering from the University of California at Santa Barbara in 2000, and the Ph.D. degree from the Norwegian University of Science and Technology (NTNU), in 2005. Prior to his studies, he was an Electrician with Aker Elektro AS on numerous oil installations for the North Sea. From 2004 to 2009, he was with Marine Cybernetics AS, where he was involved in hardware-in-the-loop simulation for testing safety-critical marine control systems. He was the Project Manager for the KMB Arctic DP Research Project. Since 2009, he has held the Kongsberg Maritime Chair of Professor in marine control engineering with the Department of Marine Technology, NTNU, where he is currently the Leader of the Research Group on Marine Structures. He is the Leader of the Ice Management Work Package with the CRI Sustainable Arctic Marine and Coastal Technology, an Associated Researcher with the CoE Center for Ships and Ocean Structures and CoE Autonomous Marine Operations and Systems, and a Principal Researcher with the CRI on Marine Operations. He is also a Co-Founder of the two companies BluEye Robotics and ArcISo. His research interests are within Arctic station keeping operations and ice management systems for ships and rigs, environmentally robust control of shipboard electric power systems, and nonlinear control theory for motion control of single and groups of marine vessels. He received the Exxon Mobil Prize for best Ph.D. thesis in applied research for his Ph.D. thesis at NTNU.

VINCENZO CALABRÒ (M'10) was born in Messina, Italy, in 1982. He received the Ph.D. degree in robotics automation and bioengineering from the University of Pisa, Italy, in 2012. In 2012, he joined the Cybernetics Research and Development Group, Kongsberg Maritime, where he developed and improved industrial solutions for Dynamic Positioning systems and related applications. Since 2017, he has been the Research and Development Manager with Norwegian Subsea AS company, developing inertial-based systems and applications. His current research interests include state observer design, neural networks, model predictive control, non-linear control, and fuzzy logic.

Paper I:

AMOS DP Research Cruise 2016: Academic Full-scale Testing of Experimental Dynamic Positioning Control Algorithms Onboard R/V Gunnerus

Roger Skjetne, Mikkel E. N. Sørensen, Morten Breivik, Svenn Are T. Værnø, Astrid H. Brodtkorb, Asgeir J. Sørensen, Øivind K. Kjerstad, Vincenzo Calabrò, Bjørn Ole Vinje

Proceedings of the ASME 2017 36th International Conference on Ocean, Offshore and Arctic Engineering, OMAE 2017, Trondheim, Norway
Paper number: OMAE2017-62045

Is not included due to copyright

Paper J:

Sensor-based Hybrid Observer for Dynamic Positioning

Astrid H. Brodtkorb, Andrew R. Teel, Asgeir J. Sørensen

2015 54th IEEE Conference on Decision and Control (CDC),
Osaka, 2015, pp. 948-953.
doi: 10.1109/CDC.2015.7401995.

Is not included due to copyright

Paper K:

Hybrid Observer Combining Measurements of Different Fidelities

Astrid H. Brodtkorb, Andrew R. Teel, Asgeir J. Sørensen

10th IFAC Conference on Control Applications in Marine Systems (CAMS 2016),
Trondheim, Norway.
IFAC-PapersOnLine. vol. 49 (23) 2016, pp. 506-511,
doi: /10.1016/j.ifacol.2016.10.486.

Available online at www.sciencedirect.com

ScienceDirect

IFAC Papers Online CONFERENCE PAPER ARCHIVE

IFAC-PapersOnLine 49-23 (2016) 506–511

Hybrid Observer Combining Measurements of Different Fidelities ⋆

Astrid H. Brodtkorb * **Andrew R. Teel** ** **Asgeir J. Sørensen** *

* *Centre for Autonomous Marine Operations (NTNU AMOS), Department of Marine Technology, Norwegian University of Science and Technology (NTNU), Otto Nielsens vei 10, 7491 Trondheim, Norway (e-mails: astrid.h.brodtkorb@ntnu.no, asgeir.sorensen@ntnu.no*

** *Department of Electrical and Computational Engineering, University of California Santa Barbara, CA USA (e-mail: teel@ece.ucsb.edu)*

Abstract: A signal-based hybrid observer combining measurements of different fidelities is proposed for position and velocity estimation of marine vessels. The concept assumes that noisy position measurements are available only sporadically at a non-constant sampling rate. Predictions of position between the samples are provided by integrating acceleration measurements, which are available at a high rate (approximated to be continuous sampling). Estimates with smaller variance are computed by averaging multiple observer copies of the position. This work is a continuation of the observer proposed in Brodtkorb et al. (2015). The main contributions of this paper is extending the observer to the more realistic scenario where linear velocity and angular acceleration measurements are not available. A simulation study showed that the observer performed well in closed loop with a controller conducting dynamic positioning operations of a marine vessel.

Keywords: Observers, hybrid systems, dynamic positioning, sensor fusion

1. INTRODUCTION

Observers are important components of dynamic positioning (DP) systems for marine vessels. Common observer types used in DP today include model-based designs such as the nonlinear passive observer (NPO), see Fossen and Strand (1999), or an exteded Kalman filter, see Sørensen (2011) for an overview and the references therein. For other examples of implementation in DP see for instance Tannuri and Morishita (2006) and Hassani et al. (2013). These observers are based on a kinetic model of the vessel, and use position measurements from e.g. Global Navigation and Sensor Systems (GNSS), hydro-acoustic, laser, or microwaves, to reconstruct unmeasured states, filter out wave frequency motions, estimate bias, and in case of signal loss, do dead reckoning.

Signal-based, or kinematic, observers are also recently proposed for DP applications. These do not contain model parameters nor vessel-specific information, in contrast to model-based observers. In general, the methods integrate acceleration and angular rate measurements from inertial measurement units (IMU) to compute position and attitude estimates, correcting the estimates from drifting using position and compass (or magnetometer) measurements. Gravity and gyro bias are also compensated. For details see e.g. Grip et al. (2012), Grip et al. (2015) and Bryne et al. (2015).

The observers mentioned here assume in the design that the measurements are available continuously, which is not the case in reality. This was addressed in Brodtkorb et al. (2015), where measurements of position, velocity and acceleration were fused in a hybrid signal-based observer. The observer design was based on the assumption that position and velocity measurements were available only sporadically, and used acceleration measurement available at a high rate for position prediction. On a similar note, Ferrante et al. (2016) considers state estimation of linear systems where the measurements are available sporadically. The work considers systems where data used for control is transmitted over networks, where data can get lost or is available intermittently.

This paper extends the observer from Brodtkorb et al. (2015) to the more realistic case where no linear velocity and angular acceleration measurements are available. The observer error dynamics are shown uniformly globally asymptotically stable (UGAS) by using theory from hybrid dynamical systems as described in Goebel et al. (2012) and cascaded systems. The observer is tested in simulations of a marine surface vessel conducting DP operations.

The paper is organized as follows: Section 2 introduces the mathematical model and available measurements used for the observer design. The observer is designed in Section 3, and stability is discussed in Section 4. The observer is

⋆ This work was supported by the Research Council of Norway through the Centres of Excellence funding scheme, project number 23254 - NTNU AMOS, and in part by NSF grant number ECCS-1508757 and AFOSR grant number FA9550-15-1-0155.

10.1016/j.ifacol.2016.10.486

tested in simulations of a surface vessel in DP in Section 5, and Section 6 concludes the paper.

2. MATHEMATICAL MODELING

Two reference frames are used thoughout this paper. The North-East-Down (NED) frame is a local Earth-fixed reference frame with origin at the mean free surface, and the second reference frame is a body-fixed frame. The NED frame is assumed inertial.

2.1 Marine Vessel Modeling

The signal-based observer is based on the kinematic (strapdown) equations relating position, velocity and acceleration of the vessel. Here, we are looking only at motions in the horizontal plane, so we only consider surge, sway and yaw motions [1] . The equations of motion are

$$\dot{p} = R(\psi)v \tag{1a}$$
$$\dot{\psi} = r \tag{1b}$$
$$\dot{v} = a \tag{1c}$$

where p is the position vector in north and east, v is the body-fixed surge and sway velocity vector, a is the body-fixed surge and sway acceleration vector, ψ is the heading angle, and r is the yaw rate. Throughout this paper the rotation matrix $R(\psi)$ refers to the 2×2 rotation matrix given by

$$R(\psi) = \begin{bmatrix} \cos(\psi) & -\sin(\psi) \\ \sin(\psi) & \cos(\psi) \end{bmatrix}. \tag{2}$$

2.2 Measurements

DP vessels have statutory class requirements on the onboard instrumentation, and system redundancy. Vessels have positioning systems, e.g. GNSS, acoustics, or laser, a compass measuring heading angle, and inertial measurement units (IMU) that combine gyroscopes for measuring angular rates and accelerometers for measuring linear acceleration. The measurements are taken at different sampling rates ranging from 0.1-2 Hz for acoustics, 0.5-4 Hz for GNSS position measurements, to 100-200 Hz for IMU angular velocity and acceleration measurements.

We assume to have measurements of position $p = [N\ E]^\top$ and heading ψ with non-constant sample time in the interval $[T_{min}, T_{max}]$, where $0 < T_{min} \leq T_{max}$. The yaw rate r, and linear acceleration a are assumed to be measured at a high rate, approximated as continuous sampling. We also assume that r and a are bounded. Notice that we do not have linear velocity or angular acceleration measurements available. Noise on the measurements is not considered in the stability analysis, but is included in the simulations.

For convenience we constrain the system states to a compact set $\mathcal{K}$, $(p, \psi, v) \in \mathcal{K} \subset \mathbb{R}^5$. The observer design does not depend on this set.

[1] Since we are considering only surge, sway and yaw motion, the coupling effects in roll and pitch are neglected, as well as the effect of gravity.

3. HYBRID OBSERVER

A hybrid observer is designed based on (1) by utilizing the measurements when they are available. The observer states, denoted $(\cdot)_i$, flow with the yaw rate and linear acceleration measurements, and are updated with the occasional position and heading measurements. To mitigate the effect of position and compass measurement noise, multiple copies of position, heading and velocity are saved in the observer and averaged. The position, heading, and velocity estimates are

$$\hat{p} := \frac{1}{N}\sum_{i=1}^{N} p_i, \quad \hat{\psi} := \frac{1}{N}\sum_{i=1}^{N} \psi_i, \quad \hat{v} \ := \frac{1}{N}\sum_{i=1}^{N} v_i \tag{3}$$

where $p_i,\ i = \{1, ..., N\}$ are the north and east position states in the observer, ψ_i are the heading states, and v_i are the linear velocity states. The observer states flow as

$$\dot{p}_i = R(\hat{\psi})v_i \tag{4a}$$
$$\dot{\psi}_i = r \tag{4b}$$
$$\dot{v}_i = a \tag{4c}$$
$$\dot{M} = R(\hat{\psi}) \tag{4d}$$
$$\dot{\tau} = -1, \tag{4e}$$

with $i = \{1, ..., N\}$ copies of position, heading and velocity flow with the available yaw rate r and acceleration measurement a. The states are allowed to flow when

$$\begin{aligned} &((p, \psi, v), (p_1, \psi_1, v_1), ..., (p_N, \psi_N, v_N), M, \tau) \in C \\ &C := \mathcal{K} \times (\mathbb{R}^2 \times \mathbb{R}^1 \times \mathbb{R}^2)^N \\ &\quad \times \left\{P \in \mathbb{R}^{2\times 2} : ||P||_2 \leq T_{max}\right\} \times [0, T_{max}]. \end{aligned} \tag{5}$$

In particular M belongs to the set of 2×2 matrices with induced 2 norm less than or equal to T_{max}, see Section 4.3 for details. The observer flows in between position and compass measurement times, when $\tau \in [0, T_{max}]$. A new position and compass measurement is available with non-constant sampling time with at least T_{min} seconds between samples and at most T_{max} seconds. Hence a jump is triggered when $\tau = 0$, with the jump dynamics

$$p_i^+ = p_{i-1} \tag{6a}$$
$$\psi_i^+ = \psi_{i-1} \tag{6b}$$
$$v_i^+ = v_i + \kappa M^{-1}(p_i - p_{i-1}), \tag{6c}$$
$$M^+ = 0, \tag{6d}$$
$$\tau^+ \in [T_{min}, T_{max}], \tag{6e}$$

with $i = \{1, .., N\}$ and the measurements $p_0 := p$ and $\psi_0 := \psi$. The measurements of position and heading are saved into the first observer states (p_1, ψ_1), and the remainder of the states are shifted one place back in the shift register. The velocity states are updated with the state itself, and a correction term consisting of a gain κ, the inverse of the matrix M involving the rotation matrix integrated over time, and the error between position states i and $i-1$. The jump set is

$$\begin{aligned} &((p, \psi, v), (p_1, \psi_1, v_1), ..., (p_N, \psi_N, v_N), M, \tau) \in D \\ &D := \mathcal{K} \times (\mathbb{R}^2 \times \mathbb{R}^1 \times \mathbb{R}^2)^N \\ &\quad \times \left\{P \in \mathbb{R}^{2\times 2} : ||P||_2 \leq T_{max},\ \det(P) \geq \rho\right\} \times \{0\}. \end{aligned} \tag{7}$$

The observer has two parameters; κ in (6c), which can be anything in $(-2, 0)$, and $\rho > 0$ in (7) which ensures that $\det(M)$ is larger than zero so that M is invertible during jumps. This last constraint is related to making sure that

the system is observable with the available measurements. The yaw dynamics are usually slow compared to the sampling period, and this makes it less likely to encounter $\det(M)$=0. The parameter ρ should be small to allow for as many signals ψ as possible.

4. STABILITY

We are using Lyapunov results for hybrid systems (Goebel et al., 2012), and cascaded systems to prove that the observer error dynamics has the origin uniformly globally asymptotically stable (UGAS).

We are analyzing stability of the plant (1) with the observer given in (4) and (6), with the flow set (5) and the jump set (7). The set for which we are analyzing stability is

$$\mathcal{A} := \{((p,\psi,v),(p_1,\psi_1,v_1),...,(p_N,\psi_N,v_N),M,\tau) \in C : p_i = p,\ \psi_i = \psi,\ v_i = v,\ \forall i \in \{1,...,N\}\}. \quad (8)$$

Theorem 1: If $\kappa \in (-2,0)$ and $\rho > 0$ then the set $\mathcal{A}$ in (8) is UGAS for the hybrid system consisting of the plant (1) the observer given in (4) and (6), with flow set (5) and jump set (7). □

The proof is done sequentially in the next sections. The observer error dynamics are first introduced. The heading error dynamics are shown UGAS, and the observer error dynamics for $N = 1$ without including heading are shown UGAS by applying a coordinate transformation. Lastly the analysis for the observer error dynamics for $N > 1$ follows from the case where $N = 1$ by using cascade theory.

4.1 Error Dynamics

Define the error states as:

$$e_i = p_i - p_{i-1},$$
$$y_i = \psi_i - \psi_{i-1},$$
$$z_i = v_i - v_{i-1},$$

for all $i \in \{1,..,N\}$, with the actual states of the system $p_0 := p,\ \psi_0 := \psi$, and $v_0 := v$. The relationship between the velocity and position is $\dot{p}_0 = R(\psi_0)v_0$. Write the observer error dynamics as:

$$\dot{e}_i = \begin{cases} R(\hat{\psi})z_i + [R(\hat{\psi}) - R(\psi)]v & i = 1 \\ R(\hat{\psi})z_i & i \in \{2,\dots,N\} \end{cases} \quad (9a)$$
$$\dot{z}_i = 0 \qquad i \in \{1,\dots,N\} \quad (9b)$$
$$\dot{M} = R(\hat{\psi}) \quad (9c)$$
$$\dot{\tau} = -1 \quad (9d)$$
$$e_i^+ = e_{i-1} \qquad i \in \{1,\dots,N\} \quad (9e)$$
$$z_i^+ = z_i + \kappa M^{-1} e_i \qquad i \in \{1,\dots,N\} \quad (9f)$$
$$M^+ = 0 \quad (9g)$$
$$\tau^+ \in [T_{min}, T_{max}], \quad (9h)$$

with position error $e_0 := p - p = 0$. Note that when the heading estimate has converged, $\hat{\psi} = \psi$, the extra term for $i = 1$ in (9a) disappears. The heading error dynamics are:

$$\dot{y}_i = 0 \qquad i \in \{1,\dots,N\} \quad (10a)$$
$$y_i^+ = y_{i-1} \qquad i \in \{1,\dots,N\}, \quad (10b)$$

with heading error $y_0 := \psi - \psi = 0$.

4.2 Heading Error Analysis

The heading error dynamics are independent of the other states, and is input to the flow dynamics of position via M.

Claim 1: The origin of the heading error dynamics (10) with states y_i are UGAS. □

Proof: The proposed Lyapunov function candidate is

$$V(y,\tau) := \exp(L\tau)\sum_{i=1}^{N} k_i y_i^\top y_i \quad (11)$$

$L > 0$, and with weights k_i chosen so that

$$k_i > \exp(LT_{max})k_{i+1},\ i \in \{1,...,N\}$$

with $k_{N+1} := 0$. The Lyapunov function $V(y,\tau)$ can be lower bounded by choosing $\tau = 0$ and upper bounded by choosing $\tau = T_{max}$. The time derivative of V along the trajectories of the state, and the difference between V before and after a jump are

$$\langle \nabla V(y,\tau), f\rangle = \exp(L\tau)\left(L\dot{\tau}\sum_{i=1}^{N} k_i y_i^\top y_i + 2\sum_{i=1}^{N} k_i y_i^\top \dot{y}_i\right) = -LV(y,\tau).$$

$$V(y^+,\tau^+) - V(y,\tau) \le \exp(LT_{max})\sum_{i=1}^{N} k_i y_{i-1}^\top y_{i-1} - \sum_{i=1}^{N} k_i y_i^\top y_i$$

$y_0 = \psi - \psi = 0$, so the first sum can be contracted.

$$V(y^+,\tau^+) - V(y,\tau) \le \exp(LT_{max})\sum_{i=2}^{N} k_i y_{i-1}^\top y_{i-1} - \sum_{i=1}^{N} k_i y_i^\top y_i$$
$$\le \exp(LT_{max})\sum_{i=1}^{N-1} k_{i+1} y_i^\top y_i - \sum_{i=1}^{N} k_i y_i^\top y_i$$
$$\le \sum_{i=1}^{N} \left(\exp(LT_{max})k_{i+1} - k_i\right) y_i^\top y_i$$

Due to the definition of $k_i\ \forall i$, the terms in the first sum can be dominated by the terms in the second sum. Then there exists a $\delta > 0$ such that

$$V(y^+,\tau^+) - V(y,\tau) \le -\delta y^\top y.$$

□

4.3 Lyapunov Analysis for $N = 1$

Assume that $\hat{\psi}$ has converged to ψ, so that $R(\hat{\psi}) - R(\psi) = 0$.

Claim 2: Given that $\hat{\psi} = \psi$, the origin of the observer error dynamics given by (9) is UGAS. □

Proof: We introduce new coordinates

$$x_1 := e_1 - Mz_1$$
$$x_2 := z_1, \quad (12)$$

and rewrite the error dynamics as

$$\dot{x}_1 = 0 \tag{13a}$$
$$\dot{x}_2 = 0 \tag{13b}$$
$$\dot{\tau} = -1 \tag{13c}$$
$$x_1^+ = 0 \tag{13d}$$
$$x_2^+ = (1+\kappa)x_2 + \kappa M^{-1}x_1 \tag{13e}$$
$$\tau^+ \in [T_{min}, T_{max}]. \tag{13f}$$

Choose the following Lyapunov function candidate:

$$V(x,\tau) := \exp(\mu\tau)(\ell x_1^\top x_1 + x_2^\top x_2) \tag{14}$$

with $0 < \mu \ll 1$, and a large number ℓ. The time derivative of V along the trajectories of (x,τ) is

$$\begin{aligned}\langle \nabla V(x,\tau), f(x,\tau)\rangle &= -\mu V(x,\tau) + 2\exp(\mu\tau)\left(x_1^\top \dot{x}_1 + x_2^\top \dot{x}_2\right)\\ &= -\mu V(x,\tau).\end{aligned}$$

Before investigating what happens during jumps, we calculate a convenient bound on $V(x^+,\tau^+) - V(x,\tau)$ using the induced 2 norm of M^{-1}

$$||M^{-1}||_2 = \frac{||M||_2}{\det(M)},$$

where $\det(M)$ is the determinant of M. The induced 2 norm of a matrix is defined as

$$||M||_2 := \max_{|v|_2=1} |Mv|_2,$$

with the vector norm $|v|_2 = 1$. In this case M evolves as $\dot{M}(t) = R(\hat{\psi}(t))$ with initial condition $M(0) = 0$. The induced 2 norm of M is computed in the following:

$$\begin{aligned}|M(t)v|_2 &= \left|\int_0^t R(\hat{\psi}(s))ds\ v\right|_2\\ &\le \int_0^t \left|R(\hat{\psi}(s))v\right|_2 ds.\end{aligned}$$

Use that $R(\hat{\psi}(s))$ is a rotation matrix for all s, so it rotates v, not altering the magnitude of the vector.

$$\begin{aligned}|M(t)v|_2 &\le \int_0^t |v|_2\, ds\\ &\le \int_0^t ds = t \le T_{max},\end{aligned}$$

so $||M||_2 \le T_{max}$. The determinant of M cannot be smaller than ρ in the jump map, so we get that

$$||M^{-1}||_2 \le \frac{T_{max}}{\rho}.$$

During jumps we get

$$\begin{aligned}V(x^+,\tau^+) - V(x,\tau) &\le \exp(\mu T_{max})[(1+\kappa)x_2 + \kappa M^{-1}x_1)^\top\\ &\quad ((1+\kappa)x_2 + \kappa M^{-1}x_1] - \ell x_1^\top x_1 - x_2^\top x_2\\ &\le \exp(\mu T_{max})[(1+\kappa)^2 x_2^\top x_2 + \kappa^2 x_1^\top (M^{-1})^\top M^{-1}x_1\\ &\quad + 2\kappa(1+\kappa)x_1^\top (M^{-1})^\top x_2] - \ell x_1^\top x_1 - x_2^\top x_2\\ &\le \exp(\mu T_{max})[(1+\kappa)^2 x_2^\top x_2 + \kappa^2 \frac{T_{max}^2}{\rho^2} x_1^\top x_1\\ &\quad + 2(1+\kappa)\kappa\frac{T_{max}}{\rho}x_1^\top x_2] - \ell x_1^\top x_1 - x_2^\top x_2.\end{aligned}$$

We use Young's inequality for completion of squares

$$2a^\top b \le \frac{1}{\varepsilon}a^\top a + \varepsilon b^\top b, \qquad \forall \varepsilon > 0.$$

By choosing $a = \kappa\frac{T_{max}}{\rho}x_1$, and $b = (1+\kappa)x_2$, we get

$$\begin{aligned}&V(x^+,\tau^+) - V(x,\tau)\\ &\quad \le \left[\exp(\mu T_{max})\left(\kappa^2\frac{T_{max}^2}{\rho^2} + \kappa^2\frac{T_{max}^2}{\rho^2}\frac{1}{\varepsilon}\right) - \ell\right]x_1^\top x_1\\ &\quad + \left[\exp(\mu T_{max})\left((1+\kappa)^2 + (1+\kappa)^2\varepsilon\right) - 1\right]x_2^\top x_2\end{aligned}$$

The Lyapunov function decreases during jumps if

$$\ell > \exp(\mu T_{max})\kappa^2\frac{T_{max}^2}{\rho^2}\left(1 + \frac{1}{\varepsilon}\right) \tag{15a}$$
$$1 > \exp(\mu T_{max})(1+\kappa)^2(1+\varepsilon). \tag{15b}$$

When $\mu = 0$ and $\varepsilon = 0$ (15b) holds since $\kappa \in (-2, 0)$. By continuity it still holds for $\mu > 0$ and $\varepsilon > 0$ sufficiently small. After picking such a $\mu > 0$ and $\varepsilon > 0$, we choose ℓ to satisfy (15a).

We can bound the Lyapunov function given in (14) with the original states (e_1, z_1) by noting that

$$\begin{aligned}V(x,\tau) &\le \ell\exp(\mu T_{max})\left|\begin{bmatrix}x_1\\ x_2\end{bmatrix}\right|^2\\ &\le \ell\exp(\mu T_{max})(1+T_{max})^2\left|\begin{bmatrix}e_1\\ z_1\end{bmatrix}\right|^2,\end{aligned} \tag{16}$$

and

$$\begin{aligned}V(x,\tau) &\ge \left|\begin{bmatrix}x_1\\ x_2\end{bmatrix}\right|^2\\ &= \frac{(1+T_{max})^2}{(1+T_{max})^2}\left|\begin{bmatrix}x_1\\ x_2\end{bmatrix}\right|^2\\ &\ge \frac{1}{(1+T_{max})^2}\left|\begin{bmatrix}e_1\\ z_1\end{bmatrix}\right|^2.\end{aligned} \tag{17}$$

By Theorem 3.18 Goebel et al. (2012) the set $\mathcal{A}$ in (8) is globally asymptotically stable for (9) with $\hat{\psi} = \psi$ and $N = 1$ given that (15) holds. □

4.4 Lyapunov Analysis for $N > 1$

When $N > 1$ there are two considerations we have to take. Firstly, the flow dynamics get an extra term when the heading estimate is not equal to the actual heading, and secondly, the position estimates $e_{i-1},\ i = \{2, ..., N\}$ in the jump dynamics are not zero.

Flow Dynamics with $\hat{\psi} \neq \psi$ When $\hat{\psi}$ has not converged to ψ yet, we are left with an extra term in the position error dynamics of e_1. Using (12), the error dynamics are

$$\dot{x}_1 = [R(\hat{\psi}) - R(\psi)]v \tag{18a}$$
$$\dot{x}_2 = 0 \tag{18b}$$
$$\dot{\tau} = -1 \tag{18c}$$
$$x_1^+ = 0 \tag{18d}$$
$$x_2^+ = (1+\kappa)x_2 + \kappa M^{-1}x_1 \tag{18e}$$
$$\tau^+ \in [T_{min}, T_{max}] \tag{18f}$$

The rotation matrix is bounded for all $\hat{\psi}$ and ψ, and the velocity v is bounded, since it is contained in the compact set $\mathcal{K}$. The jump dynamics are unchanged.

Claim 3: The system given by (18) with input v is input-to-state stable (ISS). □

Proof (from the proof of Proposition 2.7, Cai and Teel (2009)): The Lyapunov function $V(x,\tau)$ in (14) is bounded by two κ_∞-functions in (17). Furthermore, we get the time derivative along the state trajectories

$$\begin{aligned}&\langle \nabla V(x,\tau), f(x,\tau)\rangle\\ &\quad\le -\mu V(x,\tau) + 2\exp(\mu\tau)\ell x_1^\top [R(\hat\psi) - R(\psi)]v,\end{aligned}$$

where the first term is from the unperturbed e_1 dynamics, and the second term is due to the difference $\hat\psi - \psi$. Using Young's inequality for completion of squares with $a = \sqrt{\ell}x_1$ and $b = 2\sqrt{\ell}\exp(\mu\tau)[R(\hat\psi) - R(\psi)]v$, we get

$$\begin{aligned}&\langle \nabla V(x,\tau), f(x,\tau)\rangle\\ &\quad\le -\mu V(x,\tau) + \frac{1}{2}\mu\ell x_1^\top x_1 + \frac{1}{2\mu}\ell\exp(2\mu T_{max})(2|v|)^2\\ &\quad\le -\frac{1}{2}\mu V(x,\tau) + \alpha_1(|v|).\end{aligned}$$

We know that $V(x,\tau)$ can be lower bounded as in (17), and $\alpha_1(s) := \frac{2}{\mu}\ell\exp(2\mu T_{max})s^2$, $\forall s \ge 0$ is a class κ-function since $\alpha_1(0) = 0$ and it is strictly increasing. Then the Lyapunov function $V(x,\tau)$ in (14) is an ISS-Lyapunov function w.r.t the input v, and the hybrid system (18) is ISS w.r.t. v. □

Theorem 2: Given that $\kappa \in (-2, 0)$ and (15) holds, the origin of the cascaded system (18) and (10) is UGAS. □

The proof follows from Goebel et al. (2009) Corollary 19. Consider the hybrid system $\mathcal{H} = (C, F, C, G)$ consisting of the position and velocity error dynamics (18) and the heading error dynamics (10). The compact set

$$\begin{aligned}\mathcal{A}_1 =\{&((p,\psi,v),(p_1,\psi_1,v_1),...,(p_N,\psi_N,v_N),M,\tau)\in C :\\ &p_i = \beta\mathbb{B},\ \psi_i = \psi,\ v_i = \beta\mathbb{B},\ \forall i\in\{1,...,N\}\},\end{aligned}$$

with $\beta > 0$ and $\mathbb{B}$ the unit ball is globally pre-asymptotically stable (GpAS) for $\mathcal{H}$ (Claim 1). Further, the compact set $\mathcal{A}$ from (8), which is a subset of $\mathcal{A}_1$ is GpAS for $\mathcal{H}|_{\mathcal{A}_1} := (C\cap\mathcal{A}_1, F, D\cap\mathcal{A}_1, G\cap\mathcal{A}_1)$ (Claim 2). Then set $\mathcal{A}$ in (8) is UGAS for $\mathcal{H}$, given by (18) and (10). □

Jump Dynamics with $e_{i-1} \neq 0$ Again, we assume that $\hat\psi = \psi$ so that $R(\hat\psi) - R(\psi) = 0$. In general, the system (9) with $i = \{1, ..., N\}$ can be written as

$$\dot e_i = R(\hat\psi)z_i \tag{19a}$$
$$\dot z_i = 0 \tag{19b}$$
$$\dot M = R(\hat\psi) \tag{19c}$$
$$e_i^+ = e_{i-1} \tag{19d}$$
$$z_i^+ = z_i + \kappa M^{-1}e_i \tag{19e}$$
$$M^+ = 0. \tag{19f}$$

In Section 4.3 the case with $N = 1$ was proved. The error dynamics for $i \in \{2, ..., N\}$ are identical to the case where $N = 1$, except for the position error jumps $e_i^+ = e_{i-1}$, in stead of $e_1^+ = 0$.

Claim 4: Assuming that $\hat\psi = \psi$, the system given by (19) with input e_{i-1} is ISS, implying that the origin of the unforced system (19) with $e_{i-1} = 0$ is UGAS. □

Proof: The position jump dynamics changes the x_1 jump dynamics in (13d), which adds an extra term in the Lyapunov function during jumps. The flow dynamics are unchanged. The change in the $V(x,\tau)$ in (14) can be written as

$$\begin{aligned}&V(x^+,\tau^+) - V(x,\tau)\\ &\quad\le -\gamma_1 x_1^\top x_1 - \gamma_2 x_2^\top x_2 + \exp(\mu T_{max})\ell e_{i-1}^\top e_{i-1}\\ &\quad\le -\alpha_2(|x|) + \alpha_3(|e_{i-1}|),\end{aligned}$$

where $\alpha_2(|x|)$ is a class κ_∞-function given that (15) holds, and $\alpha_3(|e_{i-1}|)$ is a class κ-function. It follows that $V(x,\tau)$ (14) is an ISS-Lyapunov function for (19), then the system (19) is ISS with respect to the input e_{i-1} (Cai and Teel, 2009, Proposition 2.7). □

5. SIMULATION RESULTS AND DISCUSSION

The observer was implemented in MATLAB/Simulink, and simulated with a platform supply vessel in DP. The vessel has length 80 meters and breadth 17.4 meters. The control objective was to control the vessel to the desired time-varying reference $p_d(t)$ with the desired velocity trajectory $v_d(t)$:

$$\lim_{t\to\infty} p(t) - p_d(t) = 0$$
$$\lim_{t\to\infty} v(t) - v_d(t) = 0.$$

A nonlinear proportional, integral, derivative (nPID) controller was used to achieve trajectory tracking using output feedback, with current as the only environmental force. The current speed was $[-0.3\ 0.5]$ m/s in the North-East frame. Realistic noise values were used, where the position noise variance σ_p^2 was varied in the simulations.

Figures 1 and 2 show the actual and estimated north position and surge velocity for different values of N when the vessel changes setpoint and heading several times. At 200 seconds the vessel starts changing to the first setpoint; 3 m north, -5 m east, and with a heading of $-90°$. At 500 seconds the vessel does a new setpoint change to -2 m north, 5 m east, and heading angle $-60°$. The observer performance in the other degrees of freedom was comparable to the north position and surge velocity.

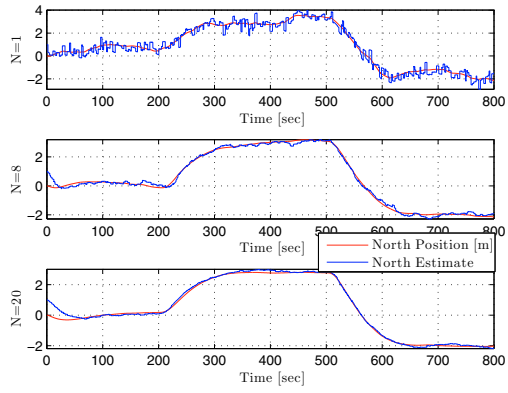

Fig. 1. Position and estimated position, for $N = 1, N = 8$ and $N = 20$. $T_{min} = 1$ $T_{max} = 5$ with noisy measurements $\sigma_p^2 = 0.3^2$ and estimates in feedback.

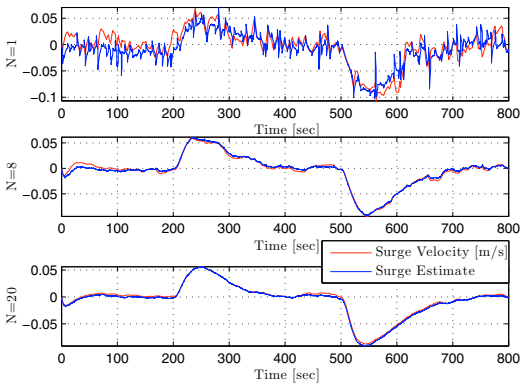

Fig. 2. Velocity and estimated velocity, for $N = 1, N = 8$ and $N = 20$. $T_{min} = 1$ $T_{max} = 5$ with noisy measurements $\sigma_p^2 = 0.3^2$ and estimates in feedback.

The observer states were initialized as $p_i = 1$ m, $\psi_i = 1°$ and $v_i = 0$ m/s, with the vessel states all starting at zero. It is clear from Figure 1 that as the number of states in the observer increases, the variance on the estimates decreases. Table 1 shows the variance for $N = 1$, $N = 8$, and $N = 20$. The estimation error also decreases for increasing N, and the overall reference tracking performance increases when the estimates are less oscillatory. The performance is similar for $N = 8$ and $N = 20$, with a longer initialization phase for $N = 20$ and some induced oscillations on the position for $N = 8$. Decreasing N and T_{max} decreases the convergence time greatly since $p_i - p_{i-1}$ is used as correction term in the velocity update dynamics. It was also found that with higher noise variance, the effect of increasing N was greater.

	Position variance [m^2]	Velocity variance [m^2/s^2]
$N = 1$	0.1016	$6.53 \cdot 10^{-5}$
$N = 8$	0.0162	$1.34 \cdot 10^{-5}$
$N = 20$	0.0030	$1.21 \cdot 10^{-5}$

Table 1. Variance of the estimates with $T_{min} = 1$ $T_{max} = 5$, and $\sigma_p^2 = 0.3^2$

The velocity estimates in Figure 2 were also better for larger N. The best velocity estimates were achieved by choosing κ just large enough so the velocity estimates did not drift. In particular for $N = 1$, $\kappa = -0.08$, for $N = 8, \kappa = -0.03$, and for $N = 20, \kappa = -0.02$. In general it was found that for increasing N, the value of κ could beneficially be decreased slightly. Without noise $\kappa = -1$ provided perfect position and velocity estimation.

The velocity dynamics were sensitive to position noise. For high position noise variance, small feedback gain on velocity produced less oscillatory estimates, but too low gain caused the velocity estimates to drift. Increasing N improved the estimation. The frequency of the position updates also influences the choice of κ, see (15). With frequent position measurements, κ could be chosen smaller, and vice versa in the simulations.

6. CONCLUSION

The signal-based observer without velocity and angular acceleration measurements updates worked well in simulations with and without measurement noise. Having a large number of states N in the observer was beneficial to mitigate noise with large variance.

For future work, rigorously analyzing the effect of the noise in the position and compass measurements is of interest. In addition, we may consider extending the velocity update dynamics to the case where M is not necessarily invertible at every sampling time.

REFERENCES

Brodtkorb, A., Teel, A., and Sørensen, A.J. (2015). Sensor-based hybrid observer for dynamic positioning. *Proceedings of the IEEE Conference on Decision and Control*, 2015-December, 948–953.

Bryne, T., Fossen, T., and Johansen, T. (2015). A virtual vertical reference concept for GNSS/INS applications at the sea surface. *IFAC Proceedings Volumes (IFAC-PapersOnline)*, 48(16), 127–133.

Cai, C. and Teel, A. (2009). Characterizations of input-to-state stability for hybrid systems. *Systems and Control Letters*, 58(1), 47–53.

Ferrante, F., Gouaisbaut, F., and Sanfelice, R.G. (2016). State estimation of linear systems in the presence of sporadic measurements. *To appear in: Automatica*.

Fossen, T.I. and Strand, J.P. (1999). Passive nonlinear observer design for ships using Lyapunov methods: full-scale experiments with a supply vessel. *Automatica*, 35(1), 3 – 16.

Goebel, R., Sanfelice, R., and Teel, A.R. (2009). Hybrid dynamical systems robust stability and control for systems that combine continuous-time and discrete-time dynamics. *IEEE Control Systems Magazine, April 2009*, 28–93.

Goebel, R., Sanfelice, R.G., and Teel, A.R. (2012). *Hybrid Dynamical Systems, Modelling, Stability and Robustness*. Princeton University Press.

Grip, H.F., Fossen, T.I., Johansen, T.A., and Saberi, A. (2012). Attitude estimation using biased gyro and vector measurements with time-varying reference vectors. *IEEE Transactions on Automatic Control*, 57(5), 1332–1338.

Grip, H.F., Fossen, T.I., Johansen, T.A., and Saberi, A. (2015). Globally esponentially stable attitude and gyro bias estimation with application to GNSS/INS integration. *Automatica*, 51, 158–166.

Hassani, V., Sørensen, A.J., and Pascoal, A.M. (2013). A novel methodology for robust dynamic positioning of marine vessels: Theory and experiments. *Proceedings of the American Control Conference*, 560–565.

Sørensen, A.J. (2011). A survey of dynamic positioning control systems. *Annual Reviews in Control*, 35(1), 123–136.

Tannuri, E.A. and Morishita, H.M. (2006). Experimental and numerical evaluation of a typical dynamic positioning system. *Applied Ocean Research*, 28(2), 133–146.

PhD Theses Published at the Department of Marine Technology

Previous PhD theses published at the Departement of Marine Technology
(earlier: Faculty of Marine Technology)
NORWEGIAN UNIVERSITY OF SCIENCE AND TECHNOLOGY

Report No.	Author	Title
	Kavlie, Dag	Optimization of Plane Elastic Grillages, 1967
	Hansen, Hans R.	Man-Machine Communication and Data-Storage Methods in Ship Structural Design, 1971
	Gisvold, Kaare M.	A Method for non-linear mixed -integer programming and its Application to Design Problems, 1971
	Lund, Sverre	Tanker Frame Optimalization by means of SUMT-Transformation and Behaviour Models, 1971
	Vinje, Tor	On Vibration of Spherical Shells Interacting with Fluid, 1972
	Lorentz, Jan D.	Tank Arrangement for Crude Oil Carriers in Accordance with the new Anti-Pollution Regulations, 1975
	Carlsen, Carl A.	Computer-Aided Design of Tanker Structures, 1975
	Larsen, Carl M.	Static and Dynamic Analysis of Offshore Pipelines during Installation, 1976
UR-79-01	Brigt Hatlestad, MK	The finite element method used in a fatigue evaluation of fixed offshore platforms. (Dr.Ing. Thesis)
UR-79-02	Erik Pettersen, MK	Analysis and design of cellular structures. (Dr.Ing. Thesis)
UR-79-03	Sverre Valsgård, MK	Finite difference and finite element methods applied to nonlinear analysis of plated structures. (Dr.Ing. Thesis)
UR-79-04	Nils T. Nordsve, MK	Finite element collapse analysis of structural members considering imperfections and stresses due to fabrication. (Dr.Ing. Thesis)
UR-79-05	Ivar J. Fylling, MK	Analysis of towline forces in ocean towing systems. (Dr.Ing. Thesis)
UR-80-06	Nils Sandsmark, MM	Analysis of Stationary and Transient Heat Conduction by the Use of the Finite Element Method. (Dr.Ing. Thesis)
UR-80-09	Sverre Haver, MK	Analysis of uncertainties related to the stochastic modeling of ocean waves. (Dr.Ing. Thesis)
UR-81-15	Odland, Jonas	On the Strength of welded Ring stiffened cylindrical Shells primarily subjected to axial Compression
UR-82-17	Engesvik, Knut	Analysis of Uncertainties in the fatigue Capacity of

		Welded Joints
UR-82-18	Rye, Henrik	Ocean wave groups
UR-83-30	Eide, Oddvar Inge	On Cumulative Fatigue Damage in Steel Welded Joints
UR-83-33	Mo, Olav	Stochastic Time Domain Analysis of Slender Offshore Structures
UR-83-34	Amdahl, Jørgen	Energy absorption in Ship-platform impacts
UR-84-37	Mørch, Morten	Motions and mooring forces of semi submersibles as determined by full-scale measurements and theoretical analysis
UR-84-38	Soares, C. Guedes	Probabilistic models for load effects in ship structures
UR-84-39	Aarsnes, Jan V.	Current forces on ships
UR-84-40	Czujko, Jerzy	Collapse Analysis of Plates subjected to Biaxial Compression and Lateral Load
UR-85-46	Alf G. Engseth, MK	Finite element collapse analysis of tubular steel offshore structures. (Dr.Ing. Thesis)
UR-86-47	Dengody Sheshappa, MP	A Computer Design Model for Optimizing Fishing Vessel Designs Based on Techno-Economic Analysis. (Dr.Ing. Thesis)
UR-86-48	Vidar Aanesland, MH	A Theoretical and Numerical Study of Ship Wave Resistance. (Dr.Ing. Thesis)
UR-86-49	Heinz-Joachim Wessel, MK	Fracture Mechanics Analysis of Crack Growth in Plate Girders. (Dr.Ing. Thesis)
UR-86-50	Jon Taby, MK	Ultimate and Post-ultimate Strength of Dented Tubular Members. (Dr.Ing. Thesis)
UR-86-51	Walter Lian, MH	A Numerical Study of Two-Dimensional Separated Flow Past Bluff Bodies at Moderate KC-Numbers. (Dr.Ing. Thesis)
UR-86-52	Bjørn Sortland, MH	Force Measurements in Oscillating Flow on Ship Sections and Circular Cylinders in a U-Tube Water Tank. (Dr.Ing. Thesis)
UR-86-53	Kurt Strand, MM	A System Dynamic Approach to One-dimensional Fluid Flow. (Dr.Ing. Thesis)
UR-86-54	Arne Edvin Løken, MH	Three Dimensional Second Order Hydrodynamic Effects on Ocean Structures in Waves. (Dr.Ing. Thesis)
UR-86-55	Sigurd Falch, MH	A Numerical Study of Slamming of Two-Dimensional Bodies. (Dr.Ing. Thesis)
UR-87-56	Arne Braathen, MH	Application of a Vortex Tracking Method to the Prediction of Roll Damping of a Two-Dimension Floating Body. (Dr.Ing. Thesis)

UR-87-57	Bernt Leira, MK	Gaussian Vector Processes for Reliability Analysis involving Wave-Induced Load Effects. (Dr.Ing. Thesis)
UR-87-58	Magnus Småvik, MM	Thermal Load and Process Characteristics in a Two-Stroke Diesel Engine with Thermal Barriers (in Norwegian). (Dr.Ing. Thesis)
MTA-88-59	Bernt Arild Bremdal, MP	An Investigation of Marine Installation Processes – A Knowledge - Based Planning Approach. (Dr.Ing. Thesis)
MTA-88-60	Xu Jun, MK	Non-linear Dynamic Analysis of Space-framed Offshore Structures. (Dr.Ing. Thesis)
MTA-89-61	Gang Miao, MH	Hydrodynamic Forces and Dynamic Responses of Circular Cylinders in Wave Zones. (Dr.Ing. Thesis)
MTA-89-62	Martin Greenhow, MH	Linear and Non-Linear Studies of Waves and Floating Bodies. Part I and Part II. (Dr.Techn. Thesis)
MTA-89-63	Chang Li, MH	Force Coefficients of Spheres and Cubes in Oscillatory Flow with and without Current. (Dr.Ing. Thesis
MTA-89-64	Hu Ying, MP	A Study of Marketing and Design in Development of Marine Transport Systems. (Dr.Ing. Thesis)
MTA-89-65	Arild Jæger, MH	Seakeeping, Dynamic Stability and Performance of a Wedge Shaped Planing Hull. (Dr.Ing. Thesis)
MTA-89-66	Chan Siu Hung, MM	The dynamic characteristics of tilting-pad bearings
MTA-89-67	Kim Wikstrøm, MP	Analysis av projekteringen for ett offshore projekt. (Licenciat-avhandling)
MTA-89-68	Jiao Guoyang, MK	Reliability Analysis of Crack Growth under Random Loading, considering Model Updating. (Dr.Ing. Thesis)
MTA-89-69	Arnt Olufsen, MK	Uncertainty and Reliability Analysis of Fixed Offshore Structures. (Dr.Ing. Thesis)
MTA-89-70	Wu Yu-Lin, MR	System Reliability Analyses of Offshore Structures using improved Truss and Beam Models. (Dr.Ing. Thesis)
MTA-90-71	Jan Roger Hoff, MH	Three-dimensional Green function of a vessel with forward speed in waves. (Dr.Ing. Thesis)
MTA-90-72	Rong Zhao, MH	Slow-Drift Motions of a Moored Two-Dimensional Body in Irregular Waves. (Dr.Ing. Thesis)
MTA-90-73	Atle Minsaas, MP	Economical Risk Analysis. (Dr.Ing. Thesis)
MTA-90-74	Knut-Aril Farnes, MK	Long-term Statistics of Response in Non-linear Marine Structures. (Dr.Ing. Thesis)
MTA-90-75	Torbjørn Sotberg, MK	Application of Reliability Methods for Safety Assessment of Submarine Pipelines. (Dr.Ing.

		Thesis)
MTA-90-76	Zeuthen, Steffen, MP	SEAMAID. A computational model of the design process in a constraint-based logic programming environment. An example from the offshore domain. (Dr.Ing. Thesis)
MTA-91-77	Haagensen, Sven, MM	Fuel Dependant Cyclic Variability in a Spark Ignition Engine - An Optical Approach. (Dr.Ing. Thesis)
MTA-91-78	Løland, Geir, MH	Current forces on and flow through fish farms. (Dr.Ing. Thesis)
MTA-91-79	Hoen, Christopher, MK	System Identification of Structures Excited by Stochastic Load Processes. (Dr.Ing. Thesis)
MTA-91-80	Haugen, Stein, MK	Probabilistic Evaluation of Frequency of Collision between Ships and Offshore Platforms. (Dr.Ing. Thesis)
MTA-91-81	Sødahl, Nils, MK	Methods for Design and Analysis of Flexible Risers. (Dr.Ing. Thesis)
MTA-91-82	Ormberg, Harald, MK	Non-linear Response Analysis of Floating Fish Farm Systems. (Dr.Ing. Thesis)
MTA-91-83	Marley, Mark J., MK	Time Variant Reliability under Fatigue Degradation. (Dr.Ing. Thesis)
MTA-91-84	Krokstad, Jørgen R., MH	Second-order Loads in Multidirectional Seas. (Dr.Ing. Thesis)
MTA-91-85	Molteberg, Gunnar A., MM	The Application of System Identification Techniques to Performance Monitoring of Four Stroke Turbocharged Diesel Engines. (Dr.Ing. Thesis)
MTA-92-86	Mørch, Hans Jørgen Bjelke, MH	Aspects of Hydrofoil Design: with Emphasis on Hydrofoil Interaction in Calm Water. (Dr.Ing. Thesis)
MTA-92-87	Chan Siu Hung, MM	Nonlinear Analysis of Rotordynamic Instabilities in Highspeed Turbomachinery. (Dr.Ing. Thesis)
MTA-92-88	Bessason, Bjarni, MK	Assessment of Earthquake Loading and Response of Seismically Isolated Bridges. (Dr.Ing. Thesis)
MTA-92-89	Langli, Geir, MP	Improving Operational Safety through exploitation of Design Knowledge - an investigation of offshore platform safety. (Dr.Ing. Thesis)
MTA-92-90	Sævik, Svein, MK	On Stresses and Fatigue in Flexible Pipes. (Dr.Ing. Thesis)
MTA-92-91	Ask, Tor Ø., MM	Ignition and Flame Growth in Lean Gas-Air Mixtures. An Experimental Study with a Schlieren System. (Dr.Ing. Thesis)
MTA-86-92	Hessen, Gunnar, MK	Fracture Mechanics Analysis of Stiffened Tubular Members. (Dr.Ing. Thesis)

MTA-93-93	Steinebach, Christian, MM	Knowledge Based Systems for Diagnosis of Rotating Machinery. (Dr.Ing. Thesis)
MTA-93-94	Dalane, Jan Inge, MK	System Reliability in Design and Maintenance of Fixed Offshore Structures. (Dr.Ing. Thesis)
MTA-93-95	Steen, Sverre, MH	Cobblestone Effect on SES. (Dr.Ing. Thesis)
MTA-93-96	Karunakaran, Daniel, MK	Nonlinear Dynamic Response and Reliability Analysis of Drag-dominated Offshore Platforms. (Dr.Ing. Thesis)
MTA-93-97	Hagen, Arnulf, MP	The Framework of a Design Process Language. (Dr.Ing. Thesis)
MTA-93-98	Nordrik, Rune, MM	Investigation of Spark Ignition and Autoignition in Methane and Air Using Computational Fluid Dynamics and Chemical Reaction Kinetics. A Numerical Study of Ignition Processes in Internal Combustion Engines. (Dr.Ing. Thesis)
MTA-94-99	Passano, Elizabeth, MK	Efficient Analysis of Nonlinear Slender Marine Structures. (Dr.Ing. Thesis)
MTA-94-100	Kvålsvold, Jan, MH	Hydroelastic Modelling of Wetdeck Slamming on Multihull Vessels. (Dr.Ing. Thesis)
MTA-94-102	Bech, Sidsel M., MK	Experimental and Numerical Determination of Stiffness and Strength of GRP/PVC Sandwich Structures. (Dr.Ing. Thesis)
MTA-95-103	Paulsen, Hallvard, MM	A Study of Transient Jet and Spray using a Schlieren Method and Digital Image Processing. (Dr.Ing. Thesis)
MTA-95-104	Hovde, Geir Olav, MK	Fatigue and Overload Reliability of Offshore Structural Systems, Considering the Effect of Inspection and Repair. (Dr.Ing. Thesis)
MTA-95-105	Wang, Xiaozhi, MK	Reliability Analysis of Production Ships with Emphasis on Load Combination and Ultimate Strength. (Dr.Ing. Thesis)
MTA-95-106	Ulstein, Tore, MH	Nonlinear Effects of a Flexible Stern Seal Bag on Cobblestone Oscillations of an SES. (Dr.Ing. Thesis)
MTA-95-107	Solaas, Frøydis, MH	Analytical and Numerical Studies of Sloshing in Tanks. (Dr.Ing. Thesis)
MTA-95-108	Hellan, Øyvind, MK	Nonlinear Pushover and Cyclic Analyses in Ultimate Limit State Design and Reassessment of Tubular Steel Offshore Structures. (Dr.Ing. Thesis)
MTA-95-109	Hermundstad, Ole A., MK	Theoretical and Experimental Hydroelastic Analysis of High Speed Vessels. (Dr.Ing. Thesis)
MTA-96-110	Bratland, Anne K., MH	Wave-Current Interaction Effects on Large-Volume Bodies in Water of Finite Depth. (Dr.Ing. Thesis)
MTA-96-111	Herfjord, Kjell, MH	A Study of Two-dimensional Separated Flow by a Combination of the Finite Element Method and

		Navier-Stokes Equations. (Dr.Ing. Thesis)
MTA-96-112	Æsøy, Vilmar, MM	Hot Surface Assisted Compression Ignition in a Direct Injection Natural Gas Engine. (Dr.Ing. Thesis)
MTA-96-113	Eknes, Monika L., MK	Escalation Scenarios Initiated by Gas Explosions on Offshore Installations. (Dr.Ing. Thesis)
MTA-96-114	Erikstad, Stein O., MP	A Decision Support Model for Preliminary Ship Design. (Dr.Ing. Thesis)
MTA-96-115	Pedersen, Egil, MH	A Nautical Study of Towed Marine Seismic Streamer Cable Configurations. (Dr.Ing. Thesis)
MTA-97-116	Moksnes, Paul O., MM	Modelling Two-Phase Thermo-Fluid Systems Using Bond Graphs. (Dr.Ing. Thesis)
MTA-97-117	Halse, Karl H., MK	On Vortex Shedding and Prediction of Vortex-Induced Vibrations of Circular Cylinders. (Dr.Ing. Thesis)
MTA-97-118	Igland, Ragnar T., MK	Reliability Analysis of Pipelines during Laying, considering Ultimate Strength under Combined Loads. (Dr.Ing. Thesis)
MTA-97-119	Pedersen, Hans-P., MP	Levendefiskteknologi for fiskefartøy. (Dr.Ing. Thesis)
MTA-98-120	Vikestad, Kyrre, MK	Multi-Frequency Response of a Cylinder Subjected to Vortex Shedding and Support Motions. (Dr.Ing. Thesis)
MTA-98-121	Azadi, Mohammad R. E., MK	Analysis of Static and Dynamic Pile-Soil-Jacket Behaviour. (Dr.Ing. Thesis)
MTA-98-122	Ulltang, Terje, MP	A Communication Model for Product Information. (Dr.Ing. Thesis)
MTA-98-123	Torbergsen, Erik, MM	Impeller/Diffuser Interaction Forces in Centrifugal Pumps. (Dr.Ing. Thesis)
MTA-98-124	Hansen, Edmond, MH	A Discrete Element Model to Study Marginal Ice Zone Dynamics and the Behaviour of Vessels Moored in Broken Ice. (Dr.Ing. Thesis)
MTA-98-125	Videiro, Paulo M., MK	Reliability Based Design of Marine Structures. (Dr.Ing. Thesis)
MTA-99-126	Mainçon, Philippe, MK	Fatigue Reliability of Long Welds Application to Titanium Risers. (Dr.Ing. Thesis)
MTA-99-127	Haugen, Elin M., MH	Hydroelastic Analysis of Slamming on Stiffened Plates with Application to Catamaran Wetdecks. (Dr.Ing. Thesis)
MTA-99-128	Langhelle, Nina K., MK	Experimental Validation and Calibration of Nonlinear Finite Element Models for Use in Design of Aluminium Structures Exposed to Fire. (Dr.Ing. Thesis)
MTA-99-	Berstad, Are J., MK	Calculation of Fatigue Damage in Ship Structures.

129		(Dr.Ing. Thesis)
MTA-99-130	Andersen, Trond M., MM	Short Term Maintenance Planning. (Dr.Ing. Thesis)
MTA-99-131	Tveiten, Bård Wathne, MK	Fatigue Assessment of Welded Aluminium Ship Details. (Dr.Ing. Thesis)
MTA-99-132	Søreide, Fredrik, MP	Applications of underwater technology in deep water archaeology. Principles and practice. (Dr.Ing. Thesis)
MTA-99-133	Tønnessen, Rune, MH	A Finite Element Method Applied to Unsteady Viscous Flow Around 2D Blunt Bodies With Sharp Corners. (Dr.Ing. Thesis)
MTA-99-134	Elvekrok, Dag R., MP	Engineering Integration in Field Development Projects in the Norwegian Oil and Gas Industry. The Supplier Management of Norne. (Dr.Ing. Thesis)
MTA-99-135	Fagerholt, Kjetil, MP	Optimeringsbaserte Metoder for Ruteplanlegging innen skipsfart. (Dr.Ing. Thesis)
MTA-99-136	Bysveen, Marie, MM	Visualization in Two Directions on a Dynamic Combustion Rig for Studies of Fuel Quality. (Dr.Ing. Thesis)
MTA-2000-137	Storteig, Eskild, MM	Dynamic characteristics and leakage performance of liquid annular seals in centrifugal pumps. (Dr.Ing. Thesis)
MTA-2000-138	Sagli, Gro, MK	Model uncertainty and simplified estimates of long term extremes of hull girder loads in ships. (Dr.Ing. Thesis)
MTA-2000-139	Tronstad, Harald, MK	Nonlinear analysis and design of cable net structures like fishing gear based on the finite element method. (Dr.Ing. Thesis)
MTA-2000-140	Kroneberg, André, MP	Innovation in shipping by using scenarios. (Dr.Ing. Thesis)
MTA-2000-141	Haslum, Herbjørn Alf, MH	Simplified methods applied to nonlinear motion of spar platforms. (Dr.Ing. Thesis)
MTA-2001-142	Samdal, Ole Johan, MM	Modelling of Degradation Mechanisms and Stressor Interaction on Static Mechanical Equipment Residual Lifetime. (Dr.Ing. Thesis)
MTA-2001-143	Baarholm, Rolf Jarle, MH	Theoretical and experimental studies of wave impact underneath decks of offshore platforms. (Dr.Ing. Thesis)
MTA-2001-144	Wang, Lihua, MK	Probabilistic Analysis of Nonlinear Wave-induced Loads on Ships. (Dr.Ing. Thesis)
MTA-2001-145	Kristensen, Odd H. Holt, MK	Ultimate Capacity of Aluminium Plates under Multiple Loads, Considering HAZ Properties. (Dr.Ing. Thesis)
MTA-2001-146	Greco, Marilena, MH	A Two-Dimensional Study of Green-Water

		Loading. (Dr.Ing. Thesis)
MTA-2001-147	Heggelund, Svein E., MK	Calculation of Global Design Loads and Load Effects in Large High Speed Catamarans. (Dr.Ing. Thesis)
MTA-2001-148	Babalola, Olusegun T., MK	Fatigue Strength of Titanium Risers – Defect Sensitivity. (Dr.Ing. Thesis)
MTA-2001-149	Mohammed, Abuu K., MK	Nonlinear Shell Finite Elements for Ultimate Strength and Collapse Analysis of Ship Structures. (Dr.Ing. Thesis)
MTA-2002-150	Holmedal, Lars E., MH	Wave-current interactions in the vicinity of the sea bed. (Dr.Ing. Thesis)
MTA-2002-151	Rognebakke, Olav F., MH	Sloshing in rectangular tanks and interaction with ship motions. (Dr.Ing. Thesis)
MTA-2002-152	Lader, Pål Furset, MH	Geometry and Kinematics of Breaking Waves. (Dr.Ing. Thesis)
MTA-2002-153	Yang, Qinzheng, MH	Wash and wave resistance of ships in finite water depth. (Dr.Ing. Thesis)
MTA-2002-154	Melhus, Øyvin, MM	Utilization of VOC in Diesel Engines. Ignition and combustion of VOC released by crude oil tankers. (Dr.Ing. Thesis)
MTA-2002-155	Ronæss, Marit, MH	Wave Induced Motions of Two Ships Advancing on Parallel Course. (Dr.Ing. Thesis)
MTA-2002-156	Økland, Ole D., MK	Numerical and experimental investigation of whipping in twin hull vessels exposed to severe wet deck slamming. (Dr.Ing. Thesis)
MTA-2002-157	Ge, Chunhua, MK	Global Hydroelastic Response of Catamarans due to Wet Deck Slamming. (Dr.Ing. Thesis)
MTA-2002-158	Byklum, Eirik, MK	Nonlinear Shell Finite Elements for Ultimate Strength and Collapse Analysis of Ship Structures. (Dr.Ing. Thesis)
IMT-2003-1	Chen, Haibo, MK	Probabilistic Evaluation of FPSO-Tanker Collision in Tandem Offloading Operation. (Dr.Ing. Thesis)
IMT-2003-2	Skaugset, Kjetil Bjørn, MK	On the Suppression of Vortex Induced Vibrations of Circular Cylinders by Radial Water Jets. (Dr.Ing. Thesis)
IMT-2003-3	Chezhian, Muthu	Three-Dimensional Analysis of Slamming. (Dr.Ing. Thesis)
IMT-2003-4	Buhaug, Øyvind	Deposit Formation on Cylinder Liner Surfaces in Medium Speed Engines. (Dr.Ing. Thesis)
IMT-2003-5	Tregde, Vidar	Aspects of Ship Design: Optimization of Aft Hull with Inverse Geometry Design. (Dr.Ing. Thesis)
IMT-	Wist, Hanne Therese	Statistical Properties of Successive Ocean Wave

2003-6		Parameters. (Dr.Ing. Thesis)
IMT-2004-7	Ransau, Samuel	Numerical Methods for Flows with Evolving Interfaces. (Dr.Ing. Thesis)
IMT-2004-8	Soma, Torkel	Blue-Chip or Sub-Standard. A data interrogation approach of identity safety characteristics of shipping organization. (Dr.Ing. Thesis)
IMT-2004-9	Ersdal, Svein	An experimental study of hydrodynamic forces on cylinders and cables in near axial flow. (Dr.Ing. Thesis)
IMT-2005-10	Brodtkorb, Per Andreas	The Probability of Occurrence of Dangerous Wave Situations at Sea. (Dr.Ing. Thesis)
IMT-2005-11	Yttervik, Rune	Ocean current variability in relation to offshore engineering. (Dr.Ing. Thesis)
IMT-2005-12	Fredheim, Arne	Current Forces on Net-Structures. (Dr.Ing. Thesis)
IMT-2005-13	Heggernes, Kjetil	Flow around marine structures. (Dr.Ing. Thesis
IMT-2005-14	Fouques, Sebastien	Lagrangian Modelling of Ocean Surface Waves and Synthetic Aperture Radar Wave Measurements. (Dr.Ing. Thesis)
IMT-2006-15	Holm, Håvard	Numerical calculation of viscous free surface flow around marine structures. (Dr.Ing. Thesis)
IMT-2006-16	Bjørheim, Lars G.	Failure Assessment of Long Through Thickness Fatigue Cracks in Ship Hulls. (Dr.Ing. Thesis)
IMT-2006-17	Hansson, Lisbeth	Safety Management for Prevention of Occupational Accidents. (Dr.Ing. Thesis)
IMT-2006-18	Zhu, Xinying	Application of the CIP Method to Strongly Nonlinear Wave-Body Interaction Problems. (Dr.Ing. Thesis)
IMT-2006-19	Reite, Karl Johan	Modelling and Control of Trawl Systems. (Dr.Ing. Thesis)
IMT-2006-20	Smogeli, Øyvind Notland	Control of Marine Propellers. From Normal to Extreme Conditions. (Dr.Ing. Thesis)
IMT-2007-21	Storhaug, Gaute	Experimental Investigation of Wave Induced Vibrations and Their Effect on the Fatigue Loading of Ships. (Dr.Ing. Thesis)
IMT-2007-22	Sun, Hui	A Boundary Element Method Applied to Strongly Nonlinear Wave-Body Interaction Problems. (PhD Thesis, CeSOS)
IMT-2007-23	Rustad, Anne Marthine	Modelling and Control of Top Tensioned Risers. (PhD Thesis, CeSOS)
IMT-2007-24	Johansen, Vegar	Modelling flexible slender system for real-time simulations and control applications
IMT-2007-25	Wroldsen, Anders Sunde	Modelling and control of tensegrity structures.

		(PhD Thesis, CeSOS)
IMT-2007-26	Aronsen, Kristoffer Høye	An experimental investigation of in-line and combined inline and cross flow vortex induced vibrations. (Dr. avhandling, IMT)
IMT-2007-27	Gao, Zhen	Stochastic Response Analysis of Mooring Systems with Emphasis on Frequency-domain Analysis of Fatigue due to Wide-band Response Processes (PhD Thesis, CeSOS)
IMT-2007-28	Thorstensen, Tom Anders	Lifetime Profit Modelling of Ageing Systems Utilizing Information about Technical Condition. (Dr.ing. thesis, IMT)
IMT-2008-29	Refsnes, Jon Erling Gorset	Nonlinear Model-Based Control of Slender Body AUVs (PhD Thesis, IMT)
IMT-2008-30	Berntsen, Per Ivar B.	Structural Reliability Based Position Mooring. (PhD-Thesis, IMT)
IMT-2008-31	Ye, Naiquan	Fatigue Assessment of Aluminium Welded Box-stiffener Joints in Ships (Dr.ing. thesis, IMT)
IMT-2008-32	Radan, Damir	Integrated Control of Marine Electrical Power Systems. (PhD-Thesis, IMT)
IMT-2008-33	Thomassen, Paul	Methods for Dynamic Response Analysis and Fatigue Life Estimation of Floating Fish Cages. (Dr.ing. thesis, IMT)
IMT-2008-34	Pákozdi, Csaba	A Smoothed Particle Hydrodynamics Study of Two-dimensional Nonlinear Sloshing in Rectangular Tanks. (Dr.ing.thesis, IMT/ CeSOS)
IMT-2007-35	Grytøyr, Guttorm	A Higher-Order Boundary Element Method and Applications to Marine Hydrodynamics. (Dr.ing.thesis, IMT)
IMT-2008-36	Drummen, Ingo	Experimental and Numerical Investigation of Nonlinear Wave-Induced Load Effects in Containerships considering Hydroelasticity. (PhD thesis, CeSOS)
IMT-2008-37	Skejic, Renato	Maneuvering and Seakeeping of a Singel Ship and of Two Ships in Interaction. (PhD-Thesis, CeSOS)
IMT-2008-38	Harlem, Alf	An Age-Based Replacement Model for Repairable Systems with Attention to High-Speed Marine Diesel Engines. (PhD-Thesis, IMT)
IMT-2008-39	Alsos, Hagbart S.	Ship Grounding. Analysis of Ductile Fracture, Bottom Damage and Hull Girder Response. (PhD-thesis, IMT)
IMT-2008-40	Graczyk, Mateusz	Experimental Investigation of Sloshing Loading and Load Effects in Membrane LNG Tanks Subjected to Random Excitation. (PhD-thesis, CeSOS)
IMT-2008-41	Taghipour, Reza	Efficient Prediction of Dynamic Response for Flexible amd Multi-body Marine Structures. (PhD-

		thesis, CeSOS)
IMT-2008-42	Ruth, Eivind	Propulsion control and thrust allocation on marine vessels. (PhD thesis, CeSOS)
IMT-2008-43	Nystad, Bent Helge	Technical Condition Indexes and Remaining Useful Life of Aggregated Systems. PhD thesis, IMT
IMT-2008-44	Soni, Prashant Kumar	Hydrodynamic Coefficients for Vortex Induced Vibrations of Flexible Beams, PhD thesis, CeSOS
IMT-2009-45	Amlashi, Hadi K.K.	Ultimate Strength and Reliability-based Design of Ship Hulls with Emphasis on Combined Global and Local Loads. PhD Thesis, IMT
IMT-2009-46	Pedersen, Tom Arne	Bond Graph Modelling of Marine Power Systems. PhD Thesis, IMT
IMT-2009-47	Kristiansen, Trygve	Two-Dimensional Numerical and Experimental Studies of Piston-Mode Resonance. PhD-Thesis, CeSOS
IMT-2009-48	Ong, Muk Chen	Applications of a Standard High Reynolds Number Model and a Stochastic Scour Prediction Model for Marine Structures. PhD-thesis, IMT
IMT-2009-49	Hong, Lin	Simplified Analysis and Design of Ships subjected to Collision and Grounding. PhD-thesis, IMT
IMT-2009-50	Koushan, Kamran	Vortex Induced Vibrations of Free Span Pipelines, PhD thesis, IMT
IMT-2009-51	Korsvik, Jarl Eirik	Heuristic Methods for Ship Routing and Scheduling. PhD-thesis, IMT
IMT-2009-52	Lee, Jihoon	Experimental Investigation and Numerical in Analyzing the Ocean Current Displacement of Longlines. Ph.d.-Thesis, IMT.
IMT-2009-53	Vestbøstad, Tone Gran	A Numerical Study of Wave-in-Deck Impact usin a Two-Dimensional Constrained Interpolation Profile Method, Ph.d.thesis, CeSOS.
IMT-2009-54	Bruun, Kristine	Bond Graph Modelling of Fuel Cells for Marine Power Plants. Ph.d.-thesis, IMT
IMT 2009-55	Holstad, Anders	Numerical Investigation of Turbulence in a Sekwed Three-Dimensional Channel Flow, Ph.d.-thesis, IMT.
IMT 2009-56	Ayala-Uraga, Efren	Reliability-Based Assessment of Deteriorating Ship-shaped Offshore Structures, Ph.d.-thesis, IMT
IMT 2009-57	Kong, Xiangjun	A Numerical Study of a Damaged Ship in Beam Sea Waves. Ph.d.-thesis, IMT/CeSOS.
IMT 2010-58	Kristiansen, David	Wave Induced Effects on Floaters of Aquaculture Plants, Ph.d.-thesis, CeSOS.

IMT 2010-59	Ludvigsen, Martin	An ROV-Toolbox for Optical and Acoustic Scientific Seabed Investigation. Ph.d.-thesis IMT.
IMT 2010-60	Hals, Jørgen	Modelling and Phase Control of Wave-Energy Converters. Ph.d.thesis, CeSOS.
IMT 2010- 61	Shu, Zhi	Uncertainty Assessment of Wave Loads and Ultimate Strength of Tankers and Bulk Carriers in a Reliability Framework. Ph.d. Thesis, IMT/ CeSOS
IMT 2010-62	Shao, Yanlin	Numerical Potential-Flow Studies on Weakly-Nonlinear Wave-Body Interactions with/without Small Forward Speed, Ph.d.thesis,CeSOS.
IMT 2010-63	Califano, Andrea	Dynamic Loads on Marine Propellers due to Intermittent Ventilation. Ph.d.thesis, IMT.
IMT 2010-64	El Khoury, George	Numerical Simulations of Massively Separated Turbulent Flows, Ph.d.-thesis, IMT
IMT 2010-65	Seim, Knut Sponheim	Mixing Process in Dense Overflows with Emphasis on the Faroe Bank Channel Overflow. Ph.d.thesis, IMT
IMT 2010-66	Jia, Huirong	Structural Analysis of Intect and Damaged Ships in a Collission Risk Analysis Perspective. Ph.d.thesis CeSoS.
IMT 2010-67	Jiao, Linlin	Wave-Induced Effects on a Pontoon-type Very Large Floating Structures (VLFS). Ph.D.-thesis, CeSOS.
IMT 2010-68	Abrahamsen, Bjørn Christian	Sloshing Induced Tank Roof with Entrapped Air Pocket. Ph.d.thesis, CeSOS.
IMT 2011-69	Karimirad, Madjid	Stochastic Dynamic Response Analysis of Spar-Type Wind Turbines with Catenary or Taut Mooring Systems. Ph.d.-thesis, CeSOS.
IMT - 2011-70	Erlend Meland	Condition Monitoring of Safety Critical Valves. Ph.d.-thesis, IMT.
IMT – 2011-71	Yang, Limin	Stochastic Dynamic System Analysis of Wave Energy Converter with Hydraulic Power Take-Off, with Particular Reference to Wear Damage Analysis, Ph.d. Thesis, CeSOS.
IMT – 2011-72	Visscher, Jan	Application of Particla Image Velocimetry on Turbulent Marine Flows, Ph.d.Thesis, IMT.
IMT – 2011-73	Su, Biao	Numerical Predictions of Global and Local Ice Loads on Ships. Ph.d.Thesis, CeSOS.
IMT – 2011-74	Liu, Zhenhui	Analytical and Numerical Analysis of Iceberg Collision with Ship Structures. Ph.d.Thesis, IMT.
IMT – 2011-75	Aarsæther, Karl Gunnar	Modeling and Analysis of Ship Traffic by Observation and Numerical Simulation. Ph.d.Thesis, IMT.

Imt – 2011-76	Wu, Jie	Hydrodynamic Force Identification from Stochastic Vortex Induced Vibration Experiments with Slender Beams. Ph.d.Thesis, IMT.
Imt – 2011-77	Amini, Hamid	Azimuth Propulsors in Off-design Conditions. Ph.d.Thesis, IMT.
IMT – 2011-78	Nguyen, Tan-Hoi	Toward a System of Real-Time Prediction and Monitoring of Bottom Damage Conditions During Ship Grounding. Ph.d.thesis, IMT.
IMT- 2011-79	Tavakoli, Mohammad T.	Assessment of Oil Spill in Ship Collision and Grounding, Ph.d.thesis, IMT.
IMT- 2011-80	Guo, Bingjie	Numerical and Experimental Investigation of Added Resistance in Waves. Ph.d.Thesis, IMT.
IMT- 2011-81	Chen, Qiaofeng	Ultimate Strength of Aluminium Panels, considering HAZ Effects, IMT
IMT- 2012-82	Kota, Ravikiran S.	Wave Loads on Decks of Offshore Structures in Random Seas, CeSOS.
IMT- 2012-83	Sten, Ronny	Dynamic Simulation of Deep Water Drilling Risers with Heave Compensating System, IMT.
IMT- 2012-84	Berle, Øyvind	Risk and resilience in global maritime supply chains, IMT.
IMT- 2012-85	Fang, Shaoji	Fault Tolerant Position Mooring Control Based on Structural Reliability, CeSOS.
IMT- 2012-86	You, Jikun	Numerical studies on wave forces and moored ship motions in intermediate and shallow water, CeSOS.
IMT- 2012-87	Xiang ,Xu	Maneuvering of two interacting ships in waves, CeSOS
IMT- 2012-88	Dong, Wenbin	Time-domain fatigue response and reliability analysis of offshore wind turbines with emphasis on welded tubular joints and gear components, CeSOS
IMT- 2012-89	Zhu, Suji	Investigation of Wave-Induced Nonlinear Load Effects in Open Ships considering Hull Girder Vibrations in Bending and Torsion, CeSOS
IMT- 2012-90	Zhou, Li	Numerical and Experimental Investigation of Station-keeping in Level Ice, CeSOS
IMT- 2012-91	Ushakov, Sergey	Particulate matter emission characteristics from diesel enignes operating on conventional and alternative marine fuels, IMT
IMT- 2013-1	Yin, Decao	Experimental and Numerical Analysis of Combined In-line and Cross-flow Vortex Induced Vibrations, CeSOS

IMT-2013-2	Kurniawan, Adi	Modelling and geometry optimisation of wave energy converters, CeSOS
IMT-2013-3	Al Ryati, Nabil	Technical condition indexes doe auxiliary marine diesel engines, IMT
IMT-2013-4	Firoozkoohi, Reza	Experimental, numerical and analytical investigation of the effect of screens on sloshing, CeSOS
IMT-2013-5	Ommani, Babak	Potential-Flow Predictions of a Semi-Displacement Vessel Including Applications to Calm Water Broaching, CeSOS
IMT-2013-6	Xing, Yihan	Modelling and analysis of the gearbox in a floating spar-type wind turbine, CeSOS
IMT-7-2013	Balland, Océane	Optimization models for reducing air emissions from ships, IMT
IMT-8-2013	Yang, Dan	Transitional wake flow behind an inclined flat plate-----Computation and analysis, IMT
IMT-9-2013	Abdillah, Suyuthi	Prediction of Extreme Loads and Fatigue Damage for a Ship Hull due to Ice Action, IMT
IMT-10-2013	Ramìrez, Pedro Agustìn Pèrez	Ageing management and life extension of technical systems- Concepts and methods applied to oil and gas facilities, IMT
IMT-11-2013	Chuang, Zhenju	Experimental and Numerical Investigation of Speed Loss due to Seakeeping and Maneuvering. IMT
IMT-12-2013	Etemaddar, Mahmoud	Load and Response Analysis of Wind Turbines under Atmospheric Icing and Controller System Faults with Emphasis on Spar Type Floating Wind Turbines, IMT
IMT-13-2013	Lindstad, Haakon	Strategies and measures for reducing maritime CO2 emissons, IMT
IMT-14-2013	Haris, Sabril	Damage interaction analysis of ship collisions, IMT
IMT-15-2013	Shainee, Mohamed	Conceptual Design, Numerical and Experimental Investigation of a SPM Cage Concept for Offshore Mariculture, IMT
IMT-16-2013	Gansel, Lars	Flow past porous cylinders and effects of biofouling and fish behavior on the flow in and around Atlantic salmon net cages, IMT
IMT-17-2013	Gaspar, Henrique	Handling Aspects of Complexity in Conceptual Ship Design, IMT
IMT-18-2013	Thys, Maxime	Theoretical and Experimental Investigation of a Free Running Fishing Vessel at Small Frequency of Encounter, CeSOS
IMT-19-2013	Aglen, Ida	VIV in Free Spanning Pipelines, CeSOS

IMT-1-2014	Song, An	Theoretical and experimental studies of wave diffraction and radiation loads on a horizontally submerged perforated plate, CeSOS
IMT-2-2014	Rogne, Øyvind Ygre	Numerical and Experimental Investigation of a Hinged 5-body Wave Energy Converter, CeSOS
IMT-3-2014	Dai, Lijuan	Safe and efficient operation and maintenance of offshore wind farms ,IMT
IMT-4-2014	Bachynski, Erin Elizabeth	Design and Dynamic Analysis of Tension Leg Platform Wind Turbines, CeSOS
IMT-5-2014	Wang, Jingbo	Water Entry of Freefall Wedged – Wedge motions and Cavity Dynamics, CeSOS
IMT-6-2014	Kim, Ekaterina	Experimental and numerical studies related to the coupled behavior of ice mass and steel structures during accidental collisions, IMT
IMT-7-2014	Tan, Xiang	Numerical investigation of ship's continuous- mode icebreaking in leverl ice, CeSOS
IMT-8-2014	Muliawan, Made Jaya	Design and Analysis of Combined Floating Wave and Wind Power Facilities, with Emphasis on Extreme Load Effects of the Mooring System, CeSOS
IMT-9-2014	Jiang, Zhiyu	Long-term response analysis of wind turbines with an emphasis on fault and shutdown conditions, IMT
IMT-10-2014	Dukan, Fredrik	ROV Motion Control Systems, IMT
IMT-11-2014	Grimsmo, Nils I.	Dynamic simulations of hydraulic cylinder for heave compensation of deep water drilling risers, IMT
IMT-12-2014	Kvittem, Marit I.	Modelling and response analysis for fatigue design of a semisubmersible wind turbine, CeSOS
IMT-13-2014	Akhtar, Juned	The Effects of Human Fatigue on Risk at Sea, IMT
IMT-14-2014	Syahroni, Nur	Fatigue Assessment of Welded Joints Taking into Account Effects of Residual Stress, IMT
IMT-1-2015	Bøckmann, Eirik	Wave Propulsion of ships, IMT
IMT-2-2015	Wang, Kai	Modelling and dynamic analysis of a semi-submersible floating vertical axis wind turbine, CeSOS
IMT-3-2015	Fredriksen, Arnt Gunvald	A numerical and experimental study of a two-dimensional body with moonpool in waves and current, CeSOS
IMT-4-2015	Jose Patricio Gallardo Canabes	Numerical studies of viscous flow around bluff bodies, IMT

IMT-5-2015	Vegard Longva	Formulation and application of finite element techniques for slender marine structures subjected to contact interactions, IMT
IMT-6-2015	Jacobus De Vaal	Aerodynamic modelling of floating wind turbines, CeSOS
IMT-7-2015	Fachri Nasution	Fatigue Performance of Copper Power Conductors, IMT
IMT-8-2015	Oleh I Karpa	Development of bivariate extreme value distributions for applications in marine technology,CeSOS
IMT-9-2015	Daniel de Almeida Fernandes	An output feedback motion control system for ROVs, AMOS
IMT-10-2015	Bo Zhao	Particle Filter for Fault Diagnosis: Application to Dynamic Positioning Vessel and Underwater Robotics, CeSOS
IMT-11-2015	Wenting Zhu	Impact of emission allocation in maritime transportation, IMT
IMT-12-2015	Amir Rasekhi Nejad	Dynamic Analysis and Design of Gearboxes in Offshore Wind Turbines in a Structural Reliability Perspective, CeSOS
IMT-13-2015	Arturo Jesùs Ortega Malca	Dynamic Response of Flexibles Risers due to Unsteady Slug Flow, CeSOS
IMT-14-2015	Dagfinn Husjord	Guidance and decision-support system for safe navigation of ships operating in close proximity, IMT
IMT-15-2015	Anirban Bhattacharyya	Ducted Propellers: Behaviour in Waves and Scale Effects, IMT
IMT-16-2015	Qin Zhang	Image Processing for Ice Parameter Identification in Ice Management, IMT
IMT-1-2016	Vincentius Rumawas	Human Factors in Ship Design and Operation: An Experiential Learning, IMT
IMT-2-2016	Martin Storheim	Structural response in ship-platform and ship-ice collisions, IMT
IMT-3-2016	Mia Abrahamsen Prsic	Numerical Simulations of the Flow around single and Tandem Circular Cylinders Close to a Plane Wall, IMT
IMT-4-2016	Tufan Arslan	Large-eddy simulations of cross-flow around ship sections, IMT

IMT-5-2016	Pierre Yves-Henry	Parametrisation of aquatic vegetation in hydraulic and coastal research,IMT
IMT-6-2016	Lin Li	Dynamic Analysis of the Instalation of Monopiles for Offshore Wind Turbines, CeSOS
IMT-7-2016	Øivind Kåre Kjerstad	Dynamic Positioning of Marine Vessels in Ice, IMT
IMT-8-2016	Xiaopeng Wu	Numerical Analysis of Anchor Handling and Fish Trawling Operations in a Safety Perspective, CeSOS
IMT-9-2016	Zhengshun Cheng	Integrated Dynamic Analysis of Floating Vertical Axis Wind Turbines, CeSOS
IMT-10-2016	Ling Wan	Experimental and Numerical Study of a Combined Offshore Wind and Wave Energy Converter Concept
IMT-11-2016	Wei Chai	Stochastic dynamic analysis and reliability evaluation of the roll motion for ships in random seas, CeSOS
IMT-12-2016	Øyvind Selnes Patricksson	Decision support for conceptual ship design with focus on a changing life cycle and future uncertainty, IMT
IMT-13-2016	Mats Jørgen Thorsen	Time domain analysis of vortex-induced vibrations, IMT
IMT-14-2016	Edgar McGuinness	Safety in the Norwegian Fishing Fleet – Analysis and measures for improvement, IMT
IMT-15-2016	Sepideh Jafarzadeh	Energy effiency and emission abatement in the fishing fleet, IMT
IMT-16-2016	Wilson Ivan Guachamin Acero	Assessment of marine operations for offshore wind turbine installation with emphasis on response-based operational limits, IMT
IMT-17-2016	Mauro Candeloro	Tools and Methods for Autonomous Operations on Seabed and Water Coumn using Underwater Vehicles, IMT
IMT-18-2016	Valentin Chabaud	Real-Time Hybrid Model Testing of Floating Wind Tubines, IMT
IMT-1-2017	Mohammad Saud Afzal	Three-dimensional streaming in a sea bed boundary layer
IMT-2-2017	Peng Li	A Theoretical and Experimental Study of Wave-induced Hydroelastic Response of a Circular Floating Collar
IMT-3-2017	Martin Bergström	A simulation-based design method for arctic maritime transport systems

IMT-4-2017	Bhushan Taskar	The effect of waves on marine propellers and propulsion
IMT-5-2017	Mohsen Bardestani	A two-dimensional numerical and experimental study of a floater with net and sinker tube in waves and current
IMT-6-2017	Fatemeh Hoseini Dadmarzi	Direct Numerical Simualtion of turbulent wakes behind different plate configurations
IMT-7-2017	Michel R. Miyazaki	Modeling and control of hybrid marine power plants
IMT-8-2017	Giri Rajasekhar Gunnu	Safety and effiency enhancement of anchor handling operations with particular emphasis on the stability of anchor handling vessels
IMT-9-2017	Kevin Koosup Yum	Transient Performance and Emissions of a Turbocharged Diesel Engine for Marine Power Plants
IMT-10-2017	Zhaolong Yu	Hydrodynamic and structural aspects of ship collisions
IMT-11-2017	Martin Hassel	Risk Analysis and Modelling of Allisions between Passing Vessels and Offshore Installations
IMT-12-2017	Astrid H. Brodtkorb	Hybrid Control of Marine Vessels – Dynamic Positioning in Varying Conditions